Technische Universität München
Fakultät für Medizin

The immune response of CRISPR-Cas9 generated *B2M* knockout and MHC-I deficient human induced pluripotent stem cells

Lina Ottelé

Vollständiger Abdruck der von der Fakultät für Medizin der Technischen Universität München zur Erlangung einer **Doktorin der Medizin (Dr.med.)** genehmigten Dissertation.

Vorsitz: apl. Prof. Dr. Ute Reuning

Prüfer der Dissertation:
1. apl. Prof. Dr. Markus Krane
2. Priv.-Doz. Dr. Bastian Höchst

Die Dissertation wurde am 07.12.2022 bei der Fakultät für Medizin der Technischen Universität München eingereicht und durch die Fakultät für Medizin am 13.06.2023 angenommen.

List of Abbreviations

AAV adeno-associated virus

ACTB β-Actin

aq. bidest. aqua bidestillata (Latin name for double-distilled water)

ATP adenosine triphosphate

AU absorbance units

AU arbitrary units

B2M β2-microglobulin

BLAST Basic Local Alignment Search Tool

bp base pairs

BSA bovine serum albumin

CAD coronary artery disease

CD cluster of differentiation

CDM3 Chemically defined medium, 3 components

cDNA complementary deoxyribonucleic acid

CMs cardiomyocytes

CRISPR-Cas9 clustered regularly interspaced short palindromic repeats-associated endonuclease 9

Ct threshold cycle

CTLA4 cytotoxic T-lymphocyte antigen 4

CVDs cardiovascular diseases

D day

DAPI 4',6-diamidino-2-phenylindole

DMSO dimethyl sulfoxide

dNTP desoxynucleotide triphosphate

D-PBS Dulbecco's phosphat buffered saline

DNA deoxyribonucleic acid

DSB double-strand break

DTT dithiothreitol

E. coli Escherichia coli

E:T effector to target

EDTA ethylenediamine tetraacetic acid

EHS Engelbreth-Holm-Swarm

ELISA enzyme-linked immunosorbent assay

ER endoplasmic reticulum

ESCs embryonic stem cells

FACS fluorescence-activated cell sorting

FCS fetal calf serum

FGF fibroblast growth factor

FITC fluorescein isothiocyanate

FSC forward scatter

G418 Geneticin 418

GATA4 GATA binding protein 4

GFR growth factor reduced

GSK3 glycogen synthase kinase 3

GZMB granzyme B

HDR homology-directed repair

HEK human embryonic kidney

hiPS human induced pluripotent stem

hiPSC human induced pluripotent stem cell

HLA human leukocyte antigen

HRP horseradish peroxidase

ICC immunocytochemistry

ICM inner cell mass

IFNγ interferon gamma

IL10 interleukin 10

IL12 interleukin 12

IL15 interleukin 15

IL2 interleukin 2

iPSCs induced pluripotent stem cells

KIR killer immunoglobulin-like receptor

KLF4 Krüppel-like factor 4

LB lysogeny broth

LDH lactate dehydrogenase

loxP locus of X-over P1

M-MLV RT Moloney murine leukemia virus reverse transcriptase

MACS magnetic cell sorting

MEF2C myocyte enhancer factor 2C

MHC major histocompatibility complex

MHC-I major histocompatibility complex class I

MLC2a myosin light chain-2, atrial isoform, encoded by *MYL7*

MLC2v myosin light chain-2, ventrical isoform, encoded by *MYL2*

NAD nicotinamide adenine dinucleotide

NCBI National Center for Biotechnology Information

NHEJ non-homologous end joining

NK natural killer

NKX2.5 NK2 Homeobox 5

OCT3/4 Octamer binding transcription factor 3/4

p passage

PAM protospacer adjacent motif

PBMCs peripheral blood mononuclear cells

PBS phosphat buffered saline

PBS-T phosphate buffered saline with Triton X-100

PCR polymerase chain reaction

PD-L1 programmed death ligand-1

Pen-Strep Penicillin-Streptomycin

PFA paraformaldehyde

pH power of hydrogen

PHA phytohemagglutinin

PS Polystyrene

PSCs pluripotent stem cells

qRT-PCR quantitative real-time polymerase chain reaction

RFP red fluorescent protein

RIPA radioimmunoprecipitation assay

RNA ribonucleic acid

RNAi RNA interference

ROCK rho-associated protein kinase

RPMI Roswell Park Memorial Institute

RT room temperature (15-25 °C)

SDS sodium dodecyl sulfate

sgRNA single guide RNA

SOB super optimal broth

SOC super optimal broth with catabolite repression

SOX2 SRY [sex determining region Y]-box transcription factor 2

SSC side scatter

TALEN transcription activator-like effector nuclease

TBE TRIS borate EDTA buffer

TBX5 T-Box 5

TCR T-cell receptor

TGF transforming growth factor

TGFβ transforming growth factor beta

TNFα tumor necrosis factor alpha

TNNT2 cardiac troponin T

Tregs regulatory T-cells

WB western blot

WNT wingless and int-1

ZFN zinc-finger nuclease

List of Figures

List of Tables

Zusammenfassung

Herz-Kreislauf-Erkrankungen stellen weltweit die häufigste Todesursache dar und haben einen erheblichen Einfluss auf die globale Morbidität. In den letzten Jahren haben sich die aus humanen induzierten pluripotenten Stammzellen (hiPSCs) abgeleiteten Kardiomyozyten (CMs) zu einer vielversprechenden Zellquelle für kardiale Regenerationstherapien entwickelt. Nach Transplantation ist das Überleben transplantierter hiPSCs vor allem durch die immunologische Abstoßungsreaktion begrenzt. Diese ist in erster Linie auf die Major Histocompatibility Complex (MHC) Klasse I Histoinkompatibilität zurückzuführen. Das Hauptziel dieser Arbeit war deshalb, die Generierung einer hypoimmunogenen hiPSC-Linie, die das Potential hat, nach Transplantation eine verminderte Immunantwort durch den Empfängers zu induzieren. Die Erzeugung einer Zelllinie ohne MHC-I-Oberflächenexpression hat die Kapazität, ihre Immunogenität gegenüber alloreaktiven T-Zellen zu reduzieren. Um diese Annahme zu überprüfen, wurde eine gut etablierte und charakterisierte MLC2v-tdTomato Reporter-hiPSC-Linie mit Hilfe der CRISPR-Cas9-Technologie genetisch verändert. Dabei wurden die Exone 2 und 3 des *β2-Mikroglobulin (B2M)* Gens auf einem oder beiden Allelen durch eine Neomycin-Resistenzkassette über homologe Rekombination ersetzt. Durch diesen Ansatz konnten mehrere hetero- und homozygote *B2M*-defiziente Zellklone generiert werden. Durchflusszytometrische und immunzytochemische Untersuchungen zeigten, dass B2M auf der Zelloberfläche für eine funktionelle MHC-I-Komplexbildung unerlässlich ist. So führte die gezielte Deletion des *B2M* Gens zu einer reduzierten MHC-I-Oberflächenexpression in heterozygoten und zu einer fehlenden MHC-I-Oberflächenexpression in homozygoten *B2M*-defizienten hiPSCs. Immunzytochemie und Genexpressionsanalysen herzspezifischer Marker während der gerichteten kardialen Differenzierung bestätigten, dass die manipulierten Zellklone das Potential haben, sich effizient in die kardiale Richtung differenzieren zu können. Da MLC2v ein robuster Marker für ventrikuläre CMs ist, ermöglichte das MLC2v-tdTomato Knock-in der Zelllinie die Identifizierung von CMs mit einem ventrikulären Phänotyp anhand ihrer roten Fluoreszenz. Parallel dazu wurden verschiedene Immunzell-basierte Experimente durchgeführt, um die Immunogenität der erzeugten *B2M*-defizienten hiPSC-Klone zu untersuchen. Durchgeführte LDH-basierte Zytotoxizitätstests bestätigten die signifikante Verringerung der CD8+ T-Zell-vermittelten Immunantwort gegen homozygote *B2M*-defiziente hiPSC-Klone im Vergleich zur Wildtyp-Zelllinie. Diese Ergebnisse zeigen, dass die genetische Manipulation von MHC-I eine effiziente Strategie zur Verringerung der immunologischen Abstoßung von hiPSCs darstellt. Die erzeugten hypoimmunogenen hiPSCs stellen einen ersten Schritt zur Generierung von universell einsetzbaren Spenderzellen dar und werden dazu beitragen, die Effizienz

und den Erfolg der zellbasierten kardialen Regenerationstherapie zu verbessern.

Abstract

Cardiovascular diseases represent the leading cause of mortality worldwide and have a substantial impact on global morbidity. In recent years, cell therapy using human induced pluripotent stem cell (hiPSC)-derived cardiomyocytes (CMs) has become a promising strategy for cardiac regeneration. However, successful engraftment and survival of transplanted hiPSCs are limited by immune rejection, predominantly due to major histocompatibility complex (MHC) class I histoincompatibility. Hence, the main goal of this thesis was the generation of an hypoimmunogenic hiPSC line for cardiac regeneration therapy, which is able to trigger a reduced immune response of the recipient upon transplantation. Generating a cell line devoid of MHC-I surface expression has the potential to reduce its immunogenicity towards alloreactive T-cells. To verify this postulation, a well-established and characterized MLC2v-tdTomato reporter hiPSC line was genetically modified using the CRISPR-Cas9 technology. In fact, exons 2 and 3 of the *β2-microglobulin (B2M)* gene were replaced on one or both alleles by a neomycin resistance cassette via homologous recombination. This approach generated several successfully manipulated hetero- and homozygous *B2M*-deficient cell clones. Flow cytometry and immunocytochemistry demonstrated that B2M on the cell surface is essential for functional MHC-I complex formation. Thus, targeted disruption of the *B2M* gene resulted in reduced MHC-I surface expression in heterozygous and completely absent MHC-I surface expression in homozygous *B2M*-deficient hiPSCs. Immunocytochemical and gene expression analysis of cardiac-specific markers, during directed cardiac differentiation of successfully manipulated cell clones, confirmed their potential to efficiently differentiate towards the cardiac lineage. As MLC2v is a robust marker for ventricular CMs, the MLC2v-tdTomato knock-in of the cell line enabled the identification of CMs with a developing ventricular phenotype by their red fluorescence. In parallel, different immune cell-based assays were established to evaluate the immunogenicity of the generated *B2M*-deficient hiPSC clones. LDH-Cytotoxicity assays confirmed the significant reduction of the CD8+ T-cell-mediated immune response against homozygous *B2M*-deficient hiPSC clones in comparison to the wild-type cell line. These results demonstrate that genetic manipulation of MHC-I is an efficient strategy to reduce the immune rejection of hiPSCs. The generated hypoimmunogenic hiPSCs represent a first step to establish universal donor cells and will notably help to improve the efficiency and success of cell-based cardiac regeneration therapy.

Contents

1 Introduction

1.1 Cardiovascular diseases

Cardiovascular diseases (CVDs) comprise heart and blood vessel disorders and represent the leading cause of mortality worldwide, accounting for around 18.6 million deaths per year (Roth et al., 2020). CVDs have a substantial impact on global morbidity and are associated with high healthcare costs, making them a topic of great public health relevance (Roth et al., 2020). CVDs include, among others, coronary heart disease, cerebrovascular disease, peripheral arterial disease and aortic disease (Lopez, Ballard, & Jan, 2021). Non-modifiable risk factors for CVDs are age, sex, ethnicity, and a positive family history (Brown, Gerhardt, & Kwon, 2021). Behavioral determinants associated with CVDs include a poor diet, physical inactivity, tobacco use and high alcohol consumption (Alageel, Wright, & Gulliford, 2016). In Europe, coronary artery disease (CAD) represents the most frequent cause of cardiovascular death, corresponding to 38 % of all CVDs deaths in women and 44 % in men (Timmis et al., 2020). The underlying pathophysiological process leading to CAD is atherosclerosis, a multifactorial inflammatory disease of the intima of medium-sized arteries, which develops and progresses over time (Ambrose & Singh, 2015). Multiple factors, such as dyslipidemia, immune responses, inflammation, and endothelial dysfunction lead to the formation of an atherosclerotic plaque (Lopez et al., 2021). Atherosclerotic disease progression and associated arterial remodelling contribute to vessel luminal narrowing (Birnbaum, Fishbein, Luo, Nishioka, & Siegel, 1997; Pasterkamp, Galis, & De Kleijn, 2004). Total or partial coronary occlusion compromises myocardial blood flow and reduces the amount of oxygen-rich blood supplied to the heart (Boyette & Manna, 2021). Extended periods of ischemia lead to myocardial necrosis, causing significant loss of CMs and formation of collagenous scar tissue (Richardson, Clarke, Alexander Quinn, & Holmes, 2015). Reactive tissue scarring triggers a cardiac remodelling process, which results in continuous loss of CMs, contractile dysfunction, cardiac dilation and eventually progression to heart failure (Hashimoto, Olson, & Bassel-Duby, 2018; Park & Yoon, 2018). Despite significant advancements in the treatment of ischemic heart disease by pharmacological, interventional and surgical therapies, leading to a reduced cardiac mortality and improved quality of life, heart transplantation remains the only definitive treatment option for progressed heart failure allowing complete cardiac recovery (Schaun et al., 2016; Ford et al., 2009; Park & Yoon, 2018; Cambria et al., 2017). However, major challenges in cardiac transplantation involve organ donor shortage, chronic immunosuppression, surgery risk and posttransplantational complications (Tonsho, Michel, Ahmed, Alessandrini, & Madsen, 2014; Gupta & Krim, 2019).

Hence, there is an urgent need for new therapeutic strategies to improve cardiac repair.

1.2 Therapeutic approaches for cardiac regeneration

1.2.1 Regenerative capacity of the heart

The adult human heart itself possesses restricted self-renewal capacity, limiting endogenous cardiac regeneration (Hashimoto et al., 2018). The highest rate of cardiac cell proliferation is found in adolescents and decreases to <1 % per year in adulthood (Bergmann et al., 2015). Main processes contributing to endogenous cardiac regeneration are proliferation of endogenous adult CMs and differentiation of both resident and migrating bone marrow-derived progenitor and stem cells (Parmacek & Epstein, 2009; Maximilian Buja & Vela, 2008; Finan & Richard, 2015). Hurdles and limitations of natural cardiac repair are, amongst others, low proliferation potency of adult CMs, inadequate proliferation and differentiation of resident stem cells and insufficient mobilization of bone marrow-derived stem cells (Segers & Lee, 2008).

1.2.2 Cell-based therapies for cardiac regeneration

In recent years, cardiac regeneration medicine has become an emerging field of research. Among the most promising strategies for generation of functional cardiac tissue are stem cell-based regenerative therapies (Lemcke, Voronina, Steinhoff, & David, 2018). Cell-based therapeutic approaches aim to replace damaged and dysfunctional CMs by transplantation of exogenous cells proficient of cardiomyogenesis (Liew, Ho, & Soh, 2020). In the last decade, pluripotent stem cells (PSCs) have emerged as the most propitious cell type for cardiac repair. PSCs possess unlimited self-renewal capacity *in vitro* and can differentiate into various specialized cell types derived from one of the three embryonic germ layers (ectoderm, endoderm, and mesoderm) (Abu-Dawud, Graffmann, Ferber, Wruck, & Adjaye, 2018; G. Liu, David, Trawczynski, & Fessler, 2020). Both embryonic stem cells (ESCs) and human induced pluripotent stem (hiPS) cells show great cardiomyogenic potential and are able to generate clinically relevant numbers of stem cell-derived CMs, making them central sources for cell-based cardiovascular regenerative therapy (Shiba, Hauch, & Laflamme, 2009; Chao, Chen, Tseng, & Li, 2014).

Embryonic stem cells (ESCs)

In 1998, Thomson and colleagues generated the first human ESCs from the inner cell mass (ICM) of preimplantation blastocyst stage embryos (Thomson et al., 1998). In humans, blastocyst stage begins about 5 to 6 days after fertilization (Hackett & Fortier, 2011). Application of mechanical pressure, microsurgery, laser dissection and immunosurgical procedures are common methods for isolation of the ICM (Khan, Almohazey, Alomari, & Almofty, 2018). Numerous efficient and reproducible protocols have been

established to differentiate ESCs towards the cardiac lineage (Shiba et al., 2009). Upon cardiac differentiation, ESCs reveal a cardiac phenotype, which is supported by the expression of cardiac differentiation markers (*GATA binding protein 4 (GATA4)*, *NK2 Homeobox 5 (NKX2.5)*, and *myocyte enhancer factor 2C (MEF2C)*), cardiac specific proteins (α-actinin, cardiac troponin I and T, atrial natriuretic peptide, atrial and ventricular myosin light chains) and spontaneous contractility (Gepstein, 2002; Zhu, Hauch, Xu, & Laflamme, 2009; C. Xu, Police, Rao, & Carpenter, 2002). Moreover, animal studies confirmed the ability of ESCs-derived CMs to integrate functionally and partially remuscularize infarcted cardiac areas after transplantation (Pawani & Bhartiya, 2013; Laflamme et al., 2007). However, there are some limitations to the clinical implementation of ESCs. Firstly, the application of ESCs in cardiac regeneration therapy is compromised by ethical concerns, as ESCs are derived from human embryos and the isolation of ESCs leads to the destruction of the embryo (Raval, Kamp, & Hogle, 2008). Secondly, there is the risk of immune rejection upon allogenic transplantation of ESCs-derived CMs by the recipient's immune system (Park & Yoon, 2018).

Human induced pluripotent stem cells (hiPSCs)

In 2006, Takahashi and Yamanaka revolutionized stem cell research with the generation of induced pluripotent stem cells (iPSCs) directly from murine fibroblasts (Takahashi & Yamanaka, 2006), thereby avoiding the ethical challenges associated with ESCs. Subsequently, the first hiPS cells were derived from adult human fibroblasts under defined culture conditions by introduction of four factors (*Octamer binding transcription factor 3/4 (OCT3/4)*, *SRY [sex determining region Y]-box transcription factor 2 (SOX2)*, *Krüppel-like factor 4 (KLF4)* and *c-MYC*) through retroviral transduction (Takahashi et al., 2007). Since then, hiPS cells from different somatic cell sources, such as, neuronal cells, keratinocytes and peripheral blood cells have been successfully reprogrammed to a pluripotent state using the same strategy (Patel & Yang, 2010; Staerk et al., 2010). Besides, this technology has greatly influenced human disease modelling, *in vitro* drug screening and cell-based regenerative medicine (J. Li, Song, Pan, & Zhou, 2014; Chao et al., 2014). Particularly, the use of hiPS cell-derived CMs in cardiac regeneration therapy has shown promising results (Park & Yoon, 2018). Currently employed approaches for cardiac differentiation of hiPS cells are spontaneous embryoid body-based differentiation, inductive co-culture with endoderm-like cells and directed cardiac differentiation using growth factors or small molecules (Rajala, Pekkanen-Mattila, & Aalto-Setälä, 2011; Mummery et al., 2012; Burridge et al., 2014). The latter shows great differentiation efficiency and allows generating clinically relevant quantities of hiPS cell-derived CMs with high purity (Burridge et al., 2014). HiPS cell-derived CMs express markers like endogenous cardiomyocytes including cardiac transcription factors, structural proteins, hormones, ion-channels, and gap junction proteins (Rajala et al., 2011). Transplantation into experimental animal models for myocardial regeneration showed that hiPS cell-derived CMs are capable of engrafting, structurally integrating into the recipient's

cardiac tissue and of restoring cardiac function (Zwi-Dantsis et al., 2013; Chao et al., 2014; L. Ye et al., 2014). Thus far in all approaches, correct electrophysiological coupling remains a major issue (Oikonomopoulos, Kitani, & Wu, 2018; Silver, Barrs, & Mei, 2021).

1.2.3 Applications for cardiac regeneration

In the last years, different cell delivery strategies have been developed for administration of hiPS cell-derived CMs to the site of cardiac injury. Two major approaches encompass cell delivery with injectable cell-loaded biomaterials and cell therapy with tissue-engineered patches (Park & Yoon, 2018). Injectable hydrogels have displayed great potential in the enhancement of cell engraftment and cardiac regeneration (Laflamme et al., 2007; Chong et al., 2014; Park & Yoon, 2018). The three main application routes are intracoronary delivery, epicardial and trans-endocardial injection (Hastings et al., 2015). A clear advantage of this application is the precise, directed and minimally invasive administration of cells (Hastings et al., 2015; Hasan et al., 2015; Bar & Cohen, 2020). Furthermore, tissue-engineered patches are used for cardiac repair. Typically, these patches are implanted surgically and fixed epicardially (Hastings et al., 2015). The great advantage of this technique is the structural support for the delivered cells provided by the engineered tissue, which has shown to positively influence cardiac wall thickening and reinforcement (Hastings et al., 2015; Di Franco, Amarelli, Montalto, Loforte, & Musumeci, 2018).

1.3 Immunological barriers to hiPS cell-based cardiac regeneration

Regardless of the cell delivery technique, immune rejection remains a major hurdle in hiPS cell mediated cardiac regeneration therapy limiting graft survival rate and efficient cardiac repair. Studying the immunogenicity of hiPS cells and their derivatives and developing strategies to minimize their immunogenicity is therefore essential for their efficient clinical implementation (Scheiner, Talib, & Feigal, 2014; X. Liu, Li, Fu, & Xu, 2017). Notably, the mechanism underlying the immune response against hiPS cells is based on the origin of the transplanted cells (allogeneic or autologous) (Miyagawa et al., 2016).

1.3.1 Immune response to autologous iPS cell-derived cells

In fact, the initially recognized advantage of using autologous patient-specific hiPS cells for transplantation to escape the acquired immune response of the recipient, was challenged by studies performed by Zhao and colleagues (T. Zhao, Zhang, Rong, & Xu, 2011; Boyd, Rodrigues, Lui, Fu, & Xu, 2012). In their murine C57BL/6 (B6) teratoma

model, they showed that despite syngeneic transplantation, allowing cell histocompatibility, iPS cells were rejected by a T-cell mediated immune response (T. Zhao et al., 2011) Potential causes of autologous iPS cell immunogenicity could be genetic and epigenetic changes attributable to reprogramming and culture conditions (T. Zhao et al., 2011; Scheiner et al., 2014). On the one hand, the somatic parental cell origin could influence the transcriptional profile of iPS cells and contribute to cell surface antigen expression differences among iPS cells (Polo et al., 2010; Ghosh et al., 2010; Scheiner et al., 2014). iPS cells derived from umbilical cord mesenchymal cells, for example, have been discovered to be less immunogenic than iPS cells derived from adult skin fibroblasts (P. Liu et al., 2013). On the other hand, the differentiation state of the parental cell and age of the cell donor could have an impact on the quality of reprogramming and thereby influence the immunogenic properties of iPS cells (K. Kim et al., 2010). For instance, hematopoietic progenitor cells can be reprogrammed more efficiently than terminally differentiated cell types (Eminli et al., 2009). Furthermore, the immature phenotype of transplanted iPS cells could enhance their immunogenicity (Scheiner et al., 2014). In particular, undifferentiated iPS cells have been found to express low levels of MHC-I, which renders them susceptible to natural killer (NK) cell-mediated targeting and leads to immune rejection of autologous iPS cells (Miyagawa et al., 2016; Scheiner et al., 2014).

1.3.2 Immune response to allogeneic iPS cell-derived cells

Immune rejection of allogeneic cells is predominately mediated by major histocompatibility complex (MHC) molecules, referred to as human leukocyte antigen (HLA) in humans (Cruz-Tapias, Castiblanco, & Anaya, 2013; W. Zhao et al., 2020). In fact, foreign MHC proteins on the surface of donor cells represent an antigenic stimulus to the recipient's immune system (Marino, Paster, & Benichou, 2016; García, Yebra, Flores, & Guerra, 2012). The immunological phenomenon by which the recipient's immune system then initiates an immune response against 'non-self' donor antigens is called allorecognition (García et al., 2012). Two main effector cells capable of targeting allogeneic hiPS cells and their derivatives are cytotoxic T-lymphocytes and NK cells (De Rham & Villard, 2014).

The role of MHC-I in the immune response

MHC-I proteins are polymorphic glycoproteins present on the cell surface of all nucleated cells in the human body (Chaplin, 2010). The MHC-I molecule is composed of a polymorphic heavy alpha chain, encoded by HLA-A, -B, or -C genes on chromosome 6, which interacts non-covalently with a non-polymorphic B2M unit, encoded by the *B2M* gene on chromosome 15 to form a complex (Drukker et al., 2002; Chaplin, 2010; García et al., 2012). MHC-I molecules play a dominant role in cell transplantation, as they control the function and recruitment of cytotoxic T-cells and NK cells (Nakamura,

Shirouzu, Nakata, Yoshimura, & Ushigome, 2019; X. C. Li & Raghavan, 2010).

Cytotoxic T-cells

T-lymphocytes are primarily responsible for cell-mediated allograft rejection (Ingulli, 2010; LaRosa, Rahman, & Turka, 2007). T-cell allorecognition of donor MHC antigens mainly takes place by two distinct pathways (De Almeida, Ransohoff, Nahid, & Wu, 2013). Firstly, the indirect pathway, which describes the ability of recipient T-cells to recognize processed donor MHC molecules that are presented as MHC-I bound peptides by the recipient's antigen presenting cells (García et al., 2012; Ingulli, 2010). This mechanism has been found to play a predominant role in chronic immune rejection (García et al., 2012; Bharat & Mohanakumar, 2007). Secondly, the direct pathway, by which recipient T-cells directly recognize intact allogeneic MHC-I molecules on the surface of transplanted donor cells (Marino et al., 2016; Ingulli, 2010). This mechanism can be observed in acute graft rejection and causes a strong immune response (García et al., 2012). In particular, direct allorecognition leads to an effector cell response mediated by cytotoxic T-lymphocytes (CD8+ T-cells) (Boardman, Jacob, Smyth, Lombardi, & Lechler, 2016). Cytotoxic T-lymphocytes are activated by interaction of their allogen-specific T-cell receptor (TCR) with foreign MHC-I molecules and eliminate target cells by inducing apoptosis (Marino et al., 2016; Alberts B, Johnson A, Lewis J, & al., 2002; Chávez-Galán, Arenas-Del Angel, Zenteno, Chávez, & Lascurain, 2009). The principal mechanism through which activated cytotoxic T-lymphocytes respond is the release of cytolytic granules, such as, the pore-forming protein perforin and serine proteases called granzymes (displayed in figure 1) (Choy, 2010; Charles A Janeway, Travers, Walport, & Shlomchik, 2001).

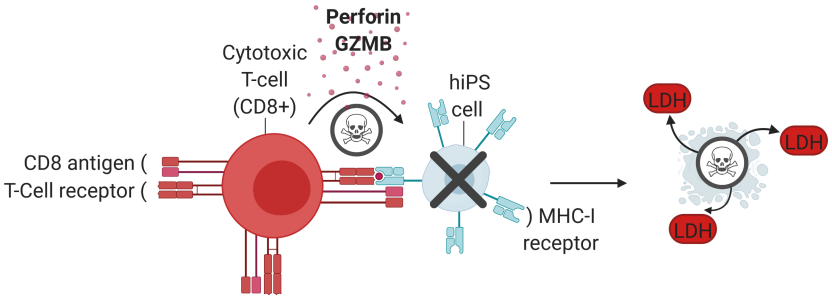

Figure 1: Overview of the cytotoxic T-lymphocyte response

Created with BioRender.com; **Abbreviations**: **LDH**: lactate dehydrogenase; **GZMB**: granzyme B; **CD**: cluster of differentiation; **MHC-I**: major histocompatibility complex class I; **hiPS cell**: human induced pluripotent stem cell

Furthermore, cytotoxic T-lymphocytes can transmit death signals by Fas-Fas ligand interaction, leading to activation of caspases and induction of apoptosis (Charles A Janeway et al., 2001). In addition, cytotoxic T-lymphocytes are capable of secreting

immune cell-activating cytokines, such as tumor necrosis factor alpha (TNFα) and interferon gamma (IFNγ) (Charles A Janeway et al., 2001).

Natural killer (NK) cells

NK cells are effector cells of the innate immune system and competent to recognize self-MHC-I molecules (Hamerman, Ogasawara, & Lanier, 2005). Their activity is mediated by a large variety of surface receptors with activating and inhibitory functions (Chávez-Galán et al., 2009; X. C. Li & Raghavan, 2010; Chan, Smyth, & Martinet, 2014). The balance of these activating and inhibiting signals determines the function of NK cells, which include cytolytic activity, cytokine production and proliferation (Morvan & Lanier, 2016). Notably, MHC-I molecules represent central determinants of NK cell responses (Benjamin, Gill, & Negrin, 2010). In autologous transplant settings, NK cells primarily attack cells with low expression of MHC-I molecules (Frenzel et al., 2009; De Almeida et al., 2013). In allogeneic transplantation, however, NK cell alloreactivity is due to a mismatch between inhibitory receptors for self-MHC-I molecules on donor NK cells and MHC-I ligands on recipient cells (Ruggeri et al., 2006). In humans, this 'missing self' response is primarily modulated by inhibitory receptors that belong to the killer immunoglobulin-like receptor (KIR) family (Yawata et al., 2008; Benjamin et al., 2010; De Almeida et al., 2013). In the absence of a corresponding MHC-I molecule, the inhibitory signal is missing. The resulting excess of activating over inhibiting signals is believed to activate NK cells (Bessoles et al., 2014; Ichise et al., 2017). Activated NK cells possess strong cytotoxic potential, which is mediated through exocytosis of cytolytic granules using a perforin/granzyme-dependent mechanism, and the production and release of cytokines (Barao & Murphy, 2003; X. C. Li & Raghavan, 2010; Benjamin et al., 2010). Furthermore, NK cells can eliminate target cells via the engagement of cell surface death receptors (FAS ligand and TNF-related apoptosis-inducing ligand), leading to target cell apoptosis (Barao & Murphy, 2003; Morvan & Lanier, 2016).

1.4 The role of cytokines in the alloimmune response

Cytokines are soluble molecules secreted by the recipient's immune cells and play a central role in the process of both graft rejection and tolerance (Walsh, Strom, & Turka, 2004; Noakes & Michaelis, 2013). During the alloimmune response, proinflammatory cytokines, such as tumor necrosis factor alpha (TNFα), granzyme B (GZMB), interferon gamma (IFNγ), interleukin 2 (IL2), interleukin 12 (IL12), interleukin 15 (IL15) promote graft rejection and immunosuppressive cytokines, such as transforming growth factor beta (TGFβ) and interleukin 10 (IL10), encourage graft survival (Walsh et al., 2004). Production and release of cytokines enable the communication between the innate and adaptive immune system and lead to the activation and clonal expansion of specific T and B cell clones and the recruitment of cytotoxic T cells and NK cells (Pirenne et al.,

1994; Lacy & Stow, 2011; Walsh et al., 2004). Moreover, the secreted cytokines promote the upregulation of MHC class I and II expression and possess a direct cytotoxic effect on the transplanted cells (Pirenne et al., 1994).

1.5 Strategies to protect allogeneic hiPS cell-derived cells from immune rejection

To evade the immunological challenges associated with the transplantation of allogeneic hiPS-cell derived CMs, different strategies have been developed during the last years. One approach to reduce cell rejection would be the use of immunosuppressive pharmacological drugs. Long-term immunosuppression, however, often leads to toxic side effects, such as, infections, and malignancy, caused by systemic immune suppression (Otsuka, Wada, Murata, & Seino, 2020; Taylor, Bolton, & Bradley, 2011; P. Liu et al., 2013). Another strategy would be the creation of HLA-typed hiPS cell banks. In fact, HLA matching, enabling immunological compatibility between donor and recipient, has been shown to reduce donor cell immunogenicity and lower the risk of graft rejection (Umekage, Sato, & Takasu, 2019). Due to high HLA allele diversity in the human population a large number of hiPS cell lines would be necessary to ensure optimal compatibility with a wide number of recipients (Riolobos et al., 2013; Barry, Hyllner, Stacey, Taylor, & Turner, 2015; De Rham & Villard, 2014). Nevertheless, prevailing registry and HLA-typed hiPS cell banks around the world would not be able to provide matches for the majority of the population, thus limiting this approach (W. Zhao et al., 2020). Moreover, allograft rejection may be suppressed by inducing peripheral immunological tolerance towards the transplanted cells (Martin, 2017; Boyd et al., 2012). Regulatory T-cells (Tregs) play an important role in the induction and maintenance of peripheral tolerance (Romano, Fanelli, Albany, Giganti, & Lombardi, 2019). Co-transplantation of therapeutic donor cell-derived antigen-specific Tregs during allogeneic hiPS cell transplantation could prevent graft rejection (Y. Zhou et al., 2014). However, clinical barriers include the need for additional immunosuppression, Treg specificity, cost-effective production, and reliable expansion of high quality Tregs (Tang & Bluestone, 2013). Substantially, a key strategy to overcome the need for immunosuppression and HLA matching would be the generation of an immunotolerant universal donor cell line. Recent advances in gene editing technologies have enabled the reduction of allogeneic cell immunogenicity by targeted gene manipulation (Malik, Jenkins, Mellon, & Bailey, 2019; Han et al., 2019; Deuse et al., 2019; W. Zhao et al., 2020). Several studies have found that HLA-I engineering by targeted disruption of the *B2M* gene is an effective strategy for the reduction of immunogenicity (Mandal et al., 2014; Riolobos et al., 2013; Mattapally et al., 2018). As the B2M subunit is indispensable for MHC-I complex assembly and presentation on the cell surface, targeted disruption of the *B2M* gene should lead to complete surface MHC-I deficiency and result in a significant decrease of CD8+ T-cell-

mediated cytotoxicity (D. Wang, Quan, Yan, Morales, & Wetsel, 2015; Han et al., 2019; Norbnop, Ingrungruanglert, Israsena, Suphapeetiporn, & Shotelersuk, 2020; W. Zhao et al., 2020). Figure 2 displays an exemplary workflow for the clinical application of immunotolerant universal donor hiPS cells in cardiac regeneration therapy.

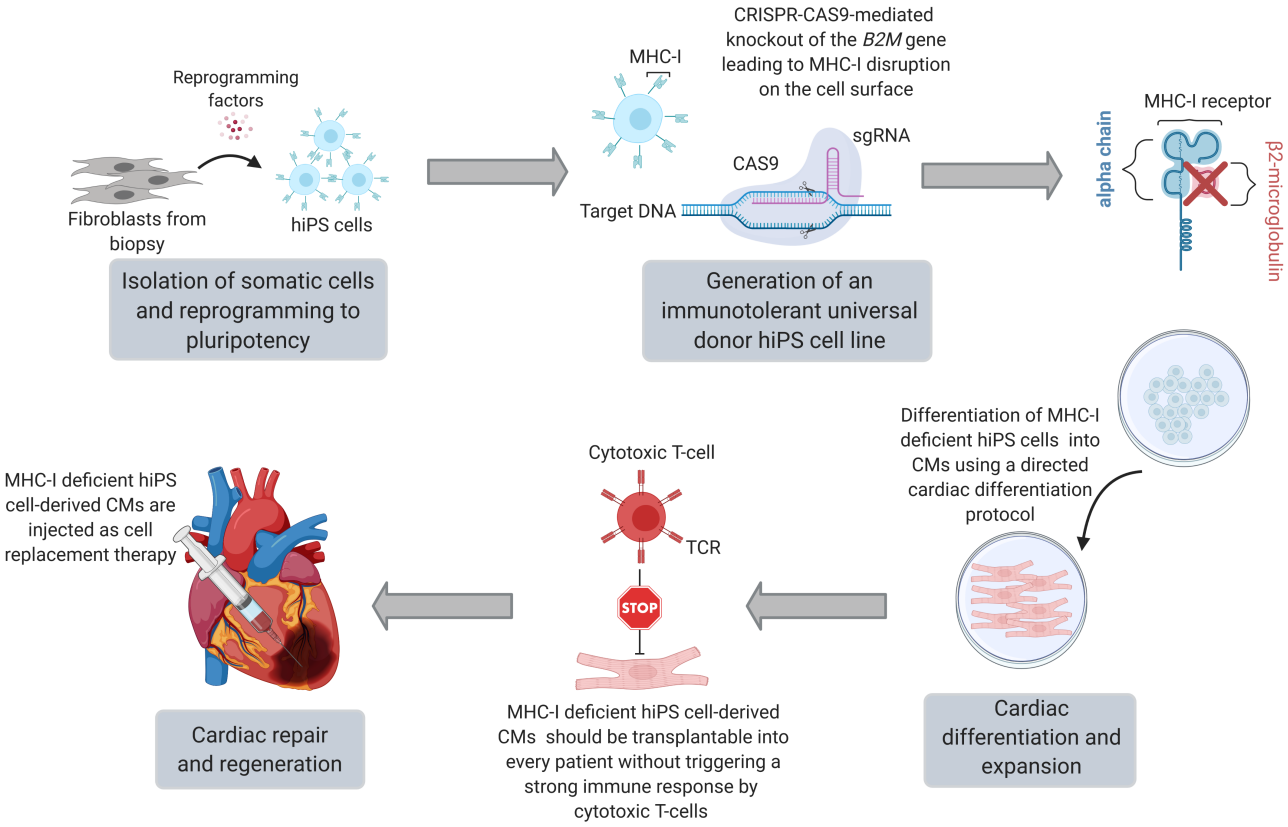

Figure 2: Immunotolerant universal donor hiPS cells for cardiac regeneration therapy
Created with BioRender.com; **Abbreviations**: **hiPS cell**: human induced pluripotent stem cell; **MHC-I**: major histocompatibility; **CRISPR-Cas9**: clustered regularly interspaced short palindromic repeats-CRISPR-associated endonuclease 9; **sgRNA**: single guide RNA; **DNA**: Deoxyribonucleic acid; **B2M**: β2-microglobulin; **MHC-I**: major histocompatibility complex class I; **CMs**: cardiomyocytes; **TCR**: T-cell receptor

MHC-I depletion could, however, concomitantly enhance NK cell-mediated recognition and destruction of hiPS cells and increase the risk for cell proliferation, after infection by pathogens or oncogenic transformation, as the cells become invisible to T-cell-mediated immune surveillance (D. Wang et al., 2015; H. Xu et al., 2019; Trounson, Boyd, & Boyd, 2019). Hence, additional gene editing approaches might be required to address these issues.

1.5.1 Advantages of an immunotolerant universal donor hiPS cell line

Generally, HLA engineering will address the immunological challenges related to allogeneic cell transplantation and will facilitate cell replacement therapy on a broader scale. Particularly, the generation of an immunotolerant universal donor cell line will save time and reduce the high costs associated with the derivation of patient-specific autologous hiPS cells (Riolobos et al., 2013; Sato et al., 2015; W. Zhao et al., 2020). In fact, reprogramming and evaluation of the pluripotency and differentiation efficacy of patient-derived hiPS cells require a considerable expenditure of time (Riolobos et al., 2013). This time-consuming process limits its use for the treatment of acute medical conditions (Mattapally et al., 2018; Malik et al., 2019; Deuse et al., 2019). Furthermore, the generation of a universal donor cell source enables bypassing the variability in gene expression patterns, culture characteristics and differentiation potential associated with the use of distinct hiPS cell lines (Riolobos et al., 2013; Huang et al., 2019).

2 Aims

Cardiovascular diseases represent the leading cause of mortality worldwide and have a substantial impact on global morbidity. Thus, it would be beneficial for cardiac regeneration to minimize the potential for allogeneic rejection in cell-based therapies. Hence, the aim of this work was the generation of an immunotolerant hiPS cell line, which is unable to trigger the natural immune response from the recipient upon transplantation. As the MHC-I plays a pivotal role in cell-mediated immune rejection, the first main objective of this thesis was to employ the CRISPR-Cas9 technology for a targeted knockout of the *B2M* gene, leading to MHC-I disruption. The second main objective of this thesis was the quantification and interpretation of the immune response against the generated *B2M*-deficient hiPS cell clones in comparison to the wild-type cell line. To this end, different immunological assays were established within the framework of this thesis, which will help to evaluate the cell-mediated immune response.

3 Materials and Methods

All materials and methods used in this work are described below.

3.1 Material and laboratory equipment

3.1.1 Devices

All devices used in this work are listed in table 1.

Table 1: Devices

Devices	**Manufacturer**
Analytical balance ABT 220-5 DNM Kern	Sohn GmbH, Bahlingen, Germany
Autoclave HICLAVE HI-50	HMC Europe GmbH, Tüßling, Germany
Axiovert 200 M Inverted Fluorescent Microscope	Carl Zeiss AG, Oberkochen, Germany
BD LSRFortessa^{TM} flow cytometer	BD Biosciences, Becton, Dickinson and Company, San Jose, CA
Bio-Rad Mini Protean® Tetra Cell System	Bio-Rad Laboratories GmbH, München, Germany
C1000^{TM} Thermal Cycler	Bio-Rad Laboratories GmbH, München, Germany
Drying Chamber Model ED 56	Binder GmbH, Tuttlingen, Germany
Eppendorf Thermomixer comfort	Eppendorf AG, Hamburg, Germany
EVOS XL Core Microscope	Thermo Fisher Scientific, Waltham, MA
Gel chamber Sub-Cell Modell 96	Bio-Rad Laboratories GmbH, München, Germany
Gel documentation instrument ChemDoc XR System	Bio-Rad Laboratories GmbH, München, Germany
Heidolph Polymax 1040 Platform Shaker	ProfiLab24 GmbH, Berlin, Germany
HERA Freezer Basic (-80°C)	Thermo Fisher Scientific, Waltham, MA
HERACell^{TM} 240i CO_2 incubator	Thermo Fisher Scientific, Waltham, MA
Heraeus Megafuge 40R	Thermo Fisher Scientific, Waltham, MA
Incubator Shaker INFORS HT Ecotron	Infors AG, Bottmingen, Switzerland
Infinite® 200 PRO	Tecan, Tecan Group AG, Männedorf, Switzerland
Lauda Aqualine AL 12, water bath	LAUDA-Brinkmann LP, Delran, NJ
Liquid Nitrogen Storage Tank	Messer Griesheim GmbH, Bad Soden, Germany
Microwave MW 7849 900W	Severin, Sundern, Germany
MilliQ©	Merck Millipore, Merck KGaA, Darmstadt, Germany
Nalgene® Mr. Frosty® Cryo 1°C Freezing Container	Thermo Fisher Scientific, Waltham, MA
NanoDrop 2000c Spectrophotometer	Thermo Fisher Scientific, Waltham, MA
Neubauer counting chamber	Thomas Scientific, Swedesboro, NJ
Nucleofector^{TM} II	Amaxa Biosystems, Lonza Cologne GmbH, Köln, Germany
OctoMACS^{TM} Separator	Miltenyi Biotec, Bergisch Gladbach, Germany
PowerPac Basic Power Supply	Bio-Rad Laboratories GmbH, München, Germany

Quant Studio 3 Real-Time PCR System	Applied Biosystems™,Thermo Fisher Scientific, Waltham, MA
Refrigerator Liebherr Premium No Frost (-20°C)	Liebherr, Bulle, Switzerland
Safe 2020 Class II Biological Safety Cabinets	Thermo Fisher Scientific, Waltham, MA
Stuart™ Analogue Rocker & Roller Mixer	Sigma-Aldrich, Merck Millipore, Merck KGaA, Darmstadt, Germany
Trans-Blot® Turbo™ Transfer System	Bio-Rad Laboratories GmbH, München, Germany

3.1.2 Disposable laboratory equipment

All disposable laboratory equipment used in this work is listed in table 2.

Table 2: Disposable laboratory equipment

Disposable laboratory equipment	**Manufacturer**
BD Vacutainer® CPT™ Mononuclear Cell Preparation Tube (Sodium Heparin), #362780	BD Biosciences, Becton, Dickinson and Company, San Jose, CA
Cell culture dish (10 cm), #664160	Greiner Bio-One International GmbH, Frickenhausen, Germany
Cell Culture Multiwell Plate, 24 well, PS, clear, CELLSTAR®, sterile, #662160	Greiner Bio-One International GmbH, Frickenhausen, Germany
Cell Culture Multiwell Plate, 6 well, PS, clear, CELLSTAR®, sterile, #657160	Greiner Bio-One International GmbH, Frickenhausen, Germany
CryoTubes™, Nunc™(1.0 ml), #479-6842P	VWR International, Radnor, PA
Eppendorf Safe-Lock Tubes, 1.5 ml, Eppendorf Quality™, #30120086	Eppendorf AG, Hamburg, Germany
Eppendorf Safe-Lock Tubes, 2.0 ml, Eppendorf Quality™, #30120094	Eppendorf AG, Hamburg, Germany
Falcon® 15 ml High Clarity PP Centrifuge Tube, Conical Bottom, sterile, #734-0451	VWR International, Radnor, PA
Falcon® 50 ml High Clarity PP Centrifuge Tube, Conical Bottom, sterile, #734-0448	VWR International, Radnor, PA
Menzel™ Microscope Coverslips 24x60 mm, #11778691	Thermo Fisher Scientific, Waltham, MA
MicroAmps™ Optical 96-Well Reaction Plate, #N8010560	Thermo Fisher Scientific, Waltham, MA
MicroAmps™ Optical Adhesive Film, #4311971	Applied Biosystems™, Thermo Fisher Scientific, Waltham, MA
Millicell EZ SLIDE 4-well glass, sterile, #PEZGS0496	Merck Millipore, Merck KGaA, Darmstadt, Germany
Mini-Protean® TGX Stain-Free™ Protein Gel, #4568094	Bio-Rad Laboratories GmbH, München, Germany
MS Columns, #130-042-201	Miltenyi Biotec, Bergisch Gladbach, Germany
Nunc™ 96-Well Polystyrene Round Bottom Microwell Plates, #143761	Thermo Fisher Scientific, Waltham, MA
PVDF-Filter 0.22 μm, #P666.1	Carl Roth GmbH + Co. KG, Karlsruhe, Germany
Serological Pipettes 10 ml, sterile, (scale: 0.1 ml; color: orange), #GPS-10.0	Kisker Biotech GmbH & Co. KG, Steinfurt, Germany
Serological Pipettes 5 ml, sterile, (scale: 0.1 ml; color: blue), #GPS-5.0	Kisker Biotech GmbH & Co. KG, Steinfurt, Germany
SurPhob Pipette Tips Reload without filter (1250μL), #VT0173	Biozym Scientific GmbH, Hessisch Oldendorf, Germany
Trans-Blot® Turbo™ Mini PVDF Transfer Pack, #1704156	Bio-Rad Laboratories GmbH, München, Germany

3.1.3 Chemicals and laboratory reagents

All chemicals and laboratory reagents listed in table 3 have been stored and used as described below or as specified by the manufacturer.

Table 3: Chemicals and laboratory reagents

Chemicals and laboratory reagents	Manufacturer
10x Red cell lysis buffer, #130-094-183	Miltenyi Biotec, Bergisch Gladbach, Germany
10x T4 Ligation Buffer, #B69	New England Biolabs GmbH, Frankfurt am Main, Germany
10x Tango buffer, #BY5	Thermo Scientific™, Thermo Fisher Scientific, Waltham, MA
2-Propanol≥ 99.9%, #AE73.1	Carl Roth GmbH + Co. KG, Karlsruhe, Germany
4',6-Diamidino-2-Phenylindole (DAPI), #422801	Biolegend, San Diego, CA
4x Laemmli Sample Buffer, #161-0747	Bio-Rad Laboratories GmbH, München, Germany
Accutase, #7920	StemCell™ Technologies, Köln, Germany
Agar, #2266.3	Carl Roth GmbH + Co. KG, Karlsruhe, Germany
Agarose (PeqGOLD Universal), #35-1020	PEQLAB GmbH, VWR Life Science Competence, Erlangen, Germany
Albumin human, recombinant, expressed in rice, lyophilized powder, cell culture tested, low endotoxin, ≥ 96%, #A9731-10G	Sigma-Aldrich, Merck Millipore, Merck KGaA, Darmstadt, Germany
Ampicillin sodium salt, #K029.1	Carl Roth GmbH + Co. KG, Karlsruhe, Germany
ATP (100 mM), #R0441	Thermo Scientific™, Thermo Fisher Scientific, Waltham, MA
autoMACS Running Buffer (MACS separation buffer), #130-090-221	Miltenyi Biotec, Bergisch Gladbach, Germany
Boric acid, #6943.1	Carl Roth GmbH + Co. KG, Karlsruhe, Germany
BSA (bovine serum albumin), #A7906	Sigma-Aldrich, Merck Millipore, Merck KGaA, Darmstadt, Germany
CD16 MicroBeads, human, #130-045-701	Miltenyi Biotec, Bergisch Gladbach, Germany
CD3 MicroBeads, human, #130-050-101	Miltenyi Biotec, Bergisch Gladbach, Germany
CD8 MicroBeads, human, #130-045-201	Miltenyi Biotec, Bergisch Gladbach, Germany
CHIR99021, #C-6556	LC Laboratories, Woburn, MA
CloneR™, #05889	StemCell™ Technologies, Köln, Germany
Color Prestained Protein Standard, Broad Range (11-245 kDa), #P77125	New England Biolabs, Ipswich, MA
Corning® Matrigel® growth factor reduced (GFR) basement membrane matrix, #356231	Corning, Tewksbury, MA
Cre Vector (20 μg), #sc-418923	Santa Cruz Biotechnology, Dallas, TX
deoxynucleotide triphosphates dNTP-Set 1 (100 mM dATP, dGTP, dCTP, dTTP), #K039.1	Carl Roth GmbH + Co. KG, Karlsruhe, Germany
Dimethyl sulfoxid (DMSO), #A994.1	Carl Roth GmbH + Co. KG, Karlsruhe, Germany
DNA Gel Loading Dye (6x), #R0611	Thermo Scientific™, Thermo Fisher Scientific, Waltham, MA
DTT (1 mM), #28025013	Invitrogen™, Thermo Fisher Scientific, Waltham, MA
EDTA, #CN06.1	Carl Roth GmbH + Co. KG, Karlsruhe, Germany
Ethanol absolut ≥ 99.8%, AnalaR NORMAPUR®, #20821330	VWR International, Radnor, PA
Ethanol denaturated ≥ 99.5%, GPR RECTAPUR® (denaturated with 1% MEK), #85033-460	VWR International, Radnor, PA
FastDigest BbsI, #FD1014	Thermo Scientific™, Thermo Fisher Scientific, Waltham, MA
Fetal Bovine Serum, EU approved origin, South America, #10270-106	Gibco© by Life Technologies ™, Thermo Fisher Scientific, Waltham, MA

Fetal Bovine Serum, FCS, South America, GE Healthcare Hyclone, #SV30160.03	Hyclone Laboratories Inc, GE Healthcare, Thermo Fisher Scientific, Waltham, MA
Fluoroshield Mounting Medium with DAPI, #ab104138	Abcam, Cambridge, UK
FuGENE ® HD Transfection Reagent, #E2311	Promega Corporation, Fitchburg, WI
G418 (25.000 U/ml), #A2912	Biochrom, Merck Millipore, Merck KGaA, Darmstadt, Germany
GeneRuler 100 bp DNA Ladder, #SM0241	Thermo Scientific™, Thermo Fisher Scientific, Waltham, MA
Glucose, #G8270	Sigma-Aldrich, Merck Millipore, Merck KGaA, Darmstadt, Germany
Glycerol, #3783	Carl Roth GmbH + Co. KG, Karlsruhe, Germany
Hydrochloric acid, c(HCl) = 0,1 mol/l (0,1 N) Titripur® Reag. Ph Eur, Reag. USP, #109060	Merck Millipore, Merck KGaA, Darmstadt, Germany
Incidin OxyFoam S, #3087450	Ecolab, Saint Paul, MN
L-Ascorbic acid-2-phosphate, #A8960	Sigma-Aldrich, Merck Millipore, Merck KGaA, Darmstadt, Germany
Magnesium chloride, MgCl2 Hexahydrat, #105833	Sigma-Aldrich, Merck Millipore, Merck KGaA, Darmstadt, Germany
Milk Powder, #A0830	PanReac AppliChem, AppliChem GmbH, Darmstadt, Germany
Normal goat serum, #ab7841	Abcam, Cambridge, UK
Normal rabbit serum, #ab7487	Abcam, Cambridge, UK
Nuclease Free Water, #10977-035	Invitrogen™, Thermo Fisher Scientific, Waltham, MA
Paraformaldehyde, #0335	Carl Roth GmbH + Co. KG, Karlsruhe, Germany
PBS powder without calcium and magnesium, #L-182-50	Biochrom, Merck Millipore, Merck KGaA, Darmstadt, Germany
Penicillin-Streptomycin (100x) for cell culture, #A8943	PanReac AppliChem, AppliChem GmbH, Darmstadt, Germany
peqGREEN 20000X DNA/RNA binding dye, #732-2960	VWR International, Radnor, PA
Phytohemagglutinin-M (PHA-M), #11082132001	Roche Applied Science, Penzberg, Germany
Pierce™ Bovine Serum Albumin Standard Ampules, #23209	Pierce Biotechnology, Thermo Fisher Scientific, Waltham, MA
Plasmid Transfection Medium (20 ml), #sc-108062	Santa Cruz Biotechnology, Dallas, TX
Plasmid-Safe™ ATP-Dependent DNase (10 U/μl), #E3101K	Biozym Scientific GmbH, Hessisch Oldendorf, Germany
Potassium chloride, KCl $\geq$ 99,0%, #P9541	Sigma-Aldrich, Merck Millipore, Merck KGaA, Darmstadt, Germany
Puromycin hydrochlorid-25 mg, #P8833	Sigma-Aldrich, Merck Millipore, Merck KGaA, Darmstadt, Germany
Quantitas DNA Marker 25-500 bp, #250216	Biozym Scientific GmbH, Hessisch Oldendorf, Germany
Random Hexamer Oligonucleotides, #48190011	Invitrogen™, Thermo Fisher Scientific, Waltham, MA
ReLeSR™, #05872	StemCell™ Technologies, Köln, Germany
RIPA Puffer, #9806	Cell Signaling Technology, Danvers, MA
ROCK Inhibitor Y-27632, #72304	StemCell™ Technologies, Köln, Germany
Sodium chloride, NaCl, #3957.1	Carl Roth GmbH + Co. KG, Karlsruhe, Germany
Sodium hydroxide solution, c(NaOH)=0,1 mol/l (0,1 N) Titripur® Reag. Ph Eur, Reag. USP, #1.09141	Sigma-Aldrich, Merck Millipore, Merck KGaA, Darmstadt, Germany
T4 Polynucleotide Kinase PNK (10.000 U/ml), #M0201S	New England Biolabs GmbH, Frankfurt am Main, Germany
T7 DNA Ligase (3,000,000 U/ml), #M0318S	New England Biolabs GmbH, Frankfurt am Main, Germany
TrisBase, #5429.3	Carl Roth GmbH + Co. KG, Karlsruhe, Germany
Tris-glycine-SDS buffer 10x, #161-0772	Bio-Rad Laboratories GmbH, München, Germany
Triton® X 100, #3051.3	Carl Roth GmbH + Co. KG, Karlsruhe, Germany
Trypan blue 0.5%, #L6323	Biochrom, Merck Millipore, Merck KGaA, Darmstadt, Germany
TrypLE™ Select Enzym 10x, #A12177-01	Thermo Scientific™, Thermo Fisher Scientific, Waltham, MA
Trypton, #8952.3	Carl Roth GmbH + Co. KG, Karlsruhe, Germany
UltraCruz® transfection plasmid reagent (0.2 ml), #sc-395739	Santa Cruz Biotechnology, Dallas, TX

UltraPure ™ 0.5 M EDTA, pH 8.0, #15575-038	Gibco® by Life Technologies ™, Thermo Fisher Scientific, Waltham, MA
Water (PCR grade), #3315843001	Roche Applied Science, Penzberg, Germany
Water, RNase-free, DEPC treated, Molecular Biology Grade, Ultrapure, #J70783	Thermo Fisher Scientific, Waltham, MA
Wnt-C59, #S7037	Selleckchem, Houston, TX
Yeast extract, #2363.3	Carl Roth GmbH + Co. KG, Karlsruhe, Deutschland
β-Mercaptoethanol (55 mM), #21985-023	Gibco® by Life Technologies ™, Thermo Fisher Scientific, Waltham, MA

3.1.4 Buffers and solutions

All buffers and solutions used in this work have been listed below with a description of the composition, the manufacture, the use, and the storage. Aqua bidestillata (Latin name for double-distilled water) (aq. bidest.), used to dilute buffers and solutions, was supplied by the Milli-Q© water purification and dispensing system (Merck Millipore, Merck KGaA, Darmstadt, Germany) at the Research Center of the German Heart Center. Sterile filtration was performed with a 0.22 μm PVDF filter (Carl Roth GmbH + Co. KG, Karlsruhe, Germany). Sterilization of buffers and solutions was performed by autoclaving in a HICLAVE HI-50 (HMC Europe GmbH, Tüßling, Germany).

Bovine serum albumin (BSA)

In this work, BSA (Sigma-Aldrich, Merck Millipore, Merck KGaA, Darmstadt, Germany) solution was used for various applications. BSA was dissolved in sterile 1x Dulbecco's phosphat buffered saline (D-PBS) to produce a 10 % BSA solution. The solution was sterile-filtered, aliquoted and stored at -20 °C. BSA solution (10 %) used for immunocytochemistry (ICC) was diluted to produce the desired concentration specified in the immunocytochemical protocol. BSA solution (10 %) used as a component of the lactate dehydrogenase (LDH) cytotoxicity assay medium was diluted with Roswell Park Memorial Institute (RPMI) 1640 medium (Biochrom, Merck Millipore, Merck KGaA) to produce the desired concentration of 1 % BSA in RPMI 1640.

CHIR99021

CHIR99021 is a small molecule used to stimulate the initiation of the directed cardiac differentiation of hiPS. As a potent inhibitor of glycogen synthase kinase 3 (GSK3), CHIR99021 increases free cytosolic β-catenin and functions as a wingless and int-1 (WNT) signal pathway activator (Laco et al., 2018). CHIR99021 (LC Laboratories, Woburn, MA) was stored at -80 °C. Dimethyl sulfoxide (DMSO) (Carl Roth GmbH + Co. KG) was used to obtain a 6 mM stock solution. The solution was sterile-filtered, aliquoted and stored for up to 6 months at -80 °C.

CloneR™

CloneR™ (StemCell™ Technologies, Köln, Germany) is a serum-free 10-fold concentrated cell culture medium supplement used to enhance cloning efficiency and single-cell survival of hiPS cells. CloneR™ (StemCell™ Technologies) was thawed at room temperature (15-25 °C) (RT), aliquoted and stored for up to 6 months at -20 °C. After thawing an aliquot, CloneR™ (StemCell™ Technologies) (2.5 ml) was supplemented to 22.5 ml of complete TeSR™-E8™ cell culture medium (StemCell™ Technologies).

4',6-diamidino-2-phenylindole (DAPI)

DAPI (Biolegend, San Diego, CA) was used as a stain to assess cell viability in flow cytometry assays. DAPI is an exclusion dye which labels only dead cells with a compromised plasma membrane (Kepp, Galluzzi, Lipinski, Yuan, & Kroemer, 2011). DAPI was dissolved in aq. bidest. to obtain a stock solution of 5 mg/ml, which was aliquoted and stored at -20 °C. The stock solution was diluted to a working solution of 0.1 mg/ml and was stored for up to 3 months at 4 °C in the dark. For flow cytometry assays, the working solution was supplemented to the cell suspension to produce a final concentration of 1 μg/ml.

D-PBS

Phosphat buffered saline (PBS) powder without calcium and magnesium (Biochrom, Merck Millipore, Merck KGaA, Darmstadt, Germany) was dissolved in aq. bidest. to produce a 10x stock solution. D-PBS 10x (Biochrom, Merck Millipore, Merck KGaA) was used to prepare 1x D-PBS by dilution with aq. bidest. 1x D-PBS was sterilized by autoclaving and was stored at RT.

Ethanol

Ethanol was used for various applications. Ethanol absolute $\geq$ 99.8 % AnalaR NORMAPUR® (VWR International, Radnor, PA) was diluted with aq. bidest. to produce the desired concentration.

Ethanol 70 %

Ethanol denatured 70 % was used for sterilization of laboratory equipment and for decontamination of Safe 2020 Class II Biological Safety Cabinets (Thermo Fisher Scientific, Waltham, MA). Ethanol denaturated $\geq$ 99.5 % GPR RECTAPUR® (VWR International) was diluted with aq. bidest. to produce the required concentration. The solution was stored at RT.

FACS buffer (PBS/ 0.5% BSA/ 4 mM ethylenediamine tetraacetic acid (EDTA))

FACS buffer was used to collect cells in suspension for flow cytometry analysis and to reduce cell clumping. To maintain a single cell suspension 1.0 g BSA (Sigma-Aldrich, Merck Millipore, Merck KGaA) and 0.22 g of EDTA (Carl Roth GmbH + Co. KG) were dissolved in 200 ml 1x D-PBS. The buffer was sterile-filtered and stored for up to 4 weeks at 4°C.

Fetal calf serum (FCS)

FCS, EU approved origin, South America (Gibco® by Life Technologies™, Thermo Fisher Scientific) was thawed overnight at 4 °C. The solution was aliquoted and stored at -20 °C.

Geneticin 418 (G418)

G418 solution is an aminoglycoside antibiotic and an analog of neomycin used to select transfected hiPS cells. The antibiotic inhibits protein synthesis by interfering with the function of ribosomes, resulting in cell death. Transfection of a neomycin resistance gene into cells results in resistance to G418 and enables cell growth in a culture medium containing G418 (Volarevic, Wu, Smolic, Andorfer, & Wu, 2007). G418 (Biochrom, Merck Millipore, Merck KGaA) was purchased with an activity of 25,000 U/ml, equivalent to a weight of 50 mg/ml. The solution was aliquoted and stored at -20 °C.

L-Ascorbic acid-2-phosphate

L-ascorbic acid-2-phosphate (Sigma-Aldrich, Merck Millipore, Merck KGaA) was used as a supplement for the directed cardiac differentiation medium CDM3. The stock solution of 64 mg/ml in aq. bidest. was sterile-filtered, aliquoted, and stored for up to 6 months at -20 °C. At each medium change the CDM3 differentiation medium was freshly supplemented with L-ascorbic acid-2-phosphate.

Matrigel

Corning® Matrigel® growth factor reduced (GFR) basement membrane matrix (Corning, Tewksbury, MA) was used for coating of cell culture plates. The matrigel was aliquoted depending on the protein concentration determined in the certificate of analysis and was stored at -20 °C.

5 % milk solution

5 % milk solution was used as blocking buffer in the western blot (WB) protocol. By blocking free binding sites it prevents non-specific binding of antibodies to the membrane (Mahmood & Yang, 2012). Milk powder (PanReac AppliChem, AppliChem GmbH,

Darmstadt, Germany) was dissolved in 1x PBS-T to produce a 5 % milk solution. The solution was freshly produced for each WB.

2.5 % milk solution

2.5 % milk solution was used to dilute the secondary antibody in the WB protocol. Milk powder (PanReac AppliChem, AppliChem GmbH) was dissolved in 1x PBS-T to produce a 2.5 % milk solution. The solution was freshly produced for each WB.

Normal goat serum

Normal goat serum was used to reduce non-specific interactions of the secondary antibody in the immunocytochemistry (ICC). Commercially purchased normal goat serum (Abcam, Cambridge, UK) was aliquoted and stored for up to 6 months at -20 °C.

Normal rabbit serum

Normal rabbit serum was used to reduce non-specific interactions of the secondary antibody in the ICC. Commercially purchased normal rabbit serum (Abcam) was aliquoted and stored for up to 6 months at -20 °C.

Paraformaldehyde (PFA)

PFA was used to fix cells in the ICC. PFA (Carl Roth GmbH + Co. KG) was dissolved in 1x phosphate buffered saline with Triton X-100 (PBS-T) to produce a 4 % PFA solution and was stored at 4 °C.

PBS-EDTA solution (0.5 mM)

PBS-EDTA solution (0.5 mM) was used to dissociate adherent hiPS cells. UltraPure ™ 0.5 M EDTA (Gibco© by Life Technologies™, Thermo Fisher Scientific) was diluted with sterile 1x D-PBS. The solution was sterile-filtered and stored for up to 6 months at RT.

PBS-T (0.1 %)

Triton X 100 (Carl Roth GmbH + Co. KG) was diluted with 1x D-PBS to produce PBS-T (0.1 %).The solution was used in the immunocytochemical protocol and was stored at RT.

Penicillin-Streptomycin (Pen-Strep)

Pen-Strep was used as a supplement for the directed cardiac differentiation medium CDM3 to prevent bacterial contamination. Penicillin-Streptomycin 100x for cell culture (PanReac AppliChem, AppliChem GmbH) contains 10,000 U/ml of penicillin and 10 mg/ml of streptomycin. The stock solution was aliquoted and stored for up to 6 months at -20 °C. Thawed aliquots can be stored for up to 4 weeks at 4 °C.

Puromycin

Puromycin is an aminonucleoside antibiotic used to select transfected hiPS cells. The antibiotic inhibits protein synthesis and enables transfected cells carrying a puromycin resistance gene to grow in a culture medium containing puromycin (Steyer et al., 2018; Nathans, 1964). Puromycin hydrochloride (Sigma-Aldrich, Merck Millipore, Merck KGaA) was diluted with aq. bidest. to a concentration of 50 mg/ml. The solution was sterile-filtered, aliquoted and stored at -20 °C.

Recombinant human serum albumin

Recombinant human serum albumin (Sigma-Aldrich, Merck Millipore, Merck KGaA) was used as a supplement for the directed cardiac differentiation medium CDM3. The stock solution of 75 mg/ml in aq. bidest. was sterile-filtered, aliquoted and stored for up to 6 months at -20 °C.

Radioimmunoprecipitation assay (RIPA) buffer

RIPA buffer was used for cell lysis and for protein isolation from cells. RIPA buffer 10x (Cell Signaling Technology, Danvers, MA) was diluted with aq. bidest. and the produced RIPA buffer 1x was aliquoted and stored at -20 °C.

ROCK inhibitor Y-27632

ROCK Inhibitor Y-27632 is used in hiPS cell culture to enhance the recovery of cryopreserved hiPS cells and to improve their growth after splitting (Claassen, Desler, & Rizzino, 2009). Y-27632 is a selective, adenosine triphosphate (ATP)-competitive inhibitor of the rho-associated protein kinase (ROCK) family of kinases (Ishizaki et al., 2000). The concentration of Y-27632 (10 μM) used in this work is described in various publications as beneficial for promoting the characteristic properties of PSCs and the self-renewal ability of hiPS cells (X. Li, Meng, Krawetz, Liu, & Rancourt, 2008; Vernardis, Terzoudis, Panoskaltsis, & Mantalaris, 2017; Ungrin, Joshi, Nica, Bauwens, & Zandstra, 2008). Furthermore, the addition of Y-27632 modulates the differentiation of hiPS cells towards the mesendodermal lineage (Maldonado, Luu, Ramos, & Nam, 2016). 1 mg of Rock inhibitor Y-27632 (StemCell^{TM} Technologies) was dissolved in 312

μl sterile 1x D-PBS to produce a 10 mM stock solution. The solution was aliquoted and stored for up to 6 months at -20 °C. After thawing an aliquot, Rock inhibitor Y-27632 was supplemented to the cell culture medium to produce a final concentration of 10 μM. Thawed aliquots can be stored for up to 2 weeks at 4 °C.

1x TRIS borate EDTA buffer (TBE)

1x TBE was used as a running buffer for gel electrophoresis and was used to produce agarose gels. A 10x TBE buffer was prepared by dissolving 55.03 g of boric acid (Carl Roth GmbH + Co. KG), 107.81 g of Tris Base (Carl Roth GmbH + Co. KG) and 5.85 g of EDTA (Carl Roth GmbH + Co. KG) in 750 ml aq. bidest. A hydrochloric acid and sodium hydroxide solution, c(HCl) = 0,1 mol/l (0,1 N), (Merck Millipore, Merck KGaA) was used to adjust the power of hydrogen (pH) of the buffer to 8.3. The buffer was then filled up to 1 l with aq. bidest. to produce a 10x TBE buffer. The 10x TBE buffer was diluted with aq. bidest. to produce 1x TBE.

10x Tris-glycine-SDS buffer

10x Tris-glycine-SDS buffer (Bio-Rad Laboratories GmbH, München, Germany) was diluted with aq. bidest. to produce a 1x Tris-glycine-SDS and was stored at RT. The buffer contains 25 mM Tris, 192 mM glycine and 0.1 % sodium dodecyl sulfate (SDS) and has a pH of 8.3.

Trypan blue solution (0.2 %)

Trypan blue solution (0.2 %) was used as a vital stain to assess cell viability (Strober, 1997). Trypan blue 0.5 % (Biochrome, Merck Millipore, Merck KGaA) was diluted with sterile 1x D-PBS to a 0.2 % solution, was aliquoted and stored at 4 °C.

WNT-C59

WNT-C59 is a small molecule used to inhibit the WNT signal pathway during the directed cardiac differentiation (M. Zhao, Tang, Zhou, & Zhang, 2019). Undissolved WNT-C59 (Selleckchem, Houston, TX) can be stored for up to 3 years at -20 °C. A stock solution of 2 mM was manufactured in DMSO, sterile-filtered, aliquoted and stored at -80 °C.

3.1.5 Cell culture media and supplements

All cell culture media and supplements used in this work have been listed below with a description of the composition, the manufacture, the use, and the storage specified by the manufacturer or by cited publications. All commercially acquired media are listed in table 4.

Table 4: Commercially acquired media

Media	Description	Manufacturer
DMEM/Ham's F12, #FG-4815	DMEM/Ham's F-12 (Dulbecco's Modified Eagle Medium/Nutrient Mixture F-12) Basal Medium with L-glutamine	Biochrom, Merck Millipore, Merck KGaA, Darmstadt, Germany
Ham's F-12, #FG-0815	Ham's F-12 (Nutrient Mixture F-12) Basal Medium with L-glutamine	Biochrom, Merck Millipore, Merck KGaA, Darmstadt, Germany
mFreSR™, #05854	Defined, serum-free cryopreservation medium for hiPS cells	StemCell™ Technologies, Köln, Germany
mTeSR™ Plus, #05826	Feeder-free and serum-free stabilized cell culture medium for maintenance and expansion of hiPS cells consisting of 2 components: mTeSR™ Plus Basal Medium (400 ml) and mTeSR™ Plus 5X Supplement (100 ml)	StemCell™ Technologies, Köln, Germany
RPMI 1640 Medium, #FG-1215	Roswell Park Memorial Institute (RPMI) 1640 Medium (500 ml) with L-glutamine and 2.0 g/l sodium bicarbonate	Biochrom, Merck Millipore, Merck KGaA, Darmstadt, Germany
TeSR™-E8™, #05990	Feeder-free, animal component-free cell culture medium for maintenance of hiPS cells consisting of 2 components: TeSR™-E8™ Basal Medium (480 ml) and TeSR™-E8™ 25X Supplement (20 ml)	StemCell™ Technologies, Köln, Germany

Abbreviations: **DMEM**: Dulbecco's Modified Eagle Medium; **hiPS cells**: human induced pluripotent stem cells; **RPMI**: Roswell Park Memorial Institute

mFreSR™

mFreSR™ (StemCell™ Technologies) was used as cryopreservation medium for hiPS cells. The serum-free medium contains DMSO and is ready-to-use. The medium was

thawed, aliquoted and stored for up to 12 months at -20 °C. At the day of cryopreservation, an aliquot was thawed and used according to the manufacturer's instructions.

mTeSR™ Plus

mTeSR™ Plus (StemCell™ Technologies) is a feeder-free and serum-free cell culture medium and was used for maintenance and expansion of hiPS cells. The medium enables weekend-free cell culture with routine passaging on Fridays. To skip medium change on 2 consecutive days, the standard feeding volume was doubled. According to the manufacturer, this culture protocol for hiPS cells allows an extension of the feeding interval without compromising culture quality (StemCell™ Technologies). The medium consists of 2 components: mTeSR™ Plus Basal Medium (stable until expiry date on label at 2-8 °C) and mTeSR™ Plus 5X Supplement (stable until expiry date on label at -20 °C). To prepare complete medium, the supplement was thawed overnight at 4 °C and was supplemented to the basal medium. The complete medium was mixed thoroughly and stored for up to 2 weeks at 2-8 °C.

Chemically defined medium, 3 components (CDM3)

The directed cardiac differentiation medium CDM3 is based on the publication by Burridge and colleagues (Burridge et al., 2014). The components of the medium are listed in table 5. CDM3 is a chemically defined medium consisting of RPMI 1640 Medium, recombinant human albumin, L-ascorbic acid 2-phosphate and Pen-Strep. RPMI 1640 Medium (Biochrom, Merck Millipore, Merck KGaA) was supplemented with recombinant human serum albumin (Sigma-Aldrich, Merck Millipore, Merck KGaA) and Penicillin-Streptomycin 100x (PanReac AppliChem, AppliChem GmbH) and was stored for up to 2 weeks at 4 °C. At each medium change, L-ascorbic acid-2-phosphate (Sigma-Aldrich, Merck Millipore, Merck KGaA) was freshly supplemented to CDM3 differentiation medium.

Table 5: Composition of the directed cardiac differentiation medium CDM3

Components	Final concentration in medium
RPMI 1640 Medium	
Recombinant human serum albumin (75 mg/ml)	500 μg/ml
Penicillin (10,000 U/ml) - Streptomycin 100x (10 mg/ml)	29.91 U/ml Penicillin- 29.91 μg/ml Streptomycin
L-ascorbic acid-2-phosphate (64 mg/ml)	213 μg/ml

Abbreviations: **RPMI**: Roswell Park Memorial Institute

TeSR™-E8™

TeSR™-E8™ (StemCell™ Technologies) is a feeder-free and animal component-free cell culture medium and was used for maintenance of hiPS cells. TeSR™-E8™ is a

simplified variant of the popular mTeSR^{TM}1 medium, a widely used feeder-free culture medium for pluripotent stem cells, based on publications by the laboratory of Dr. James Thomson (University of Wisconsin-Madison) (G. Chen et al., 2011; Beers et al., 2012; Ludwig, Levenstein, et al., 2006; Ludwig, Bergendahl, et al., 2006). The components of the medium are listed in table 6 and are based on the publication by Chen and colleagues (G. Chen et al., 2011).

Table 6: Composition of TeSR^{TM}-E8^{TM}

Components	**Final concentration in medium**
DMEM/F12	
fibroblast growth factor (FGF)2	100 μg/l
Insulin	19.4 mg/l
L-ascorbic acid-2-phosphate	64 mg/ml
$NaHCO_3$	543 mg/l
Sodium-Selenium	14 μg/l
Transferrin	10.7 mg/l
transforming growth factor (TGF)β1 or Nodal	2 μg/l or 100 μg/l

Abbreviations: **DMEM**: Dulbecco's Modified Eagle Medium; **FGF**: fibroblast growth factor; **TGF**: transforming growth factor

The medium consists of 2 components: TeSR^{TM}-E8^{TM} Basal Medium (stable for up to 12 months at 2-8 °C) and TeSR^{TM}-E8^{TM} 25X Supplement (stable for up to 12 months at -20 °C). To prepare the complete medium, the supplement was thawed overnight at 4 °C and was supplemented to the basal medium. The complete medium was mixed thoroughly and was stored for up to 2 weeks at 2-8 °C. The cultivation of hiPS cells in TeSR^{TM}-E8^{TM} requires matrigel coated culture plates. The medium enables long-term passaging and expansion of hiPS cells, while maintaining normal cell karyotypes (Y. Wang et al., 2013).

Human embryonic kidney (HEK) 293 medium

HEK 293 cells ATCC® CRL-1573^{TM} (ATCC, Manassas, VA) are widely used because of their ease of growth and their high transfection efficiency (Ooi, Wong, Esau, Lemtiri-Chlieh, & Gehring, 2016). HEK 293 medium consists of 475 ml DMEM/Ham's F12 (Biochrom, Merck Millipore, Merck KGaA) and 25 ml FCS (Hyclone Laboratories Inc, GE Healthcare, Thermo Fisher Scientific, Waltham, MA). The medium was supplemented with Penicillin-Streptomycin 100x (PanReac AppliChem, AppliChem GmbH) to produce a final activity of 100 U/ml penicillin and a final concentration of 100 μg/ml streptomycin. The complete medium was stored for up to 4 weeks at 4 °C.

HEK 293 cryopreservation medium

HEK 293 cryopreservation medium consists of HEK 293 medium with 10 % FCS (Hyclone, Hyclone Laboratories Inc, GE Healthcare) and 10 % DMSO (Carl Roth GmbH + Co. KG). At the day of cryopreservation, the medium was freshly produced.

3.1.6 Bacterial culture

LB medium

LB medium is a nutritionally rich medium and was used for the cultivation of *Escherichia coli (E. coli)*. The components of the medium are listed in table 7. The complete LB medium was autoclaved for 20 minutes at 121 °C.

Table 7: Composition of the LB medium

Components	Added amount
Tryptone (Carl Roth GmbH + Co. KG)	1.0 g
Yeast extract (Carl Roth GmbH + Co. KG)	2.5 g
Sodium chloride (Carl Roth GmbH + Co. KG)	5.0 g
Demineralised water	1 l

Demineralised water was supplied by the water purification system at the Research Center of the German Heart Center.

LB agar

LB agar plates were used as a growth substrate for the cultivation of *E. coli*. The components of the agar are listed in table 8. The complete LB agar was autoclaved for 20 minutes at 121 °C.

Table 8: Composition of the LB agar

Components	Added amount
Tryptone (Carl Roth GmbH + Co. KG)	5.0 g
Yeast extract (Carl Roth GmbH + Co. KG)	2.5 g
Sodium chloride (Carl Roth GmbH + Co. KG)	5.0 g
Agar (Carl Roth GmbH + Co. KG)	7.5 g
Demineralised water	500 ml

Demineralised water was supplied by the water purification system at the Research Center of the German Heart Center.

SOC medium

SOC medium is a nutritionally rich medium and was used for cultivation of competent *E. coli* to maximize the efficiency of bacterial plasmid transformations. SOC medium is

an adjusted version of super optimal broth (SOB) medium with catabolite repression. 20 mM of glucose were supplemented to the SOB medium, creating optimal metabolic conditions for bacterial growth. The components of the SOC medium are listed in table 9. The complete SOC medium was autoclaved for 20 minutes at 121 °C. The medium was aliquoted and stored for up to 6 months at -20 °C.

Table 9: Composition of the SOC medium

Components	Final concentration in medium
Tryptone (Carl Roth GmbH + Co. KG)	2 %
Yeast extract (Carl Roth GmbH + Co. KG)	0.5 %
Sodium chloride (Carl Roth GmbH + Co. KG)	10 mM
Potassium chloride (Sigma-Aldrich, Merck Millipore, Merck KGaA)	2.5 mM
Magnesium chloride Hexahydrat (Sigma-Aldrich, Merck Millipore, Merck KGaA)	10 mM
Glucose (Sigma-Aldrich, Merck Millipore, Merck KGaA)	10 mM
Demineralised water	

Demineralised water was supplied by the water purification system at the Research Center of the German Heart Center.

3.1.7 Cell lines and organisms

All purchased cell lines and organisms used in this work are listed in table 10.

Table 10: Purchased cell lines and organisms

Cell lines and organisms	Manufacturer
Human embryonic kidney cells, HEK 293, #CRL-1573	American Type Culture Collection, Manassas, VA
One Shot ^{TM} TOP 10 Chemically Competent E. Coli, #C404010	Invitrogen^{TM}, Thermo Fisher Scientific, Waltham, MA

The hiPS cell line 'E5', used for genome editing, originates from human fibroblasts, which were reprogrammed in the laboratory of Professor Joseph Wu (Stanford Cardiovascular Institute, Stanford University School of Medicine, Stanford, CA). The hiPS cell line 'E5' is fully characterized and published (Sun et al., 2012) and was provided to the Division of Experimental Surgery at the German Heart Center in cooperation with Professor Joseph Wu and Professor Sean Wu (Institute of Stem Cell and Regenerative Medicine, Stanford, CA).

3.1.8 Oligonucleotides

All oligonucleotide sequences used in this work are listed in tables 11 and 12 and were designed by Roche Diagnostics Deutschland GmbH (Mannheim, Germany) with an annealing temperature of 60 °C. Oligonucleotides used to amplify genomic DNA were de-

signed using the National Center for Biotechnology Information (NCBI) (Available from: https://www.ncbi.nlm.nih.gov/) database. Oligonucleotides used to amplify cDNA were obtained using the Universal ProbeLibrary System Assay Design website, (Available from: *https://lifescience.roche.com/en_de/brands/universal-probe-library.html#assay-design-center*) After checking their specificity with the Basic Local Alignment Search Tool (BLAST) (Available from:
https://blast.ncbi.nlm.nih.gov/), the designed oligonucleotides were ordered and synthesized by Ella Biotech GmbH (Martinsried, Germany) and were reconstituted and stored according to the manufacturer's instructions.

Table 11: Oligonucleotides used to amplify cDNA

Official gene symbol	Official name	GenBank accession numbers	Forward sequence 5 → 3	Reverse sequence 5 → 3
ACTB F382/R478	Homo sapiens actin beta	NM_001101.3	CCA ACC GCG AGA AGA TGA	CCA GAG GCG TAC AGG GAT AG
B2M F75/R160	Homo sapiens beta-2-microglobulin	NM_004048.4	TTC TGG CCT GGA GGC TAT C	TCA GGA AAT TTG ACT TTC CAT TC
GZMB F597/R793	Homo sapiens granzyme B	NM_004131.6	GGG GGA CCC AGA GAT TAA AA	CCA TTG TTT CGT CCA TAG GAG
IFNG F243/R320	Homo sapiens interferon gamma	NM_000619.3	GCA GGT CAT TCA GAT GTA GCG	TCT GTC ACT CTC CTC TTT CCA
IL10 F197/R299	Homo sapiens interleukin 10	NM_000572.3	TGC CTT CAG CAG AGT GAA GA	GCA ACC CAG GTA ACC CTT AAA
IL2 F220/R315	Homo sapiens interleukin 2	NM_000586.4	ACT CAC CAG GAT GCT CAC ATT	TCC AGA GGT TTG AGT TCT TCT T
MYL2 F446/R519	Homo sapiens myosin light chain 2	NM_000432.3	GCA GGC GGA GAG GTT TTC	AGT TGC CAG TCA CGT CAG G
MYL7 F371/R463	Homo sapiens myosin light chain 7	NM_021223.2	GGG TGG TGA ACA AGG ATG AG	GCA GAC CTG AGG GAG ACC TA
NKX2.5 F450/R552	Homo sapiens NK2 homeobox 5	NM_004387.3	TTC TAT CCA CGT GCC TAC AGC	CTG TCT TCT CCA GCT CCA CC
TBX5 F888/R953	Homo sapiens T-box 5	NM_000192.3	TGA TCA TAA CCA AGG CTG GA	GAT TAA GGC CCG TCA CCT TC

Table 12: Oligonucleotides used to amplify genomic DNA

Target sequence	Forward sequence 5 → 3	Reverse sequence 5 → 3
B2M Exon 2 (WT)	GAA CAT ACC TTG GGT TGA TCC	TCA ACT TCA ATG TCG GAT GGA T
B2M Exon 2 (KO)	GAA CAT ACC TTG GGT TGA TCC	GAG ATC CTA AGC TTG GCT GG
B2M Exon 3 (WT)	TGC CAG CCT TAT TTC TAA CCA T	TTA AGA TGA CGG GTC CCAT GT
B2M Exon 3 (KO)	TCT AAT TCC ATC AGA AGC TGG T	TTA AGA TGA CGG GTC CCAT GT
tdTomato (PURO)	GGA CAC CAA GCT GGA CAT CA	CTA CCG GTG GAT GTG GAA TG
tdTomato (CRE)	GGA CAC CAA GCT GGA CAT CA	TTG TAC CGG AGA CCT ACC TAA

3.1.9 Plasmids

All vectors and gene targeting constructs used in this work are listed in table 13. The associated vector maps are shown in figures S1 and S2.

Table 13: Vectors and gene targeting constructs

Plasmid	Source
pUC57-Simple	GenScript (Piscataway, NJ)
pSpCas9(BB)-2A-Puro (pX459) V2.0	Addgene (Watertown, MA)

3.1.10 Antibodies

All primary and secondary antibodies used in this work are listed in tables 14 (primary antibodies) and 15 (secondary antibodies) and have been stored according to the manufacturer's specifications.

Table 14: Primary antibodies

Antibody	Specificity	Manufacturer	Order number	Concentration	Dilution
Anti-beta 2 Microglobulin antibody [EP2978Y]	rabbit monoclonal IgG	Abcam, Cambridge, UK	ab75853	0.18 mg/ml	1:5000 (WB)
Anti-Cardiac Troponin T antibody [1C11]	mouse monoclonal IgG1	Abcam, Cambridge, UK	ab8295	1 mg/ml	1:200 (ICC)
Anti-Myosin Light Chain 2 (MYL2) antibody, synonym MLC2V	rabbit, polyclonal IgG	Proteintech Group Inc., Rosemont, IL, UK	10906-1-AP	1 mg/ml	1:200 (ICC)
Anti-Myosin Light Chain 7 (MYL7) antibody, synonym MLC2A	mouse monoclonal IgG2b	Synaptic Systems GmbH, Göttingen, Germany	311011	1 mg/ml	1:400 (ICC)
Anti-RFP antibody (FITC)	rabbit polyclonal IgG	Abcam, Cambridge, UK	ab34764	1 mg/ml	1:500 (ICC)
Anti-Sarcomeric Alpha Actinin antibody [EA-53]	mouse monoclonal IgG1	Abcam, Cambridge, UK	ab9465	0.125 mg/ml	1:200 (ICC)
CD3-FITC, human	mouse monoclonal $IgG2_{ak}$	Miltenyi Biotec, Bergisch Gladbach, Germany	#130-113-128		1:50 (FACS)
CD8-FITC, human	mouse monoclonal $IgG2_{ak}$	Miltenyi Biotec, Bergisch Gladbach, Germany	#130-113-157		1:50 (FACS)
CD16-FITC, human	recombinant human IgG1	Miltenyi Biotec, Bergisch Gladbach, Germany	#130-113-392		1:50 (FACS)
HLA-ABC Monoclonal Antibody (W6/32)	mouse monoclonal IgG2a	Invitrogen^{TM}, Thermo Fisher Scientific, Waltham, MA	MA5-11723	0.2 mg/ml	1:75 (ICC) 1:100 (WB) 1:40 (FACS)

Table 15: Secondary antibodies

Antibody	Specificity	Manufacturer	Order number	Concentration	Dilution
Goat Anti-Mouse IgG H&L (Alexa Fluor© 488)	polyclonal, IgG	Abcam, Cambridge, UK	ab150113	2 mg/ml	1:500 (ICC) 1:1000 (FACS)
Goat Anti-Mouse IgG-HRP	polyclonal, IgG	Santa Cruz Biotechnology, Dallas, TX	sc-2005	0.4 mg/ml	1:10000 (WB)
Goat Anti-Rabbit IgG Antibody, (H+L) HRP conjugate	polyclonal, IgG	Sigma-Aldrich, Merck Millipore, Merck KGaA, Darmstadt, Germany	AP307P	1 mg/ml	1:5000 (WB)
Goat Anti-Rabbit IgG H&L (Alexa Fluor© 488)	polyclonal, IgG	Abcam, Cambridge, UK	ab150077	2 mg/ml	1:1000 (FACS)
Goat Anti-Rabbit IgG H&L (Alexa Fluor© 647)	polyclonal, IgG	Abcam, Cambridge, UK	ab150079	2 mg/ml	1:500 (ICC)

3.1.11 Purchased services

All oligonucleotides used for qRT-PCR were ordered from Ella Biotech GmbH (Martinsried, Germany). Plasmid and PCR product sequencing was performed by Eurofins GmbH (Ebersberg, Germany). Synthesis of the B2M donor construct by GenScript (Leiden, The Netherlands).

3.1.12 Websites and databases

All websites and databases used in this work are listed in table 16.

Table 16: Websites and databases

Website/data base	**Online access**
Basic Local Alignment Search Tool (BLAST)	https://blast.ncbi.nlm.nih.gov/
Benchling CRISPR gRNA Design program	https://benchling.com/
Biorender	https://app.biorender.com/
National Center for Biotechnology Information (NCBI)	https://www.ncbi.nlm.nih.gov/
TIDE webtool	https://tide.deskgen.com/
Universal ProbeLibrary System Assay Design website	https://lifescience.roche.com/en_ de/brands/universal-probe-library.html#assay-design-center

3.1.13 Software

All software programs used in this work are listed in table 17.

Table 17: Software

Software	**Provider**
BD FACSDiva^{TM} Version 8.0.1	BD Biosciences, Becton, Dickinson and Company, San Jose, CA
Carl Zeiss^{TM} Axio Vision Rel. 4.8.2	Carl Zeiss AG, Oberkochen, Germany
FlowJo Version 7.6.5	FlowJow LLC, Ashland, OR
i-control^{TM} Microplate Reader Software Version 2.0	Tecan, Tecan Group AG, Männedorf, Switzerland
Image Lab^{TM} 4.0	Bio-Rad Laboratories GmbH, München, Germany
ImageQuant LAS 4000	GE Healthcare Life Sciences, General Electric Company, Boston, MA
Quant Studio Design & Analysis Software Version 1.4	Applied Biosystems^{TM} by Thermo Fisher Scientific, Waltham, MA
SigmaPlot V13.0	Systat Software Inc., San Jose, CA

3.2 Cell culture methods

3.2.1 Determination of the cell number by means of Neubauer counting chamber

Trypan blue solution (0.2 %) (described in section 3.1.4) was used as a vital stain to assess cell viability. Trypan blue labels dead cells exclusively by penetrating through their perforated cell membrane and staining their cytoplasm blue (Strober, 1997). To determine the cell number, cells were detached as a single cell suspension and pelleted by centrifugation (1500 x g, for 10 minutes at RT). The pellet was resuspended in a cell-type-specific culture medium and an aliquot of the cell suspension was diluted with 0.2 % trypan blue solution to a suitable concentration. This dilution was carefully pipetted into a Neubauer chamber slide (Thomas Scientific, Swedesboro, NJ), allowing capillary action to draw it inside. The number of living cells was determined by counting only non-stained viable cells in the 4 large squares. Since only a small volume of the diluted sample was counted, the following general formula was used to determine the total cell number:

$$\text{Cell concentration} = \frac{Total\ cell\ number}{Volume\ (ml)} = \frac{Cells\ counted\ in\ 4\ large\ squares \times 10^4}{Number\ of\ large\ squares}\ \text{x Dilution}$$

3.2.2 Preparation of single-cell solutions

Single-cell suspensions were required for FACS analysis and for all immunological assays performed within the framework of this thesis. To detach adherent hiPS cells, the culture medium was aspirated and cells were washed with 1 ml D-PBS (described in section 3.1.4). Subsequently, 1 ml PBS-EDTA solution (0.5 mM) (described in section 3.1.4) was added and the cells were incubated for 10 minutes at 37 °C until detachment. The detached cells were then transferred into a sterile 15 ml Falcon® High Clarity PP Centrifuge Tube (VWR International) (15 ml falcon tube) and filled up to 15 ml with sterile D-PBS. The single-cell suspension was centrifugated at 300 x g for 8 minutes at RT. After removing the supernatant, the cell pellet was resuspended in the corresponding assay medium.

3.2.3 General conditions for hiPS cell culture

Cell culture was performed in Safe 2020 Class II Biological Safety Cabinets (Thermo Fisher Scientific). The cells were incubated in HERACell™ 240i CO_2 incubators (Thermo Fisher Scientific) at 37 °C, 100 % humidity and 5 % CO_2. Centrifugation was carried out in the Heraeus Megafuge 40R (Thermo Fisher Scientific). EVOS XL Core Microscope (Thermo Fisher Scientific) was used to visualize cells. Incidin OxyFoam S (Ecolab, Saint Paul, MN) was used for decontamination of the interior work surface of the biological safety cabinets. Ethanol 70 % (VWR International) (described in section 3.1.4) was used for sterilization of all laboratory equipment. Eppendorf Safe-Lock Tubes 1.5 ml and 2.0 ml (Eppendorf AG, Hamburg, Germany) and SurPhob Pipette Tips Reloads without filter (1250 μl) (Biozym Scientific GmbH, Hessisch Oldendorf, Germany) were sterilized in a HICLAVE HI-50 (HMC Europe GmbH)

autoclave. Thereafter, they were dried in a Drying Chamber Model ED 56 (Binder GmbH, Tuttlingen, Germany).

Cultivation of hiPS cells

TeSR™-E8™ (StemCell™ Technologies) (described in section 3.1.5) cell culture medium was used for maintenance and expansion of hiPS cells. Cultivation of hiPS requires a surface coating matrix to ensure the attachment of cell aggregates on culture plates. Corning® Matrigel® GFR basement membrane matrix (Corning) (described in section 3.1.4) was used to coat the Cell Culture Multiwell Plate, 6 well, Polystyrene (PS), clear, CELLSTAR®, sterile (Greiner Bio-One International GmbH, Frickenhausen, Germany) (6-well culture plate). Corning® Matrigel® (Corning) is a solubilized basement membrane preparation extracted from the Engelbreth-Holm-Swarm (EHS) mouse sarcoma. It is a protein-rich extracellular matrix containing laminin, collagen IV, entactin, heparan sulfate proteoglycan and growth factors (Kleinman et al., 1982; Bissell, Arenson, Maher, & Roll, 1987; Vukicevic et al., 1992; McGuire & Seeds, 1989). At 4 °C the matrigel is a liquid solution and it solidifies at room temperature. To coat cell culture plates, an aliquot was thawed on ice and diluted with precooled (4 °C) DMEM/Ham's F12 medium (Biochrom, Merck Millipore, Merck KGaA). The dilution factor and the volume needed for coating were calculated to ensure a standardized protein concentration of 8.7 μg protein/cm^2. This protein concentration is based on publications by Lian and colleagues and Burridge and colleagues (Lian et al., 2012; Burridge et al., 2014). The matrigel was evenly distributed and the culture plate was placed at 37 °C for at least 30 minutes to allow matrigel polymerization. Coated culture plates can be stored at 37 °C for up to 1 week before use. For cell culture, the excess medium was aspirated and TeSR™-E8™ (StemCell™ Technologies) culture medium was added to each well. The maintenance of hiPS requires daily medium changes. First, the medium was aspirated and the cells were washed with Ham's F-12 (Biochrom, Merck Millipore, Merck KGaA). Then TeSR™-E8™ (StemCell™ Technologies) culture medium supplemented with CloneR™ (StemCell™ Technologies) (described in section 3.1.4) was added. Every day, hiPS cells were visually assessed under the microscope to monitor colony growth and quality and to determine the next splitting time.

Splitting of hiPS cells

Splitting of hiPS cells was carried out with ReLeSR™ (StemCell™ Technologies). ReLeSR™ (StemCell™ Technologies) is an enzyme-free reagent used for dissociation and passaging of hiPS by generating detached cell aggregates of optimal size. To split undifferentiated hiPS, the culture medium was aspirated and the cells were washed with 1 ml/well of 1x D-PBS. The wash solution was aspirated, and 1 ml/well of ReLeSR™ (StemCell™ Technologies) was added, covering the cell colonies with a thin film. ReLeSR™ (StemCell™ Technologies) was aspirated after 1-minute incubation at RT. Then the colonies were incubated for 3-5 minutes at 37 °C. Finally, TeSR™-E8™ (StemCell™ Technologies) culture medium was pipetted into the well and cells were detached by firmly tapping the side of the 6-well culture plate for approximately 30-60 seconds. The detached cell aggregates were transferred to a 15 ml falcon tube using a sterile 5 ml Serological Pipette (scale: 0.1 ml; color: blue) (Kisker Biotech GmbH & Co. KG, Steinfurt, Germany) and pelleted by centrifugation (300 x g for 5 minutes at RT).

After centrifugation, the pellet was resuspended in pre-warmed TeSR™-E8™ (StemCell™ Technologies) supplemented with CloneR™ (StemCell™ Technologies) (described in section 3.1.4) and then cells were plated at a ratio of 1:12 onto pre-coated wells. According to the manufacturer, this is the optimized splitting ratio to reach a 80 % colony confluency after 5-7 days (StemCell™ Technologies).

Cryopreservation of hiPS cells

mFreSR™ (StemCell™ Technologies) (described in section 3.1.5) was used as cryopreservation medium for hiPS cells. For all hiPS cell lines, low passage (p) cells (p10 to p20) were used to create long-time stocks. On the day of cryopreservation, an aliquot of the cryopreservation medium was thawed and used according to the manufacturer's instructions. The cells in freezing medium were then aliquoted into CryoTubes™ Nunc™ (1.0 ml) (VWR International) and quickly transferred to a Nalgene® Mr. Frosty® Cryo 1 °C Freezing Container (Thermo Fisher Scientific), which ensures a controlled cooling rate of -1 °C/minute. 2-Propanol ≥ 99.9 % (Carl Roth GmbH + Co. KG) was added to the freezing container to achieve the recommended cooling rate. First, the cryovials were placed for 2 hours at -20 °C (Refrigerator Liebherr Premium No Frost, Liebherr, Bulle, Switzerland) and then they were deposited at -80 °C (HERA Freezer Basic, Thermo Fisher Scientific) overnight. As recommended by the manufacturer, the cryovials were transferred to the Liquid Nitrogen Storage Tank (Messer Griesheim GmbH, Bad Soden, Germany) for long-time storage the next day (StemCell™ Technologies).

Thawing of hiPS cells

The thawing procedure of hiPS cells requires matrigel pre-coated cell culture plates. In general, the equivalent of one thawed cryovial was transferred into 1 well of a 6-well culture plate (Greiner Bio-One International GmbH). To enhance the recovery of cryopreserved hiPS cells, ROCK inhibitor Y-27632 (StemCell™ Technologies) (described in section 3.1.4) was supplemented to the TeSR™-E8™ (StemCell™ Technologies) culture medium at a final concentration of 10 μM. The cryovial was then placed in a 37 °C Lauda Aqualine AL 12 water bath (LAUDA-Brinkmann LP, Delran, NJ). Subsequently, the thawed cell suspension was transferred to a sterile 15 ml falcon tube (VWR International) containing 5 ml of DMEM/Ham's F12 medium and pelleted by centrifugation (300 x g for 5 minutes at RT). After centrifugation, the pellet was resuspended in pre-warmed TeSR™-E8™ (StemCell™ Technologies) supplemented with CloneR™ (StemCell™ Technologies) (described in section 3.1.4) and then cells were plated. Daily medium changes were performed using TeSR™-E8™ (StemCell™ Technologies) culture medium. Every day, hiPS cells were visually assessed under the microscope to monitor colony growth and quality and to determine the next splitting time.

3.2.4 General conditions for directed cardiac differentiation

In this work, hiPS cells were differentiated into CMs using a directed differentiation protocol based on publications by Burridge and colleagues (Burridge et al., 2014). This *in vitro* protocol allows the differentiation of pluripotent stem cells towards the cardiac lineage under fully defined conditions. By modulating signaling pathways that guide embryonic development *in*

vivo, this highly efficient protocol leads to an average yield of over 80 % CMs (Lian et al., 2012; Burridge et al., 2014; Batalov & Feinberg, 2015). The workflow of the directed cardiac differentiation protocol is shown in figure 3.

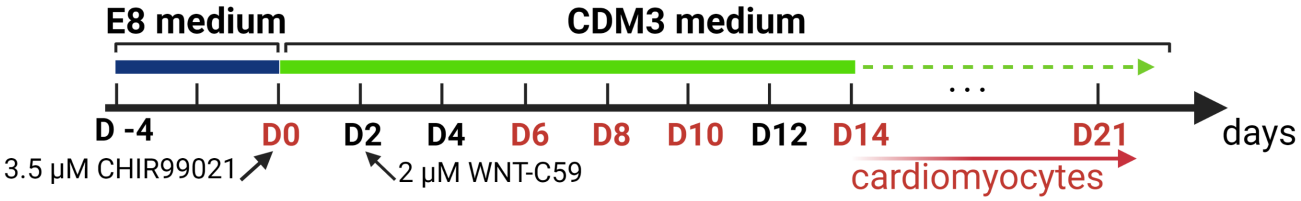

Figure 3: Directed cardiac differentiation protocol

To generate sufficient cell numbers and to maximize differentiation efficiency, hiPS cells were first expanded on three 6-well culture plates (Greiner Bio-One International GmbH) in TeSR^{TM}-E8^{TM} (StemCell^{TM} Technologies) culture medium. After reaching confluency, cells were transferred onto a pre-coated Cell Culture Multiwell Plate, 24 well, PS, clear CELLSTAR®, sterile (Greiner Bio-One International GmbH) (24-well culture plate). For this passaging procedure, culture medium was aspirated and cells were washed with 1 ml/well of 1x D-PBS. The wash solution was aspirated, and 1 ml/well of PBS-EDTA solution (0.5 mM) (described in section 3.1.4) was added. Then culture plates were incubated for 8 minutes at 37 °C and the PBS-EDTA solution was aspirated. Cells were carefully detached and were transferred to a 15 ml falcon tube using a sterile 5 ml Serological Pipette (scale: 0.1 ml; color:

blue) (Kisker Biotech GmbH & Co. KG, Steinfurt, Germany) and pelleted by centrifugation (300 x *g* for 5 minutes at RT). After centrifugation, the pellet was resuspended in pre-warmed TeSR^{TM}-E8^{TM} (StemCell^{TM} Technologies) supplemented with CloneR^{TM} (StemCell^{TM} Technologies) (described in section 3.1.4) Subsequently, 1 ml/well of the single cell suspension was pipetted onto a pre-coated 24-well plate. Daily medium changes were performed using TeSR^{TM}-E8^{TM} (StemCell^{TM} Technologies) culture medium. The medium was aspirated and cells were washed with Ham's F-12 (Biochrom, Merck Millipore, Merck KGaA) and 1 ml TeSR^{TM}-E8^{TM} (StemCell^{TM} Technologies) was added to each well. After 2 to 4 days, cultured hiPS cells had grown to a completely dense monolayer and the directed cardiac differentiation protocol was started. On day (D)0, culture medium was changed to CDM3 medium (described in section 3.1.5) containing 3.5 μM CHIR99021 (LC Laboratories, Woburn, MA) (described in section 3.1.4). On D2, culture medium was changed to CDM3 medium containing 2 μM Wnt-C59 (Selleckchem) (described in section 3.1.4). From day D4 on, medium change with CDM3 medium was performed every other day. HiPS cell-derived CMs typically started beating on D8 of the differentiation protocol and the number of contracting CMs increased continuously until day D14. RNA lysis samples were taken in duplicates or triplicates on days D0, D6, D8, D10, D14 and D21 and were stored at -20 °C until RNA isolation and purification (described in section 3.3.1). After RNA isolation and spectrophotometric assessment of the RNA concentration (described in section 3.3.3), RNA was converted into cDNA (described in section 3.3.4) and used for cardiac gene expression analysis. In this work, gene expression of the cardiac transcription factors *NKX2.5* (NM_004387.3), *T-Box 5 (TBX5)* (NM_000192.3), *myosin light chain-2, ventrical isoform, encoded by MYL2 (MLC2v)* (NM_000432.3) and *myosin light chain-2, atrial isoform, encoded by MYL7 (MLC2a)* (NM_021223.2) was measured as described in section 3.3.5. The oligonucleotide primer sequences used for qRT-PCR are given in table 11. For relative quantification, the expression of the target genes was normalized using *β-Actin (ACTB)* (NM_001101.3) as a reference gene (described in section 3.3.6). Within the framework of this thesis, the E5V cell line (parental line) and all derivatives were differentiated according to this protocol.

3.3 Molecular biology methods

3.3.1 RNA isolation and purification

RNA extraction is a commonly used molecular biology method for the purification of RNA from biological samples (Peirson & Butler, 2007). In this work, RNA was isolated from hiPS cells and HEK 293 cells using the peqGOLD Total RNA Kit (S-Line) (VWR International) according to the manufacturer's instructions. To lyse the cells, culture medium was aspirated and lysis buffer was added to each well and mixed thoroughly to ensure complete lysis. After disruption, the RNA lysates were stored at -20 °C until further use. In the first step of the RNA purification protocol, the lysates were pipetted directly onto DNA removing columns to selectively remove genomic DNA. After centrifugation, the flow-through was transferred to a PerfectBind RNA column containing a silica membrane that selectively binds RNA. The amount of contaminating DNA was effectively reduced by using the on-column peqGOLD DNase I Digest Kit (Peqlab Biotechnologie GmbH, Erlangen, Germany) according to the man-

ufacturer's instructions. Subsequent wash steps ensured the removal of remaining cell debris. In the last step, purified and highly concentrated RNA was eluted with RNase-free water and stored at -20 °C until further use.

3.3.2 DNA isolation and purification

To isolate genomic DNA from hiPS or HEK 293 cells, adherent cells were dissociated with PBS-EDTA solution (0.5 mM) (described in section 3.1.4). The detached single cells were transferred to a 15 ml falcon tube. After centrifugation (300 x *g*, 10 minutes at RT), supernatant was aspirated and the cell pellet was stored at -20 °C until subsequent use. DNA isolation was carried out with the DNeasy Blood & Tissue Kit (Qiagen, Hilden, Germany) according to the manufacturer's instructions. This DNA extraction and purification procedure uses a buffer system to achieve cell lysis. Lysates were then pipetted directly onto DNeasy spin-columns containing a silica membrane that selectively binds DNA. Subsequent wash steps ensured the removal of remaining contaminants. Finally, the kit-specific buffer was used to elute the purified and highly concentrated DNA which was stored at -20 °C until further use.

3.3.3 Measurement of the concentration of RNA and DNA

Spectrophotometric assessment of the concentration and purity of RNA and DNA was performed with a NanoDrop 2000c spectrophotometer (Thermo Fisher Scientific). This instrument is designed to measure the absorbance and calculate the concentration of nucleic acids by applying a sample volume of 1 μl. The concentration of nucleic acids was calculated by applying a modification of the Beer-Lambert equation to correlate absorbance with concentration:

$$c = \frac{A}{\epsilon * b}$$

c: nucleic acid concentration in ng/μl
A: absorbance in absorbance units (AU)
ϵ: wavelength-dependent extinction coefficient in ng-cm/μl
b: pathlength in cm

Generally accepted extinction coefficients for nucleic acids are as follows:

double-stranded DNA: 50 ng-cm/μl
single-stranded DNA: 33 ng-cm/μl
single-stranded RNA: 40 ng-cm/μl

Absorbance values at 230 nm, 260 nm and 280 nm are used for quality control. A260/280 and A230/260 ratios are used to calculate RNA purity of the measured nucleic acid samples. An A260/280 ratio between $\approx$ 1.8 and 2.0 is considered as indicative of highly pure DNA and RNA. A lower ratio indicates the presence of protein contaminants. Absorbance values of the measured nucleic acids are standardized to a 10 mm pathlength. To enable the quantification of concentrated samples, the spectrophotometer selects pathlengths between 1.0 mm to 0.05 mm. All absorbance measurements were performed according to the manufacturer's instructions.

3.3.4 Synthesis of cDNA

Reverse transcription of RNA to cDNA was performed with the M-MLV Reverse Transcriptase Kit (Invitrogen^{TM}, Thermo Fisher Scientific). The kit was used according to the manufacturer's instructions. The newly synthesized cDNA was then employed for analysis of gene expression using qRT-PCR (Haddad & Baldwin, 2010). Synthesis of cDNA requires the application of Random hexamer oligonucleotides (Invitrogen^{TM}, Thermo Fisher Scientific). These are short oligodeoxyribonucleotides of random sequence that bind to random complementary sites on the target RNA template and initiate reverse transcription. Before use, 100 μl of the random hexamers (3 μg/μl) were diluted with 1100 μl Water, RNase-free, DEPC treated, Molecular Biology Grade, Ultrapure (Thermo Scientific, Waltham, MA) to a final concentration of 250 ng/μl. The diluted random hexamers were aliquoted and stored at -20 °C. The enzyme Moloney murine leukemia virus reverse transcriptase (M-MLV RT) used in the protocol is a recombinant DNA polymerase that synthesizes a complementary DNA strand from the single-stranded RNA template (specification by the manufacturer). In the first step of cDNA production, 100 ng RNA were mixed with random hexamers and desoxynucleotide triphosphate (dNTP)-Set 1 (100 mM dATP, dGTP, dCTP, dTTP) (Carl Roth GmbH + Co. KG). The mixture was incubated in the C1000^{TM} Thermal Cycler (Bio-Rad Laboratories GmbH, München, Germany) for 5 minutes at 65 °C. The components of the reverse transcription mastermix 1 used for the first reaction of cDNA synthesis are listed in table 18.

Table 18: Composition of the reverse transcription mastermix 1

Components	Volume
RNA (100 ng)	16 μl
random hexamers (250 ng/ml)	3 μl
dNTPs (100 mM dATP, dGTP, dCTP, dTTP)	1.5 μl

Abbreviations: **RNA**: ribonucleic acid; **dNTP**: deoxynucleotide triphosphate

The mixture was chilled by transferring the tubes on ice. To prepare the reverse transcription mastermix 2, 5x First Strand Buffer (M-MLV Reverse Transcriptase Kit, Invitrogen^{TM}, Thermo Fisher Scientific) was mixed with 0.1 M dithiothreitol (DTT) (M-MLV Reverse Transcriptase Kit, Invitrogen^{TM}, Thermo Fisher Scientific). In the second step of cDNA production, reverse transcription mastermix 2 was added to the reverse transcription mastermix 1 containing the RNA. The mixture was then incubated in the C1000^{TM} Thermal Cycler (Bio-Rad Laboratories GmbH) for 2 minutes at 37 °C. The components of the reverse transcription mastermix 2 used for the second reaction of cDNA synthesis are listed in table 19.

0.5 μl of the M-MLV Reverse Transcriptase (200 U/μl) (M-MLV Reverse Transcriptase Kit, Invitrogen^{TM}, Thermo Fisher Scientific) were then added to the reaction mixture (mastermix 1 and mastermix 2) and the complete mixture was incubated in the C1000^{TM} Thermal Cycler (Bio-Rad Laboratories GmbH) under defined reaction conditions specified in table 20. The newly synthesized cDNA was stored at -20 °C until subsequent use.

Table 19: Composition of the reverse transcription mastermix 2

Components	Volume
5x First Strand Buffer	6 μl
0.1 M DTT	3 μl

Abbreviation: **DTT**: dithiothreitol

Table 20: Reaction conditions for cDNA synthesis

Reaction	Temperature	Incubation time
Incubation	25 °C	10 min
cDNA synthesis	37 °C	50 min
Enzyme inactivation	75 °C	15 min
Hold	4 °C	∞

Abbreviation: **cDNA**: complementary deoxyribonucleic acid

3.3.5 Amplification of DNA fragments

Polymerase chain reaction (PCR)

PCR is a commonly used method for enzyme-dependent amplification of a specific DNA sequence. The PCR assay requires the presence of the DNA template, oligonucleotides (described in section 3.1.8), dNTPs, PCR reaction buffer + DMSO (optional) and the key enzyme Taq DNA polymerase. Amplification of DNA fragments was carried out in the C1000^{TM} Thermal Cycler (Bio-Rad Laboratories GmbH) under defined cycling conditions specified in table 21. First, the key enzyme FastStart^{TM} High Fidelity Polymerase (FastStart^{TM} High Fidelity PCR System, dNTPack (Kit), Sigma-Aldrich, Merck Millipore, Merck KGaA) was activated during a 2-minute incubation period at 95 °C. Activation of the DNA polymerase was then followed by a three-step thermocycling protocol. During the first step of the cycling protocol, the reaction mixture (described in table 22) was heated to separate the double-stranded target DNA into 2 single strands. This denaturation process was followed by an annealing step. During the annealing process, the temperature was lowered to allow the hybridization of complementary oligonucleotide sequences to the target DNA. During the following extension step, the temperature was raised again. Raising temperature allows the DNA polymerase to extend the attached oligonucleotides at their 3' end in the 5'→ 3' direction by adding free nucleotides to the developing DNA strand. The thermocycling protocol was usually repeated 40 times to produce the desired yield of PCR product by exponential replication (Garibyan & Avashia, 2013). In this work, PCR analysis was employed to verify correct homologous recombination.

Table 21: PCR cycling conditions

Cycle step	Reaction	Temperature	Incubation time	Number of cycles
Initial activation		95 °C	2 min	1
Amplification				30-40
	Denaturation	95 °C	30 s	
	Annealing	60 °C	30 s	
	Extension	72 °C	120 s	
Final extension		72 °C	7 min	1
Hold		4 °C	∞	1

Table 22: Reaction mixture for DNA amplification

Components	Volume per reaction	Final concentration
DNA template	variable	100 ng
FastStart High Fidelity Reaction Buffer*, 10x	2 µl	1x; 1.8 mM magnesiumchlorid
DMSO*	1 µl	5 %
PCR Grade Nucleotide Mix (200 µM each)*	1 µl	10 µM
Oligonucleotide (forward), 5 µM	1.6 µl	0.4 µM
Oligonucleotide (reverse), 5 µM	1.6 µl	0.4 µM
FastStart High Fidelity Enzyme Blend, 5 U/µl*	0.5 µl	2.5 U per reaction
Water (PCR grade)	filled up to 20 µl	

Abbreviations: **DNA**: deoxyribonucleic acid; **DMSO**: dimethyl sulfoxide; **PCR**: polymerase chain reaction;
All * marked components were delivered with the FastStart™ High Fidelity PCR System, dNTPack (Kit) (Sigma-Aldrich, Merck Millipore, Merck KGaA).
Water (PCR grade) was purchased from Roche Applied Science (Penzberg, Germany).

Quantitative real-time polymerase chain reaction (qRT-PCR)

qRT-PCR is a commonly used method for real-time detection of gene expression. The PCR based detection technology allows real-time quantification of amplified target DNA by employing a fluorescent dye (Deepak et al., 2007). The fluorescent reporter signal strength increases proportionally to the number of amplified DNA molecules. Recording the fluorescent reporter signal in each PCR cycle enables to monitor the amplified DNA during the exponential phase of the PCR reaction (Green & Sambrook, 2018). In this work, the fluorescent dye SYBR Green I was used to detect gene-specific PCR products. This dye binds to the minor groove of double-stranded DNA (Dragan et al., 2012). During the initial cycles of PCR, the fluorescence signal is weak and referred to as baseline. The baseline fluorescent signal is used to accurately determine the threshold cycle (Ct) value. The Ct value is defined as the cycle number, where the fluorescent intensity rises significantly above the baseline signal. The quantification of the PCR product relies on the detection of the Ct value (Jia, 2012). To determine the quality of the amplified PCR product, a melting curve analysis can be performed. During the melting protocol, the temperature is gradually increased and fluorescence intensity changes are continuously documented. As the temperature increases, double-stranded DNA denatures into two single strands, causing the fluorescent dye to dissociate and resulting in

a decreased fluorescence signal. Since differences in melting temperature are based on both length and specific nucleotide sequence composition of the DNA fragment, this method enables the characterization of the amplification product and reveals the presence of unspecific products. In this work, qRT-PCR was performed with the Quant Studio 3 Real-Time PCR and the Quant Studio Design & Analysis Software Version 1.4 (Applied Biosystems^{TM}, Thermo Fisher Scientific) under defined cycling conditions, specified in table 23. The components required for the qRT-PCR protocol were provided from the Power SYBR® Green PCR Master Mix (Applied Biosystems^{TM} by Life Technologies^{TM}, Thermo Fisher Scientific) Kit and the oligonucleotides (described in section 3.1.8) were obtained from Ella Biotech GmbH (Martinsried, Germany). Before starting the protocol, the reaction mixture (described in table 24) was transferred into each well of the MicroAmps^{TM} Optical 96-Well Reaction Plate (Thermo Fisher Scientific) (96-well plate), which was sealed using a MicroAmps^{TM} Optical Adhesive Film (Applied Biosystems^{TM}, Thermo Fisher Scientific).

Table 23: qRT-PCR cycling conditions

Cycle step	**Reaction**	**Temperature**	**Incubation time**	**Number of cycles**	**Rate**
		50 °C	2 min	1	1.6 °C/s
Initial activation		95 °C	10 min	1	1.6 °C/s
Amplification				30-40	
	Denaturation	95 °C	15 s		1.6 °C/s
	Annealing/ Extension	60 °C	1 min		1.6 °C/s
Melting curve analysis				1	
	1. Segment	95 °C	15 s		1.6 °C/s
	2. Segment	60 °C	1 min		1.6 °C/s
	3. Segment	95 °C	235 s		0.15 °C/s
Hold		4 °C	∞	1	

Table 24: Reaction mixture for qRT-PCR

Components	**Volume per reaction**	**Final concentration**
cDNA template	variable	≈ 3 ng per reaction
Power SYBR® Green PCR Master Mix, 2x	10 μl	1x; 2.5 mM magnesiumchlorid
Oligonucleotide (forward), 5 μM	1.2 μl	0.3 μM
Oligonucleotide (reverse), 5 μM	1.2 μl	0.3 μM
Water (RNase-free)	variable	filled up to 20 μl
Total reaction volume	**20 μl**	

Abbreviations: **cDNA**: complementary deoxyribonucleic acid; **PCR**: polymerase chain reaction; **RNase**: ribonuclease;
Water (RNase-free) was purchased from Thermo Fisher Scientific.

3.3.6 Analysis of relative gene expression

The relative gene expression quantification is a commonly used methodology to analyze data from qRT-PCR assays. To calculate the relative gene expression, the amplification efficiency was first determined. For this purpose, a standard dilution series was performed in duplicates for each primer set over six log10 stages. After performing qRT-PCR, the standard curve was generated by plotting the Ct values (y-axis) along with the corresponding DNA concentrations (x-axis). The linear regression curve was obtained using the following formula:

$$y = -m \ln x + zp$$

m: slope; zp: y-axis intercept

Amplification efficiency (E) was calculated using the following equation:

$$E = 10^{-\frac{1}{m}}$$

The desired amplification efficiencies range from 90 % to 100 %, corresponding to efficiency values (E) of 1.8 to 2.0. The coefficient of determination R^2 was then calculated, to examine how well the regression predictions validate the real data. An R^2 value of 1 indicates perfect prediction. For relative quantification, the expression of the target gene is compared to a steadily expressed reference gene, a so-called housekeeping gene. In this work, *ACTB* (NM_001101.3) was used as reference gene. Before calculation of the relative gene expression, the Ct values were converted into arbitrary units (AU) using the slope and y-axis intercept of the appropriate linear regression curve as follows:

$$AU = e^{\frac{Ct\ value - zp}{m}}$$

Finally relative gene expression was calculated as follows:

$$\text{Relative gene expression} = \frac{Target\ gene}{ACTB}$$

The unpaired Student‘s t-test was used to determine statistically significant differences in gene expression.

3.3.7 Detection and analysis of DNA

Agarose gel electrophoresis

Agarose gel electrophoresis is a commonly used molecular biology method for separation and visualization of nucleic acids. The application of an electric field permits to separate DNA fragments according to their size and charge. The DNA molecules can be detected under ultraviolet light by staining the gel with an appropriate dye (P. Y. Lee, Costumbrado, Hsu, & Kim, 2012). In this work, the technique was used to analyse PCR and qRT-PCR products. Separation of target-specific amplification products, with a fragment size between 100 and 200 base pairs (bp), was carried out in a 2 % agarose gel. To prepare the agarose gel, 1 g agarose (PeqGOLD Universal, PEQLAB GmbH, VWR Life Science Competence) was weighed using

the Analytical balance ABT 220-5 DNM (Kern & Sohn GmbH, Bahlingen, Germany) and was dissolved in 50 ml 1x TBE buffer (described in section 3.1.4). The solution was heated with the Microwave MW 7849 900W (Severin, Sundern, Germany) until the agarose crystals were completely dissolved. After cooling the solution to 52 °C, 3 μl of peqGREEN 20000X DNA/RNA binding dye (VWR, Radnor, PA) were added to 50 ml agarose solution. According to the manufacturer, peqGREEN is a non-toxic and ecofriendly dye with a sensitivity comparable to ethidium bromide and was used to detect nucleic acids. The prepared agarose solution was poured into a gel tray with the well comb in place. Once solidified, the agarose gel was transferred into a gel chamber (Gel chamber Sub-Cell Modell 96, Bio-Rad Laboratories GmbH) filled with 1x TBE buffer. To check the amplification products of PCR, the complete PCR reaction (20 μl) was mixed with 4 μl of the 6x DNA Gel Loading Dye (Thermo Scientific^{TM}, Thermo Fisher Scientific). To check the amplification products of qRT-PCR, 4 μl of the qRT-PCR product were mixed with 16 μl of aq. bidest. and 4 μl of the 6x DNA Gel Loading Dye (Thermo Scientific^{TM}, Thermo Fisher Scientific). The markers used to assess the DNA fragment sizes were either Quantitas DNA Marker 25-500 bp (Biozym Scientific GmbH, Hessisch Oldendorf, Germany) or GeneRuler^{TM} 100 bp DNA Ladder (Thermo Scientific^{TM}, Thermo Fisher Scientific). 1 μl of the appropriate marker was mixed with 19 μl of aq. bidest. and 4 μl of the 6x DNA Gel Loading Dye (Thermo Scientific^{TM}, Thermo Fisher Scientific). Marker mixture was carefully loaded into the first sample well of the gel. Then, DNA samples were loaded into the additional sample wells. Gel electrophoresis was performed with the PowerPac Basic Power supply (Bio-Rad Laboratories GmbH) at 120 V for 40 minutes. Finally, DNA bands were visualized directly upon illumination with ultraviolet light, using the Gel documentation instrument ChemDoc XR System (Bio-Rad Laboratories GmbH) and the software Image Lab^{TM} 4.0 (Bio-Rad Laboratories GmbH, München, Germany).

3.3.8 Sequence analysis

Purification of plasmids and PCR products was performed with the High Pure PCR Product Purification Kit (Sigma-Aldrich, Merck Millipore, Merck KGaA) according to the manufacturer's instructions. Spectrophotometric assessment of the concentration and the purity of plasmids and PCR products was carried out with NanoDrop 2000c spectrophotometer (Thermo Fisher Scientific) (described in section 3.3.3). To determine quality and DNA fragment sizes, an agarose gel electrophoresis was performed (described in section 3.3.7). Plasmid and PCR product sequencing was executed by Eurofins GmbH (Ebersberg, Germany). The respective sequencing requirements are summarized in table 25.

Table 25: Sequencing requirements (Eurofins GmbH)

Sample	Concentration	Volume	Oligonucleotide concentration	Oligonucleotide volume
Plasmid DNA	50-100 ng/μl	15 μl	10 pmol/μl	2 μl
PCR product	1 ng/μl (150-300 bp) 5 ng/μl (300-1000 bp) 10 ng/μl (1000-3000 bp)	15 μl	10 pmol/μl	2 μl

Abbreviations: **DNA**: deoxyribonucleic acid; **PCR**: polymerase chain reaction; **bp**: base pair;
All oligonucleotides used for sequencing are listed in table 12.

3.4 Gene editing methods

3.4.1 Gene editing by CRISPR-Cas9 technology

The CRISPR-Cas9 technology is a commonly used molecular biology technique for controlled manipulation and targeting of DNA (Newman & Ausubel, 2016; Doudna & Charpentier, 2014). By inducing targeted deletions, insertions and precise mutations, this technique enables to modify the function of specific genes and regulatory elements in a wide range of cell types and organisms (Sander & Joung, 2014; Hsu, Lander, & Zhang, 2014). The CRISPR-Cas9 technology is derived from the CRISPR-Cas9 system, an adaptive defense system used by many bacteria to protect themselves against viruses or phages (Jinek et al., 2012; Horvath & Barrangou, 2010; Loureiro & Da Silva, 2019). This genetic tool uses the programmable and well-characterized Cas9 endonuclease of *Streptococcus pyogenes* to cut the DNA in the region of interest by introducing a double-strand break (DSB) (Rodríguez-Rodríguez, Ramírez-Solís, Garza-Elizondo, Garza-Rodríguez, & Barrera-Saldaña, 2019). The resulting DNA DSB activates natural DNA repair mechanisms, which include the error-prone non-homologous end joining (NHEJ) and the error-free homology-directed repair (HDR) (Brunner et al., 2019). For controlled and precise gene editing purposes, the HDR mechanism is used to repair the DSB by inserting a specific donor template DNA into the target site (Brunner et al., 2019; Ryu, Hur, & Kim, 2019; Zheng et al., 2014). A schematic overview of the CRISPR-Cas9 system is shown in figure 4. The system is composed of a customed sgRNA that directs the Cas9 nuclease to create a DSB in a specific genomic sequence (Rodríguez-Rodríguez et al., 2019). Additionally, specific target recognition and cleavage of the Cas9 nuclease requires the presence of a protospacer adjacent motif (PAM), a triplet of base pairs with the canonical sequence 5'-NGG-3', flanking the DNA target sequence (Hsu et al., 2014; Gasiunas, Barrangou, Horvath, & Siksnys, 2012; Gleditzsch et al., 2019). The PAM sequence is not a part of the sgRNA.

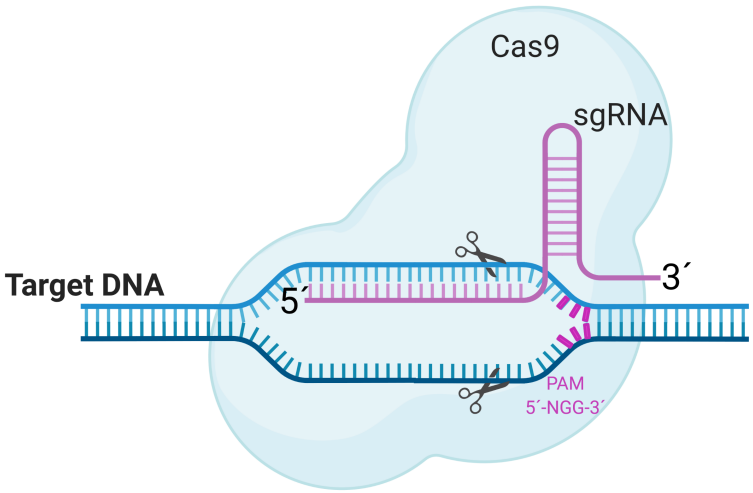

Figure 4: Schematic overview of the CRISPR-Cas9 system
Created with BioRender.com; **Abbreviations**: **DNA**: deoxyribonucleic acid; **sgRNA**: single guide RNA; **PAM**: protospacer adjacent motif

In this work, the CRISPR-Cas9 technology was employed for the generation of an immunotolerant cell line. To this end, the hiPS cell line 'E5V' (parental line), already established in the Division of Experimental Surgery, was genetically-modified. In previous work, a tomato red reporter gene has been introduced in the hiPS cell line 'E5' (described in section 3.1.7), resulting in the cell line denoted as E5V (ventricular). In fact, the tdTomato reporter cassette was inserted downstream of the *MLC2v* gene via homologous recombination using the CRISPR-Cas9 technique. The MLC2v protein is a myosin light chain regulatory protein characteristically expressed in ventricular CMs (Z. Zhang & Nam, 2018). As a robust marker for ventricular maturation during cardiogenesis, the *MLC2v* expression can be used to identify differentiated hiPS cells with a ventricular cardiac phenotype (O'Brien, Lee, & Chien, 1993; Bizy et al., 2013). Consequently, the MLC2v-tdTomato knock-in enables monitoring developing ventricular CMs by their red fluorescence upon directed cardiac differentiation. Furthermore, the E5V cells carry a puromycin resistance gene to enable the selection of successfully manipulated clones by culturing the cells in the presence of puromycin. The puromycin resistance cassette is flanked by locus of X-over P1 (loxP) sites, allowing its excision from the genome by the Cre-recombinase. The Cre-loxP system is a widely used technology for simple manipulation of DNA sequences, which does not require additional co-factors for efficient recombination (Nagy, 2000). The mechanism is based on the enzym Cre-recombinase, which recognizes two directly repeated loxP sites, excises the loxP flanked DNA and catalyzes the recombination between the target sites (Nagy, 2000; H. Kim, Kim, Im, & Fang, 2018). In this work, the Cre-LoxP system was employed to remove the puromycin resistance from the E5V cell line, resulting in the resistance-free cell line called E5Vf (free of resistance). Finally, the CRISPR-Cas9 technology was employed to knock out the *B2M* gene in the resistance-free E5Vf cell line (wild-type) via homologous recombination (described in section 3.4.8). This homozygous knockout of the *B2M* gene has the potential to cause the disruption of the MHC-I and thereby

prevent normal expression of MHC-I on the cell surface. To this end, exons 2 and 3 of the *B2M* gene were replaced on one or both alleles by a neomycin resistance cassette. Successfully edited clones were selected by culturing the cells in the presence of neomycin. Surviving clones were expanded and analyzed for the correct insertion of the donor construct. The resulting double transgenic cell line was called E5V ΔPB (free of puromycin and *B2M*). The workflow for the generation of the double transgenic E5 cells is shown in figure 5.

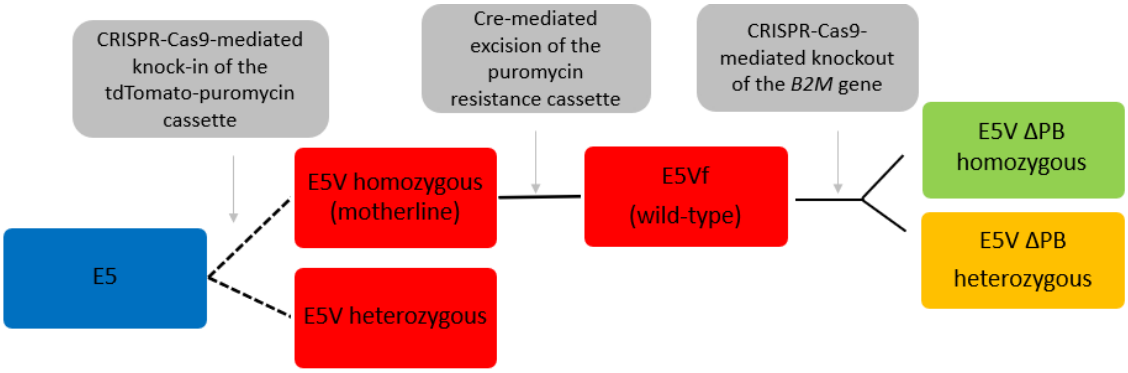

Figure 5: Schedule for the generation of double transgenic E5 cells
Created with BioRender.com; **Abbreviations**: **hiPS cells**: human induced pluripotent stem cells; **B2M**: β2-microglobulin

3.4.2 Generation of the resistance-free cell line E5Vf

In this work, the Cre-LoxP system was employed to remove the puromycin resistance from the E5V cell line. To cut out the resistance cassette, the hiPS cells were transfected with a Cre-recombinase expression vector. A schematic overview of the Cre-LoxP system is shown in figure 6.

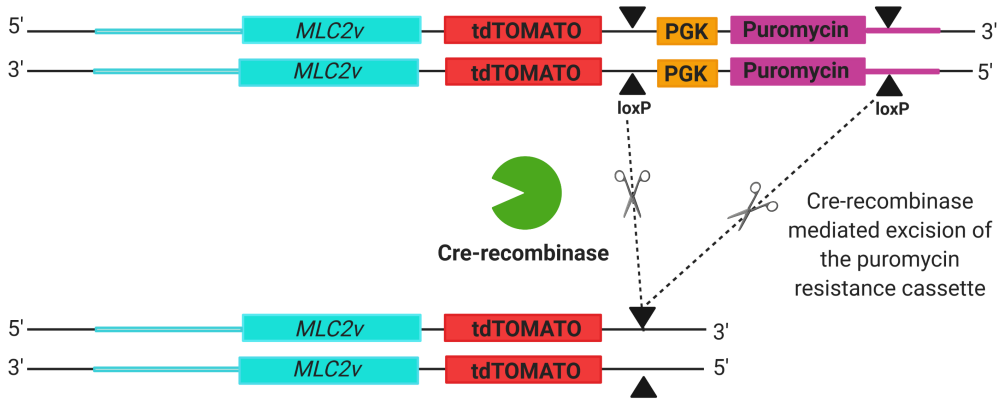

Figure 6: Cre-LoxP system
Created with BioRender.com; **Abbreviations**: **PGK**: phosphoglycerate kinase promoter; **loxP**: locus of X-over P1; **MLC2v**: myosin light chain-2 ventricular

One day prior to transfection, hiPS cells were plated at a density of 10^5 cells/ml on a

pre-coated 6-well culture plate, containing TeSR™-E8™ (StemCell™ Technologies) culture medium supplemented with CloneR™ (StemCell™ Technologies) (described in section 3.1.4). After reaching 80 % confluency, transfection was carried out according to the UltraCruz® transfection protocol (UltraCruz® transfection plasmid reagent (0.2 ml), Santa Cruz Biotechnology, Dallas, TX). For the transfection, two solutions were freshly prepared. To produce the first solution, 10 μl (1 μg per transfection) of the Cre vector (20 μg) (Santa Cruz Biotechnology) (were diluted into 140 μl of Plasmid Transfection Medium (Santa Cruz Biotechnology) to produce a final volume of 150 μl (Solution A). For the second solution, 10 μl of the UltraCruz® transfection plasmid reagent (Santa Cruz Biotechnology) were diluted into 140 μl of Plasmid Transfection Medium (Santa Cruz Biotechnology) to give a final volume of 150 μl (Solution B). The Cre vector solution (Solution A) was then added dropwise to the UltraCruz® transfection reagent solution (Solution B). Prior to transfection, a medium change was performed with TeSR™-E8™ (StemCell™ Technologies) culture medium and then 300 μl of the Cre vector/UltraCruz® transfection reagent complex (Solution A + Solution B) were added dropwise to each well. One week after transfection, clones were picked manually. Each clone was split to three wells. After expansion, one well was treated with 0.3 μg/ml puromycin (Sigma-Aldrich, Merck Millipore, Merck KGaA). Successfully transfected hiPS cells were sensitive to puromycin and died. To analyze Cre-mediated excision, DNA was extracted from the cells growing in one of the corresponding non-treated wells, as described in section 3.3.2. After assessment of the DNA concentration (described in section 3.3.3), a PCR (described in section 3.3.5) was performed to confirm the removal of the puromycin resistance cassette. The PCR reaction mixture is shown in table 27 and the applied cycling conditions are given in table 26. The oligonucleotide primer sequences used for PCR are given in table 12. All amplification products were visualized in a 2 % agarose gel (described in section 3.3.7) Purification of the amplification products was performed with the High Pure PCR Product Purification Kit (Sigma-Aldrich, Merck Millipore Merck KGaA) according to the manufacturer's instructions. Furthermore, sequencing was executed by Eurofins GmbH (Ebersberg, Germany) (described in section 3.3.8) to confirm the correct excision of the puromycin cassette. Sequencing of non-transfected E5V cells (control) served as reference sequence. The resulting resistance-free cell line was called E5Vf (free of resistance).

Table 26: PCR cycling conditions for detection of the puromycin resistance excision

Cycle step	Reaction	Temperature	Incubation time	Number of cycles
Initial activation		95 °C	2 min	1
Amplification				40
	Denaturation	95 °C	30 s	
	Annealing	60 °C	30 s	
	Extension	72 °C	90 s	
Final extension		72 °C	7 min	1
Hold		4 °C	∞	1

Table 27: Reaction mixture for detection of the puromycin resistance excision

Components	Volume per reaction	Final concentration
DNA template	variable	100 ng
FastStart High Fidelity Reaction Buffer*, 10x	2 µl	1x; 1.8 mM magnesiumchlorid
DMSO*	1 µl	5 %
PCR Grade Nucleotide Mix (200 µM each)*	1 µl	10 µM
Oligonucleotide (forward), 5 µM	1.6 µl	0.4 µM
Oligonucleotide (reverse), 5 µM	1.6 µl	0.4 µM
FastStart High Fidelity Enzyme Blend, 5 U/µl*	0.5 µl	2.5 U per reaction
Water (PCR grade)	filled up to 20 µl	

Abbreviations: **DNA**: deoxyribonucleic acid; **DMSO**: dimethyl sulfoxide; **PCR**: polymerase chain reaction; All * marked components were delivered with the FastStart™ High Fidelity PCR System, dNTPack (Kit) (Sigma-Aldrich, Merck Millipore, Merck KGaA).
Water (PCR grade) was purchased from Roche Applied Science (Penzberg, Germany).

3.4.3 Plasmid and cloning strategies

Donor construct used for the *B2M* knockout

The B2M KO Neo donor construct used for the *B2M* knockout was designed with the Benchling CRISPR gRNA Design program (Available from: https://benchling.com/). The designed donor construct was cloned into the vector pUC57-Simple by GenScript (Leiden, The Netherlands). To confirm correct insertion of the donor construct, a restriction digestion of the modified vector was performed by GenScript (Leiden, The Netherlands). The designed plasmid was then reconstituted according to the manufacturer's instructions and used to transform One Shot ™ TOP 10 Chemically Competent *E. Coli* (Invitrogen™, Thermo Fisher Scientific) (described in section 3.4.5). Plasmid minipreps were performed to isolate plasmid DNA from the transformed bacteria (described in section 3.4.6). After sequence analysis, a midiprep (described in section 3.4.6) was performed from one correct clone and glycerol stocks of the transformed bacteria were prepared (described in section 3.4.6).

sgRNA design

Gene editing was performed with the vector pSpCas9(BB)-2A-Puro (pX459) V2.0 (Addgene, #62988). As precise CRISPR-Cas9 gene targeting requires a customized sgRNA, three sgRNA sequences for exons 2 and 3 were designed with an optimal length of 20 bp, using the Benchling CRISPR gRNA Design program (Available at: https://benchling.com/). Synthesis of the sgRNA oligonucleotides was conducted by Ella Biotech GmbH (Martinsried, Germany) and their sequence is given in table 28.

Table 28: Oligonucleotides used for synthesis of sgRNA

Oligonucleotide	Sequence (5'→3')
B2M Exon2 sgRNA1 top	CACCGACTTGGTGTCAAGCTATATC
B2M Exon2 sgRNA1 bottom	aaacGATATAGCTTGACACCAAGTC
B2M Exon2 sgRNA2 top	CACCGTATTTCACTTGGGGCTAACT
B2M Exon2 sgRNA2 bottom	aaacAGTTAGCCCCAAGTGAAATAC
B2M Exon2 sgRNA3 top	CACCGTTGCCAGGGTATTTCACTTG
B2M Exon2 sgRNA3 bottom	aaacCAAGTGAAATACCCTGGCAAC
B2M Exon3 sgRNA1 top	CACCGTTTTTGTTTCACTGTCCTG
B2M Exon3 sgRNA1 bottom	aaacCAGGACAGTGAAACAAAAAC
B2M Exon3 sgRNA2 top	CACCGCTGTCTATAAATAGTCCTC
B2M Exon3 sgRNA2 bottom	aaacGAGGACTATTTATAGACAGC
B2M Exon3 sgRNA3 top	CACCGCAATGTTCTCCACATAGTGA
B2M Exon3 sgRNA3 bottom	aaacTCACTATGTGGAGAACATTGC

Abbreviations: **B2M**: β-microglobulin; **sgRNA**: single guide RNA; **RNA**: ribonucleic acid;
overhang sequences (black); sgRNA sequences (red)

To clone the designed sgRNA into the pX459 V2.0 vector, a three-step protocol was performed. Annealing of the oligonucleotides (1st step) was carried out in a C1000 Thermal Cycler (Bio-Rad Laboratories GmbH) under defined reaction conditions, specified in table 29. The reaction mixture for the annealing of oligonucleotides is given in table 30.

Table 29: Reaction conditions for the phosphorylation and annealing of oligonucleotides

Temperature	Incubation time
37 °C	30 min
95 °C	5 min
95 °C → 25 °C	5 °C/min (ramp-down rate)

Table 30: Reaction mixture for the phosphorylation and annealing of oligonucleotides

Components	Volume per reaction	Final concentration
Oligonucleotide top (100 μM)	1 μl	10 μM
Oligonucleotide bottom (100 μM)	1 μl	10 μM
10x T4 Ligation Buffer*	1 μl	1x
aq. bidest.	6 μl	
T4 Polynucleotide Kinase PNK (10.000 U/ml)*	1 μl	10 U

Abbreviation: **aq. bidest.**: aqua bidestillata (Latin name for double-distilled water)
All * marked components were purchased from New England Biolabs GmbH (Frankfurt am Main, Germany).

In the following ligation reaction (2nd step), the phosporylated and annealed oligonucleotide duplexes were cloned into the vector backbone. The ligation reaction was carried out in a C1000

Thermal Cycler (Bio-Rad Laboratories GmbH) under defined reaction conditions, specified in table 31. The reaction mixture for the ligation reaction is given in table 32.

Table 31: Ligation reaction conditions

Reaction	Temperature	Incubation time	Number of cycles
Ligation			6
	37 °C	5 min	
	23 °C	5 min	
Hold	4 °C	∞	1

Table 32: Reaction mixture for the ligation

Components	Volume per reaction	Final concentration
Annealed oligonucleotide duplexes (1. step) (1:200 dilution)	2 µl	
vector pSpCas9(BB)-2A-Puro (pX459) V2.0 (Addgene)	1 µl	100 ng
10x Tango buffer (Thermo Fisher Scientific)	2 µl	1x
DTT (10 mM) (Invitrogen™, Thermo Fisher Scientific)	1 µl	0.5 mM
ATP (10 mM) (Thermo Fisher Scientific)	1 µl	0.5 mM
FastDigest BbsI (10 U/µl) (Thermo Fisher Scientific)	1 µl	1 U
T7 DNA Ligase (3,000,000 U/ml) (New England Biolabs GmbH)	0.5 µl	1500 U
aq. bidest.	filled up to 20 µl	

Abbreviations: **aq. bidest.**: aqua bidestillata (Latin name for double-distilled water); **DTT**: dithiothreitol; **ATP**: adenosine triphosphate; **DNA**: deoxyribonucleic acid

After ligation, the ligation reaction mixture was treated with an ATP-dependent DNase to remove non-specific recombination products (3rd step). The reaction mixture (given in table 33) was incubated in the Eppendorf Thermomixer comfort (Eppendorf) at 37 °C for 30 minutes.

Table 33: Reaction mixture for the removal of non-specific recombination products

Components	Volume per reaction	Final concentration
Ligation reaction mixture (2. step)	11 µl	
10x Plasmid-Safe™ buffer⋆	1.5 µl	1x
ATP (10 mM)⋆	1.5 µl	1 mM
Plasmid-Safe™ ATP-Dependent DNase (10 U/µl)⋆	1 µl	0.66 U

Abbreviations: **ATP**: adenosine triphosphate; **DNase**: desoxyribonuclease;
All ⋆ marked components were delivered with the Plasmid-Safe™ ATP-Dependent DNase (10 U/µl) (Biozym Scientific GmbH).

Each customized sgRNA expression vector was transformed into chemically competent *E. coli* (described in section 3.4.5). For each cloned sgRNA, single colonies were picked manually

and plasmid preparations were performed (described in section 3.4.6). A sequence analysis was accomplished to confirm correct insertion of the sgRNA sequence (described in section 3.3.8). Furthermore, glycerol stocks of the successfully transformed bacteria were prepared (described in section 3.4.6).

3.4.4 General conditions for bacterial cell culture

For bacterial culture, the desired bacteria were either suspended in LB medium or plated on LB agar plates (described in section 3.1.5). To obtain a clonal bacterial culture, a single bacterial colony was picked manually and transferred to LB medium or plated on a new agar plate. Incubation of bacterial cultures was carried out at 37 °C in an incubator shaker INFORS HT Ecotron (Infors AG, Bottmingen, Switzerland).

3.4.5 Bacterial transformation

Bacterial transformation is a key step in molecular cloning and is used to introduce foreign plasmid DNA into chemically competent cells (Froger & Hall, 2007). The transformed bacteria then enable the replication of the DNA sequence of interest (Lodish et al., 2000). The workflow for transformation is shown in figure 7. In this work, One Shot ^{TM} TOP 10 Chemically Competent *E. coli* (Invitrogen^{TM}, Thermo Fisher Scientific) were used for bacterial transformation. All plasmids used carried an ampicillin resistance gene to ensure the selection of successfully transformed bacteria by growing them in the presence of ampicillin. For bacterial transformation, 50 μl of the chemically competent *E. coli* cells were thawed on ice. Two μl of the recombinant plasmid were added to the bacterial cells to produce a final concentration of 10 ng/μl. The mixture was incubated on ice for 30 minutes. To introduce the desired plasmid vector into the chemically competent cells, a heat shock protocol was applied. For this step, the mixture of chemically competent bacteria and DNA was placed at 42 °C for 30 seconds (heat shock) in an Eppendorf Thermomixer comfort (Eppendorf AG), allowing the plasmid DNA to enter the bacterial cell through the disrupted cell membrane. After a short incubation on ice (5 minutes), 600 μl SOC medium (described in section 3.1.5) were added and the mixture was placed for 1 hour at 37 °C in an Eppendorf Thermomixer comfort (Eppendorf AG) (1000 rpm). Five and 50 μl of the transformed bacteria were plated onto LB agar plates (10 cm) (Greiner Bio-One International GmbH) in the presence of ampicillin (50 μg/ml). The LB agar plates were incubated upside down overnight at 37 °C in an incubator (Infors AG). For the subsequent plasmid DNA purification and isolation protocol, single bacterial clones were picked manually and transferred to 3 ml LB medium (described in section 3.1.5) supplemented with 100 μg/ml ampicillin sodium salt (Carl Roth GmbH + Co. KG). Tubes were incubated overnight at 37 °C with vigorous shaking (2000 rpm).

3.4.6 Purification and isolation of plasmid DNA from bacteria

Plasmid preparations allow the preparative purification and isolation of plasmid DNA from transformed bacteria. Depending on the amount of required plasmid DNA, different isolation methods were used. For small scale plasmid preparation, the miniprep protocol was applied. To purify larger amounts of plasmid DNA, the midiprep protocol was used.

Small-scale plasmid preparation (Miniprep)

For small-scale plasmid preparation, the QIAGEN Plasmid Mini Kit (Qiagen) was used according to the manufacturer's instructions. The principle of this kit is based on alkaline lysis of bacteria followed by adsorption of their DNA onto a silica column. Subsequent wash steps ensure the removal of remaining contaminants. Finally, a buffer is used to elute the purified plasmid DNA. For the miniprep protocol, single colonies of the transformed bacteria (described in section 3.4.5) were incubated overnight in 3 ml LB medium and 100 μg/ml ampicillin in a shaker incubator (Infors AG) (200 rpm, 16 hours at 37 °C). After the plasmid purification procedure, sequence analysis of the purified plasmid DNA was performed (described in section 3.3.8).

Mid-scale plasmid preparation (Midiprep)

Mini preparations, in which sequencing confirmed the insertion of the sequence of interest, were used for mid-scale plasmid preparation. For midipreps, the QIAGEN Plasmid Midi Kit (Qiagen) was used according to the manufacturer's instructions. For the midiprep protocol, 50 μl of the mini preparation were inoculated in 250 ml LB medium (described in section 3.1.5) supplemented with 100 μg/ml ampicillin. The mixture was incubated overnight in a shaker incubator (Infors AG) (200 rpm, 16 hours at 37 °C). After the plasmid purification procedure, sequence analysis of the purified plasmid DNA was performed (described in section 3.3.8).

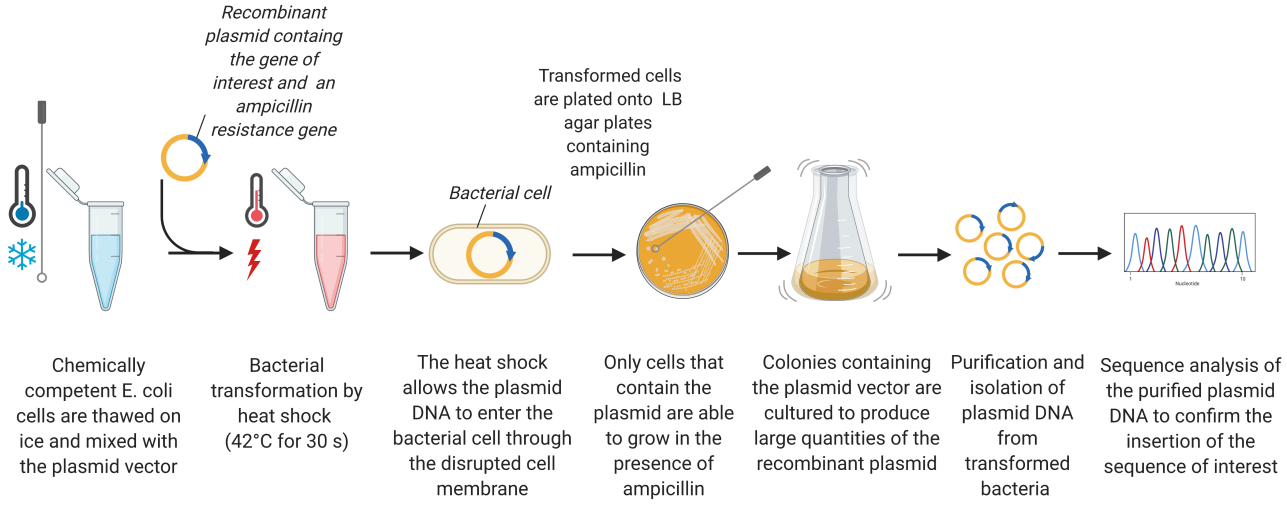

Figure 7: Transformation workflow

Created with BioRender.com; **Abbreviations**: **E. coli**: Escherichia coli; **LB**: Lysogeny broth; **DNA**: deoxyribonucleic acid

Glycerol stock preparation

For long-term storage of transformed bacteria, glycerol stocks of all colonies with confirmed sequence of interest were prepared. For this purpose, 300 μl of glycerol (Carl Roth GmbH + Co. KG) were mixed with 700 μl of bacterial culture and stored at -80 °C.

3.4.7 Cell transfection

Transfection of HEK 293 cells

To determine the sgRNA cleavage efficiency, HEK 293 cells were transfected with the customized sgRNA expression vectors (described in section 3.4.3). Two days prior to transfection, HEK 293 cells were plated at a density of $3x10^5$ cells/well on a 6-well culture plate, containing DMEM/Ham's F12 medium (Biochrom, Merck Millipore, Merck KGaA) supplemented with 5 % FCS (described in section 3.1.4). After reaching 80 % confluency, transfection was carried out according to the Fugene transfection reagent protocol (FuGENE® HD transfection reagent, Promega Corporation, Fitchburg, WI). One day after transfection, the HEK 293 culture medium (described in section 3.1.5) was supplemented with 0.5 μg/ml puromycin (Sigma-Aldrich, Merck Millipore, Merck KGaA) to select successfully transfected HEK 293 cells. DNA was extracted after three days from successfully transfected HEK 293 cells (described in section 3.3.2). After assessment of the DNA concentration (described in section 3.3.3), a PCR was performed to amplify the DNA sequence of interest (described in section 3.3.5). The PCR reaction mixture is shown in table 22 and the applied cycling conditions are given in table 21. The oligonucleotide primer sequences used for PCR are given in table 12. Purification of the amplification products was performed with the High Pure PCR Product Purification Kit (SigmaAldrich, Merck Millipore Merck KGaA) according to the manufacturer's instructions. Sequencing was executed by Eurofins GmbH (Ebersberg, Germany) (described in section 3.3.8). The obtained sequencing chromatograms were loaded into the TIDE webtool (Available from: https://tide.deskgen.com/) and sgRNA cleavage efficiency was determined. Sequencing of non-transfected HEK 293 cells (control) served as reference sequence.

Electroporation

The Human Stem Nucleofector® Kit 1 (Lonza Cologne GmbH, Köln, Germany) was used according to the manufacturer's instructions for transfection of hiPS cells by electroporation. Before proceeding to electroporation, the hiPS cells were washed with 1x D-PBS (described in section 3.1.4). For cell detachment, cells were incubated with Accutase (StemCell™ Technologies) in a HERACell™ 240i CO_2 incubator (Thermo Fisher Scientific) for 5 minutes at 37 °C. Then, Accutase was inactivated by adding twice the amount of TeSR™-E8™ (StemCell™ Technologies) (described in section 3.1.5) culture medium supplemented with ROCK inhibitor Y-27632 (StemCell™ Technologies) (described in section 3.1.4). The detached cells were transferred into a sterile 50 ml Falcon® High Clarity PP Centrifuge Tube (VWR International) (50 ml falcon tube) and a single cell suspension was achieved by carefully pipetting up and down, using a sterile 10 ml Serological Pipette (scale: 0,1 ml; color: orange) (Kisker Biotech GmbH & Co. KG, Steinfurt, Germany). The hiPS cells were pelleted by centrifugation (1000 x rpm, for 5 minutes at RT) and the number of living cells was determined as described in section

3.2.1. 1x10^6 cells were resuspended in 750 μl TeSR^{TM}-E8^{TM} (StemCell^{TM} Technologies) culture medium supplemented with ROCK inhibitor Y-27632 (StemCell^{TM} Technologies). After centrifugation (2800 x rpm, 5 min at RT), the supernatant was aspirated and the cell pellet was resuspended in 100 μl Nucleofector Solution (Lonza Cologne GmbH). 1 μg of the respective donor construct and 1 μg of the respective vectors were then added to the cell suspension. The mixture was transferred into a cuvette provided by the kit. Electroporation was performed with the Nucleofector^{TM} II (Amaxa Biosystems, Lonza Cologne GmbH) by applying the program B-016, which is proposed by the manufacturer.

3.4.8 Generation of the *B2M*-deficient cell line

In this work, the CRISPR-Cas9 technology was employed to knock out the *B2M* gene in the E5Vf cell line via homologous recombination. Exons 2 and 3 of the *B2M* gene were replaced on one or both alleles by a neomycin resistance cassette. The design of the construct used for genome editing is shown schematically in figure 8.

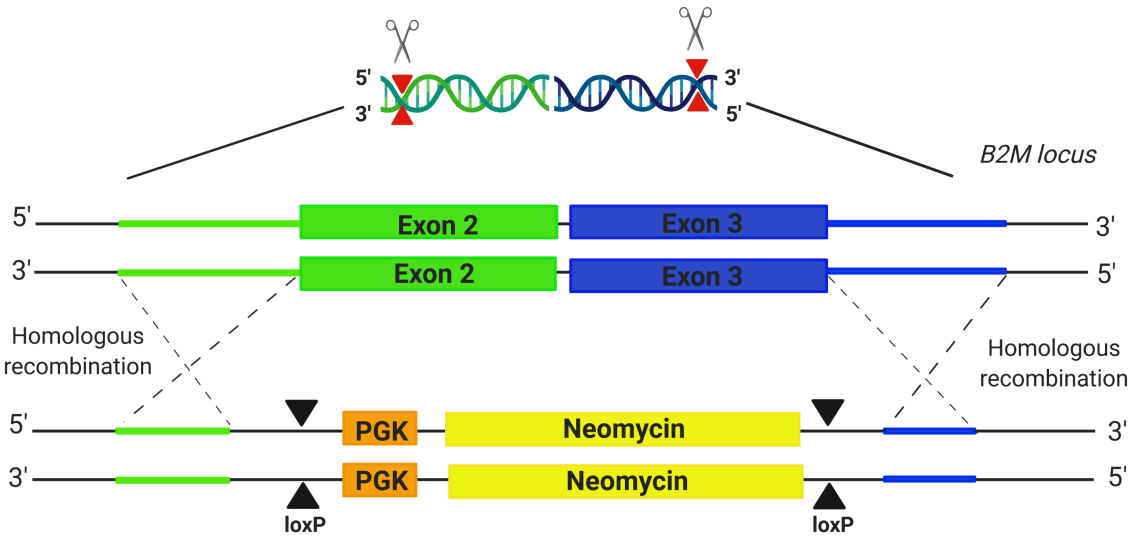

Figure 8: Design of the B2M KO Neo donor construct
Created with BioRender.com; **Abbreviations**: **PGK**: phosphoglycerate kinase promoter; **loxP**: locus of X-over P1; ***B2M***: β-microglobulin

To knock out the *B2M* gene in E5Vf hiPS cells an electroporation protocol was applied (described in section 3.4.7). For cell transfection, 1 μg the B2M KO Neo donor construct

(described in section 3.4.3) and 1 μg of the vectors pX459 Puro V2.0 B2M-Exon2-sgRNA3-clone1 and pX459 Puro V2.0 B2M-Exon3-sgRNA3-clone3 (described in section 3.4.3) were used. After electroporation, 1 ml of TeSR^{TM}-E8^{TM} (StemCell^{TM} Technologies) cell culture medium supplemented with ROCK inhibitor Y-27632 (StemCell^{TM} Technologies) was added into the cuvette and the mixture was incubated for 2-3 minutes at RT. Electroporated cells were then plated on a pre-coated 6-well culture plate (Greiner Bio-One International GmbH) containing 1 ml TeSR^{TM}-E8^{TM} (StemCell^{TM} Technologies) culture medium supplemented with ROCK inhibitor Y-27632 (StemCell^{TM} Technologies). Cells were incubated for two days without medium change. As exons 2 and 3 of the *B2M* gene were replaced on one or both alleles by a neomycin resistance cassette, successfully edited clones could be selected by culturing the cells in the presence of G418. Selection of successfully electroporated cells was started by performing a medium change after two days with TeSR^{TM}-E8^{TM} (StemCell^{TM} Technologies) supplemented with 150 μg/ml G418 (Biochrom, Merck Millipore, Merck KGaA) (described in section 3.1.4). The optimal G418 concentration of 150 μg/ml was determined in preliminary experiments. Surviving clones were picked manually, expanded, and analyzed for correct insertion of the donor construct. To verify CRISPR-Cas9-mediated gene editing, DNA was extracted from successfully electroporated cells as described in section 3.3.2. After assessment of the DNA concentration (described in section 3.3.3), a PCR (described in section 3.3.5) was performed to confirm correct excision of the *B2M* gene. The PCR reaction mixture is shown in table 35 and the applied cycling conditions are given in table 34. The oligonucleotide primer sequences used for PCR are given in table 12. All amplification products were visualized in a 2 % agarose gel (described in section 3.3.7) Purification of the amplification products was performed with the High Pure PCR Product Purification Kit (Sigma-Aldrich, Merck Millipore Merck KGaA) according to the manufacturer's instructions. Furthermore, sequencing was executed by Eurofins GmbH (Ebersberg, Germany) (described in section 3.3.8) to confirm the *B2M* gene knockout. Sequencing of non-transfected E5Vf cells (control) served as reference sequence. The resulting double transgenic cell line was called E5V ΔPB (free of puromycin and *B2M*).

Table 34: PCR cycling conditions for detection of the *B2M* knockout

Cycle step	Reaction	Temperature	Incubation time	Number of cycles
Initial activation		95 °C	15 min	1
Amplification				30-40
	Denaturation	95 °C	30 s	
	Annealing	60 °C	30 s	
	Extension	72 °C	120 s	
Final extension		72 °C	7 min	1
Hold		4 °C	∞	1

Table 35: Reaction mixture for detection of the *B2M* knockout

Components	Volume per reaction	Final concentration
DNA template	variable	100 ng
FastStart High Fidelity Reaction Buffer*, 10x	2 μl	1x; 1.8 mM magnesiumchlorid
DMSO*	1 μl	5 %
PCR Grade Nucleotide Mix*	0.4 μl	200 μM
Oligonucleotide (forward), 2 μM	1.6 μl	0.16 μM
Oligonucleotide (reverse), 2 μM	1.6 μl	0.16 μM
FastStart High Fidelity Enzyme Blend, 5 U/μl*	0.5 μl	2.5 U per reaction
Water (PCR grade)	filled up to 20 μl	

Abbreviations: **DNA**: deoxyribonucleic acid; **DMSO**: dimethyl sulfoxide; **PCR**: polymerase chain reaction; All * marked components were delivered with the FastStart^{TM} High Fidelity PCR System, dNTPack (Kit) (Sigma-Aldrich, Merck Millipore, Merck KGaA).
Water (PCR grade) was purchased from Roche Applied Science (Penzberg, Germany).

3.5 Cell characterization

In this work, the following techniques were employed for molecular characterization of cells. To analyze *B2M* gene expression in the generated hiPS cell clones, total RNA was extracted as described in section 3.3.1 and was converted to cDNA by reverse transcription (described in section 3.3.4). Relative gene expression for *B2M* (NM_004048.4) was then evaluated by qRT-PCR (described in section 3.3.5). The oligonucleotide primer sequences used for qRT-PCR are given in table 3.11. A western blot (WB) analysis (described in section 3.5.3) was carried out to measure the endogenous cellular B2M and MHC-I protein expression. Detection of MHC-I on the surface of the generated homozygous and heterozygous *B2M*-deficient hiPS cell clones was analyzed by fluorescence-activated cell sorting (FACS) (described in section 3.5.2). Furthermore, the selected hiPS cell clones were immunocytochemically stained for MHC-I (described in section 3.5.1). To further characterize and assess the cardiac differentiation potential of the generated *B2M*-deficient homozygous and heterozygous clones, two independent directed cardiac differentiation assays were accomplished as described in section 3.2.4. Upon directed cardiac differentiation, the MLC2v-tdTomato knock-in of the cell lines enabled to track the expression of *MLC2v* over time by documenting the red fluorescence of CMs with the Axiovert 200 M Inverted Fluorescent Microscope (Carl Zeiss AG, Oberkochen, Germany), using the program Carl Zeiss^{TM} Axio Vision Rel. 4.8.2 software (Carl Zeiss AG). Subsequently, cardiac gene expression analysis during directed cardiac differentiation of homozygous and heterozygous *B2M*-deficient hiPS cell clones was compared to wild-type cells (E5V cell line).

3.5.1 Immunocytochemistry (ICC)

Immunocytochemistry (ICC) is a commonly used technique for the detection and visualization of specific proteins and cellular components (Maity, Sheff, & Fisher, 2013; Im, Mareninov, Diaz, & Yong, 2019). This method is based on the employment of a specific fluorescent antibody, which binds to a target antigen and thereby allows visualization under a fluorescent microscope

(Bauer, 2014). In this work, an indirect immunofluorescence staining protocol was applied, in which a secondary antibody labeled with a fluorophore is directed against a primary antibody, which binds to the target epitope (Im et al., 2019; Donaldson, 1998; Barbierato, Argentini, & Skaper, 2012). The protocol consists of 5 essential steps: fixation, permeabilization, blocking, immunostaining and mounting. Two to 3 days prior to ICC, the respective cells are seeded on a pre-coated chamber slide (Millicell EZ SLIDE 4-well glass, sterile, Merck KGaA). After slide preparation, the cells are fixed to preserve cellular morphology and to immobilize target antigens. The following permeabilization step permits exposition of the antigen and allows antibodies to access intracellular epitopes. Furthermore, a blocking serum is used to prevent non-specific binding of the secondary antibody. For immuncytochemistry, the samples were incubated overnight with an optimal dilution, which is given by the manufacturer of the desired primary antibody at 4 °C. The following day, subsequent washing steps are carried out and samples are incubated with the labeled secondary antibody for 1 hour at RT protected from light. All antibodies used for ICC are given in tables 14 (primary antibodies) and 15 (secondary antibodies). Unless otherwise specified, all incubation and washing steps were performed at RT. After completing the staining procedure, the slides are air-dried in the dark and coated with mounting medium (Fluoroshield Mounting Medium with DAPI, Abcam), which contains DAPI and serves as nuclear counterstain. A coverslip (Menzel^{TM} Microscope Coverslips 24x60 mm, Thermo Fisher Scientific) is placed onto the chamber slide and is sealed with nail polish 24 hours later. Visualization of the target antigen and all images of the ICC stainings were generated with the Axiovert 200 M Inverted Fluorescent Microscope (Carl Zeiss AG, Oberkochen, Germany), using the program Carl Zeiss^{TM} Axio Vision Rel. 4.8.2 software (Carl Zeiss AG). In this work, ICC was employed for molecular characterization of the wild-type cells (E5V cell line) after their differentiation into CMs. Furthermore, this technique was used to compare the MHC-I expression of the generated homozygous and heterozygous *B2M*-deficient hiPS cell clones (E5V ΔPB cell lines) to the MHC-I expression of wild-type cells (E5Vf cell line).

ICC for characterization of CMs

Two to 3 days prior to ICC, differentiation medium was removed and beating CMs were detached with TrypLE^{TM} Select Enzym 10x (Thermo Fisher Scientific) according to the manufacturer's instructions. After detachment, CMs were transferred into a sterile 15 ml falcon tube, which was filled up to 15 ml with sterile D-PBS (described in section 3.1.4). The suspension was centrifugated for 8 minutes at 300 x g, RT. After removing the supernatant, CMs were resuspended in cardiac differentiation medium CDM3 (described in section 3.1.5) and the cells were seeded on a pre-coated chamber slide (Merck KGaA). On the day of ICC, CMs were washed for 5 minutes with 1x D-PBS (described in section 3.1.4) and fixed for 15 minutes with 4 % PFA solution (described in section 3.1.4). After two subsequent washing steps (0.1 % PBS-T for 5 minutes), blocking was performed for 30 minutes with 10 % normal goat serum (described in section 3.1.4) in PBS-T (0.1 %) to prevent non-specific antibody binding. Subsequently, cells were washed twice (0.1 % PBS-T for 5 minutes) and then incubated overnight at 4 °C with the respective primary antibody. All primary antibodies with their corresponding diluting solution are given in table 36. CMs on day 30 and 60 of the directed cardiac differentiation protocol (described in section 3.2.4) were analyzed immunocytochemically for the expression of cardiac troponin T (TNNT2), a key marker for CMs and sarcomeric

α-actinin, which is a key structural protein of the sarcomere (Waas et al., 2019; Lichter et al., 2014). Furthermore, cells were stained for MLC2a, a marker for atrial CMs, and MLC2v, a marker for ventricular CMs (Ichimura et al., 2020; Bedada, Wheelwright, & Metzger, 2016). An anti-red fluorescent protein (RFP) antibody was used for the detection of tdTomato and thereby enabled monitoring the MLC2v-tdTomato knock-in of the E5V cell line.

Table 36: Primary antibodies and their corresponding diluting solution for the ICC of CMs

Primary antibody	Diluting solution
Anti-Cardiac Troponin T antibody [1C11], mouse monoclonal IgG1	0.1 % PBS-T containing 1.5 % goat serum (dilution 1:200)
Anti-Myosin Light Chain 2 (MYL2) antibody (synonym MLC2v), rabbit polyclonal IgG	0.1 % PBS-T containing 1.5 % goat serum (dilution 1:200)
Anti-Myosin Light Chain 7 (MYL7) antibody (synonym MLC2a), mouse monoclonal IgG2b	0.1 % PBS-T containing 1.5 % goat serum (dilution 1:400)
Anti-RFP antibody (FITC), rabbit polyclonal IgG	0.1 % PBS-T containing 1.5 % rabbit serum (dilution 1:500)
Anti-Sarcomeric Alpha Actinin antibody [EA-53], mouse monoclonal IgG1	0.1 % PBS-T containing 1.5 % goat serum (dilution 1:200)

The following day, four washing steps were carried out (0.1 % PBS-T for 5 minutes) and cells were incubated with the respective secondary antibodies for 1 hour protected from light. All secondary antibodies with their corresponding diluting solution are given in table 37. Finally, cells were washed four times for 5 minutes with 1x D-PBS and once for 5 minutes with aq. bidest.

Table 37: Secondary antibodies and their corresponding diluting solution for the ICC of CMs

Primary antibody	Secondary antibody	Diluting solution
Anti-Cardiac Troponin T antibody [1C11]	Goat Anti-Mouse IgG H&L (Alexa Fluor© 488)	1 % BSA in 0.1 % PBS-T (dilution 1:500)
Anti-Myosin Light Chain 2 (MYL2) antibody (synonym MLC2v)	Goat Anti-Rabbit IgG H&L (Alexa Fluor© 488)	1 % BSA in 0.1 % PBS-T (dilution 1:500)
Anti-Myosin Light Chain 7 (MYL7) antibody (synonym MLC2a)	Goat Anti-Mouse IgG H&L (Alexa Fluor© 488)	1 % BSA in 0.1 % PBS-T (dilution 1:500)
Anti-RFP antibody (FITC)	Antibody is directly FITC-labeled	0.1% PBS-T containing 1.5% rabbit serum (dilution 1:500)
Anti-Sarcomeric Alpha Actinin antibody [EA-53]	Goat Anti-Mouse IgG H&L (Alexa Fluor© 488)	0.1% PBS-T containing 1.5% goat serum (dilution 1:500)

ICC for MHC-I detection

Furthermore, ICC was performed to compare the MHC-I expression of the generated homozygous and heterozygous *B2M*-deficient hiPS cell clones (E5V ΔPB cell lines) to the MHC-I expression of wild-type cells (E5Vf cell line). After ICC preparation procedure, cells were incubated overnight at 4 °C with the primary anti-HLA-ABC monoclonal antibody (W6/32) (MA5-11723, Invitrogen^{TM}, Thermo Fisher Scientific), which was diluted in 0.1 % PBS-T with 1.5 % normal goat serum (1:75 dilution). The following day, two washing steps were carried out (0.1 % PBS-T for 5 minutes). Protected from light, the cells were incubated for 1 hour with secondary goat anti-mouse IgG H&L antibody (Alexa Fluor© 488) (ab150113, Abcam), which was diluted in 0.1 % PBS-T with 1.5 % normal goat serum.

3.5.2 Fluorescence-activated cell sorting (FACS)

Flow cytometric analysis is a technology used to count, identify, and characterize single cells in suspension (McKinnon, 2018; Adan, Alizada, Kiraz, Baran, & Nalbant, 2017). The basic principle of flow cytometry relies on a fluidic system, that navigates single cells through a cytometer for interrogation by focused laser beams (Radcliff & Jaroszeski, 1998; Cossarizza et al., 2017). Emitted optical signals are then captured by detectors and light scattering features can be extracted (McKinnon, 2018). Scattered light is collected at two angles: forward scatter (FSC) and side scatter (SSC). This enables categorization of cells by size (FSC) and internal complexity (SSC) (Rowley, 2012). FACS is a derivative of flow cytometry, which uses a fluorescence detection system to analyze the expression of cell surface markers (Basu, Campbell, Dittel, & Ray, 2010). Phenotype detection is based on the application of fluorescent-labeled antibodies that bind to specific cell-associated molecules/markers (Liao, Makris, & Luo, 2016). The antibodies used for FACS analysis are given in tables 14 (primary antibodies) and 15 (secondary antibodies). In this work, FACS analysis was employed to characterize the E5V ΔPB cell line, by detection of the MHC-I on the surface of generated homozygous and heterozygous hiPS cell clones (described in subsection 3.5.2). Furthermore, this technique was performed to identify and quantify specific immune cell subpopulations within a heterogeneous population, by labeling cell specific surface markers with fluorescein isothiocyanate (FITC)-conjugated staining antibodies. Moreover, FACS was used to assess the purity of isolated immune cell subpopulations, after their enrichment by MACS system (described in section 3.6.3). For flow cytometric assays, all cells were resuspended in 300 μl FACS buffer (described in section 3.1.4) and cell detection was carried out in a BD LSRFortessa^{TM} flow cytometer (BD Biosciences, Becton, Dickinson and Company, San Jose, CA) using the software BD FACSDiva^{TM} Version 8.0.1 (BD Biosciences, Becton, Dickinson and Company). Analysis of flow cytometric data was carried out with the software FlowJo Version 7.6.5 (FlowJow LLC).

FACS for MHC-I detection

Among other applications, FACS was performed to compare the MHC-I expression on the surface of the generated homozygous and heterozygous *B2M*-deficient hiPS cell clones (E5V ΔPB cell lines) to the MHC-I expression of wild-type cells (E5Vf cell line). For FACS analysis, single-cell suspensions were prepared for the respective hiPS cell clones as described in section 3.2.2. The cell suspensions were then centrifugated for 8 minutes at 300 x g, RT. After removal of the supernatant, the cells were washed for 5 minutes with 1x D-PBS (described in section 3.1.4). To prevent non-specific antibody binding, a blocking step was carried out for 30 minutes with 5 % normal goat serum (described in section 3.1.4) in PBS-T (0.1 %). After a subsequent washing step (0.1 % PBS-T for 5 minutes), the cells were incubated for 30 minutes at 4 °C with the primary anti-HLA-ABC monoclonal antibody (W6/32) (MA5-11723, Invitrogen^{TM}, Thermo Fisher Scientific), which was diluted in 0.1 % PBS-T with 1.5 % normal goat serum (1:40 final dilution). Next, the cells were washed for 5 minutes with 1x D-PBS. Subsequently, the cells were incubated with the secondary goat anti-mouse IgG H&L antibody (Alexa Fluor© 488) (ab150113, Abcam) for 2 hours protected from light, which was diluted in 0.1 % PBS-T with 1.5 % normal goat serum (1:1000 final dilution). Finally, the cells were washed for 5 minutes with 1x D-PBS. Cells were pelleted by centrifugation (300 x g, 10 minutes at RT) and

were resuspended in 300 μl FACS buffer (described in section 3.1.4).

3.5.3 Western Blot (WB)

Western blotting (WB) is an analytical technique used for detection of specific proteins within a complex protein mixture (Mahmood & Yang, 2012; Eslami & Lujan, 2010). For protein analysis, extracted proteins are separated by gel electrophoresis based on their molecular weight and are blotted from the gel to a membrane support (Eslami & Lujan, 2010; Hnasko & Hnasko, 2015). This step is followed by selective immunodetection of target proteins with specific antibodies (Hnasko & Hnasko, 2015). In this work, WB analysis was carried out to measure endogenous cellular B2M and MHC-I protein expression of the generated homozygous and heterozygous E5V ΔPB clones. Unedited E5Vf hiPS cells (wild-type) served as control reference. For protein extraction, the cell culture medium was aspirated and the cells were washed with 1x D-PBS. After detaching the hiPS cells with ReLeSR^{TM} (StemCell^{TM} Technologies), they were pelleted by centrifugation (14,000 x g, 10 minutes at 4 °C). The supernatant was aspirated and the pellet was dissolved in 100 μl cold RIPA buffer (Cell Signaling Technology). Cell lysis was achieved by repeatedly pipetting up and down and the cell lysate was then incubated on ice for 30 minutes. Protein isolation was accomplished by centrifugation (16,000 x g, 15 minutes at 4 °C) and then protein quantification for each cell lysate was performed using the Pierce^{TM} BCA Protein Assay Kit (Pierce technology, Thermo Fisher Scientific) according to the manufacturer's instructions. The colorimetric readout was carried out with the device Infinite® 200 PRO (Tecan, Tecan Group AG, Männedorf, Switzerland) using the i-control^{TM} Microplate Reader Software Version 2.0 (Tecan, Tecan Group AG) at a wavelength of 562 nm. Determination of the protein concentration was achieved by comparing absorbance values of the protein samples (in duplicates) to a standard curve. The standard curve was obtained by diluting Pierce^{TM} Bovine Serum Albumin Standard Ampules (Pierce Technology, Thermo Fisher Scientific) with Nuclease Free Water (Invitrogen^{TM}, Thermo Fisher Scientific) to produce a dilution series (in duplicates) over a working range from 2 to 25 μg protein. For gel electrophoresis, 50 μg of the protein samples were mixed with 4x Laemmli Sample Buffer (Bio-Rad Laboratories GmbH) and the reducing agent β-mercaptoethanol (Gibco®by Life Technologies ^{TM}, Thermo Fisher Scientific) (9:1 ratio) to obtain a final volume of 50 μl. Protein denaturation was carried out in an Eppendorf Thermomixer comfort (Eppendorf) by boiling the mixture for 5 minutes at 95 °C. Fifty μg of the purified protein samples were then loaded into the wells of a Mini-Protean® TGX Stain-Free^{TM} Protein Gel (Bio-Rad Laboratories GmbH), which enables separation of proteins with a size of 2-400 kDa. To achieve uniform separation of proteins in the gel, diluted Laemmli sample buffer was added to all empty wells. The Color Prestained Protein Standard, Broad Range (11-245 kDa) (New England Biolabs, Ipswich, MA) was used as a molecular weight marker to estimate the size of separated proteins. The gel was then placed in a Bio-Rad Mini Protean® Tetra Cell System (Bio-Rad Laboratories GmbH), containing 1x Tris-glycine-SDS buffer (described in section 3.1.4) and gel electrophoresis was run at 300 V for 20 minutes. To further analyze the proteins, they were transferred onto a membrane using the Trans-Blot® Turbo^{TM} Mini PVDF Transfer Pack (Bio-Rad Laboratories GmbH) and the Trans-Blot® Turbo^{TM} Transfer System (Bio-Rad Laboratories GmbH) according to the manufacturer's instructions. After protein transfer, a blocking step was per-

formed with a 5 % milk powder solution (described in section 3.1.4) for 1 hour at RT to prevent non-specific antibody binding. After washing the membrane twice with deionized water, the immunodetection protocol was started to identify specific proteins blotted to the membrane. The rabbit monoclonal anti-beta 2 microglobulin antibody (ab75853, Abcam) was used to detect B2M protein expression and was diluted in 1x PBS-T with 3 % BSA (described in section 3.1.4) (1:5000 final dilution). The anti-HLA-ABC mouse monoclonal IgG2a antibody (W6/32) (MA5-11723, InvitrogenTM, Thermo Fisher Scientific) was used to detect MHC-I protein expression and was diluted in 1x PBS-T with 3 % BSA (described in section 3.1.4) (final dilution 1:100). Each blot was incubated with the respective primary antibody in a 50 ml falcon tube overnight at 4 °C on a Stuart^{TM} Analogue Rocker & Roller Mixer (Sigma-Aldrich, Merck KGaA) (33 rpm). After washing the membrane three times with 1x PBS-T for 10 minutes at RT, the membrane was incubated with a horseradish peroxidase (HRP)-conjugated secondary antibody, which binds specifically to the first antibody and enables chemiluminescent detection of target proteins. The goat polyclonal secondary anti-rabbit IgG antibody, (H+L) HRP conjugate (AP307P, Sigma-Aldrich) was used to bind the anti-B2M primary antibody and was diluted 1:5000 in 2.5 % milk powder solution (described in section 3.1.4). The goat secondary anti-mouse IgG-HRP antibody (sc-2005, Santa Cruz Biotechnology, Inc.) was used to bind the anti-MHC-I primary antibody and was diluted 1:10,000 in 2.5 % milk powder solution (described in section 3.1.4). Each blot was incubated with the respective secondary antibody in a 50 ml falcon tube for 1 hour at RT on a Heidolph Polymax 1040 Platform Shaker (ProfiLab24 GmbH, Berlin, Germany). After incubation, the membrane was washed three times with 1x PBS-T for 15 minutes. To visualize the proteins of interest, a chemiluminescence-based method was applied. After completing preparation according to the manufacturer's instructions, the chemiluminescent substrate SuperSignal^{TM} West Dura Extend Duration Substrate (Thermo Fisher Scientific) was pipetted onto the blot and enabled detection of the HRP-conjugated secondary antibody by light emission. Detection of chemiluminescence and visualization of the target proteins were carried out with the device ImageQuant LAS 4000 (GE Healthcare Life Sciences, General Electric Company, Boston, MA) using the software ImageQuant LAS 4000.

3.6 Immunological methods

In this work, two different methods were established to analyse and quantify the cell-mediated immune response against the generated *B2M*-deficient cell line E5V ΔPB. For this purpose, PBMCs were isolated from the peripheral blood of healthy donors. Subsequently, different immune cell subpopulations were isolated from peripheral blood mononuclear cells (PBMCs) to perform immune cell-based assays and to study the cytotoxic immune response.

3.6.1 Preparation of peripheral whole blood

Before using peripheral whole blood for FACS analysis, red blood cell lysis needs to be performed. For this purpose, 150 μl of peripheral whole blood, collected in a BD Vacutainer® CPT^{TM} Mononuclear Cell Preparation Tube (Sodium Heparin) (BD Biosciences, Becton, Dickinson and Company) were transferred to a 15 ml falcon tube and were treated with 5 ml of 1x red cell lysis buffer [10x Red cell lysis buffer (Miltenyi Biotec, Bergisch Gladbach, Germany)

diluted 1:10 with reagent-grade water] for 5 minutes. After red cell lysis, the falcon tube was filled up to 15 ml with sterile 1x D-PBS and all cells were pelleted by centrifugation (300 x g, 10 minutes at RT). Subsequently, the supernatant was aspirated and the cell pellet was resuspended in 300 μl FACS buffer (described in section 3.1.4).

3.6.2 Separation of peripheral blood mononuclear cells from peripheral whole blood

For isolation of PBMCs, peripheral whole blood was collected in two BD Vacutainer® CPT™ Mononuclear Cell Preparation Tubes (Sodium Heparin) (BD Biosciences, Becton, Dickinson and Company). Next, blood samples were mixed by repeated inversion and were centrifugated at 1,500 x g for 30 minutes at RT. Following density gradient centrifugation, whole blood was separated into several phases. Half of the upper plasma layer was carefully removed without disturbing the buffy coat (concentrated suspension of PBMCs). The buffy coat was then transferred to a 15 ml falcon tube and filled up to 15 ml with sterile 1x D-PBS. After careful inversion, the PBMCs were pelleted by centrifugation (300 x g, 15 minutes at RT). The supernatant was aspirated and the cell pellet was resuspended in 10 ml sterile 1x D-PBS and centrifuged (300 x g, 15 minutes at RT). Subsequently, the supernatant was aspirated and the cell pellet was dissolved in 1 to 2 ml D-PBS. The viability and cell number of PBMCs was determined as described in section 3.2.1. The workflow for PBMCs isolation from peripheral whole blood is shown in figure 9.

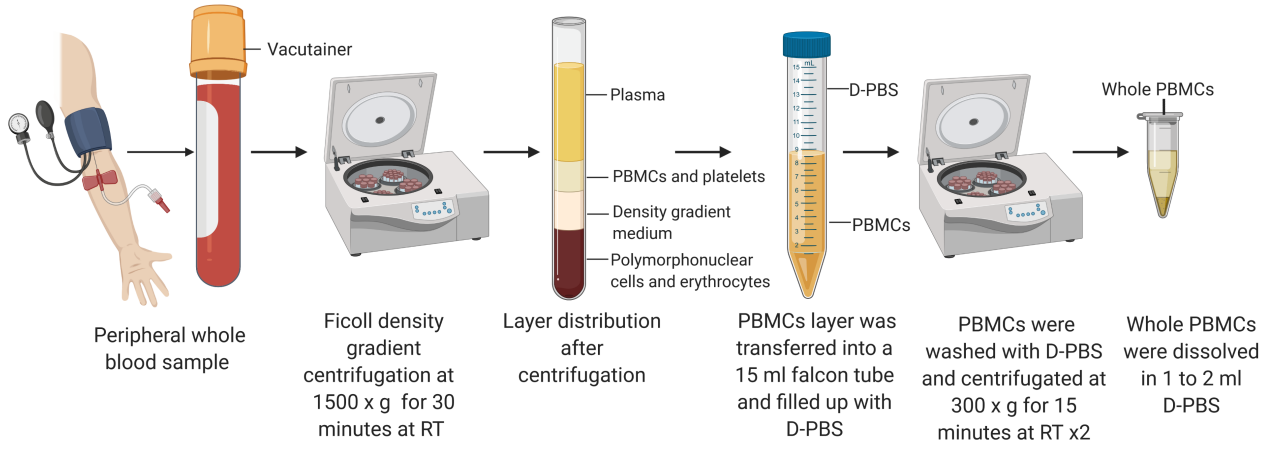

Figure 9: Workflow for PBMCs isolation
Created with BioRender.com; **Abbreviations**: **PBMCs**: peripheral blood mononuclear cells; **D-PBS**: Dulbecco's phosphat buffered saline; **RT**: room temperature

3.6.3 Isolation of immune cell subpopulations by MACS

Magnetic cell sorting (MACS) is a technique used for immunomagnetic separation of heterogeneous cell populations based on their specific surface antigens (cluster of differentiation (CD) markers) (Miltenyi, Müller, Weichel, & Radbruch, 1990; Plouffe, Murthy, & Lewis, 2015). This

method uses specific antibodies coupled to magnetic beads that bind to target cells expressing the epitope of interest (Waseem, Allen, Schreier, Udomsangpetch, & Bhakdi, 2014). In this work, the MACS® MicroBead Technology (Miltenyi Biotec), a column-based magnetic cell isolation method, was employed according to the manufacturer's instructions to perform the enrichment of immune cell subpopulations. To conduct immune cell-based assays, T-lymphocytes (CD3+), cytotoxic T-lymphocytes (CD8+) and NK cells (CD16+) were isolated from PBMCs based on their CD molecules. For immune cell isolation, isolated PBMCs (described in section 3.6.2) were first split to three equal aliquots and were then pelleted by centrifugation (300 x g, 10 minutes at 4 °C). The supernatant was aspirated and the pellet was dissolved in autoMACS Running Buffer (MACS separation buffer) (Miltenyi Biotec). The cells were then incubated with antibody-conjugated magnetic beads (20 μl anti-CD3 per 10^7 total cells, 20 μl anti-CD8 per 10^7 total cells, 50 μl anti-CD16 MicroBeads per $5x10^7$ total cells, human, Miltenyi Biotec) for 15 or 30 minutes at 4 °C, which labeled cells expressing the respective CD marker. For subsequent flow cytometric analysis, 2 μl of the corresponding FITC-labeled staining antibody (anti-CD3-FITC, anti-CD8-FITC, anti-CD16-FITC, human, Miltenyi Biotec) were added to each cell suspension (1:50 final dilution) and incubated for 5 minutes at 4 °C. Two ml MACS separation buffer were added to each cell suspension and centrifugated at 300 x g for 10 minutes at 4 °C. The supernatant was aspirated and the cells were resuspended in 500 μl MACS separation buffer. To prepare the magnetic separation, MS Columns (Miltenyi Biotec) were placed in the magnetic field of the OctoMACSTM Separator (Miltenyi Biotec) and were equilibrated with 500 μl MACS separation buffer. Each cell suspension was pipetted onto an individual column and a 15 ml falcon tube was used to collect the flow-through. The magnetic field enabled separation of target cells by positive selection. Magnetically labeled cells (CD3+, CD8+, CD16+) were retained, while unlabeled cells (CD3-, CD8-, CD16-) flowed through. After subsequent washing steps with MACS separation buffer, the columns were removed from the magnetic field and placed onto a new 15 ml falcon tube. One ml MACS separation buffer was applied onto each column and a provided plunger was pressed down firmly to recover the labeled target cells (CD3+, CD8+, CD16+). After enrichment by MACS system, cell viability and purity of the magnetically separated immune cell subpopulations were determined using FACS. The workflow for isolation of immune cell subpopulations is shown in figure 10.

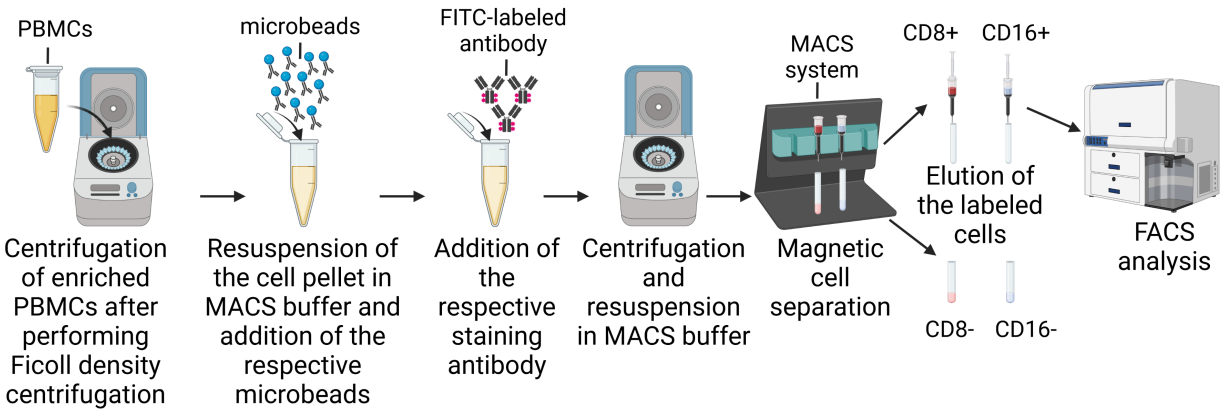

Figure 10: Workflow for isolation of immune cell subpopulations with specific antibodies using MACS system

Created with BioRender.com; **Abbreviations**: **PBMCs**: peripheral blood mononuclear cells; **MACS**: magnetic cell sorting; **FACS**: fluorescence-activated cell sorting; **FITC**: fluorescein isothiocyanate

3.6.4 FACS analysis of PBMCs

In this thesis, FACS analysis was employed to compare the heterogeneity and the FCS/SSC flow cytometric profile of isolated PBMCs to peripheral whole blood. To this end, a peripheral whole blood sample was prepared (described in section 3.6.1) and PBMCs were isolated from peripheral whole blood as described in section 3.6.2. The samples were then examined using FACS (described in section 3.5.2). Finally, the software FlowJo Version 7.6.5 (FlowJow LLC) was used to analyze the cytograms of both, the peripheral whole blood and the PBMC sample, and to identify different immune cell subpopulations by cluster analysis.

3.6.5 Determination of immune cell subpopulations frequencies

Furthermore, FACS analysis (described in section 3.5.2) was performed to quantify the relative frequencies of lymphocyte subpopulations. The percentage of T-lymphocytes, cytotoxic T-lymphocytes and NK cells was determined by labeling the cells with specific antibodies that target their CD markers. In this thesis, the peripheral blood lymphocyte cell subset distribution was studied to support the interpretation of the performed immune cell-based assays. For this purpose, PBMCs were isolated from peripheral whole blood (described in section 3.6.2). The isolated cells were then distributed to four equal aliquots and were pelleted by centrifugation (300 x g, 10 minutes at 4 °C). The supernatant was aspirated and the pellet was resuspended in

98 μl FACS buffer (described in section 3.1.4). One aliquot served as unstained control sample and the remaining aliquots were incubated with 2 μl of a FITC-labeled staining antibody (anti-CD3-FITC, anti-CD8-FITC, anti-CD16-FITC, human, Miltenyi Biotec) for 10 minutes at 4 °C in the dark. After incubation, the cells were washed with 1 ml FACS buffer and centrifugated at 300 x g for 10 minutes. The supernatant was aspirated and the pellet was resuspended in 300 μl FACS buffer. FACS analysis was carried out to investigate the frequencies of T-lymphocytes (CD3+), cytotoxic T-lymphocytes (CD8+) and natural killer (NK) cells (CD16+), respectively. A sequential gating strategy for each flow panel was performed based on the unstained PBMC control sample.

3.7 Methods for interpretation and quantification of the immune response

To analyze and quantify the cell-mediated immune response against the generated *B2M*-deficient E5V ΔPB cell line, two different immune cell-based assays were established within the scope of this thesis.

3.7.1 Quantification of the immune response by measuring gene expression of secretory factors and cytokines

A first immune cell-based assay was developed within the framework of this thesis, in the attempt to further evaluate the immunogenicity of hiPS cells. By co-culturing hiPS cells with PBMCs, this assay aims to characterize and quantify the immune response by analyzing specific immune regulatory gene expression. Upon stimulation with allogeneic cells, PBMCs are activated enabling the detection of proliferative and cytokine responses. Furthermore, studying the transcriptional profile of stimulated PBMCs may provide a better understanding of the involved immune response regulatory mechanisms. For immune response evaluation, cells were harvested after 72 hours of co-culture, which was determined in preliminary experiments (described in section 3.7.1). Next, total RNA was extracted as described in section 3.3.1 and converted to cDNA by reverse transcription (described in section 3.3.4). Relative gene expression for *GZMB* (NM_004131.6), *interferon gamma (IFNγ)* (NM_000619.3), *IL2* (NM_000586.4) and *IL10* (NM_000572.3) in stimulated PBMCs was then analyzed by qRT-PCR (described in section 3.3.5). The oligonucleotide primer sequences used for qRT-PCR are given in table 11. An overview of the assay workflow is shown in figure 11.

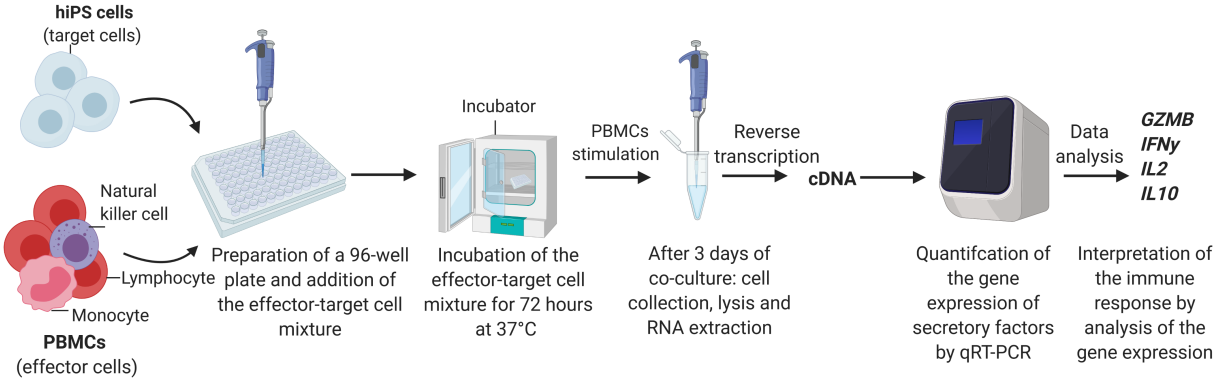

Figure 11: Interpretation of the immune response by analysis of immune regulatory gene expression

Created with BioRender.com; **Abbreviations**: **PBMCs**: peripheral blood mononuclear cells; **hiPS cell**: human induced pluripotent stem cell; **RNA**: ribonucleic acid; **cDNA**: complementary deoxyribonucleic acid; **qPCR**: quantitative real-time polymerase chain reaction; **GZMB**: granzyme B; **IL10**: interleukin 10; **IL2**: interleukin 2; **IFN**γ: interferon gamma

For each experimental setup, three controls were prepared in duplicates or triplicates and transferred to a round-bottomed 96-well plate:

- First, a target cell only control containing 100 μl of target cells (1 x10^5 hiPS cells) 100 μl assay medium [RPMI 1640 Medium (Biochrom, Merck Millipore, Merck KGaA) supplemented with 10 % FCS], providing information about specific immune regulatory gene expression in hiPS cells or CMs.
- Second, the effector cell only control containing 100 μl of effector cells (1 x10^5 PBMCs) and 100 μl assay medium, enabling to analyze specific immune regulatory gene expression in unstimulated PBMCs.
- Third, the stimulated effector cell control containing 100 μl of effector cells (1 x10^5 PBMCs) and 100 μl assay medium supplemented with 10 μg/ml of the lectin phytohemagglutinin (PHA) (Phytohemagglutinin-M (PHA-M), Roche Applied Science). PHA-mediated stimulation of PBMCs enabled studying immune regulatory gene profiles of stimulated PBMCs and served as positive control for activation of gene expression.

The optimal incubation period for co-culture and effector to target (E:T) ratio were determined in preliminary experiments.

Determination of the optimal incubation period and E:T ratio

For the determination of the optimal incubation period and E:T ratio, target cells [E5V homozygous (parental line) hiPS cells] were detached (described in section 3.2.2) and their cell number was determined as described in section 3.2.1. RPMI 1640 Medium (Biochrom, Merck Millipore, Merck KGaA) (described in section 3.1.5) supplemented with 10 % FCS (described in section 3.1.4) was used to adjust the target cell suspension to a target cell concentration of 1 x10^6cells/ml. Subsequently, the solution of target cells was diluted by two-fold serial dilution to 1 x10^4cells/ml. Next, 100 μl of each target cell concentration were pipetted in duplicate

wells into a round-bottomed 96-well plate. To prepare the effector cells, PBMCs were isolated (described in section 3.6.2) and their cell number was determined as described in section 3.2.1. The effector cell suspension was adjusted with assay medium to a cell concentration of 1 x10^6cells/ml. Next, 100 μl of the effector cell suspension was pipetted into the wells containing target cells. Furthermore, the above mentioned controls, prepared with the corresponding cell concentrations, were pipetted into the 96-well plate. Subsequently, the assay was incubated at 37 °C. To determine the optimal incubation time, the cells were harvested after 3, 4 and 5 days (72, 96 and 120 hours) of co-culture. Quantification of the specific immune regulatory gene expression was performed as described above. The E:T ratio and the incubation period, in which the gene expression profile revealed the greatest upregulation of immune regulatory genes were used for subsequent assays.

Interpretation of the immune response against the generated E5V ΔPB cell line

To compare the immune response against the generated homozygous and heterozygous *B2M*-deficient E5V ΔPB cell clones to the response against the E5Vf (wild-type) cell line, hiPS cells from the respective cell clones were detached (described in section 3.2.2) and their cell number was determined as described in section 3.2.1. The respective target cell suspensions were adjusted with assay medium to an optimal target cell concentration of 1 x10^4cells/ml. To prepare the effector cells, PBMCs were isolated (described in section 3.6.2) and their cell number was determined as described in section 3.2.1. The effector cell suspension was adjusted with assay medium to an optimal effector cell concentration of 1 x10^6cells/ml. Subsequently, 100 μl of the respective target cell suspensions were pipetted in triplicate wells into a round-bottomed 96-well plate. To produce an optimal E:T ratio of 100:1, 100 μl of the effector cell solution were then added to the wells containing target cells. Furthermore, the above mentioned controls, prepared for each hiPS cell line with the corresponding cell concentration, were pipetted into the 96-well plate. Finally, quantification of the specific immune regulatory gene expression was performed as described above.

3.7.2 Lactate dehydrogenase (LDH)-Cytotoxicity assay by ELISA readout

In the attempt to study the CD8+ T-cell and NK-cell mediated immune response against the generated homozygous and heterozygous *B2M*-deficient E5V ΔPB clones the Cytotoxicity Detection Kit (LDH) (Roche Applied Science) was employed according to the manufacturer's instructions. This colorimetric assay enables the quantification of cell lysis, based on the LDH activity released in culture medium through the damaged cell membrane of cells. LDH released from apoptotic cells catalyzes the oxidation of lactate to pyruvate with accompanying reduction of nicotinamide adenine dinucleotide (NAD)+ to NADH. In the second enzymatic reaction, yellow tetrazolium salt is converted to a colored formazan salt by using the synthesized NADH in the presence of a catalyst from the kit. The amount of formazan product can be measured colorimetrically at 490 nm using an ELISA reader and is proportional to the amount of LDH released into the culture medium. Therefore, the amount of formazan formed in the assay directly correlates to the number of lysed cells (Roche Diagnostics, 2007). A schematic

representation of the LDH-Cytotoxicity assay is shown in figure 12.

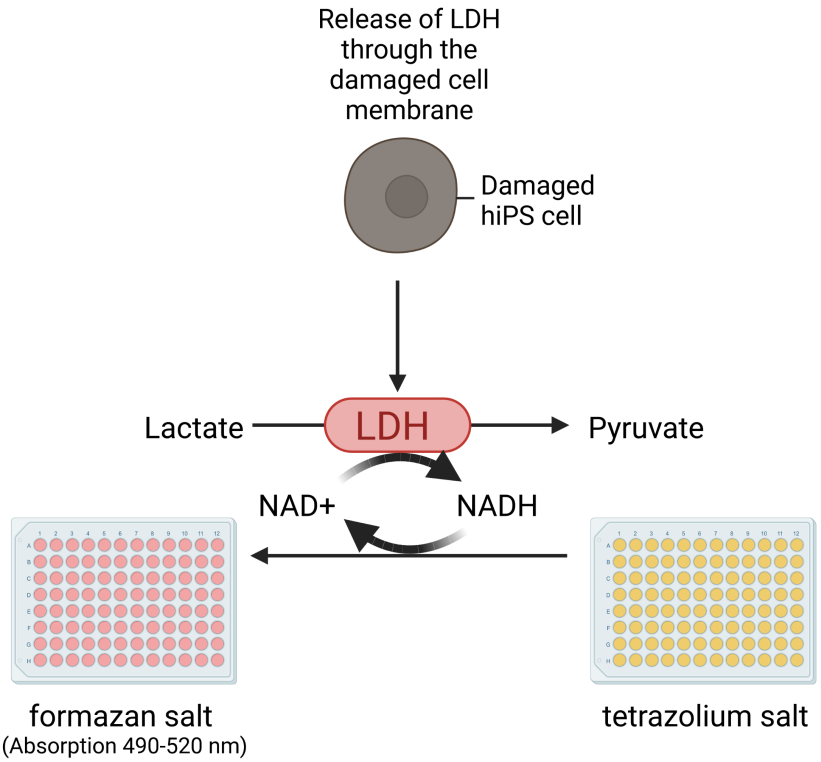

Figure 12: Visualization and quantification of cell-mediated cytotoxicity by ELISA readout
Created with BioRender.com; **Abbreviations**: **LDH**: lactate dehydrogenase; **NAD**: nicotinamide adenine dinucleotide

For each experimental setup, four controls were prepared in triplicates and transferred to a Nunc^{TM} 96-Well Polystyrene Round Bottom Microwell Plate (Thermo Fisher Scientific) (round-bottomed 96-well plate):

- First, a background control containing 200 μl assay medium [RPMI 1640 Medium (Biochrom, Merck Millipore, Merck KGaA) supplemented with 1 % BSA)], providing information about the LDH background activity from employed reagents and culture medium.
- Second, the low control containing 100 μl target cells (hiPS cells) and 100 μl assay medium, gives information about the spontaneous LDH release.
- Third, the high control containing 100 μl target cells (hiPS cells) and 100 μl assay medium supplemented with 2 % Triton X 100 (Carl Roth GmbH + Co. KG). Detergent-based lysis of all cells, determines the maximum amount of LDH released by the target cells.
- Fourth, the effector cell control (substance control) containing 100 μl effector cells (cytotoxic CD8+ T-cells or NK-cells) and 100 μl assay medium, determines the amount of

LDH released by the effector cells.

- Finally, the test sample was prepared, containing 100 μl target cells (hiPS cells) and 100 μl effector cells (CD8+ T-cells or NK-cells), which determines the amount of LDH due to cell-mediated cytotoxicity.

All assays were incubated for 4 hours at 37 °C. The incubation time of 4 hours was established in preliminary experiments and adopted for all further experiments to determine a meaningful immune response. To perform the assay, culture supernatants were harvested by centrifuging the round-bottomed 96-well plate at 250 x g for 10 minutes at RT. Next, 100 μl of culture supernatant were collected from each well and were transferred to the corresponding well of a new optically clear flat-bottomed 96-well plate. To measure LDH activity in the supernatants, 100 μl of the reconstituted reaction mixture (1:45, catalyst:dye solution) were added to each well and were incubated, protected from light, for 30 minutes at RT. Finally, absorbance of all samples was measured at 490 nm using the enzyme-linked immunosorbent assay (ELISA) reader Infinite® 200 PRO (Tecan, Tecan Group AG). An overview of the LDH assay workflow is shown in figure 13.

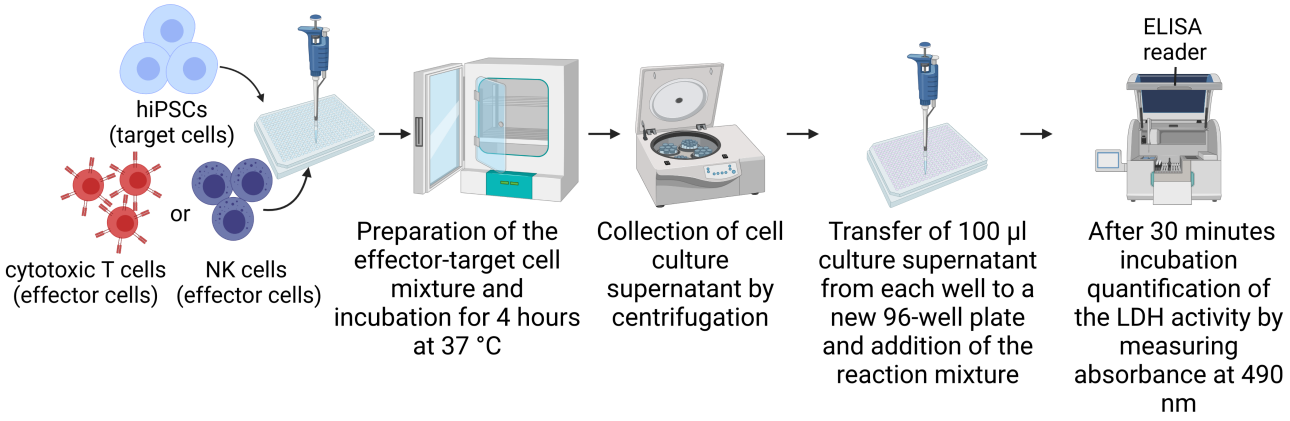

Figure 13: LDH assay workflow

Created with BioRender.com; **Abbreviations**: **CD**: cluster of differentiation **NK cell**: natural killer cell; **hiPS cell**: human induced pluripotent stem cell; **LDH**: lactate dehydrogenase; **ELISA**: enzyme-linked immunosorbent assay

To establish the LDH-Cytotoxicity assay, the optimal target cell density and E:T ratio were determined in preliminary experiments.

Determination of the optimal target cell concentration

For the determination of the optimal target cell density, hiPS cells [E5V homozygous (parental line)] were detached (described in section 3.2.2) and the cell number was determined as described in section 3.2.1. RPMI 1640 Medium (Biochrom, Merck Millipore, Merck KGaA) (described in section 3.1.5) supplemented with 1 % BSA (described in section 3.1.4) was used to adjust the cell suspension to 5 x10^5cells/ml. Subsequently, the cells were diluted by two-fold serial dilution down to 3.125 x10^4cells/ml. 100 μl of each cell concentration were pipetted in two

sets of triplicate wells into a round-bottomed 96-well plate. One set of sample wells was used to determine spontaneous LDH release and was referred to as low control. For the second set of sample wells, the assay medium was supplemented with 2 % Triton X 100 (Carl Roth GmbH + Co. KG) and was used to determine the maximum amount of releasable LDH, referred to as high control. Finally, determination of the LDH activity was performed as described above. The cell concentration corresponding to the greatest difference between the absorbance value (490 nm) (LDH activity) of the high and the low control was used for subsequent assays.

Determination of the optimal E:T ratio

For the determination of the optimal E:T ratio, target cells [E5V homozygous (parental line) hiPS cells] were detached (described in section 3.2.2) and the cell number was determined as described in section 3.2.1. The target cell suspension was adjusted with assay medium to an optimal target cell concentration of 1.25 x10^5cells/ml. To prepare the effector cells, CD8+ T-cells or NK cells were isolated from PBMCs (described in section 3.6.3) and their cell number was determined as described in section 3.2.1. The effector cell suspension was adjusted with assay medium to a cell concentration of 6.25 x10^5cells/ml (CD8+ T-cells) or to a cell concentration of 12.5 x10^5cells/ml (NK-cells). Subsequently, the effector cells were diluted by two-fold serial dilution to 7.8 x10^4cells/ml (CD8+ T-cells) or 1.56 x10^5cells/ml (NK-cells). Next, 100 μl of each effector cell concentration were pipetted in triplicate wells into a round-bottomed 96-well plate. 100 μl of the prepared target cell suspension were then added to the wells containing effector cells. Furthermore, the above mentioned controls, prepared with the corresponding cell concentrations, were pipetted into the 96-well plate. Finally, determination of the LDH activity was performed as described above. The E:T ratio and the associated effector cell concentration, in which the assay showed the greatest absorbance value (490 nm) (LDH activity), were used for subsequent assays.

Quantification and interpretation of the CD8+ T-cell and NK-cell-mediated cytotoxicity against the generated E5V $\triangle$PB cell line

To compare the cell-mediated immune response against the generated homozygous and heterozygous *B2M*-deficient E5V ΔPB cell clones to the response against the E5Vf (wild-type) cell line, hiPS cells from the respective cell clones were detached (described in section 3.2.2) and their cell number was determined as described in section 3.2.1. The respective target cell suspensions were adjusted with assay medium to an optimal target cell concentration of 1.25 x10^5cells/ml. To prepare the effector cells, CD8+ T-cells or NK-cells were isolated from PBMCs (described in section 3.6.3) and their cell number was determined as described in section 3.2.1. The effector cell suspension was adjusted with assay medium to an optimal effector cell concentration of 6.25 x10^5cells/ml (CD8+ T-cells) or 12.5 x10^5cells/ml (CD8+ T-cells). Subsequently, 100 μl of the respective target cell suspensions were pipetted in triplicate wells into a round-bottomed 96-well plate. To produce an optimal E:T ratio of 5:1 (CD8+ T-cells) or 10:1 (NK-cells), 100 μl of the respective effector cell solution were then added to the wells containing target cells. Furthermore, the above mentioned controls, prepared for each hiPS cell line with the corresponding cell concentration, were pipetted into the 96-well plate. Finally, determination of the LDH activity was performed as described above. To determine the per-

cent of cell-mediated cytotoxicity, the average absorbance value (490 nm) from each triplicate set of wells was calculated and the background control value was substracted. The obtained values were then substituted into the following equation:

$$\% \text{ Cytotoxicity} = \frac{(test\ sample\ -\ effector\ cell\ control) -\ low\ control}{high\ control\ -\ low\ control} \text{ x } 100$$

3.7.3 Statistical analysis

Unless otherwise noted, all data were expressed as mean ± standard error of the mean. Multiple comparisons were analyzed by Mann-Whitney Rank Sum Test, the umpaired Student's T-Test or One-way ANOVA using the software SigmaPlot V13.0 (Systat Software Inc., San Jose, CA). P-values < 0.05 were considered statistically significant.

4 Results

4.1 Characterization of the E5V cell line (parental line)

In this work the hiPS cell line 'E5V' (ventricular), established in the Division of Experimental Surgery, was employed for the generation of an immunotolerant cell line. Prior to the targeted knockout of the *B2M* gene, the E5V cell line was characterized. In the E5V cell line a tomato red reporter gene was introduced directly in front of the *MYL2* gene via homologous recombination using the CRISPR-Cas9 technology. The MLC2v protein is a myosin light chain regulatory protein characteristically expressed in ventricular CMs (Z. Zhang & Nam, 2018). As a robust marker for ventricular maturation during cardiogenesis, the *MLC2v* expression can be used to identify differentiated hiPS cells with a ventricular cardiac phenotype (O'Brien et al., 1993; Bizy et al., 2013). Consequently, the MLC2v-tdTomato knock-in of the cell line enables monotoring CMs by their red fluorescence upon directed cardiac differentiation. Several clones carrying the tomato-red reporter gene homozygously and heterozygously (E5V homozygous and E5V heterozygous) were selected and characterized.

4.1.1 Gene expression analysis during directed cardiac differentiation

In a first set of experiments, the capacity of E5V hiPS cells to differentiate towards the cardiac lineage was assessed. To determine the onset of cardiac transcription factor expression, to evaluate the differentiation efficiency and to analyze the maturation of E5V homozygous for tdTomato hiPS cell-derived CMs a directed cardiac differentiation protocol was applied (described in section 3.2.4). Gene expression analysis of the cardiac transcription factors *NKX2.5* (NM_004387.3) and *TBX5* (NM_000192.3) and the structural genes *MLC2v* (NM_000432.3) and *MLC2a* (NM_021223.2) was performed on days D0, D6, D8, D10, D14 and D21 of the directed cardiac differentiation protocol (shown in figure 14). The oligonucleotide primer sequences used for qRT-PCR are given in table 11. Besides, the MLC2v-tdTomato knock-in of the E5V homozygous cell line enabled to track the expression of MLC2v over time by documenting the red fluorescence of hiPS cell-derived CMs with the Axiovert 200 M Inverted Fluorescent Microscope (Carl Zeiss AG, Oberkochen, Germany). This allowed to assess their potential to differentiate into ventricular CMs.

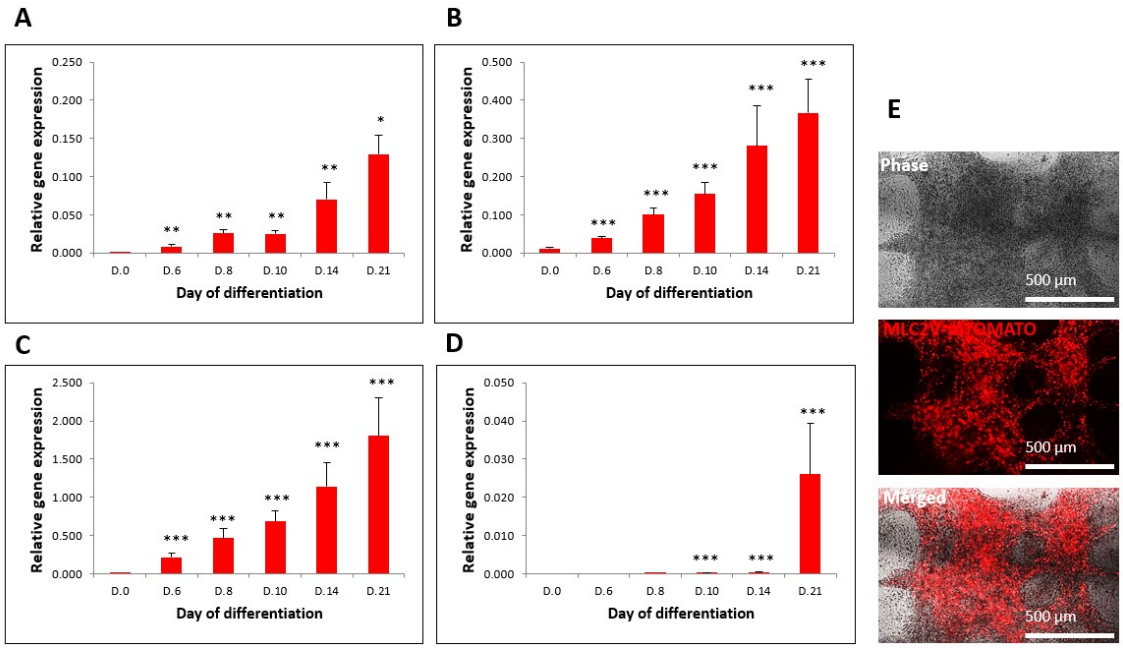

Figure 14: Gene expression analysis during directed cardiac differentiation of E5V homozygous for tdTomato hiPS cells (parental line)

Relative gene expression levels of **(A)** *NKX2.5* (NM_004387.3), **(B)** *TBX5* (NM_000192.3), **(C)** *MLC2a* (NM_021223.2) and **(D)** *MLC2v* (NM_000432.3) during directed cardiac differentiation (D0 to D21). *ACTB* (NM_001101.3) was used to normalize qRT-PCR data for relative quantification. Relative gene expression was determined in four independent differentiation assays with biological duplicates or triplicates. Deviations in gene expression are reported as standard error of the mean. **(E)** Representative phase-contrast and fluorescence image of hiPS cell-derived CMs on day 33 of the directed cardiac differentiation protocol. The MLC2v-tdTomato knock-in of the E5V cell line enabled to indirectly monitor the endogenous *MLC2v* expression (red) upon directed cardiac differentiation. The expression of the gene of interest at time 0 was compared to the induced gene expression determined for the other time points. $^{*}p < 0.05$; $^{**}p < 0.01$; $^{***}p < 0.001$ by Mann-Whitney Rank Sum Test or Student's T-Test.
Abbreviations: NKX2.5: NK2 Homeobox 5; TBX5: T-Box 5; MLC2v: ventricular Myosin Light Chain-2; MLC2a: atrial Myosin Light Chain-2; ACTB: Actin Beta.

Figure 14A shows the relative gene expression levels of the cardiomyogenic differentiation marker *NKX2.5* (George, Colombo, & Targoff, 2015). *NKX2.5* was first induced on D6 and increased continuously. Figure 14B shows the relative gene expression levels of the cardiomyogenic differentiation marker *TBX5* (Steimle & Moskowitz, 2017). *TBX5* was detectable from D0 and increased continuously. Figure 14C shows the relative gene expression levels of *MLC2a*, a cardiac marker for atrial-, nodal-, or immature ventricular-like CMs (Ichimura et al., 2020; Bedada et al., 2016). *MLC2a* was first induced on D6 and increased continuously. Figure 14D shows the relative gene expression levels of *MLC2v*, a cardiac marker for mature ventricular-like CMs (Bedada et al., 2016; Guo & Pu, 2020). *MLC2v* was first detectable on D14 and increased strongly until D21. E5V homozygous for tdTomato hiPS cell-derived CMs typically started beating on D8 and the number of contracting CMs increased continuously until D14. The tdTomato fluorescence in differentiating E5V homozygous for tdTomato hiPS cells was generally detectable around D20 of the directed cardiac differentiation protocol and increased over time. Figure 14E shows a representative phase-contrast and fluorescence image of E5V homozygous for tdTomato hiPS cell-derived CMs on D33 of the directed cardiac differentiation

protocol. An intense red fluorescence corresponding to the tdTomato expression was detected.

4.1.2 Molecular characterization of CMs

For molecular characterization, E5V hiPS cell-derived CMs on day 30 and 60 of the directed cardiac differentiation protocol were immunocytochemically analyzed for the expression of cardiac specific markers (described in section 3.5.1). Immunofluorescent analysis enabled to investigate the expression of TNNT2, a key marker for CMs, and sarcomeric α-actinin, a key structural protein of the sarcomere (Waas et al., 2019; Lichter et al., 2014). Furthermore, the cells were stained for MLC2a, a marker for atrial CMs, and MLC2v, a marker for ventricular CMs (Ichimura et al., 2020; Bedada et al., 2016). An anti-RFP antibody was used for the detection of tdTomato and thereby enabled monitoring the MLC2v-tdTomato knock-in of the E5V cell line. Clones carrying the tomato red reporter gene homozygously and heterozygously (E5V homozygous and E5V heterozygous) were analyzed to assess whether there are observable differences in their cardiac-specific protein expression and their potential to differentiate into ventricular CMs. Immunofluorescent analysis in E5V homozygous for tdTomato hiPS cell-derived CMs on day 30 (figure 15) and 60 (figure 16) of the directed cardiac differentiation protocol showed the expression of TNNT2, α-actinin, MLC2a and MLC2v, each detectable as strong green fluorescent signal. Furthermore, E5V homozygous for tdTomato hiPS cell-derived CMs stained positive for RFP, detectable as strong green fluorescent signal, which was virtually superimposable with the red fluorescent signal of the tdTomato expression (figure 15E and figure 16E). Figure 15I shows the immunofluorescent staining of α-actinin and reveals the typical striated pattern of sarcomeres, which are the basic contractile units of CMs (Lichter et al., 2014; Sweeney & Hammers, 2018). Immunofluorescent analysis in E5V heterozygous for tdTomato hiPS cell-derived CMs on day 30 (figure 17) and 60 (figure 18) of the directed cardiac differention protocol also confirmed the expression of TNNT2, α-actinin, MLC2a and MLC2v, detectable as strong green fluorescent signal. Furthermore, E5V heterozygous for tdTomato hiPS cell-derived CMs stained positive for RFP, detectable as strong green fluorescent signal, which was virtually superimposable with the red fluorescent signal of the tdTomato expression (figure 17E, figure 18E). In figures 15, 16, 17 and 18 cell nuclei were stained blue by DAPI. Besides, in all stainings an intense red fluorescence, corresponding to the tdTomato expression, was detected, and thereby enabled to indirectly monitor the endogenous *MLC2v* expression upon cardiac differentiation.

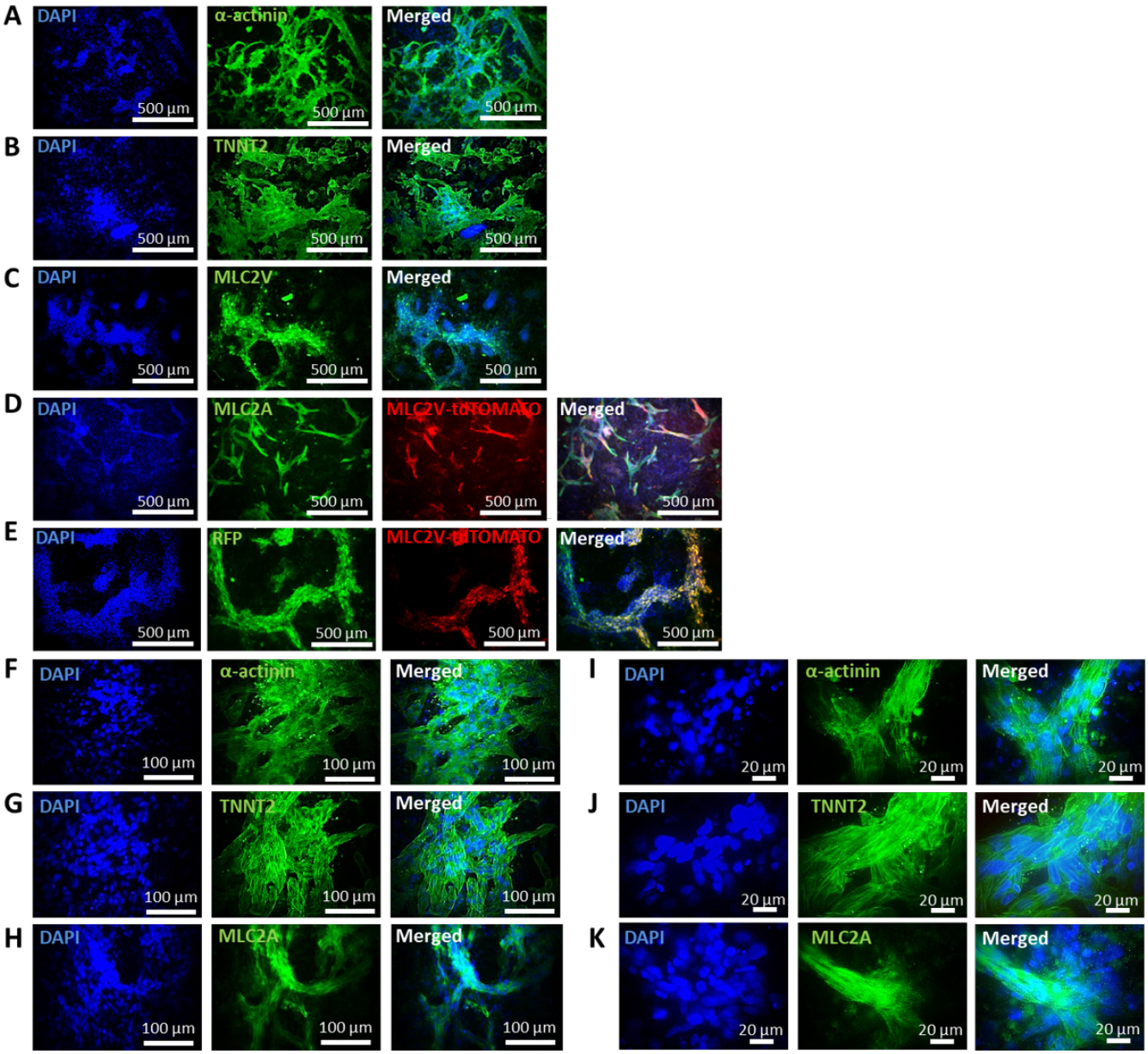

Figure 15: Immunofluorescence imaging of cardiac markers in representative E5V homozygous for tdTomato hiPS cells-derived CMs on day 30 of the directed cardiac differentiation protocol
(A) Immunofluorescent analysis of sarcomeric α-actinin (green). **(B)** Immunofluorescent analysis of TNNT2 (green). **(C)** Immunofluorescent analysis of MLC2v (green). **(D)** Immunofluorescent analysis of MLC2a (green). The MLC2v-tdTomato knock-in of the E5V cell line enabled to indirectly monitor the endogenous *MLC2v* expression (red) upon directed cardiac differentiation. **(E)** Immunofluorescent analysis of tdTomato using a FITC-labelled anti-RFP antibody (green). The MLC2v-tdTomato knock-in of the E5V cell line enabled to indirectly monitor the endogenous *MLC2v* expression (red) upon directed cardiac differentiation. **(F)** Immunofluorescent analysis of sarcomeric α-actinin (green). **(G)** Immunofluorescent analysis of cardiac TNNT2 (green). **(H)** Immunofluorescent analysis of MLC2a (green). **(I)** Immunofluorescent analysis of sarcomeric α-actinin (green). **(J)** Immunofluorescent analysis of TNNT2 (green). **(K)** Immunofluorescent analysis of MLC2a (green). DAPI (blue) was used as a nuclear counterstain.
Abbreviations: TNNT2: cardiac Troponin T; MLC2v: ventricular Myosin Light Chain-2; MLC2a: atrial Myosin Light Chain-2; RFP: red fluorescent protein; DAPI: 4',6-diamidino-2-phenylindole.

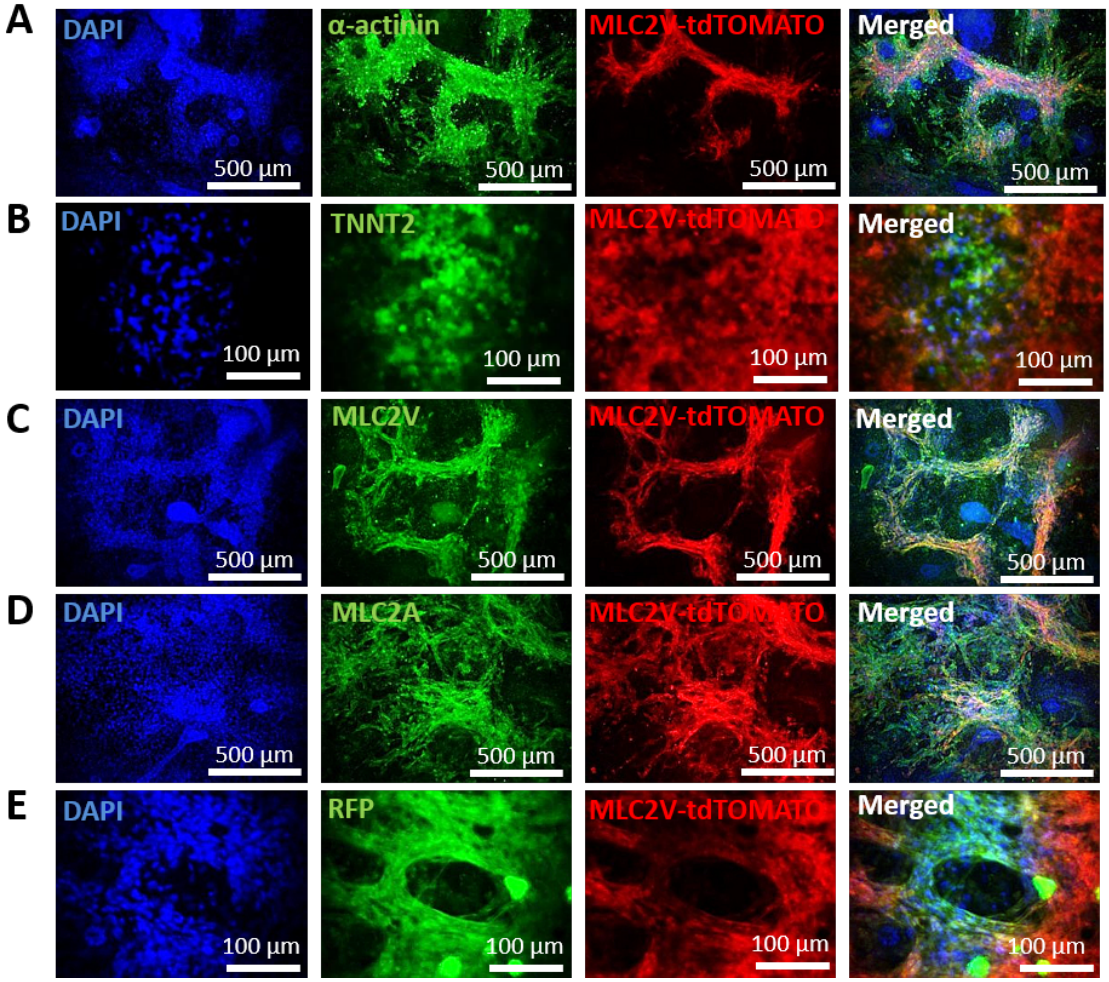

Figure 16: Immunofluorescence imaging of cardiac markers in representative E5V homozygous for tdTomato hiPS cells-derived CMs on day 60 of the directed cardiac differentiation protocol

(A) Immunofluorescent analysis of sarcomeric α-actinin (green). **(B)** Immunofluorescent analysis of TNNT2 (green). **(C)** Immunofluorescent analysis of MLC2v (green). **(D)** Immunofluorescent analysis of MLC2a (green). **(E)** Immunofluorescent analysis of tdTomato using a FITC-labelled anti-RFP antibody (green). DAPI (blue) was used as a nuclear counterstain. The MLC2v-tdTomato knock-in of the E5V cell line enabled to indirectly monitor the endogenous *MLC2v* expression (red) upon directed cardiac differentiation. **Abbreviations**: TNNT2: cardiac Troponin T; MLC2v: ventricular Myosin Light Chain-2; MLC2a: atrial Myosin Light Chain-2; RFP: red fluorescent protein; DAPI: 4',6-diamidino-2-phenylindole.

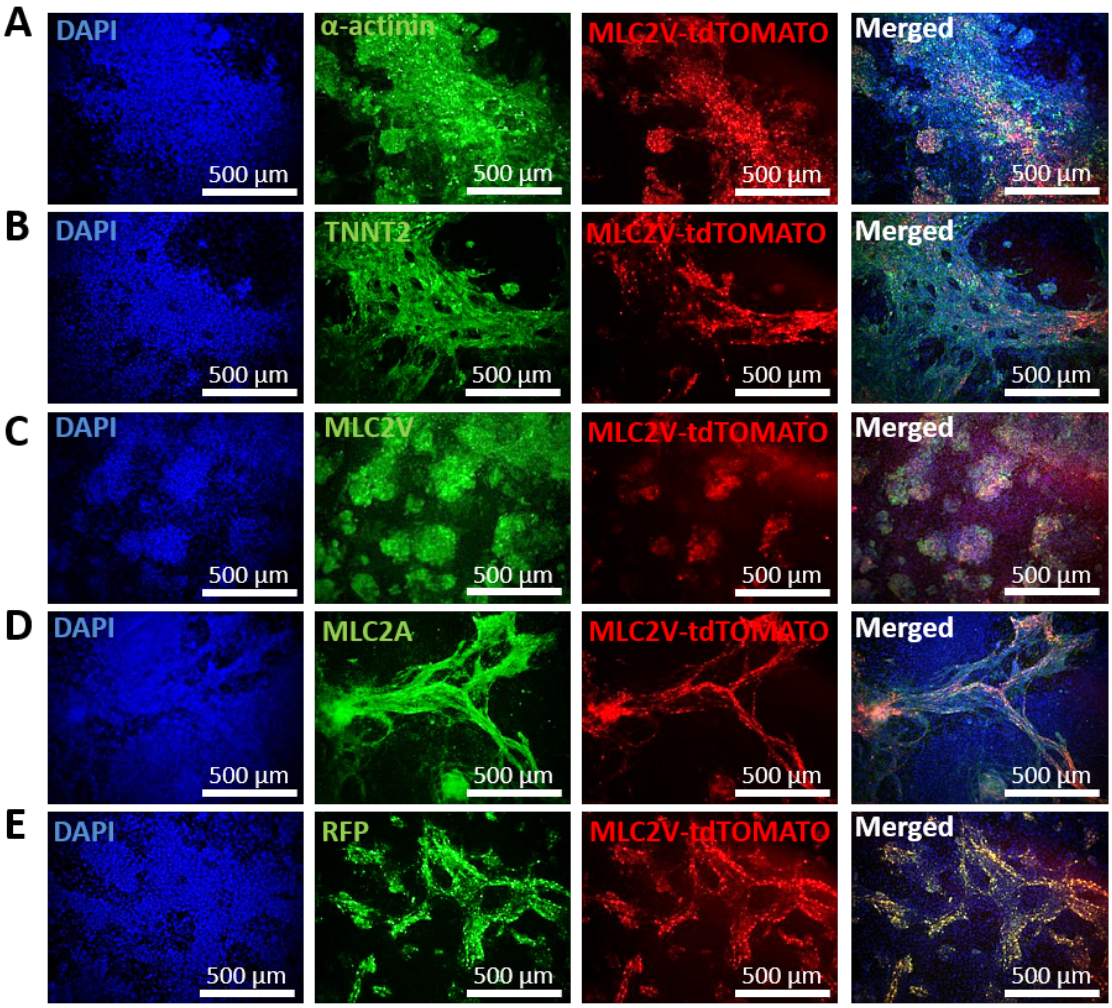

Figure 17: Immunofluorescence imaging of cardiac markers in representative E5V heterozygous for tdTomato hiPS cells-derived CMs on day 30 of the directed cardiac differentiation protocol
(A) Immunofluorescent analysis of sarcomeric α-actinin (green). **(B)** Immunofluorescent analysis of TNNT2 (green). **(C)** Immunofluorescent analysis of MLC2v (green). **(D)** Immunofluorescent analysis of MLC2a (green). **(E)** Immunofluorescent analysis of tdTomato using a FITC-labelled anti-RFP antibody (green). DAPI (blue) was used as a nuclear counterstain. The MLC2v-tdTomato knock-in of the E5V cell line enabled to indirectly monitor the endogenous *MLC2v* expression (red) upon directed cardiac differentiation. **Abbreviations**: TNNT2: cardiac Troponin T; MLC2v: ventricular Myosin Light Chain-2; MLC2a: atrial Myosin Light Chain-2; RFP: red fluorescent protein; DAPI: 4',6-diamidino-2-phenylindole.

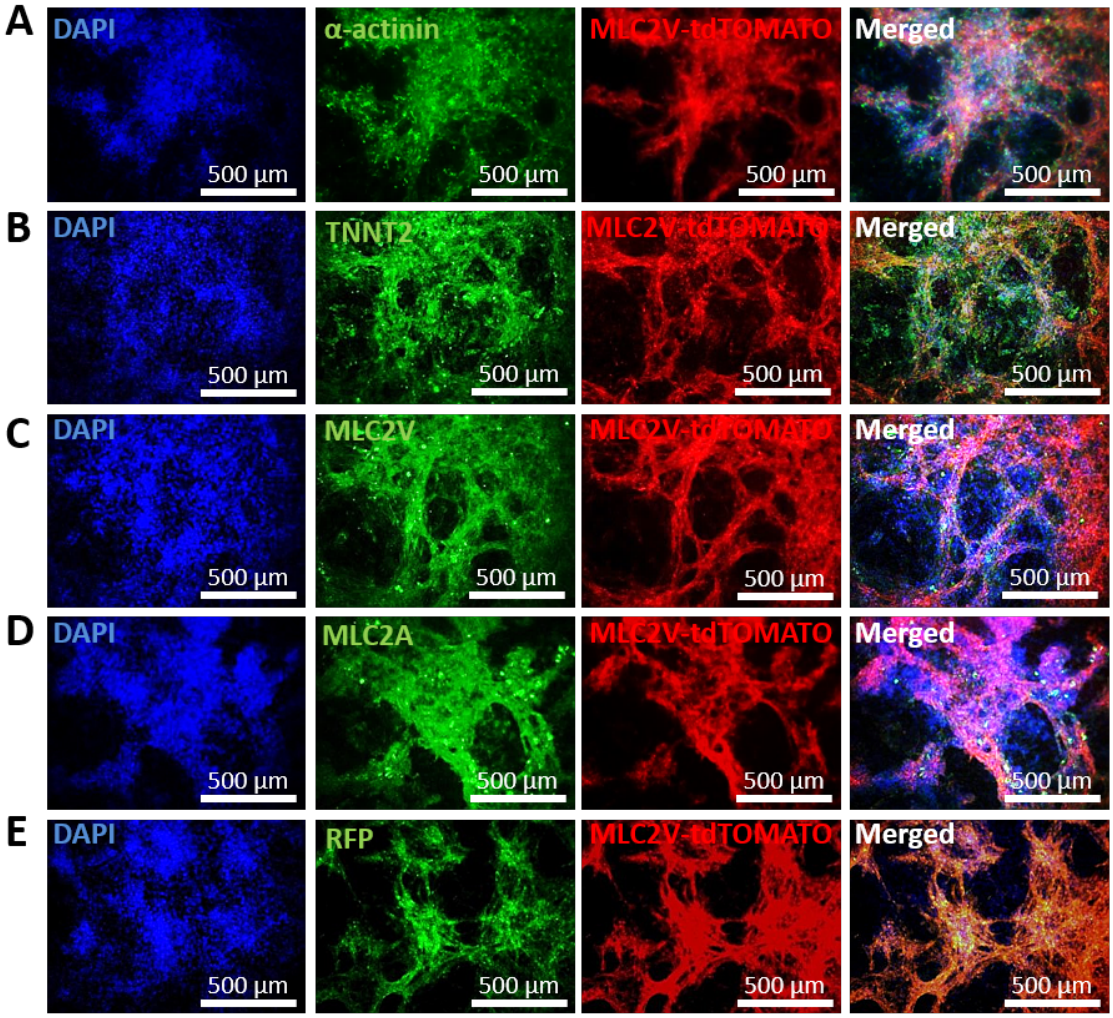

Figure 18: Immunofluorescence imaging of cardiac markers in representative E5V heterozygous for tdTomato hiPS cells-derived CMs on day 60 of the directed cardiac differentiation protocol **(A)** Immunofluorescent analysis of sarcomeric α-actinin (green). **(B)** Immunofluorescent analysis of TNNT2 (green). **(C)** Immunofluorescent analysis of MLC2v (green). **(D)** Immunofluorescent analysis of MLC2a (green). **(E)** Immunofluorescent analysis of tdTomato using a FITC-labelled anti-RFP antibody (green). DAPI (blue) was used as a nuclear counterstain. The MLC2v-tdTomato knock-in of the E5V cell line enabled to indirectly monitor the endogenous *MLC2v* expression (red) upon directed cardiac differentiation. **Abbreviations**: TNNT2: cardiac Troponin T; MLC2v: ventricular Myosin Light Chain-2; MLC2a: atrial Myosin Light Chain-2; RFP: red fluorescent protein; DAPI: 4',6-diamidino-2-phenylindole.

4.2 Evaluation of the MHC-I cell surface expression of hiPS cells and hiPS cell-derived CMs

To evaluate the MHC-I cell surface expression of hiPS cells and hiPS cell-derived CMs FACS analysis was performed (described in section 3.5.2). Figure 19 shows the flow cytometric quantification of surface MHC-I on E5V homozygous (parental line) hiPS cell-derived CMs

and E5V homozygous hiPS cells using anti-HLA-ABC monoclonal antibody (W6/32) (MA5-11723, Invitrogen^{TM}, Thermo Fisher Scientific). Flow cytometric assessment revealed that 90.9 % (figure 19C) of the analyzed E5V homozygous hiPS cells did express MHC-I. No signal was detected in the corresponding unstained cells (0.00 %, figure 19A) and cells incubated with the secondary antibody control (0.015 %, figure 19B). In contrast, 51.0 % of the analyzed E5V homozygous (parental line) hiPS cell-derived CMs were MHC-I positive (figure 19F). Again, no signal was detected in the corresponding unstained cells (0.00 %, figure 19D) and after incubation with the secondary antibody alone (0.021 %, figure 19E).

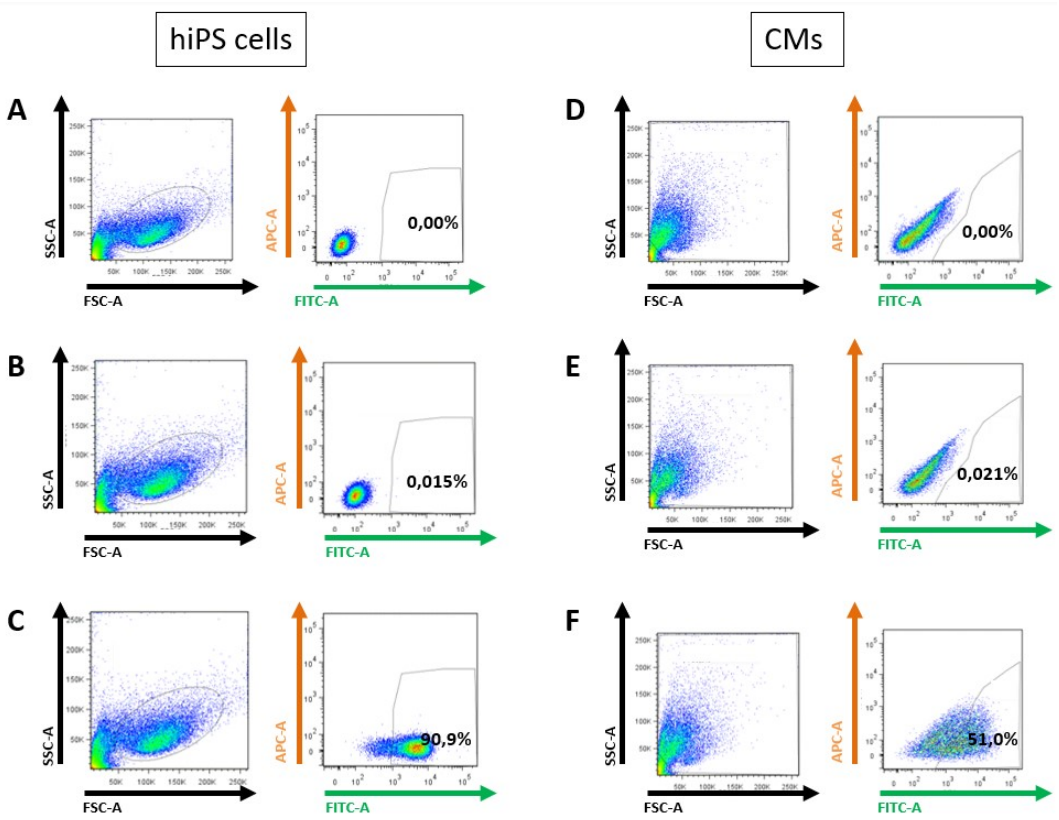

Figure 19: FACS analysis of MHC-I cell surface expression in hiPS cells and hiPS cell-derived CMs **(A)** Representative FACS analysis of unstained E5V homozygous (motherline) hiPS cells (negative control). **(B)** Representative FACS analysis of E5V homozygous (parental line) hiPS cells stained with secondary antibody alone (secondary antibody control). **(C)** Representative FACS analysis of MHC-I cell surface expression in E5V homozygous (parental line) hiPS cells. **(D)** Representative FACS analysis of unstained E5V homozygous (parental line) hiPS cell-derived CMs (negative control) **(E)** Representative FACS analysis of E5V homozygous (parental line) hiPS cell-derived CMs stained with the secondary antibody alone (secondary antibody control). **(F)** Representative FACS analysis of MHC-I cell surface expression in E5V homozygous (parental line) hiPS cell-derived CMs. **Abbreviations**: FACS: fluorescence-activated cell sorting; hiPS cells: human induced pluripotent stem cells; CMs: cardiomyocytes; MHC-I: major histocompatibility complex class I.

4.3 Gene editing

4.3.1 Gene editing overview

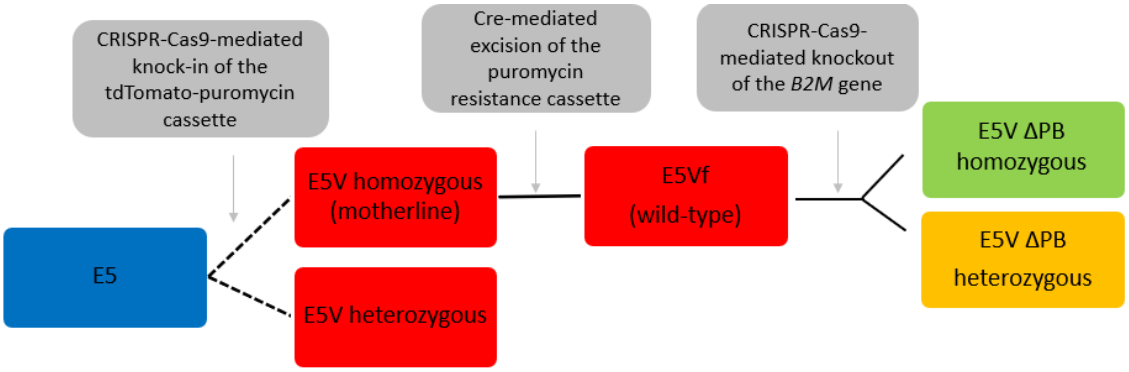

Figure 20: Schematic workflow for the generation of an immunotolerant cell line
Abbreviations: CRISPR-Cas9: clustered regularly interspaced short palindromic repeats-CRISPR-associated endonuclease 9; B2M: β2-microglobulin.

In a first step, the fully characterized and published 'E5' hiPS cell line (Sun et al., 2012) was genetically modified using the CRISPR-Cas9 technology. The 'E5' hiPS cell line originates from human fibroblasts, which were reprogrammed in the laboratory of Professor Joseph Wu (Stanford Cardiovascular Institute, Stanford University School of Medicine, Stanford, CA) and was kindly transferred to the Division of Experimental Surgery at the German Heart Center. To generate a fluorescent reporter cell line for monitoring cardiac-specific cell differentiation, a tomato red reporter gene was introduced downstream the *MLC2v* gene of the 'E5' hiPS cell line via homologous recombination as published by (Chirikian et al., 2021). This resulted in a new cell line denoted as E5V (ventricular). The E5V cell line carries a puromycin resistance which permitted the selection of successfully manipulated clones. Clones carrying the tomato red reporter gene homozygously and heterozygously (E5V homozygous and E5V heterozygous) were selected. The insertion of the tdTomato was done by Elda Dzilic in her PhD thesis. The existing line was kindly made available to me. In a next step, the puromycin resistance cassette was excised from the genome of E5V homozygous for tdTomato (parental line) hiPS cells by Cre-recombinase. Successfully manipulated clones only carried the tomato red reporter gene, resulting in the resistance-free cell line E5Vf (free of resistance). Finally, the CRISPR-Cas9 technology was employed for a targeted knockout of the *B2M* gene in the E5Vf cell line (wild-type). The *B2M* was replaced on one or both alleles by a neomycin resistance cassette via homologous recombination, resulting in the generation of the double transgenic immunotolerant cell line E5V ΔPB (free of puromycin and *B2M*).

4.3.2 Generation of the resistance-free cell line E5Vf (wild-type)

Prior to the CRISPR-Cas9-mediated knockout of the *B2M* gene, the puromycin resistance cassette was excised from the genome of E5V homozygous for tdTomato (parental line) hiPS cells. In fact, the puromycin resistance cassette enabled to select successfully manipulated

clones that carried the tdTomato reporter gene. The protocol employed for the excision of the puromycin resistance cassette is given in section 3.4.2. Figure 21A shows a schematic of the approach used for Cre-mediated excision of the puromycin resistance cassette. The mechanism is based on the enzym Cre-recombinase, which recognizes two directly repeated loxP sites, excises the loxP flanked DNA and catalyzes the recombination between the target sites (Nagy, 2000; H. Kim et al., 2018). After transfection several clones were isolated, expanded and analyzed for the absence of the puromycin resistance cassette. Figure 21B shows the strategy used for detection of correctly targeted alleles. Genotyping by PCR was performed to confirm the successful removal of the resistance cassette. After the first transfection, all examined clones were heterozygous. Figure 21C confirms the Cre-mediated excision of one puromycin resistance cassette in one representative E5Vf (free of resistance) heterozygous cell clone. Non-transfected E5V homozygous cells served as positive control. To remove the antibiotic resistance from the second allele the same Cre-transfection protocol was repeated with one confirmed E5Vf heterozygous cell clone. After transfection, several clones were isolated, expanded and 11 clones were analyzed for the absence of the second puromycin resistance cassette. Non-transfected E5V homozygous cells served as negative control and transfected E5Vf heterozygous cells served as positive control for Cre-mediated excision of the puromycin resistance. Genotype analysis by PCR confirmed the successful removal of the puromoycin resistance cassette on both alleles (figure 21C) for 2 clones (clone 4 and 7). In the remaining clones, 8 heterozygous and one mutant genotype could be identified. Successfully manipulated clones only carried the tomato red reporter gene and were referred to as E5Vf homozygous cell clones.

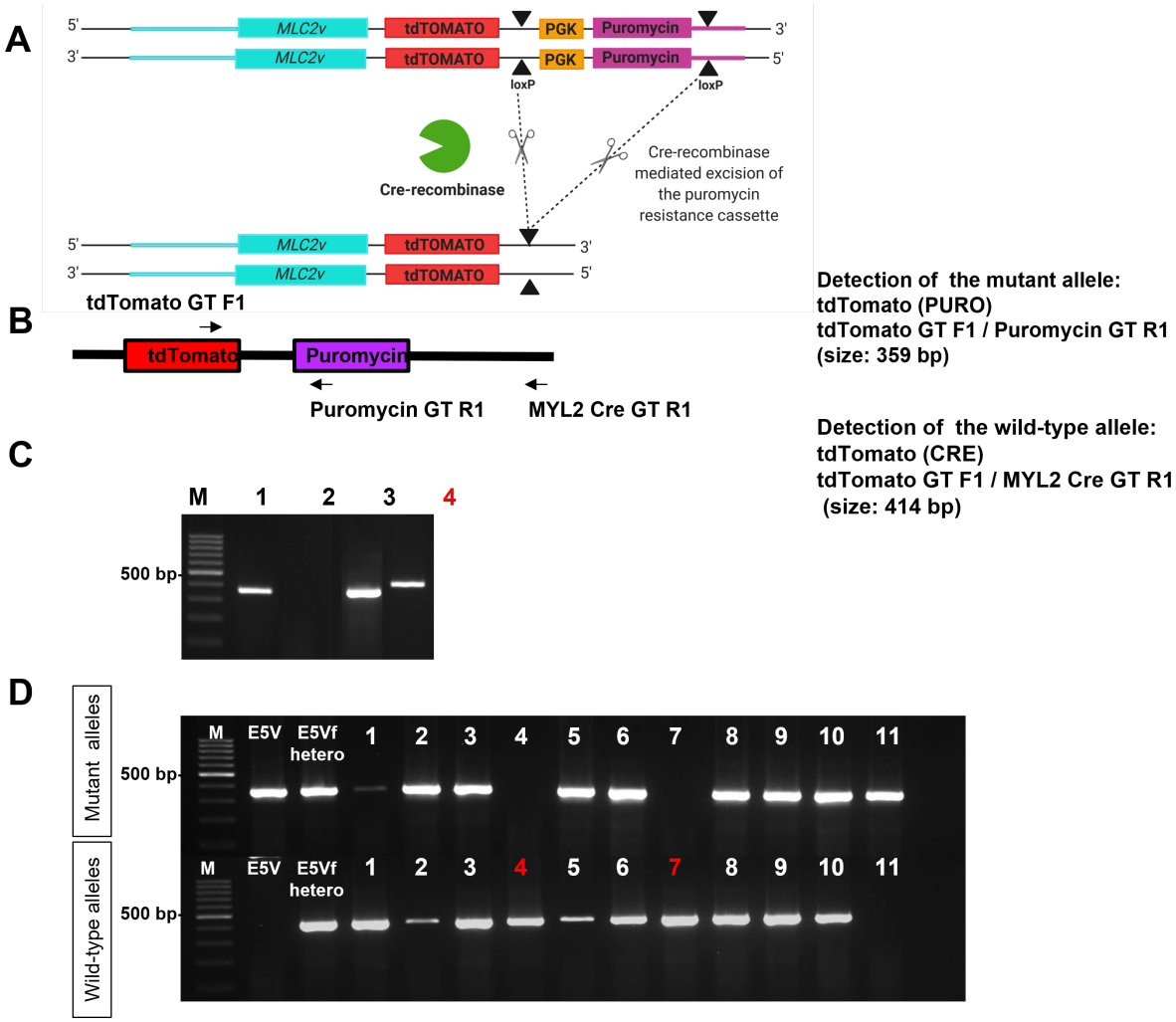

Figure 21: Cre-mediated excision of the puromycin resistance cassette for the generation of the resistance-free cell line E5Vf (wild-type)

(A) Schematic representation (Created with BioRender.com) of the Cre-mediated puromycin resistance cassette excision. The puromycin resistance cassette was flanked by loxP sites, allowing its excision from the genome by Cre-recombinase. **(B)** Schematic representation of the localization of primers used for confirmation of the puromycin resistance cassette removal. The arrows indicate the position and orientation of PCR primers used for genotyping. Primer set tdTomato (PURO) (tdTomato GT F1/ Puromycin GT R1) was used to detect mutant alleles and leads to a 359 bp amplicon. Primer set tdTomato (CRE) (tdTomato GT F1/ MYL2 Cre GT R1) was used to identify wild-type alleles and leads to a 414 bp amplicon. **(C)** Representative genotype analysis on a 2 % agarose gel after the first transfection. Lane M: marker GeneRuler^{TM} 100 bp DNA Ladder (Thermo Scientific^{TM}, Thermo Fisher Scientific), the 500 bp band is indicated. Lanes 1 and 3: mutant alleles. Lanes 2 and 4: wild-type alleles. Lanes 1 and 2 correspond to non-transfected E5V cells and serve as a positive control. Lanes 3 and 4 correspond to E5Vf heterozygous cells and the presence of one wild-type (lane 4 (red)) confirms the excision of the puromycin resistance on one allele. **(D)** Representative genotype analysis on a 2 % agarose gel after the second transfection. The upper gel shows the detection of mutant alleles using primer set tdTomato (PURO). The lower gel shows the detection of wild-type alleles using primer set tdTomato (CRE). Lane M: marker GeneRuler^{TM} 100 bp DNA Ladder (Thermo Scientific^{TM}, Thermo Fisher Scientific), the 500 bp band is indicated. Non-transfected E5V cells serve as a negative control and transfected E5Vf heterozygous cells serve as a positive control for Cre-mediated excision of the puromycin resistance. Lanes 1-11 correspond to transfected cell clones. Lanes 4 and 7 (red) represent E5Vf homozygous clones and the presence of only wild-type alleles confirms the excision of the puromycin resistance on both alleles. **Abbreviations**: MLC2v: Myosin Light Chain-2 ventricu lar; PGK: phosphoglycerate kinase; loxP: locus of X-over P1.

4.3.3 Generation of the *B2M*-deficient E5V ΔPB cell line

The main goal of this thesis was the generation of a hiPS cell line for cardiac regeneration therapy, which is unable to trigger the natural immune response of the recipient upon transplantation. The generation of a cell line lacking the MHC-I complex has the potential to reduce its immunogenicity towards alloreactive T-cells. To verify this postulation, the CRISPR-Cas9 technology was employed to replace exons 2 and 3 of the *B2M* gene in the E5Vf cell line (wild-type) on one or both alleles by a neomycin resistance cassette via homologous recombination. The resulting double transgenic immunotolerant cell line was referred to as E5V ΔPB (free of puromycin and *B2M*). The design and the cloning strategies used for the *B2M* knockout are described in section 3.4.3. For precise CRISPR-Cas9 gene targeting three customized sgRNAs for both exon 2 and 3 were cloned into the vector pSpCas9(BB)-2A-Puro (pX459) V2.0 (Addgene). Each expression vector harbouring a customized sgRNA was then transformed into chemically competent *E. coli* (described in section 3.4.5) and subsequently HEK 293 cells were transfected with these expression vectors. Three clones of each sgRNA were used to determine cleavage efficiency and the most potent and specific sgRNA was selected for subsequent gene targeting. For exon 2, sgRNA 3 clone 1 showed the best performance with 93.7 % cutting efficiency upon analysis (shown in figure S3A). For exon 3, sgRNA 3 clone 3 showed the best performance with 46.6 % cutting efficiency upon analysis (shown in figure S3B). Figure 22A shows a schematic of the approach used for the CRISPR-Cas9-mediated *B2M* gene knockout. Exons 2 and 3 of the *B2M* gene were replaced on one or both alleles by a neomycin resistance cassette via homologous recombination. For the targeted *B2M* knockout, E5Vf homozygous hiPS cells were electroporated with the designed targeting vectors pX459 Puro V2.0 B2M-Exon2-sgRNA3-clone1 and pX459 Puro V2.0 B2M-Exon3-sgRNA3-clone3 and the donor construct B2M KO Neo (described in section 3.4.8). Figure 22B shows the workflow for gene editing efficiency determination. Selection of successfully electroporated cells was started by culturing the cells in the presence of G418 (150 μg/ml). Forty-one stably transfected clones surviving G418 selection were isolated, subcultured and expanded. Genotype screening by PCR was performed to confirm correct replacement of exons 2 and 3 of the *B2M* gene and correct insertion of the donor construct. All amplification products were visualized in a 2% agarose gel. In the end only 31 of 41 clones could be analyzed due to lack of cell growth, incomplete or incorrect integration of the donor construct or failed PCR. Of 31 analyzed clones, 8 homozygous and 12 heterozygous clones could be identified. 11 clones had not integrated the B2M KO Neo donor construct and showed a wild-type genotype at the *B2M* locus. Agarose gel electrophoresis for the detection of exon 2 mutant or wild-type alleles is shown in figure S4. Agarose gel electrophoresis for the detection of exon 3 mutant or wild-type alleles is shown in figure S5. Sequencing of all amplification products was performed to verify the results. Figure 22C displays the gene editing efficiency analysis. 26 % of the analyzed clones were homozygous, 35 % were heterozygous and the frequency of wild-type clones was 39 %.

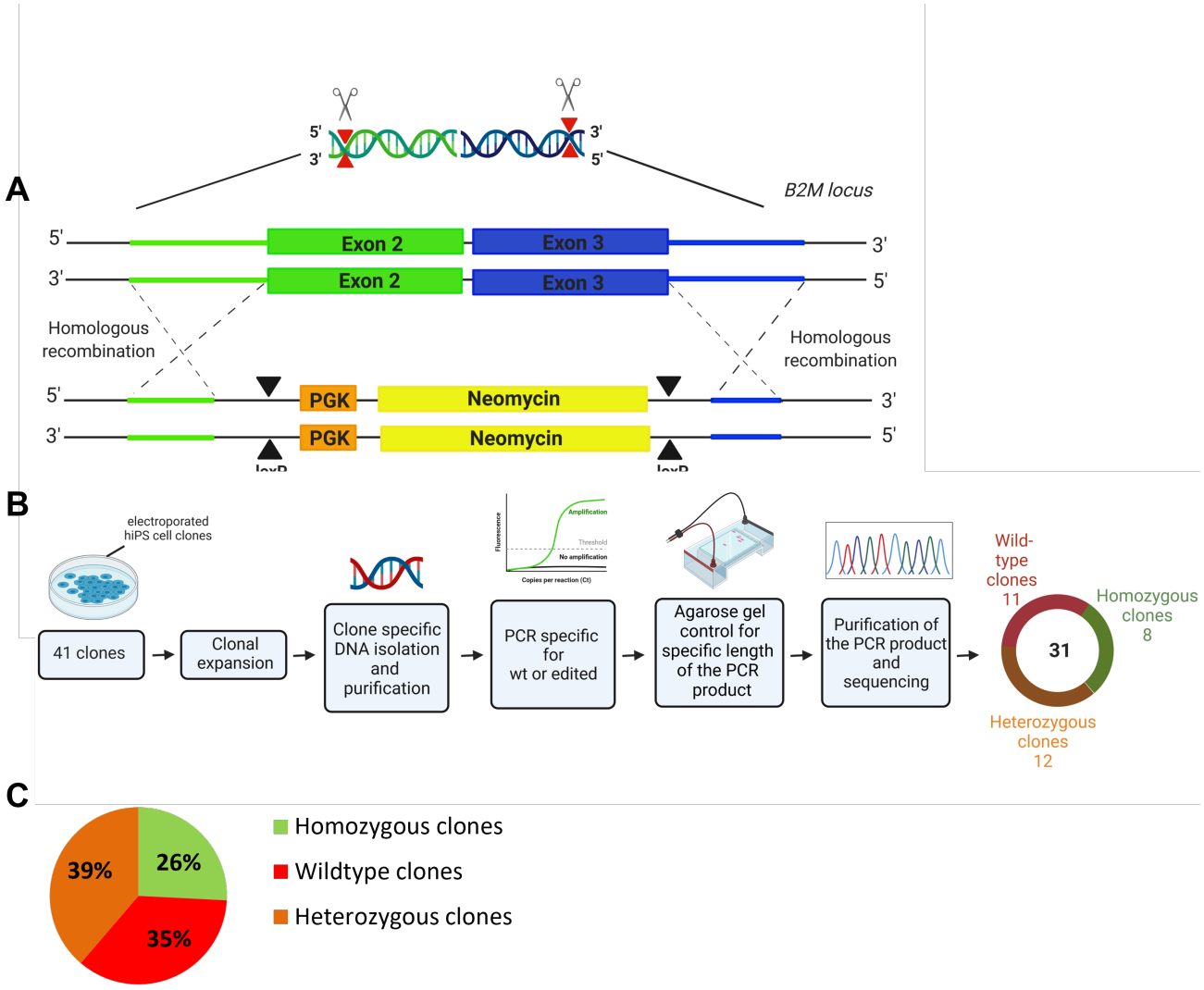

Figure 22: CRISPR-Cas9-mediated knockout of the *B2M* gene in the E5Vf cell line (wild-type) **(A)** Schematic illustration (Created with BioRender.com) of the strategy used for CRISPR-Cas9-mediated *B2M* gene knockout. Exons 2 and 3 of the *B2M* gene were replaced on one or both alleles by a neomycin resistance cassette. The neomycin resistance is under the control of a constitutive phosphoglycerate kinase promoter. **(B)** Workflow illustration (Created with BioRender.com) of the gene editing efficiency determination **(C)** Gene editing efficiency evaluation. **Abbreviations**: PGK: phosphoglycerate kinase; CRISPR-Cas9: clustered regularly interspaced short palindromic repeats-CRISPR-associated endonuclease 9; B2M: β2-microglobulin; loxP: locus of X-over P1; PCR: polymerase chain reaction.

4.4 Characterization of the generated *B2M*-deficient E5V △PB cell line

4.4.1 Confirmation of the *B2M* gene knockout by CRISPR-Cas9 and analysis of MHC-I cell surface expression

After generation and genotype screening, two homozygous (E5V ΔPB Clone 22 and Clone 28) and two heterozygous clones (E5V ΔPB Clone 5 and Clone 16) were selected to verify successful *B2M* knockout and to evaluate MHC-I cell surface expression. First, PCR was performed to verify whether the tdTomato knock-in was not damaged by the gene editing procedure and then the selected E5V ΔPB cell clones were checked for Cre-mediated excision of the puromycin resistance. The selected E5V ΔPB clones had still integrated the MLC2V-tdTomato knock-in in both alleles and were free of the puromycin resistance cassette (shown in figure 23B). E5Vf (wild-type) cells served as positive control. In a next step, the selected clones were checked for the successful knock out of *B2M* exons 2 and 3 and correct knock-in of the neomycin resistance (figures 23C and 23D). Figure 23A shows a schematic representation of the PCR primers used for genotyping. Agarose gel electrophoresis results of E5V ΔPB Clone 5 and Clone 16 revealed two bands (one mutant allele and one wild-type allele for exons 2 and 3), confirming the heterozygous genotype. In the agarose gel electrophoresis of E5V ΔPB Clones 22 and 28 only mutant alleles for exons 2 and 3 were detected, confirming the homozygous genotype. Unedited E5Vf (wild-type) cells served as a control. Except for one unspecific band (mutant exon 2) only wild-type alleles for exons 2 and 3 were detected, confirming the wild-type genotype of E5Vf cells. Moreover, qRT-PCR was performed to evaluate relative gene expression levels of *B2M* (NM_004048.4) in the generated E5V ΔPB clones and the control clone (figure 24A). *B2M* expression was detectable in both heterozygous *B2M*-deficient cell clones and in the E5Vf (wild-type) control clone. *B2M* expression was highest in the heterozygous E5V ΔPB Clone 16 followed by the E5Vf (wild-type) control clone and lowest in the heterozygous E5V ΔPB Clone 5. No *B2M* expression was detected in both homozygous E5V ΔPB Clone 22 and 28. These findings were confirmed by an agarose gel electrophoresis of the corresponding qRT-PCR products (shown in figure 24B). A WB analysis (described in section 3.5.3) was carried out to measure endogenous cellular MHC-I and B2M protein expression in the generated E5V ΔPB clones and the control clone (figure 24C). Mouse monoclonal anti-HLA-ABC IgG2a antibody (W6/32) (MA5-11723, Invitrogen™, Thermo Fisher Scientific) was used to detect MHC-I protein expression, expected to appear at 46 kDa. Rabbit monoclonal anti-beta 2 microglobulin antibody (ab75853, Abcam) was used to detect B2M protein expression, expected to appear at 14 kDa. WB analysis showed the presence of endogeneous MHC-I protein expression in all generated E5V ΔPB clones and the E5Vf (wild-type) control clone (figure 24C, left side). Furthermore, endogenous B2M protein expression was verified in the heterozygous E5V ΔPB Clones 5 and 16 and in E5Vf (wild-type) control clone. In contrast, no endogenous B2M protein could be detected in the homozygous E5V ΔPB Clones 22 and 28, confirming the successful B2M ablation (figure 24C, right side).

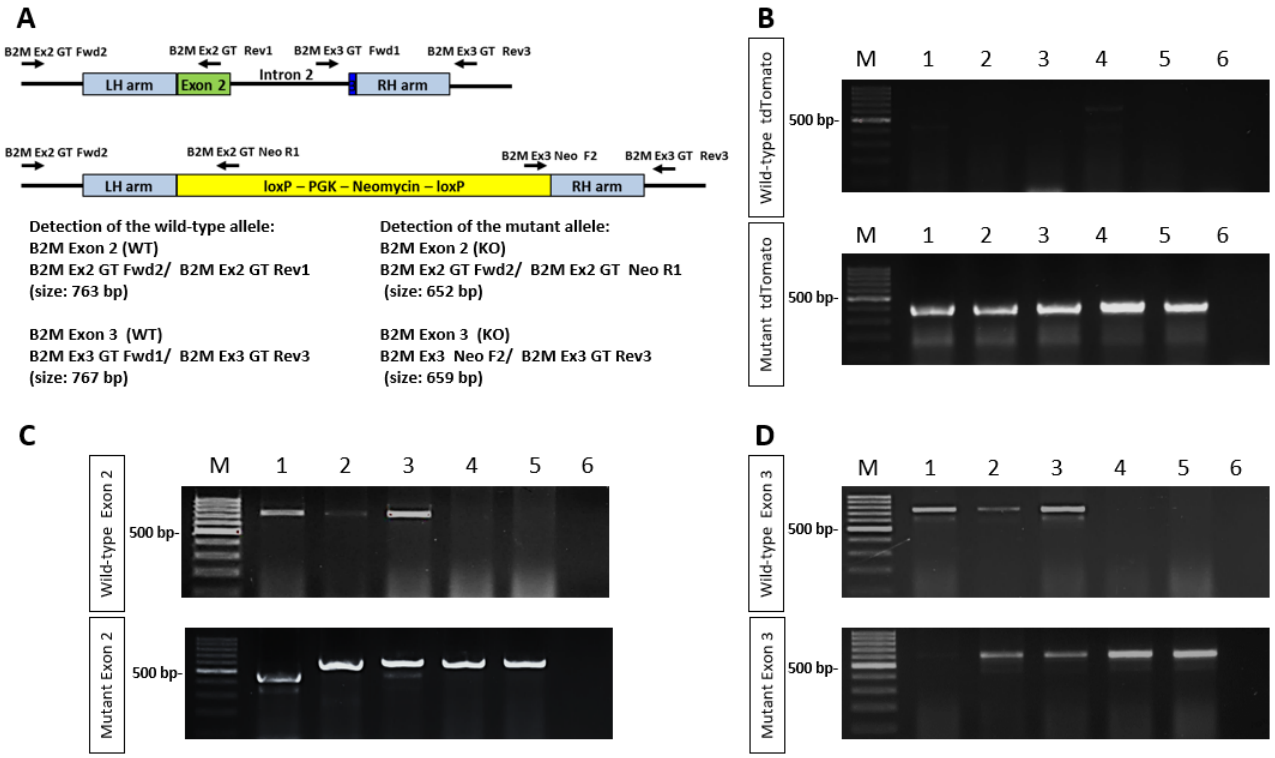

Figure 23: Genotype analysis of the generated *B2M*-deficient homozygous and heterozygous E5V ΔPB cell clones

(A) Schematic presentation of primers used for confirmation of the *B2M* gene knockout. The arrows indicate the position and orientation of PCR primers used for genotyping. The upper scheme shows exons 2 and 3 of the wild-type allele at the *B2M* locus. Primer sets B2M Exon 2 (WT) (B2M Ex2 GT Fwd2/ B2M Ex2 GT Rev1) and B2M Exon 3 (WT) (B2M Ex3 GT Fwd1/ B2M Ex3 GT Rev3) were used to detect wild-type alleles and lead to 763 bp and 767 bp amplicons, respectively. The lower scheme shows the mutant allele at the *B2M* locus, in which exons 2 and 3 of the *B2M* gene were replaced by a neomycin resistance cassette. Primer sets B2M Exon 2 (KO) (B2M Ex2 GT Fwd2/ B2M Ex2 GT Neo R1) and B2M Exon 3 (KO) (B2M Ex3 Neo F2/ B2M Ex3 GT Rev3) were used to identify mutant alleles and lead to 652 bp and 659 bp amplicons, respectively. In figures **(B)**, **(C)** and **(D)**: Lane M: marker GeneRuler^{TM} 100 bp DNA Ladder (Thermo Scientific^{TM}, Thermo Fisher Scientific), the 500 bp band is indicated; Lane 1: E5Vf wild-type (control clone); Lane 2: E5V ΔPB Clone 5 heterozygous; Lane 3: E5V ΔPB Clone 16 heterozygous; Lane 4: E5V ΔPB Clone 22 homozygous; Lane 5: E5V ΔPB Clone 28 homozygous; Lane 6: negative control. **(B)** Agarose gel electrophoresis was used to confirm the tdTomato knock-in and the Cre-mediated excision of the puromycin resistance. The upper gel shows the detection of wild-type alleles using primer set tdTomato (PURO). The lower gel shows the detection of mutant alleles using primer set tdTomato (CRE). **(C)** Agarose gel electrophoresis was used to confirm the B2M Exon 2 knockout and the knock-in of the neomycin resistance. The upper gel shows the detection of wild-type alleles using primer set B2M Exon 2 (WT). The lower gel shows the detection of mutant alleles using primer set B2M Exon 2 (KO). **(D)** Agarose gel electrophoresis to confirm the B2M Exon 3 knockout and the knock-in of the neomycin resistance. The upper gel shows the detection of wild-type alleles using primer set B2M Exon 3 (WT). The lower gel shows the detection of mutant alleles using primer set B2M Exon 3 (KO). **Abbreviations**: PGK: phosphoglycerate kinase; loxP: locus of X-over P1; LH arm: left homology arm; RH arm: right homology arm.

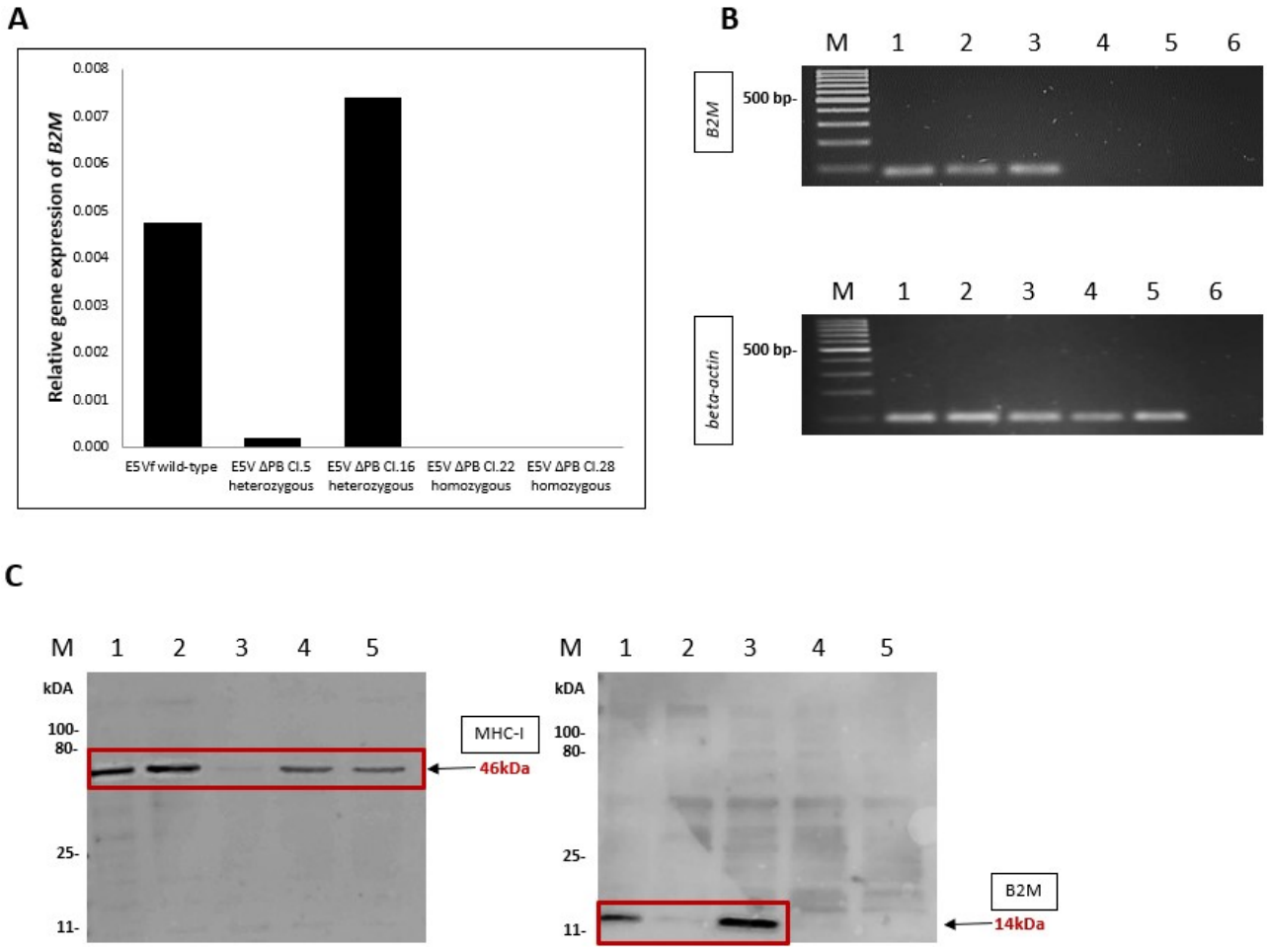

Figure 24: Characterization of the generated *B2M*-deficient homozygous and heterozygous E5V ΔPB cell clones

(A) Representative relative gene expression levels of *B2M* (NM_004048.4) in the generated homozygous and heterozygous *B2M*-deficient hiPS cell clones. *ACTB* (NM_001101.3) was used to normalize qRT-PCR data for relative quantification. **(B)** Corresponding agarose gel electrophoresis of the qRT-PCR products. The upper gel shows the detection of *B2M* (NM_004048.4) and the lower gel the detection of *ACTB* (NM_001101.3). Lane M: marker GeneRuler^{TM} 100 bp DNA Ladder (Thermo Scientific^{TM}, Thermo Fisher Scientific), the 500 bp band is indicated. Lane 1: E5Vf wild-type (control clone). Lane 2: E5V ΔPB Clone 5 heterozygous. Lane 3: E5V ΔPB Clone 16 heterozygous. Lane 4: E5V ΔPB Clone 22 homozygous. Lane 5: E5V ΔPB Clone 28 homozygous. Lane 6: negative control. **(C)** Representative western blot analysis to determine endogenous cellular B2M and MHC-I protein expression in the generated homozygous and heterozygous B2M-deficient hiPS cell clones. The left gel shows the detection of MHC-I and the right gel the detection of B2M. Lane M: marker Color Prestained Protein Standard, Broad Range (11-245 kDa) (New England Biolabs, Ipswich, MA). Lane 1: E5Vf wild-type (control clone). Lane 2: E5V ΔPB Clone 5 heterozygous. Lane 3: E5V ΔPB Clone 16 heterozygous. Lane 4: E5V ΔPB Clone 22 homozygous. Lane 5: E5V ΔPB Clone 28 homozygous. The arrow indicates the position of the protein of interest. **Abbreviations**: Cl.: clone; MHC-I: major histocompatibility complex class I; B2M: β2-microglobulin.

To evaluate the effect of gene editing on general characteristica like cell morphology and growth, hiPS cell colonies were monitored daily by microscopy. No morphological differences were found between E5Vf wild-type hiPS cell colonies (figure 25A) and edited homozygous (figure 25B) and heterozygous (figure 25C) E5V ΔPB hiPS cell colonies. After CRISPR-Cas9 gene targeting, the cell colony morphology of E5V ΔPB cell clones was preserved and

showed compact colony growth with clearly defined margins. To verify the assumption that the targeted *B2M* knockout has the potential to cause MHC-I cell surface disruption, the selected hiPS cell clones were immunocytochemically stained for MHC-I (described in section 3.5.1). The staining enabled to assess MHC-I cell surface expression changes. Immunofluorescent analysis demonstrated MHC-I surface expression in E5Vf (wild-type) control cells and in E5V ΔPB heterozygous cells. In contrast, surface MHC-I could not be detected in homozygous E5V ΔPB hiPS cells.

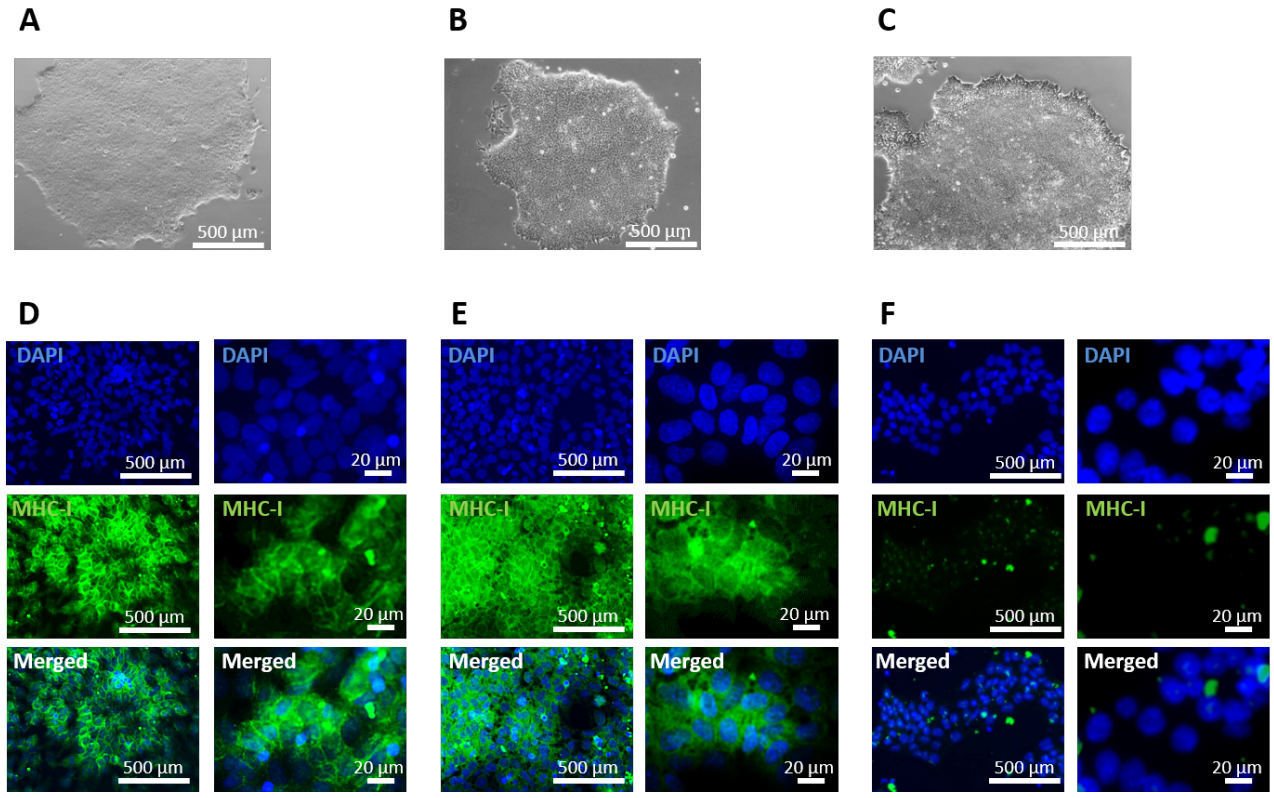

Figure 25: Monotoring of morphological and MHC-I cell surface expression changes in E5V ΔPB hiPS cells

(A) Representative phase-contrast image of an E5Vf wild-type hiPS cell colony (control clone). **(B)** Representative phase-contrast image of a heterozygous E5V ΔPB hiPS cell colony. **(C)** Representative phase-contrast image of a homozygous E5V ΔPB hiPS cell colony. **(D)** Immunofluorescence imaging of MHC-I cell surface expression (green) in E5Vf wild-type hiPS cells (control clone). **(E)** Immunofluorescence imaging of MHC-I cell surface expression (green) in E5V ΔPB heterozygous hiPS cells. **(F)** Immunofluorescence imaging of MHC-I cell surface expression (green) in E5V ΔPB homozygous hiPS cells. DAPI (blue) was used as a nuclear counterstain. **Abbreviations**: MHC-I: major histocompatibility complex class I; DAPI: 4',6-diamidino-2-phenylindole.

To further confirm the loss of a functional MHC-I complex on cell surface FACS analysis (described in section 3.5.2) was performed. Figure 26 shows the flow cytometric quantification of surface MHC-I on E5V ΔPB and control hiPS cells using anti-HLA-ABC monoclonal antibody (W6/32) (MA5-11723, Invitrogen^{TM}, Thermo Fisher Scientific). Similarly high cell viability yields (between 71.1 % and 92.3 %) for all analyzed samples could be determined. Figure S6 shows the corresponding cell viability assessment of all samples. Flow cytometric

assessment revealed that 60.2 % of the analyzed E5Vf wild-type hiPS cells (control clone) did express MHC-I (figure 26C). No signal was detected in the corresponding unstained (0.059 %, figure 26A) and secondary antibody control cells (0.454 %, figure 26B). 3.96 % of the analyzed heterozygous E5V ΔPB hiPS cells were MHC-I positive (figure 26F). No signal was detected in the corresponding unstained (0.047 %, figure 26D) and secondary antibody control cells (0.803 %, figure 26E). As expected, MHC-I complex was not expressed on homozygous E5V ΔPB hiPS cells (0.249 %, figure 26I), smiliar to unstained (0.136 % figure 26G) and secondary antibody control cells (0.634 %, figure 26H).

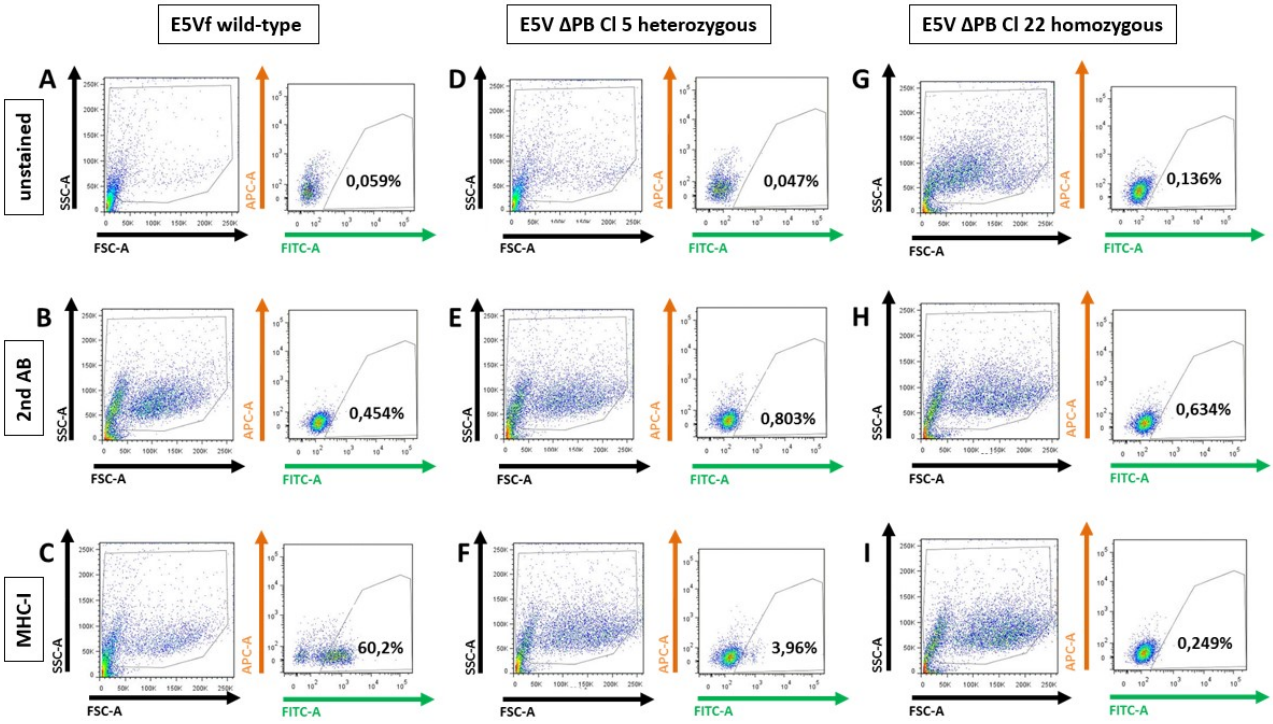

Figure 26: FACS analysis of MHC-I cell surface expression in E5V ΔPB hiPS cells
(A) Representative FACS analysis of unstained E5Vf wild-type hiPS cells (negative control) **(B)** Representative FACS analysis of E5Vf wild-type hiPS cells stained with the secondary antibody alone (secondary antibody control). **(C)** Representative FACS analysis of MHC-I cell surface expression in E5Vf wild-type hiPS cells. **(D)** Representative FACS analysis of unstained E5V ΔPB Clone 5 heterozygous hiPS cells (negative control). **(E)** Representative FACS analysis of E5V ΔPB Clone 5 heterozygous hiPS cells stained with the secondary antibody alone (secondary antibody control). **(F)** Representative FACS analysis of MHC-I cell surface expression in E5V ΔPB Clone 5 heterozygous hiPS cells. **(G)** Representative FACS analysis of unstained E5V ΔPB Clone 22 homozygous hiPS cells (negative control). **(H)** Representative FACS analysis of E5V ΔPB Clone 22 heterozygous hiPS cells stained with the secondary antibody alone (secondary antibody control). **(I)** Representative FACS analysis of MHC-I cell surface expression in E5V ΔPB Clone 22 homozygous hiPS cells. **Abbreviations**: FACS: fluorescence-activated cell sorting; hiPS cells: human induced pluripotent stem cells; MHC-I: major histocompatibility complex class I.

4.4.2 Gene expression analysis during directed cardiac differentiation

Differentiation assays (described in section 3.2.4) enabled to assess the potential of homozygous and heterozygous E5V ΔPB cell clones to differentiate towards the cardiac lineage.

Gene expression analysis of the cardiac transcription factors *NKX2.5* (NM_004387.3), *TBX5* (NM_000192.3), and the cardiomyocyte-specific markers *MLC2v* (NM_000432.3) and *MLC2a* (NM_021223.2) was performed on days D0, D6, D8, D10, D14 and D21 of the directed cardiac differentiation protocol (shown in figure 14). The oligonucleotide primer sequences used for qRT-PCR are given in table 11. Besides upon directed cardiac differentiation, the MLC2v-tdTomato knock-in of E5V ΔPB cells enabled to track the expression of *MLC2v* over time by documenting the red fluorescence of hiPS cell-derived CMs with the Axiovert 200 M Inverted Fluorescent Microscope (Carl Zeiss AG, Oberkochen, Germany). This enabled to assess their potential to differentiate into ventricular CMs.

Gene expression analysis of E5V ΔPB homozygous hiPS cells-derived CMs

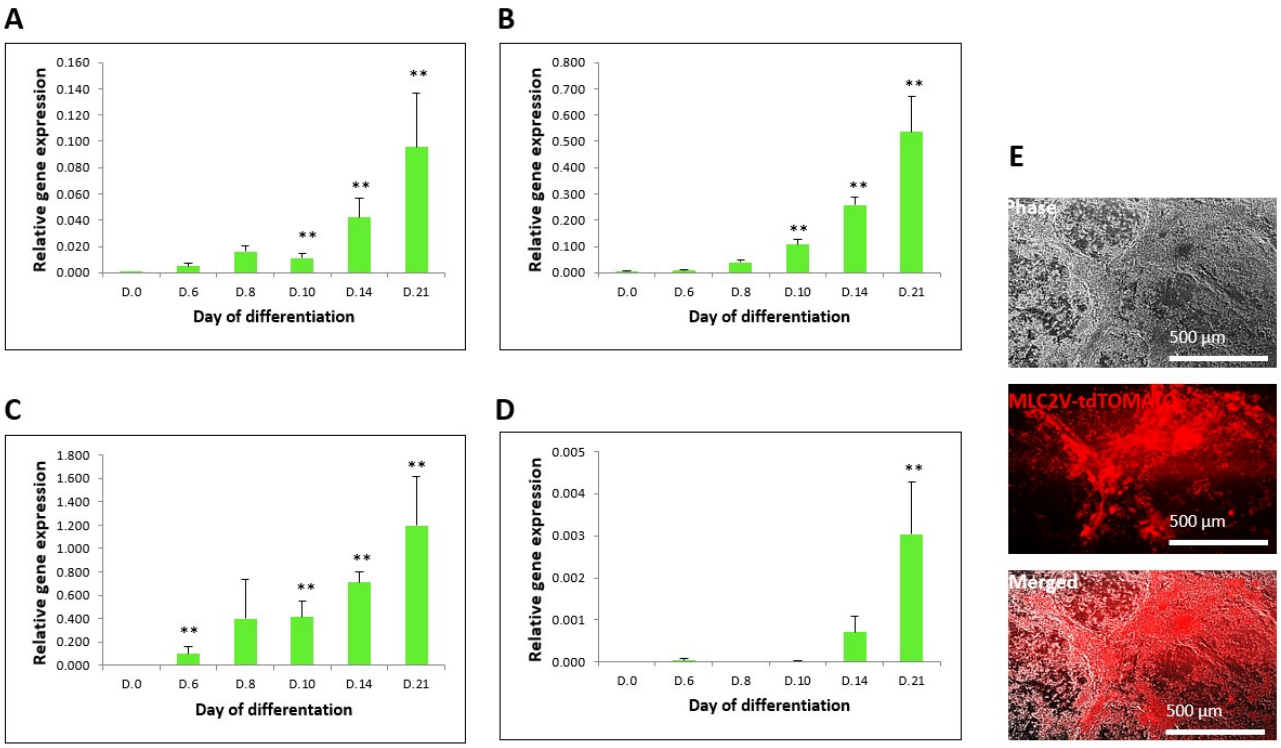

Figure 27: Gene expression analysis during directed cardiac differentiation of E5V ΔPB homozygous hiPS cells

Relative gene expression levels of **(A)** *NKX2.5* (NM_004387.3), **(B)** *TBX5* (NM_000192.3), **(C)** *MLC2a* (NM_021223.2) and **(D)** *MLC2v* (NM_000432.3) during directed cardiac differentiation (D0 to D21). *ACTB* (NM_001101.3) was used to normalize qRT-PCR data for relative quantification. Relative gene expression was determined in two independent differentiation assays with biological triplicates. Deviations in gene expression are reported as standard error of the mean. **(E)** Representative phase-contrast image of hiPS-derived CMs on day 19 of the directed cardiac differentiation protocol. The MLC2v-tdTomato knock-in of the E5V cell line enabled to indirectly monitor the endogenous *MLC2v* expression (red) upon directed cardiac differentiation. The expression of the gene of interest at time 0 was compared to the induced gene expression determined for the other time points. $^{*}p < 0.05$; $^{**}p < 0.01$; $^{***}p < 0.001$ by Mann-Whitney Rank Sum Test or Student's T-Test. **Abbreviations**: *NKX2.5*: *NK2 Homeobox 5*; *TBX5*: *T-Box 5*; *MLC2v*: *ventricular Myosin Light Chain-2*; *MLC2a*: *atrial Myosin Light Chain-2*; *ACTB*: *Actin Beta*.

Figure 27 displays the cardiac gene expression analysis of one representative homozygous E5V ΔPB cell clone (Clone 22). Figure 27A shows the relative gene expression levels of the cardiomyogenic differentiation marker *NKX2.5* (George et al., 2015). *NKX2.5* was first induced on D6 and increased continuously. Figure 27B shows the relative gene expression levels of the cardiomyogenic differentiation marker *TBX5* (Steimle & Moskowitz, 2017). *TBX5* was detectable from D0 on and increased continuously. Figure 27C shows the relative gene expression levels of *MLC2a*, a cardiac marker for atrial-, nodal-, or immature ventricular-like CMs (Ichimura et al., 2020; Bedada et al., 2016). *MLC2a* was first induced on D6 and increased continuously. Figure 27D shows the relative gene expression levels of *MLC2v*, a cardiac marker for mature ventricular-like CMs (Bedada et al., 2016; Guo & Pu, 2020). *MLC2v* was detectable at a very low level on D6 and D10. *MLC2v* expression was clearly detectable on D14 and increased strongly until D21. E5V ΔPB homozygous hiPS cell-derived CMs typically started beating on D10 and the number of contracting CMs increased continuously until D14. The tdTomato fluorescence in differentiating E5V ΔPB homozygous hiPS cells was generally detectable around D20 of the directed cardiac differentiation protocol and increased over time. Figure 27E shows a representative phase-contrast and fluorescence image of E5V ΔPB homozygous hiPS cell-derived CMs on D19 of the directed cardiac differentiation protocol. An intense red fluorescence corresponding to the tdTomato expression was detected.

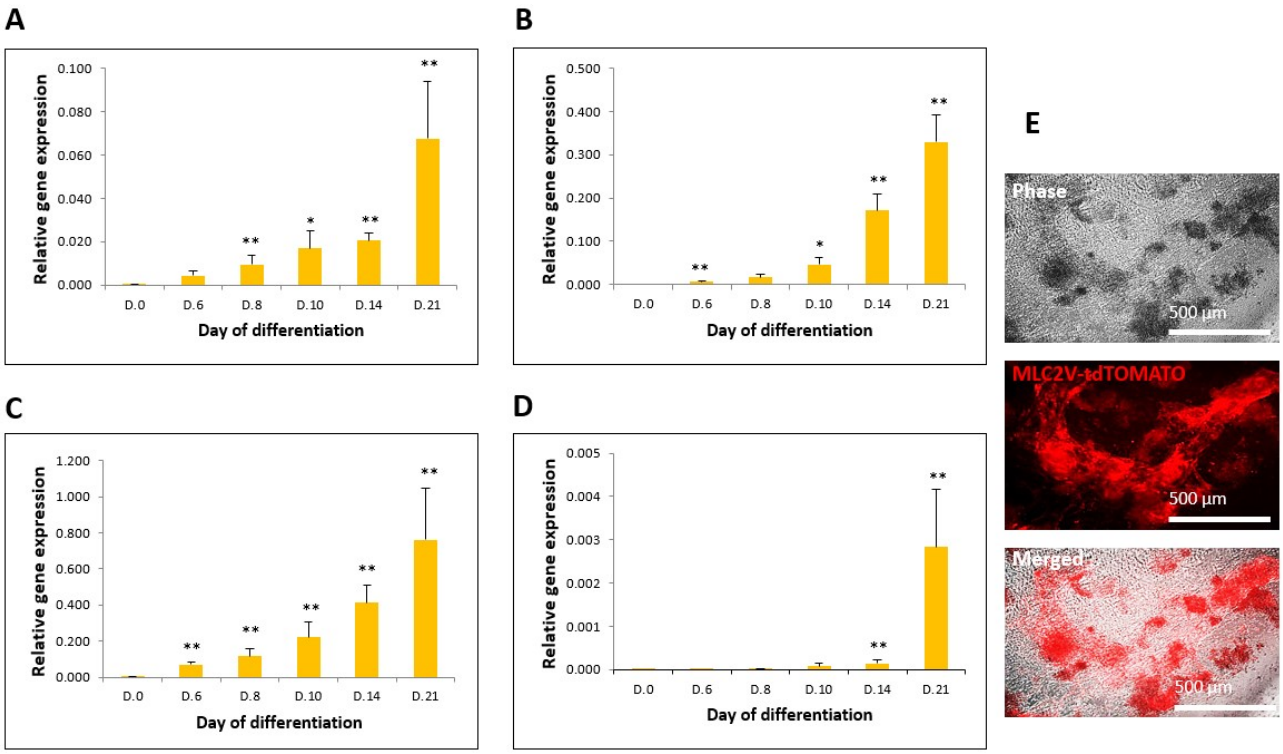

Figure 28: Gene expression analysis during directed cardiac differentiation of E5V ΔPB heterozygous hiPS cells

Relative gene expression levels of **(A)** *NKX2.5* (NM_004387.3), **(B)** *TBX5* (NM_000192.3), **(C)** *MLC2a* (NM_021223.2) and **(D)** *MLC2v* (NM_000432.3) during directed cardiac differentiation (D0 to D21). *ACTB* (NM_001101.3) was used to normalize qRT-PCR data for relative quantification. Relative gene expression was determined in two independent differentiation assays with biological triplicates. Deviations in gene expression are reported as standard error of the mean. **(E)** Representative phase-contrast image of hiPS-derived CMs on day 29 of the directed cardiac differentiation protocol. The MLC2v-tdTomato knock-in of the E5V cell line enabled to indirectly monitor the endogenous *MLC2v* expression (red) upon directed cardiac differentiation. The expression of the gene of interest at time 0 was compared to the induced gene expression determined for the other time points. $^{*}p < 0.05$; $^{**}p < 0.01$; $^{***}p < 0.001$ by Mann-Whitney Rank Sum Test or Student's T-Test. **Abbreviations**: *NKX2.5*: *NK2 Homeobox 5*; *TBX5*: *T-Box 5*; *MLC2v*: *ventricular Myosin Light Chain-2*; *MLC2a*: *atrial Myosin Light Chain-2*; *ACTB*: *Actin Beta.*.

Figure 28 displays the cardiac gene expression analysis of one representative heterozygous E5V ΔPB cell clone (Clone 5). Figure 28A shows the relative gene expression levels of the cardiomyogenic differentiation marker *NKX2.5* (George et al., 2015). *NKX2.5* was first detectable on D0 and increased continuously. Figure 28B shows the relative gene expression levels of the cardiomyogenic differentiation marker *TBX5* (Steimle & Moskowitz, 2017). *TBX5* was detectable from D6 on and increased continuously. Figure 28C shows the relative gene expression levels of *MLC2a*, a cardiac marker for atrial-, nodal-, or immature ventricular-like CMs (Ichimura et al., 2020; Bedada et al., 2016). *MLC2a* was first induced on D6 and increased continuously. Figure 28D shows the relative gene expression levels of *MLC2v*, a cardiac marker for mature ventricular-like CMs (Bedada et al., 2016; Guo & Pu, 2020). *MLC2v* was detectable at a very low level on D10 and D14 and increased strongly until D21. E5V ΔPB heterozygous

hiPS cell-derived CMs typically started beating on D10 and the number of contracting CMs increased continuously until D14. The tdTomato fluorescence in differentiating E5V ΔPB homozygous hiPS cells was generally detectable around D20 of the directed cardiac differentiation protocol and increased over time. Figure 27E shows a representative phase-contrast and fluorescence image of E5V ΔPB heterozygous hiPS cell-derived CMs on D29 of the directed cardiac differentiation protocol. An intense red fluorescence corresponding to the tdTomato expression was detected.

Comparative gene expression of cardiomyogenic differentiation markers

To verify that the CRISPR-Cas9-mediated *B2M* knockout did not compromise the capacity of E5V ΔPB cells to differentiate towards cardiac cells, cardiac gene expression during directed cardiac differentiation of homozygous and heterozygous E5V ΔPB clones was compared to the parental line (E5V cells homozygous for tdTomato). Figure 29A displays the comparative gene expression analysis of cardiomyogenic differentiation marker *NKX2.5* (George et al., 2015). In all performed differentiation assays, *NKX2.5* was first induced on D6 and increased continuously. *NKX2.5* induction and expression of differentiating homozygous and heterozygous E5V ΔPB cells showed a course similar to E5V cells homozygous for tdTomato (parental line). Only *NKX2.5* expression on D10 in homozygous E5V ΔPB cells was significantly lower than in E5V cells homozygous for tdTomato (parental line) ($p < 0.05$). Figure 29B shows the comparative gene expression analysis of cardiomyogenic differentiation marker *TBX5* (Steimle & Moskowitz, 2017). In all performed differentiation assays, *TBX5* was first detectable on D0 and increased continuously. *TBX5* expression on D6 ($p < 0.001$), D8 ($p < 0.05$) and D14 ($p < 0.05$) in homozygous E5V ΔPB cells was significantly lower than in parental cells (E5V homozygous for tdTomato). *TBX5* expression on D6 ($p < 0.001$), D8 ($p < 0.01$) and D10 ($p < 0.05$) in heterozygous E5V ΔPB cells was significantly lower than in parental line cells (E5V homozygous for tdTomato). Figure 29C shows the comparative gene expression analysis of *MLC2a*, a cardiac marker for atrial-, nodal-, or immature ventricular-like CMs (Ichimura et al., 2020; Bedada et al., 2016). In all performed differentiation assays, *MLC2a* was first induced on D6 and increased continuously. No significant changes in the *MLC2a* expression profile during directed cardiac differentiation of homozygous and heterozygous E5V ΔPB cells in comparison to the parental line (E5V homozygous for tdTomato) could be observed. Figure 29D shows the comparative gene expression analysis of *MLC2v*, a cardiac marker for mature ventricular-like CMs (Bedada et al., 2016; Guo & Pu, 2020). *MLC2v* was detectable at a very low level on D6, D8, D10 and D14 and increased until D21. Only *MLC2v* expression on D14 in homozygous E5V ΔPB cells was significantly lower than in parental line cells (E5V homozygous for tdTomato) ($p < 0.05$). In heterozygous E5V ΔPB cells *MLC2v* expression on D14 was significantly lower than in parental line cells (E5V homozygous for tdTomato ($p < 0.001$)).

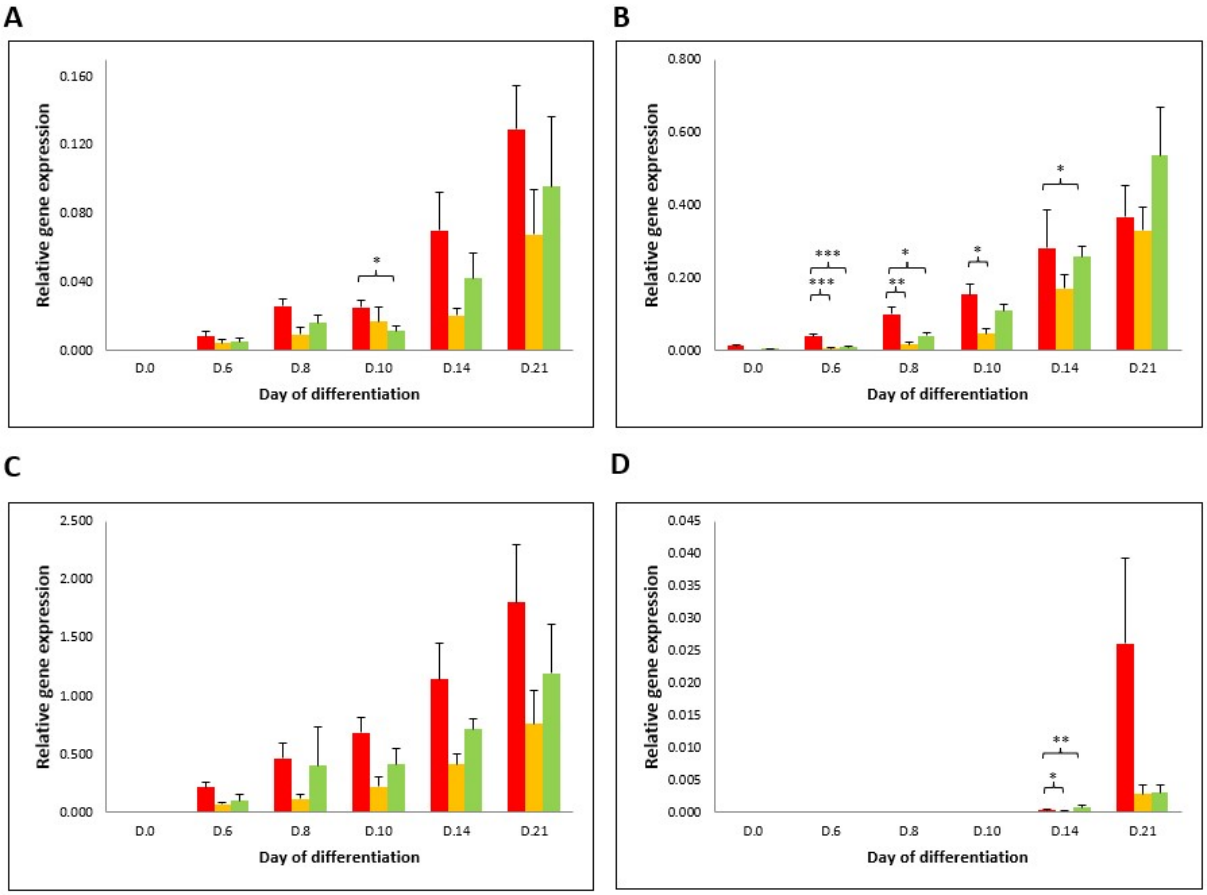

Figure 29: Comparative gene expression analysis during directed cardiac differentiation
Comparative gene expression analysis of **(A)** *NKX2.5* (NM_004387.3), **(B)** *TBX5* (NM_000192.3), **(C)** *MLC2a* (NM_021223.2) and **(D)** *MLC2v* (NM_000432.3) during directed cardiac differentiation [day 0 (D0) to day 21 (D21)]. Relative gene expression levels during directed cardiac differentiation of the generated homozygous (green) and heterozygous (orange) E5V ΔPB cell clones were compared to the E5V homozygous for tdTomato (parental line) (red). *ACTB* (NM_001101.3) was used to normalize qRT-PCR data for relative quantification. Relative gene expression of E5V ΔPB cell clones was determined in two independent differentiation assays with biological triplicates. Relative gene expression of E5V homozygous for tdTomato cell clones (parental line) was determined in four independent differentiation assays with biological duplicates or triplicates. Deviations in gene expression are reported as standard error of the mean. $^{*}p < 0.05$; $^{**}p < 0.01$; $^{***}p < 0.001$ by Mann-Whitney Rank Sum Test or Student's T-Test.
Abbreviations: *NKX2.5*: *NK2 Homeobox 5*; *TBX5*: *T-Box 5*; *MLC2v*: *ventricular Myosin Light Chain-2*; *MLC2a*: *atrial Myosin Light Chain-2*; *ACTB*: *Actin Beta.*.

4.4.3 Molecular characterization of E5V △PB hiPS cells-derived CMs

For molecular characterization, E5V ΔPB hiPS cell-derived CMs on day 30 of the directed cardiac differentiation protocol were immunocytochemically analyzed for the expression of cardiac-specific markers (described in section 3.5.1). Immunofluorescent analysis enabled to investigate the expression of TNNT2, a key marker for CMs and sarcomeric α-actinin, a key structural protein of the sarcomere (Waas et al., 2019; Lichter et al., 2014). Furthermore, the cells were stained for MLC2a, a marker for atrial CMs and MLC2v, a marker for ventricular CMs (Ichimura et al., 2020; Bedada et al., 2016). An anti-RFP antibody was used for the detection of tdTomato and thereby enabled monitoring the MLC2v-tdTomato knock-in of the E5V ΔPB cell line. Homozygous and heterozygous *B2M*-deficient clones were analyzed to assess whether there are observable differences in their cardiac-specific protein expression and their potential to differentiate into ventricular CMs.

Immunofluorescent analysis in homozygous E5V ΔPB hiPS cell-derived CMs (Clone 22) on day 30 of the directed cardiac differention protocol confirmed the expression of TNNT2, α-actinin, MLC2a and MLC2v, all detectable as a strong green fluorescent signal (figure 30). Furthermore, homozygous E5V ΔPB hiPS cell-derived CMs also stained positive for RFP, detectable as strong green fluorescent signal, which was virtually superimposable with the red fluorescent signal of the tdTomato expression (figure 30E). Figure 30I shows the immunofluorescent staining of α-actinin and reveals the typical striated pattern of sarcomeres, which are the basic contractile units of CMs (Lichter et al., 2014; Sweeney & Hammers, 2018).

Immunofluorescent analysis in heterozygous E5V ΔPB hiPS cell-derived CMs (Clone 5) on day 30 (figure 31) of the directed cardiac differentiation protocol also confirmed the expression of TNNT2, α-actinin, MLC2a and MLC2v, detectable as strong green fluorescent signal (figure 31). Furthermore, heterozygous E5V ΔPB hiPS cell-derived CMs also stained positive for RFP, detectable as strong green fluorescent signal, which was virtually superimposable with the red fluorescent signal of the tdTomato expression (figure 31E). In figures 30 and 31 cell nuclei were stained blue by DAPI and the detected intense red fluorescence corresponded to the tdTomato expression, which enabled to indirectly monitor the endogenous *MLC2v* expression upon cardiac differentiation. No differences in *MLC2v* expression could be observed in comparison to the parental line (figure 15).

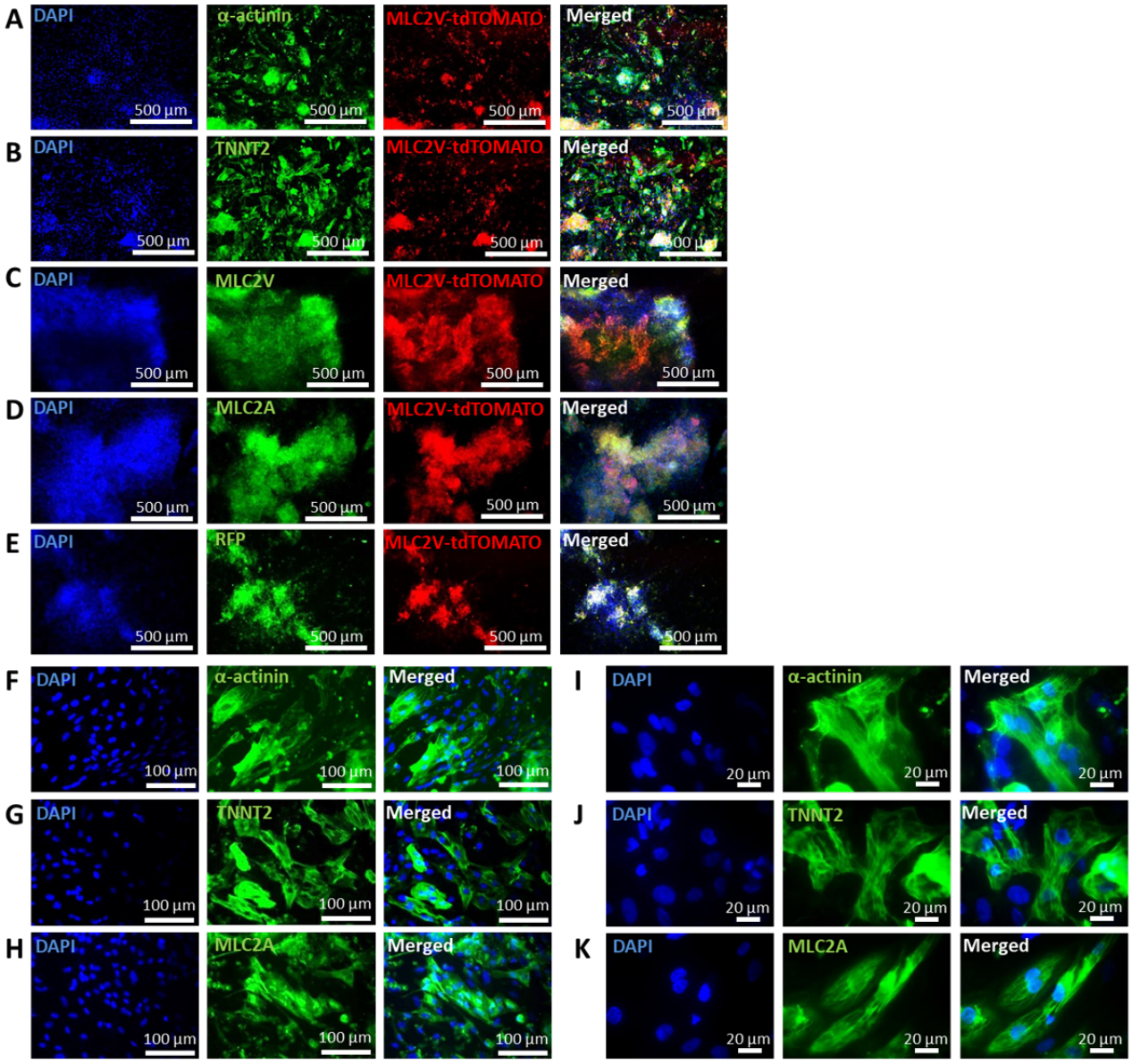

Figure 30: Immunofluorescence imaging of cardiac markers in E5V ΔPB homozygous hiPS cells-derived CMs on day 30 of the directed cardiac differentiation protocol

(A) Immunofluorescent analysis of sarcomeric α-actinin (green). **(B)** Immunofluorescent analysis of TNNT2 (green). **(C)** Immunofluorescent analysis of MLC2v (green). **(D)** Immunofluorescent analysis of MLC2a (green). **(E)** Immunofluorescent analysis of tdTomato using a FITC-labelled anti-RFP antibody (green). **(F)** Immunofluorescent analysis of sarcomeric α-actinin (green). **(G)** Immunofluorescent analysis of TNNT2 (green). **(H)** Immunofluorescent analysis of MLC2a. **(I)** Immunofluorescent analysis of sarcomeric α-actinin (green). **(J)** Immunofluorescent analysis of TNNT2 (green). **(K)** Immunofluorescent analysis of MLC2a (green). DAPI (blue) was used as a nuclear counterstain. The MLC2v-tdTomato knock-in of the E5V cell line enabled to indirectly monitor the endogenous *MLC2v* expression (red) upon directed cardiac differentiation. **Abbreviations**: TNNT2: cardiac Troponin T; MLC2v: ventricular Myosin Light Chain-2; MLC2a: atrial Myosin Light Chain-2; RFP: red fluorescent protein; DAPI: 4',6-diamidino-2-phenylindole.

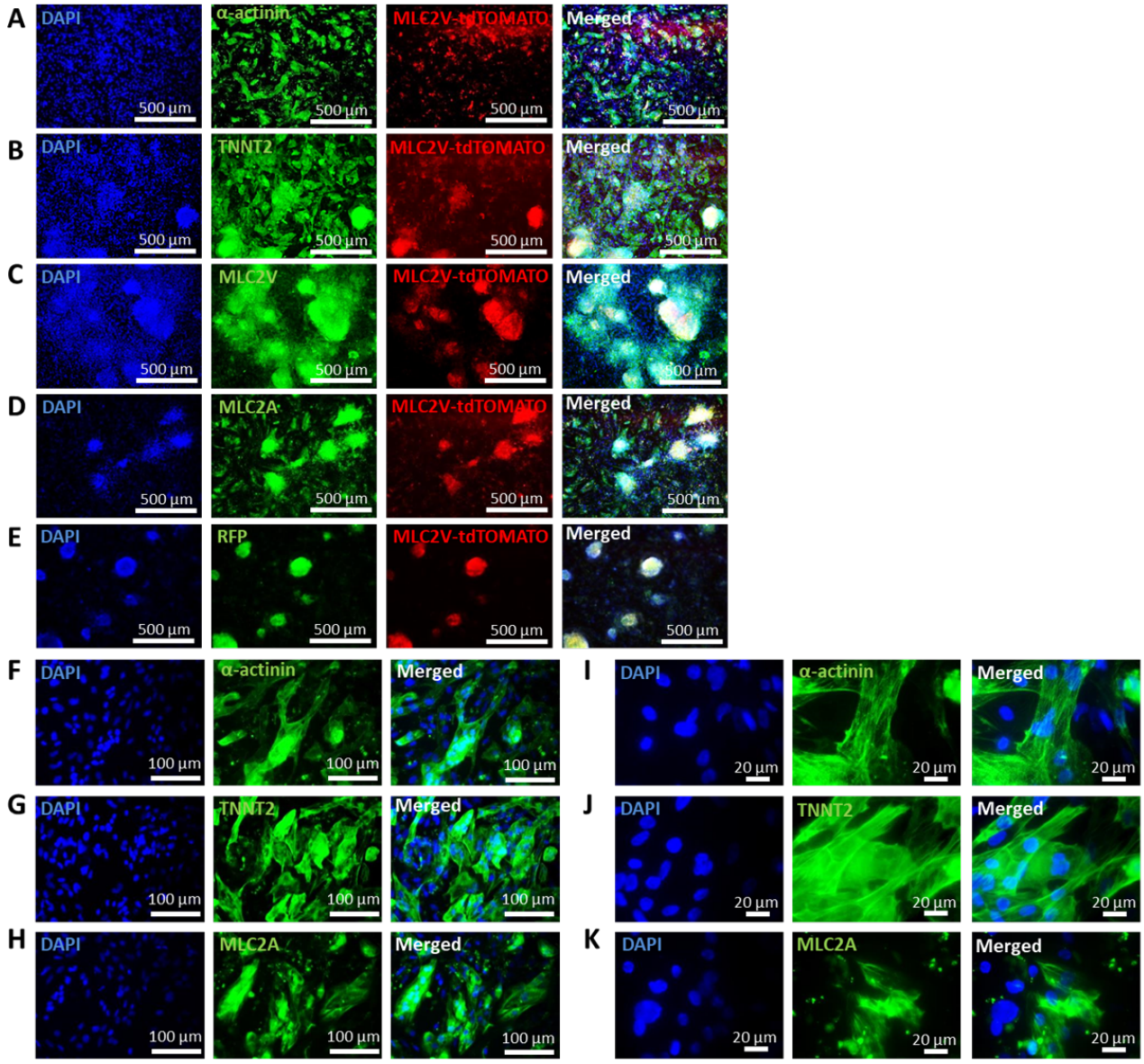

Figure 31: Immunofluorescence imaging of cardiac markers in E5V ΔPB heterozygous hiPS cells-derived CMs on day 30 of the directed cardiac differentiation protocol

(A) Immunofluorescent analysis of sarcomeric α-actinin (green). **(B)** Immunofluorescent analysis of cardiac Troponin T (green). **(C)** Immunofluorescent analysis of MLC2v (green). **(D)** Immunofluorescent analysis of MLC2a (green). **(E)** Immunofluorescent analysis of tdTomato using a FITC-labelled anti-RFP antibody (green). **(F)** Immunofluorescent analysis of sarcomeric α-actinin (green). **(G)** Immunofluorescent analysis of cardiac Troponin T (green). **(H)** Immunofluorescent analysis of MLC2a (green). **(I)** Immunofluorescent analysis of sarcomeric α-actinin (green). **(J)** Immunofluorescent analysis of cardiac Troponin T (green). **(K)** Immunofluorescent analysis of MLC2a (green). DAPI (blue) was used as a nuclear counterstain. The MLC2v-tdTomato knock-in of the E5V cell line enabled to indirectly monitor the endogenous *MLC2v* expression (red) upon directed cardiac differentiation. **Abbreviations**: TNNT2: cardiac Troponin T; MLC2v: ventricular Myosin Light Chain-2; MLC2a: atrial Myosin Light Chain-2; RFP: red fluorescent protein; DAPI: 4',6-diamidino-2-phenylindole.

4.5 Isolation of PBMCs and immune cell subpopulations

For the establishment of immunological assays that enable to quantify cell-mediated immune response against the generated *B2M*-deficient cell line E5V ΔPB, immune cell subpopulations were isolated from PBMCs and were analyzed.

4.5.1 PBMC population analysis

Before proceeding to the establishment of immunological assays, the PBMC cell population was further analyzed. First of all, FACS analysis was employed to compare the heterogeneity and the FCS/SSC flow cytometric profile of isolated PBMCs to peripheral whole blood (described in section 3.6.4). Figure 32A shows the cytograms of both a peripheral whole blood and a PBMCs sample. In the FCS/SSC flow cytometric profile of the peripheral whole blood sample three distinct cell populations corresponding to neutrophils, monocytes and lymphocytes could be identified based on their size and granularity. In the FCS/SSC flow cytometric profile of isolated PBMCs two distinct cell populations corresponding to monocytes and lymphocytes could be identified based on their size and granularity. Furthermore, the lymphocyte subset distribution within the PBMC fraction was studied using FACS to support the interpretation of the performed immune cell-based assays. The percentage of T-lymphocytes (CD3+), cytotoxic T-lymphocytes (CD8+) and natural killer (NK) cells (CD16+) was determined by labeling the cells with specific antibodies (anti-CD3-FITC, anti-CD8-FITC, anti-CD16-FITC, human, Miltenyi Biotec) that target their respective CD markers (described in section 3.6.5). Figure 32B displays a representative diagram of the different immune cell subpopulations frequencies within PBMCs showing a total of 26.9 % CD16+ NK-cells and 44.5 % CD3+ T-cells. The CD3+ T-cell fraction was composed of 11.7 % CD8+ cytotoxic T-cells. A total of 28.6 % CD3- and CD16- cells were detected, corresponding to other immune cell subsets. The associated FACS analysis is shown in figure S7.

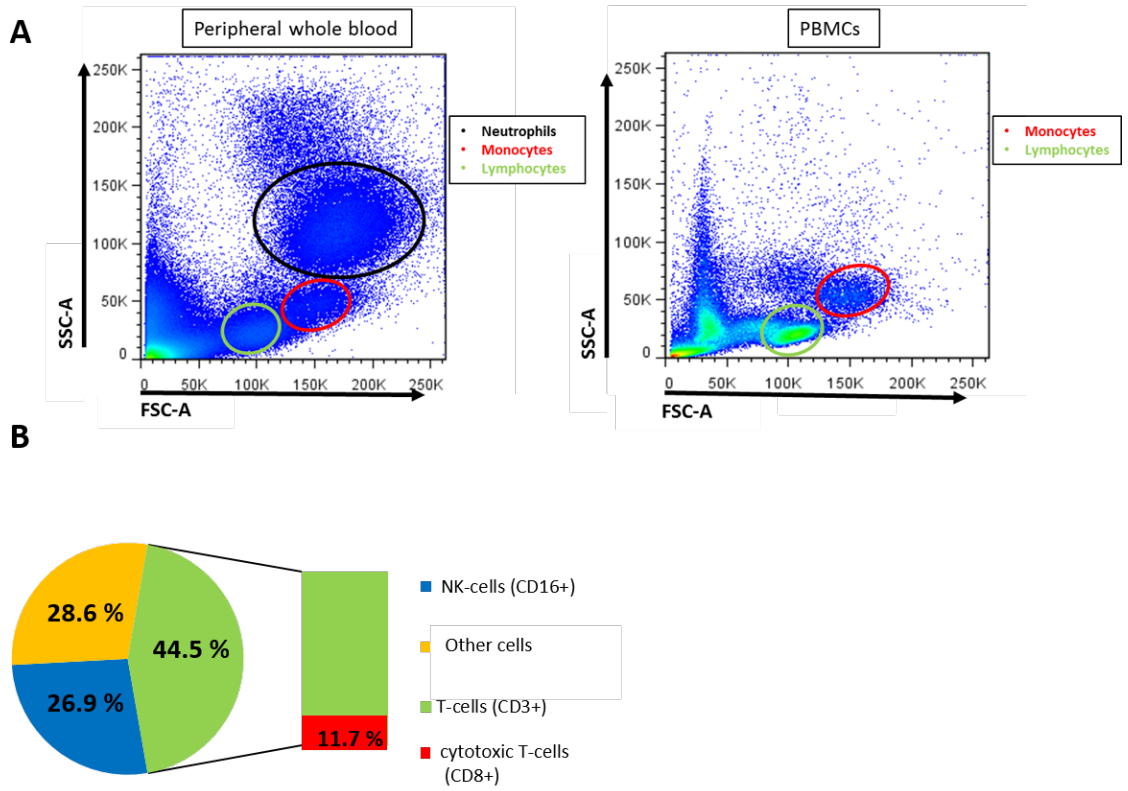

Figure 32: Cellular heterogeneity of PBMCs
(A) Flow cytometric profile of peripheral whole blood and isolated PBMCs. FCS/SSC density plot for identification of immune cell subpopulations. **(B)** Determination of immune cell subpopulations frequencies. In **(A)** and **(B)**, data from one representative experiment of two independent experiments are shown. **Abbreviations**: PBMCs: peripheral blood mononuclear cells; CD: cluster of differentiation; NK-cells: natural killer cells.

4.5.2 Enrichment of immune cell subpopulations and purity assessment

Figure 33A shows a schematic of the workflow employed for isolation of immune cell subpopulations. In a first step, PBMCs were isolated from peripheral whole blood by ficoll-density gradient centrifugation (described in section 3.6.2). In a second step, the MACS® MicroBead Technology (Miltenyi Biotec), a column-based magnetic cell isolation method, was employed according to the manufacturer's instructions to perform the enrichment of immune cell subpopulations from PBMCs (described in section 3.6.3). After isolation, purity of MACS enriched immune cell subpopulations was assessed by FACS. For this purpose, MACS enriched CD3+ T-cells, CD8+ cytotoxic T-cells and CD16+ NK-cells were stained with corresponding FITC-labeled staining antibodies (anti-CD3-FITC, anti-CD8-FITC, anti-CD16-FITC, human, Miltenyi Biotec) and were analyzed by FACS. Figures 33B and 33C show representative data of flow cytometric purity determination. Firstly, the lymphocyte population was identified based on the forward and side scatter profile (figure 33B). Secondly, gating on FITC posi-

tive cells enabled to determine cell population purity of MACS enriched and labeled CD3+, CD8+ and CD16+ cell populations (figure 33C). 99.5 % of the MACS enriched CD3+ cell fraction was CD3+ positive and 99.1 % of the MACS enriched CD8+ cell fraction was found CD8+ positive. Besides, 98.1 % of the MACS enriched CD16+ cell fraction was found CD16+ positive. Figure 33D displays the results of purity evaluation based on two independent experiments. Magnetic-column-based T-cell isolation resulted in an average of 99.15 % CD3+ T-cells. Magnetic-column-based cytotoxic T-cell isolation led to an average of 98.9 % CD8+ T-cells. Furthermore, magnetic-column-based cytotoxic NK-cell isolation enabled to enrich an average of 97.4 % CD16+ NK-cells.

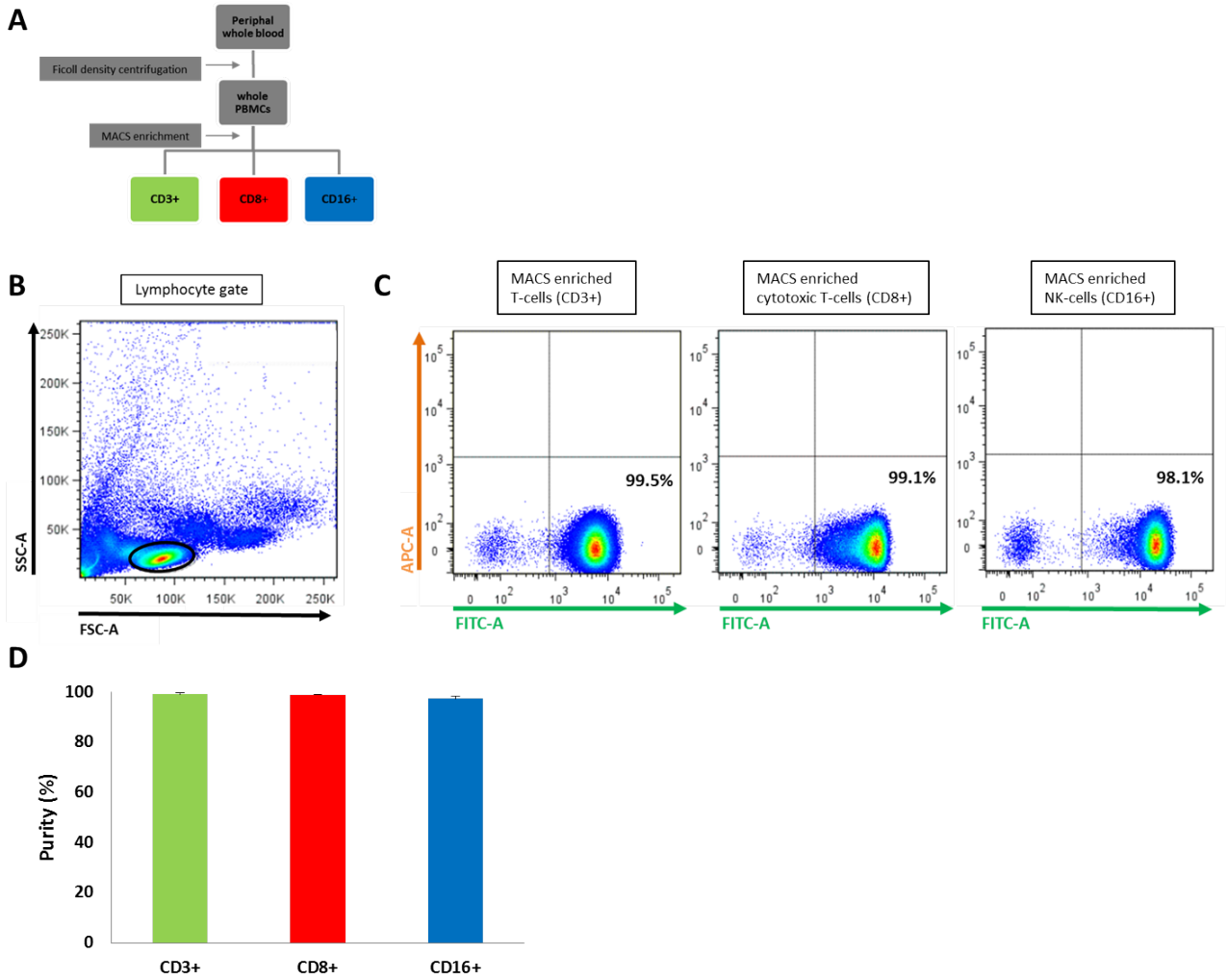

Figure 33: Purity analysis of MACS enriched immune cell subpopulations
(A) Workflow for isolation of immune cell subpopulations. **(B)** and **(C)** Purity assessment of MACS enriched immune cell subpopulations using FACS analysis. Data from one representative experiment of two independent experiments are shown. **(B)** FCS/SSC density plot. The lymphocyte gate is indicated by the circle. **(C)** MACS enriched T-cells (CD3+), cytotoxic T-cells (CD8+) and NK-cells (CD16+) were incubated with the corresponding FITC-labeled staining antibody (anti-CD3-FITC, anti-CD8-FITC, anti-CD16-FITC, human, Miltenyi Biotec) and were analyzed using FACS. **(D)** Purity evaluation. The purity of MACS enriched immune cell subpopulations was determined in two independent experiments. Deviations in percent purity are reported as standard deviation. **Abbreviations**: PBMCs: peripheral blood mononuclear cells; MACS: Magnetic cell sorting; CD: cluster of differentiation; NK-cells: natural killer cells; FACS: fluorescence-activated cell sorting.

4.6 Establishment of immunological assays

To analyze and quantify the cell-mediated immune response against the generated *B2M*-deficient E5V ΔPB cell line, two different immune cell-based assays were established within the scope of this thesis.

4.6.1 Quantification of the immune response by measuring gene expression of secretory factors and cytokines

A first immune cell-based assay was developed in an attempt to evaluate the immunogenicity of hiPS cells and CMs. By co-culturing hiPS cells or CMs with PBMCs, this assay aims to characterize and quantify the immune response by analyzing expression of specific immune regulatory genes (described in section 3.7.1). Upon stimulation with allogeneic cells PBMCs are activated, enabling the detection of proliferative and cytokine responses. For immune response evaluation, all cells were harvested after a defined incubation period (3, 4 and 5 days of co-culture). Following RNA isolation and reverse transcription into cDNA, relative gene expression for *GZMB* (NM_004131.6), *IFN*γ (NM_000619.3), *IL2* (NM_000586.4) and *IL10* (NM_000572.3) was quantified by qRT-PCR. The oligonucleotide primer sequences used for qRT-PCR are given in table 11. All preliminary experiments to establish the assay protocol were performed with immunocompetent [E5V homozygous for tdTomato (parental line)] cells. For each experimental setup, three controls were prepared. Figure 34 shows a representative agarose gel electrophoresis of qRT-PCR products from experimental controls, performed to demonstrate that the measured gene expression of secretory factors and cytokines originated from effector cells (PBMCs) and not from target cells (hiPS cells or CMs). Firstly, the "effector cell only"control, which contained 100 μl of effector cells (1 x10^5 PBMCs/well) and 100 μl assay medium, to analyze specific immune regulatory gene expression in unstimulated PBMCs (lane 1). Secondly, the "stimulated effector cell"control, which contained 100 μl of effector cells (1 x10^5 PBMCs/well) and 100 μl assay medium supplemented with 10 μg/ml of the lectin PHA (Phytohemagglutinin-M (PHA-M), Roche Applied Science) (lane 2). PHA-mediated stimulation of PBMCs enabled studying immune regulatory gene profiles of stimulated PBMCs and served as positive control for immune cell stimulation. Thirdly, a "target cell only"control, which contained 100 μl of target cells (1 x10^5 hiPS cells/well) and 100 μl assay medium [RPMI 1640 Medium (Biochrom, Merck Millipore, Merck KGaA) supplemented with 10 % FCS], to provide information about specific immune regulatory gene expression in hiPS cells (lane 3). To quantify the immunogenicity of target cells (hiPS cells), hiPS cells were co-cultured with PBMCs, enabling to analyze target cell-mediated stimulation of PBMCs (lane 4). No *GZMB* (figure 34A), *IFN*γ (figure 34B), *IL10* (figure 34C) and *IL2* (figure 34D) expression could be detected in the target cell only control (hiPS cells only). In comparison with the hiPS cell only control, unstimulated PBMCs, PHA stimulated PBMCs and hiPS cell stimulated PBMCs did express *GZMB* (figure 34A), *IFN*γ (figure 34B), *IL10* (figure 34C) and *IL2* (figure 34D).

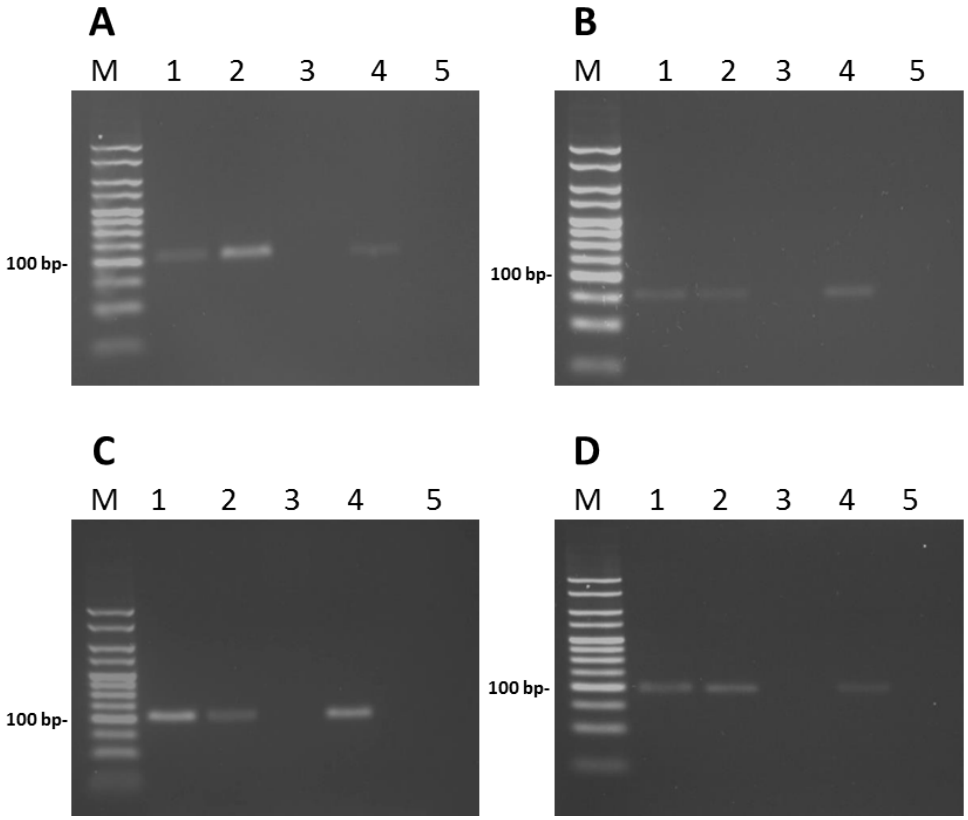

Figure 34: Agarose gel electrophoresis of experimental controls
Representative agarose gel electrophoresis of **(A)** *GZMB* (NM_004131.6), **(B)** *IFNγ* (NM_000619.3), **(C)** *IL10* (NM_000572.3), **(D)** *IL2* (NM_000586.4) qRT-PCR products from experimental controls. Lane M: marker Quantitas DNA Marker 25-500 bp (Biozym Scientific GmbH, Hessisch Oldendorf, Germany), the 100 bp band is indicated. Lane 1: effector cells only (unstimulated PBMCs). Lane 2: PHA (10 μg/ml) stimulated effector cells (positive control for PBMCs stimulation). Lane 3: target cells only (hiPS cells only). Lane 4: effector and target cell co-culture (target cell-mediated stimulation of PBMCs). Lane 5: negative control. **Abbreviations**: PBMCs: peripheral blood mononuclear cells; *GZMB*: granzyme B; *IFNγ*: *interferon γ*; *IL10*: *interleukin 10*; *IL2*: *interleukin 2*; PHA: phytohemagglutinin; hiPS cells: human induced pluripotent stem cells.

Determination of the optimal incubation period and E:T ratio

In a first pilot experiment, the optimal incubation period for co-culture (described in section 3.7.1) was determined. To define the optimal incubation period for the assay, relative gene expression levels of *GZMB* (figure 35A), *IFNγ* (figure 35B), *IL10* (figure 35C), *IL2* (figure 35D) for various E:T ratios [PBMCs (effector cells):hiPS cells (target cells); E:T 1:1 (100.000 PBMCs/well:100.000 hiPS cells/well); E:T 3.125:1 (100.000:32.000); E:T 6.25:1 (100.000:16.000); E:T 12.5:1 (100.000:8.000); E:T 25:1 (100.000:4000); E:T 50:1 (100.000:2000); E:T 100:1 (100.000:1000)] after 3, 4 and 5 days of co-culture were compared. No significant differences in gene expression could be found between 3, 4 and 5 days of co-culture. Despite the lack of significance, the *IL10* gene expression on day 3 for all E:T ratios was higher than the *IL10* expression on days 4 and 5. For practical reasons and for rapid assay feasibility an incubation period of 3 days (72 hours) was therefore chosen for subsequent experiments.

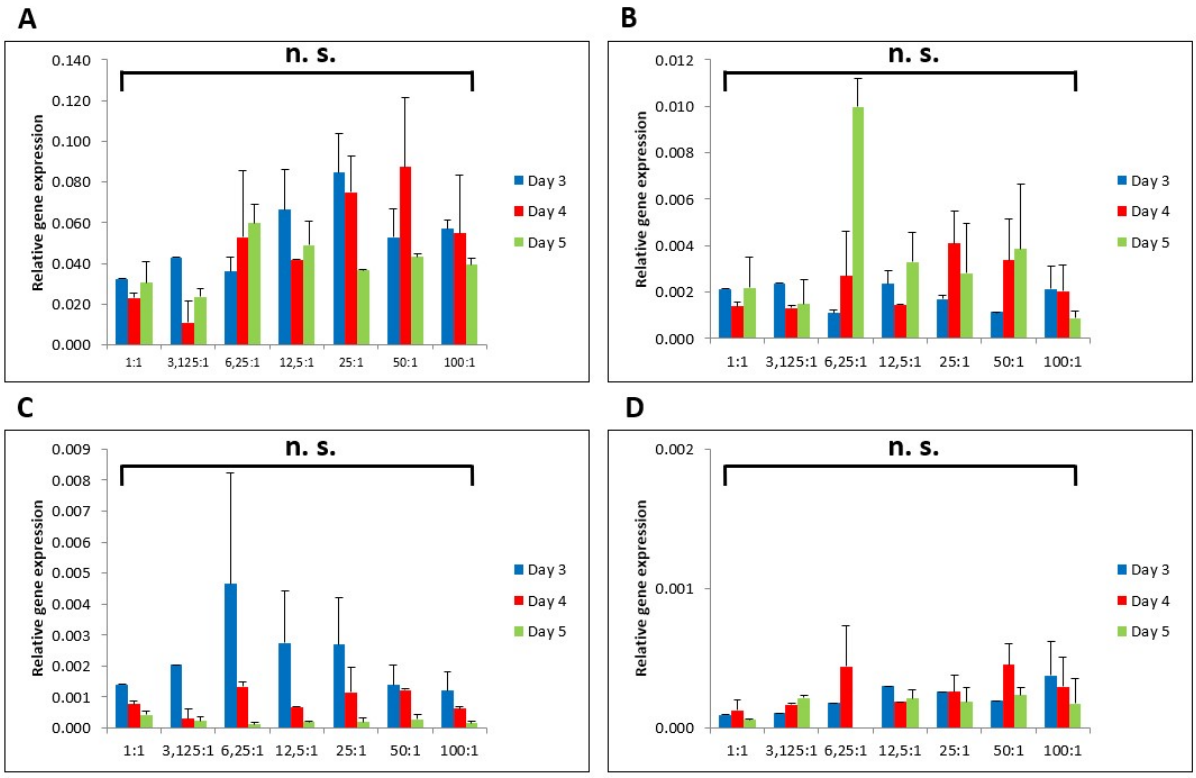

Figure 35: Determination of the optimal incubation period

Relative gene expression levels of **(A)** *GZMB* (NM_004131.6), **(B)** *IFNγ* (NM_000619.3), **(C)** *IL10* (NM_000572.3), **(D)** *IL2* (NM_000586.4) for different E:T ratios [PBMCs (effector cells) and hiPS cells (target cells)] after 3 (blue bars), 4 (red bars) and 5 days (green bars) of co-culture. A representative co-culture assay performed with biological duplicates is shown. Deviations in gene expression are reported as standard deviation. Multiple comparisons were analyzed by Mann-Whitney Rank Sum Test or Student's T-Test. P-values < 0.05 were considered statistically significant. For all analyzed E:T ratios no significant differences in gene expression could be found between 3, 4 and 5 days of co-culture. **Abbreviations**: PBMCs: peripheral blood mononuclear cells; hiPS cells: human induced pluripotent stem cells; *GZMB*: granzyme B; *IFNγ*: *interferon γ*; *IL10*: *interleukin 10*; *IL2*: *interleukin 2*; E:T ratio: effector to target ratio.

In the further course, the results of the first pilot experiment were verified and the number of biological replicates was increased. In a next step, the optimal E:T ratio for PBMCs and hiPS cell co-culture was defined. To determine the optimal E:T ratio, target cells (hiPS cells) were titrated and added to a constant number of effector cells (10^5 PBMCs). Figure 36 displays the results of relative gene expression analysis of secretory factors and cytokines for various E:T (1:1-100:1) ratios. Higher E:T ratios than E:T (100:1) were not tested due to the limiting number of PBMCs isolated. The results showed that *GZMB* (figure 36A) expression in PBMCs stimulated with immunocompetent E5V homozygous for tdTomato (parental line) hiPS cells was clearly detectable for all tested E:T ratios. The level of *GZMB* increased gradually with higher E:T ratios and was highest for a 100:1 E:T ratio. Figure 36B shows the expression of *IFNγ*. *IFNγ* gene expression was clearly detectable for all tested E:T ratios. The level of *IFNγ* increased gradually with higher E:T ratios and was highest for a 100:1 E:T ratio. Figure 36C shows the expression of *IL10*. *IL10* gene expression was clearly detectable for all tested E:T ratios and was highest for a 12.5:1 E:T ratio. Furthermore, low levels of *IL2* expression (figure 36D) were observed for 1:1 to 50:1 E:T ratios and increased greatly for a 100:1 E:T ratio.

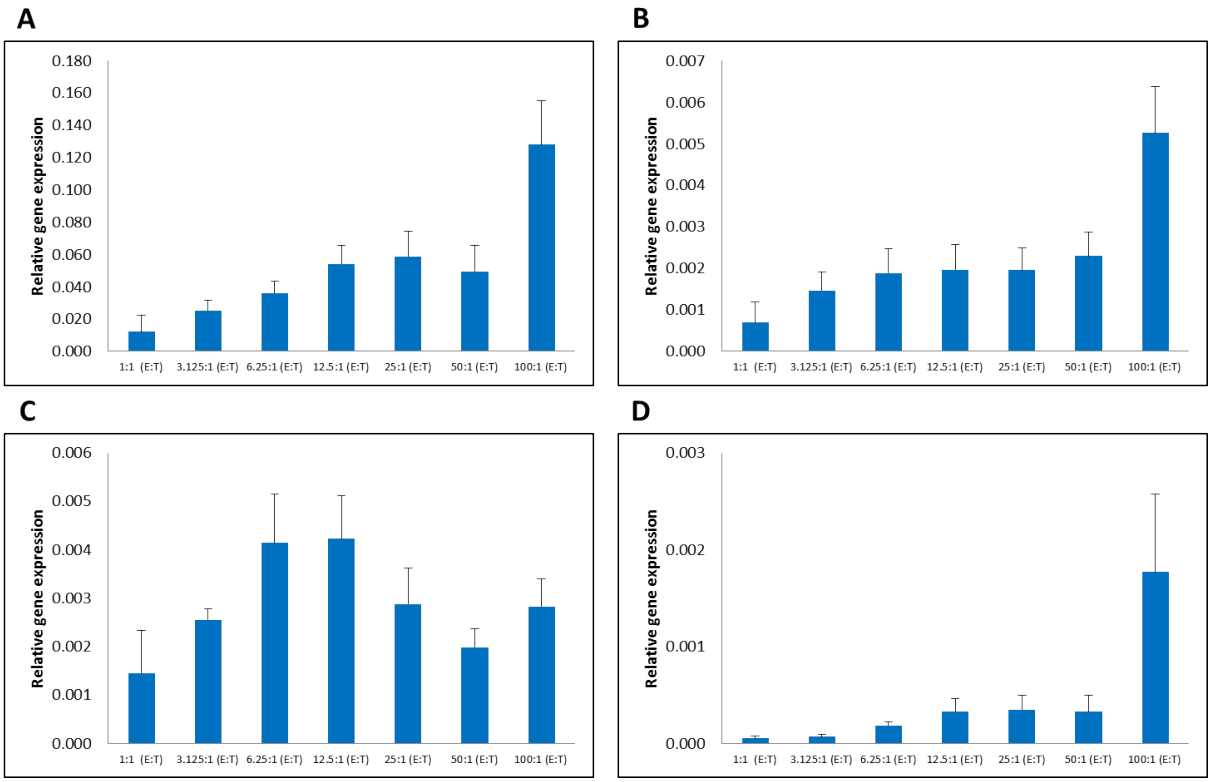

Figure 36: Determination of the optimal E:T ratio for hiPS cells
Relative gene expression levels of **(A)** *GZMB* (NM_004131.6), **(B)** *IFNγ* (NM_000619.3), **(C)** *IL10* (NM_000572.3) and **(D)** *IL2* (NM_000586.4) for different E:T ratios [PBMCs (effector cells) and hiPS cells (target cells)] after 3 days of co-culture. Relative gene expression was determined in three independent co-culture assays performed with biological duplicates. Deviations in gene expression are reported as standard error of the mean. Since it is not possible to determine which ratio is the reference ratio to which all other ratios are compared, statistical evaluation was not carried out here. **Abbreviations**: PBMCs: peripheral blood mononuclear cells; hiPS cells: human induced pluripotent stem cells; *GZMB*: granzyme B; *IFNγ*: *interferon γ*; *IL10*: *interleukin 10*; *IL2*: *interleukin 2*; E:T ratio: effector to target ratio.

Subsequently, the optimal E:T ratio for PBMCs and hiPS cell-derived CMs co-culture was defined. To determine the optimal E:T ratio, target cells (hiPS cell-derived CMs) were titrated and added to a constant concentration of effector cells (PBMCs) (1 x10^6cells/ml). Figure 37 displays the results of relative gene expression analysis of secretory factors and cytokines for various E:T ratios. The results showed that *GZMB* (figure 37A) expression in PBMCs stimulated with immunocompetent E5V homozygous for tdTomato (parental line) and other control hiPS cell-derived CMs was clearly detectable for all tested E:T ratios. The level of *GZMB* increased continuously with higher E:T ratios and was highest for a 100:1 E:T ratio. Figure 37B shows the expression of *IFNγ*. *IFNγ* gene expression was clearly detectable for all tested E:T ratios and was highest for a 100:1 E:T ratio. *IL10* (figure 37C) gene expression was clearly detectable for all tested E:T ratios. The level of *IL10* increased continuously with higher E:T ratios and was highest for a 100:1 E:T ratio. Furthermore, low levels of *IL2* expression (figure 37D) were observed for 1:1 to 50:1 E:T ratios. *IL2* expression increased slightly for a 100:1 E:T ratio.

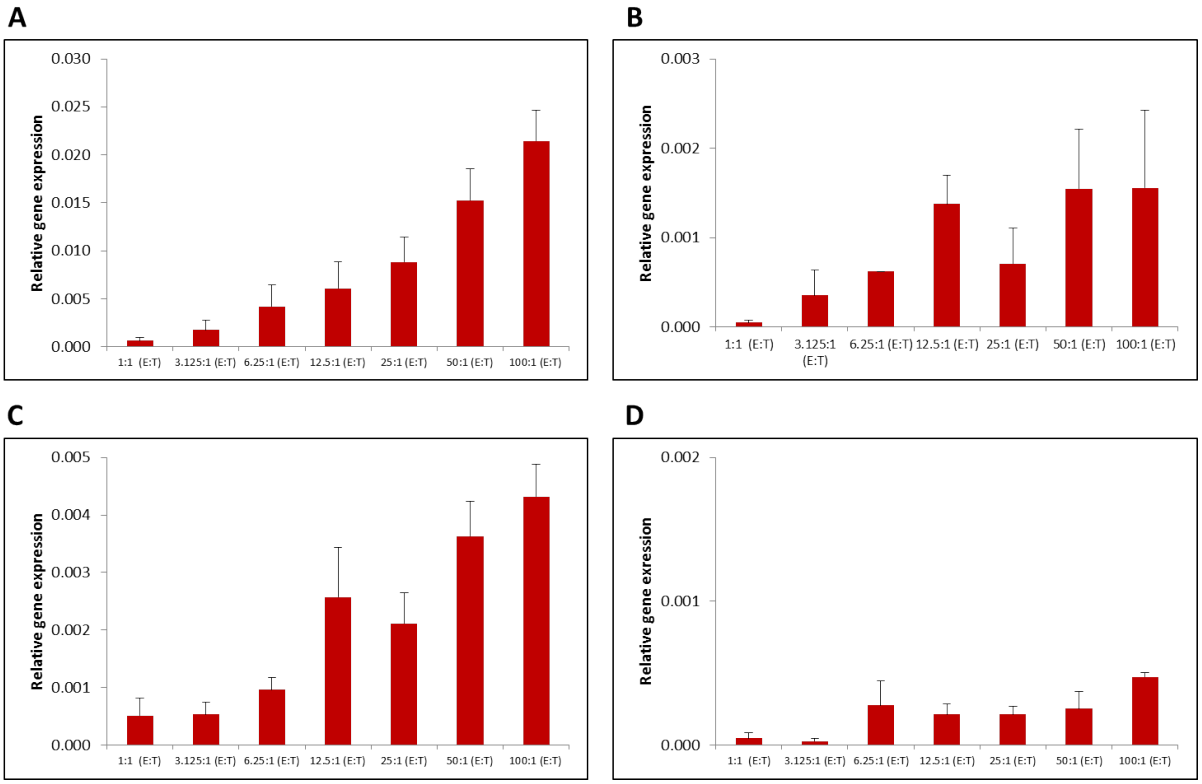

Figure 37: Determination of the optimal E:T ratio for hiPS cell-derived CMs
Relative gene expression levels of **(A)** *GZMB* (NM_004131.6), **(B)** *IFNγ* (NM_000619.3), **(C)** *IL10* (NM_000572.3) and **(D)** *IL2* (NM_000586.4) for different E:T ratios [PBMCs (effector cells) and hiPS cell-derived CMs (target cells)] after 3 days of co-culture. Relative gene expression was determined in two independent co-culture assays performed with biological duplicates. Deviations in gene expression are reported as standard error of the mean. Since it is not possible to determine which ratio is the reference ratio to which all other ratios are compared, statistical evaluation was not carried out here. **Abbreviations**: PBMCs: peripheral blood mononuclear cells; hiPS cell: human induced pluripotent stem cell; CMs: cardiomyocytes; *GZMB*: granzyme B; *IFNγ*: *interferon γ*; *IL10*: *interleukin 10*; *IL2*: *interleukin 2*; E:T ratio: effector to target ratio.

For both hiPS cells and hiPS-cell derived CMs, an E:T ratio of 100:1 showed the highest gene expression levels for all analyzed secretory factors and cytokines and was chosen for subsequent assays. Higher E:T ratios than E:T (100:1) were not tested due to the limiting number of PBMCs isolated.

Evaluation of the immunogenicity of hiPS cells and hiPS cells-derived CMs

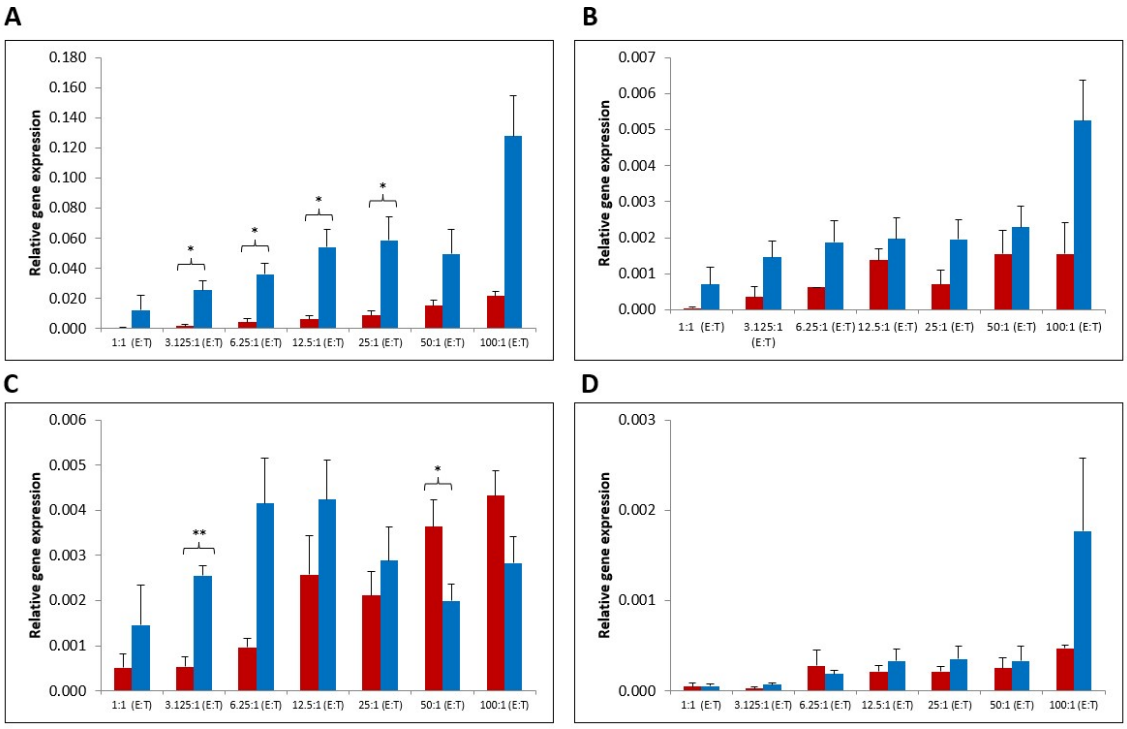

Figure 38: Comparison of the immunogenicity of hiPS cells and hiPS cells-derived CMs
Comparative gene expression analysis of **(A)** *GZMB* (NM_004131.6), **(B)** *IFNγ* (NM_000619.3), **(C)** *IL10* (NM_000572.3), **(D)** *IL2* (NM_000586.4) for different E:T ratios [effector cells (PBMCs) and target cells (hiPS cells (blue) or CMs (red)] after 3 days of co-culture. For immune response evaluation, relative gene expression levels of proliferative and cytokine responses from PBMCs stimulated with hiPS cells was compared to the transcriptional profile of PBMCs stimulated with hiPS cell-derived CMs. *ACTB* (NM_001101.3) was used to normalize qRT-PCR data for relative quantification. Relative gene expression of hiPS cell was determined in three independent co-culture assays with biological duplicates and was determined in two independent co-culture assays with biological duplicates. Multiple comparisons were analyzed by Mann-Whitney Rank Sum Test or Student's T-Test. **Abbreviations**: *PBMCs*: *peripheral blood mononuclear cells*; *hiPS cells*: *human induced pluripotent stem cells*; *GZMB*: granzyme B; *IFNγ*: *interferon γ*; *IL10*: *interleukin 10*; *IL2*: *interleukin 2*; E:T ratio: effector to target ratio.

To compare the immunogenicity of hiPS cells and hiPS cell-derived CMs a comparative gene expression analysis of secretory factors and cytokines was performed after 3 days of co-culture with PBMCs (figure 38). The results showed that *GZMB* expression for 3.125 to 25:1 E:T ratios ($p < 0.05$) in PBMCs stimulated with immunocompetent E5V homozygous (parental line) hiPS cells was significantly higher than in PBMCs stimulated with immunocompetent E5V homozygous hiPS cell-derived CMs (figure 38A). Figure 38B displays the comparative *IFNγ* expression analysis. All E:T ratios showed similar gene expression levels and no significant differences could be found between the transcriptional profile of PBMCs stimulated with hiPS cells and PBMCs stimulated with hiPS-cell derived CMs. Figure 38C shows the comparative expression of *IL10*. *IL10* expression for a 3.125:1 ratio ($p < 0.01$) in PBMCs stimulated with hiPS cells was significantly higher than in PBMCs stimulated with hiPS cell-derived CMs. For a 50:1 ratio ($p < 0.05$) *IL10* expression levels in PBMCs stimulated with hiPS cell-derived

CMs were significantly higher than in PBMCs stimulated with hiPS cells. Figure 38D displays the comparative *IL2* expression analysis. All E:T ratios showed similar gene expression levels and no significant differences could be found between hiPS cell-mediated and hiPS cell-derived CMs-mediated stimulation of PBMCs. Though there were rather few significant differences between the two target cell populations, the immune response against CMs tended to be less pronounced compared to that against hiPS cells.

4.7 Evaluation of the immune response against the generated E5V △PB cell lines

4.7.1 Evaluation of the immune response against the generated E5V △PB cell lines by measuring gene expression of secretory factors and cytokines in PBMCs

To compare the immunogenicity of the generated homozygous and heterozygous *B2M*-deficient E5V ΔPB hiPS cells and E5Vf (wild-type) hiPS cells, a comparative gene expression analysis of secretory factors and cytokines was performed after 72 hours of co-culture with PBMCs. Figure 39A displays a schematic of the employed experimental co-culture conditions. Relative gene expression levels of *GZMB* (figure 39B), *IFNγ* (figure 39C), *IL10* (figure 39D) and *IL2* (figure 39E) expression analysis showed no significant gene expression differences between homozygous and heterozygous E5V ΔPB hiPS cell clones and E5Vf (wild-type) hiPS cells. Despite the lack of significance, gene expression levels of *GZMB* (figure 39B) and *IFNγ* (figure 39C) was higher in PBMCs co-cultured with homozygous *B2M*-deficient E5V ΔPB hiPS cells than in PBMCs co-cultured with heteozygous E5V ΔPB and E5Vf (wild-type) hiPS cells. Besides, despite the lack of significance *IL10* (figure 39D) and *IL2* (figure 39E) gene expression was higher in PBMCs co-cultured with E5Vf (wild-type) hiPS cells than in PBMCs co-cultured with homozygous and heterozygous E5V ΔPB hiPS cell clones.

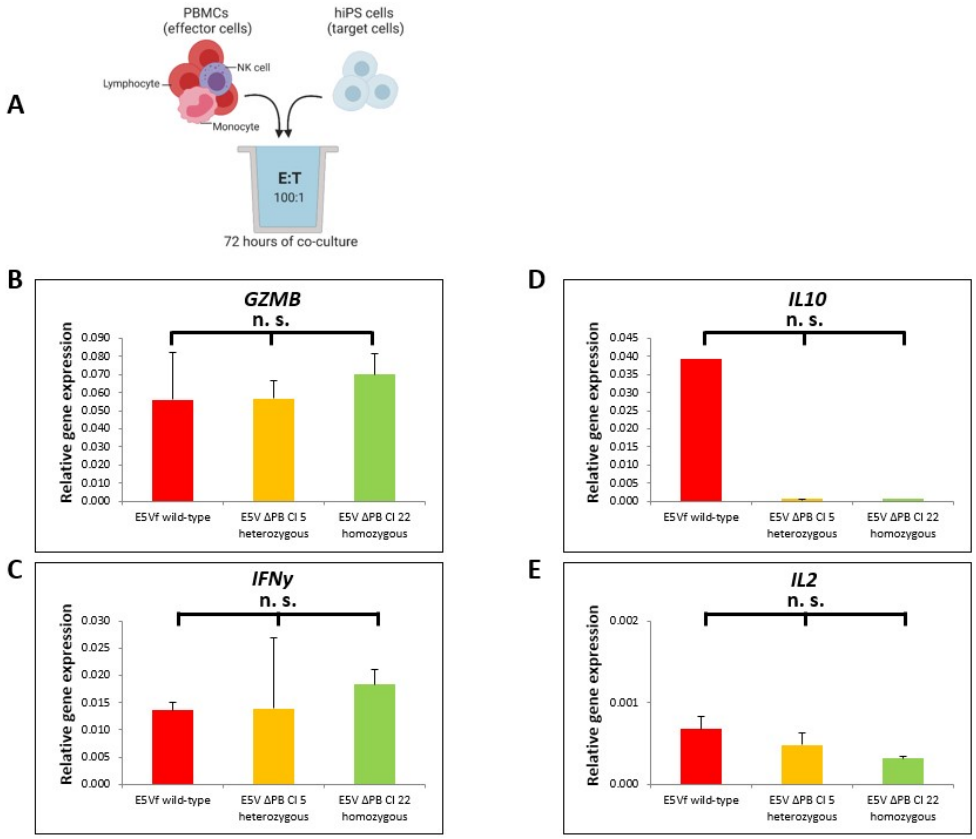

Figure 39: Evaluation of the immune response against the generated *B2M*-deficient hiPS cell clones by measuring gene expression of secretory factors and cytokines

(A) Schematic (Created with BioRender.com) showing the experimental setup of the co-culture assay (Created with BioRender.com). To analyze specific immune regulatory gene expression, PBMCs (effector cells) were co-cultured with hiPS cells (target cells) for 72 hours at a 100:1 E:T ratio. For immune response evaluation against the generated *B2M*-deficient hiPS cell clones, relative gene expression levels of **(B)** *GZMB* (NM_004131.6), **(C)** *IFNγ* (NM_000619.3), **(D)** *IL10* (NM_000572.3), **(E)** *IL2* (NM_000586.4) were determined. Relative gene expression levels of proliferative and cytokine responses from PBMCs stimulated with the generated homozygous (green) and heterozygous (orange) E5V ΔPB hiPS cell clones were compared to the transcriptional profile of PBMCs stimulated with the E5Vf hiPS cells (wild-type) (red). *ACTB* (NM_001101.3) was used to normalize qRT-PCR data for relative quantification. A representative co-culture assay performed with biological triplicates is shown. Deviations in gene expression are reported as standard error of the mean. Multiple comparisons were analyzed by Mann-Whitney Rank Sum Test or Student's T-Test. For all analyzed secretory factors and cytokines no significant differences in gene expression could be found between the generated homozygous and heterozygous *B2M*-deficient E5V ΔPB hiPS cells and E5Vf (wild-type) hiPS cells. **Abbreviations**: PBMCs: peripheral blood mononuclear cells; hiPS cells: human induced pluripotent stem cells; *GZMB*: granzyme B; *IFNγ*: *interferon γ*; *IL10*: *interleukin 10*; *IL2*: *interleukin 2*; E:T ratio: effector to target ratio.

4.7.2 LDH-Cytotoxicity assay by ELISA readout

A second assay was developed within the scope of this thesis to characterize the cytotoxic T-cell and NK-cell-mediated immune response. By co-culturing cytotoxic T-cells or NK-cells with hiPS cells this assay aims to quantify cell-mediated cytotoxicity (described in section 3.7.2). Figure 40A displays a schematic of the LDH-Cytotoxicity assay workflow. In a first set of experiments, the optimal target cell concentration and E:T ratio were defined. All preliminary experiments for assay establishment were performed with immunocompetent [E5V homozygous

(parental line)] cells. Figure 40B shows the results of target cell concentration assessment (described in section 3.7.2). The target cell concentration (1.25 x10^5cells/ml) corresponding to the greatest difference between the absorbance value at 490 nm (LDH activity) of the high and the low control was used for following assays. To define the optimal E:T ratio (described in section 3.7.2) a fixed optimal number of target cells (1.25x10^4 hiPS cells) was co-cultured with effector cells (cytotoxic CD8+ T-cells or NK-cells) at different E:T ratios and the absorbance value at 490 nm (LDH activity) was measured. The E:T ratio and the associated effector cell concentration, in which the assay showed the greatest absorbance value (490 nm) were used for subsequent assays. Figure 40C shows the results of E:T ratio determination for cytotoxic T-cells. The level of cytotoxic T-cell mediated cytotoxicity was highest for a 5:1 E:T ratio and decreased with lower E:T ratios. Figure 40D shows the results of E:T ratio determination for NK-cells. The level of NK-cell mediated cytotoxicity was highest for a 10:1 E:T ratio and decreased with lower E:T ratios. In figures 40C and 40D, background control, low control (target cells only) and substance control (effector cells only) showed low levels of LDH activity in comparison with the high control (target cells + Triton X 100), which enabled to determine maximum releasable LDH activity in the assay. Based on these results an E:T ratio of 5:1 (CD8+ T-cells) and 10:1 (CD16+ NK-cells) was used to evaluate cell-mediated cytotoxicity in all further experiments.

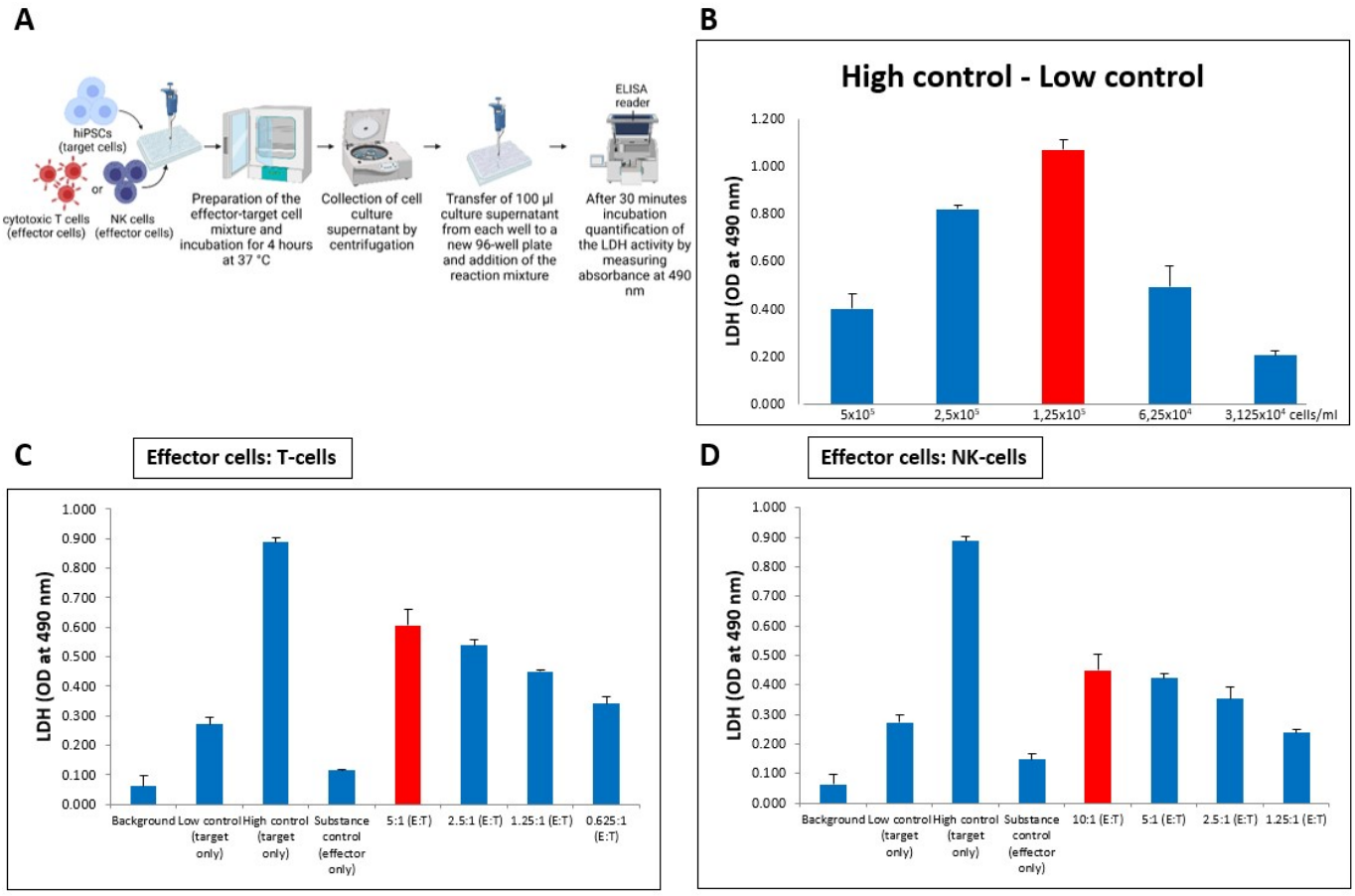

Figure 40: Evaluation of the cell-mediated immune response against the generated *B2M*-deficient hiPS cell clones

(A) Schematic (Created with BioRender.com) showing the experimental setup of the LDH-Cytotoxicity assay (Created with BioRender.com). The Cytotoxicity Detection Kit (LDH) (Roche Applied Science) was employed for cytotoxicity determination and the amount of LDH released in cell culture medium was measured colorimetrically using an ELISA reader. **(B)** Determination of the optimal target cell concentration. The cell concentration used for subsequent assays was indicated by a red bar. A representative LDH-Cytotoxicity assay performed with triplicates is shown. Deviations in absorbance are reported as standard error of the mean. **(C)** Determination of the optimal E:T ratio using cytotoxic CD8+ T-cells as effector cells. The E:T ratio used for subsequent assays was indicated by a red bar. A representative LDH-Cytotoxicity assay performed with triplicates is shown. Deviations in absorbance are reported as standard error of the mean. **(D)** Determination of the optimal E:T ratio using NK-cells as effector cells. The E:T ratio used for subsequent assays was indicated by a red bar. A representative LDH-Cytotoxicity assay performed with triplicates is shown. Deviations in absorbance are reported as standard error of the mean. **Abbreviations**: CD: cluster of differentiation; NK-cell: natural killer cell; hiPS cell: human induced pluripotent stem cell; E:T ratio: effector to target ratio; LDH: lactate dehydrogenase; ELISA: enzyme-linked immunosorbent assay.

4.7.3 Assessment of the CD8+ T-cell-mediated cytotoxicity

In organ transplantation, cell-mediated allograft rejection is mainly attributable to cytotoxic T-cells (Harper et al., 2015). Direct alloantigen recognition leads to activation of CD8+ T-cells by interaction of their specific TCR with foreign MHC-I molecules on target cells (Marino et al., 2016; Boardman et al., 2016). Targeted knockout of the *B2M* gene in the generated E5V ΔPB cell lines, leading to MHC-I disruption on the cell surface, should therefore result in a

significant decrease of CD8+ T-cell-mediated cytotoxicity (D. Wang et al., 2015).

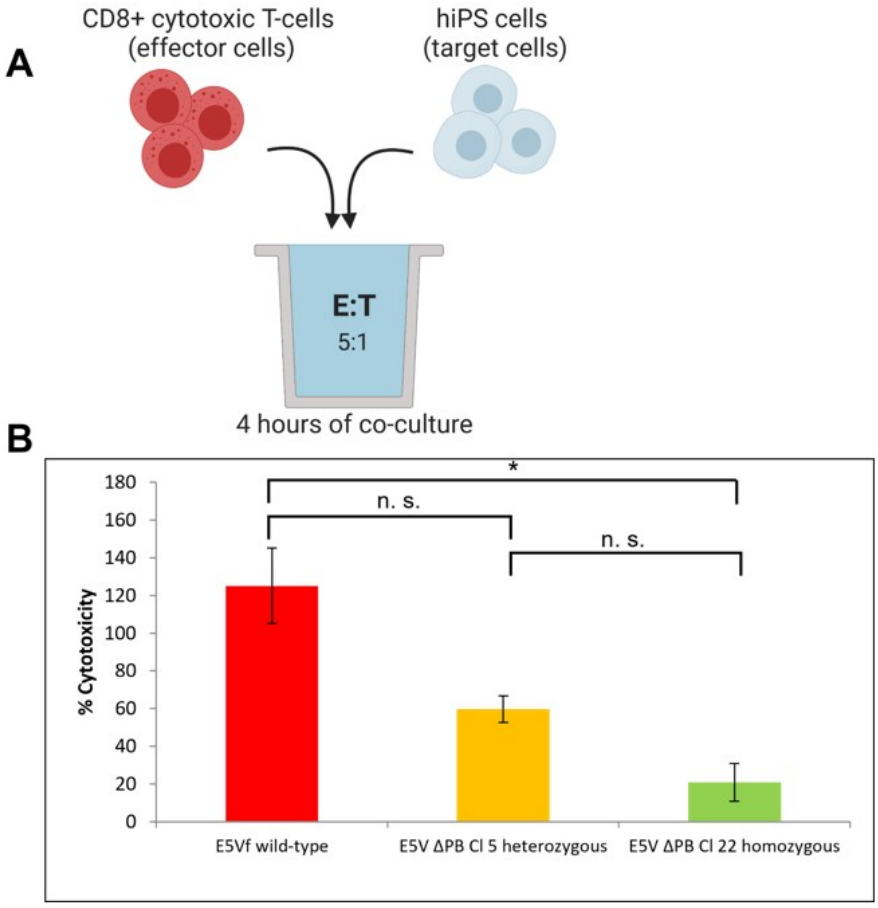

Figure 41: Evaluation of the cytotoxic T-cell-mediated immune response against the generated *B2M*-deficient hiPS cell clones

(A) Schematic (Created with BioRender.com) showing the experimental setup of the LDH-Cytotoxicity assay. To determine the T-cell-mediated cytotoxicity, cytotoxic CD8+ T-cells (effector cells) were co-cultured with hiPS cells (target cells) for 4 hours at a 5:1 E:T ratio. The Cytotoxicity Detection Kit (LDH) (Roche Applied Science) was employed for cytotoxicity determination and the amount of LDH released in cell culture medium was measured colorimetrically using an ELISA reader. **(B)** Quantification of the CD8+ T-cell-mediated cytotoxicity against E5Vf and the generated E5V ΔPB cell lines. The CD8+ T-cell-mediated immune response against the generated homozygous (green) and heterozygous (orange) E5V ΔPB cell clones was compared to the response against the E5Vf cell line (wild-type) (red). Representative data from two independent LDH-Cytotoxicity assays performed with triplicates are shown. Deviations in percent cytotoxicity are reported as standard error of the mean. $^{*}p < 0.05$ by One-way ANOVA. **Abbreviations**: CD: cluster of differentiation; hiPS cells: human induced pluripotent stem cells; E:T ratio: effector to target ratio; LDH: lactate dehydrogenase; ELISA: enzyme-linked immunosorbent assay.

To quantify CD8+ T-cell mediated cytotoxicity against the generated homozygous and heterozygous E5V ΔPB hiPS cells, the LDH-Cytotoxicity assay was performed (described in section 3.7.2). Figure 41A displays a schematic of the employed experimental co-culture conditions. Figure 41B presents the results of the CD8+ T-cell-mediated cytotoxicity evaluation. The results showed strong cytotoxic activity of CD8+ T-cells against E5Vf (wild-type) hiPS cells. By contrast, a significant reduction of the CD8+ T-cell-mediated cytotoxicity for ho-

mozygous ($p < 0.05$) could be observed compared to wild-type hiPS cells. No significant reduction of the CD8+ T-cell-mediated cytotoxicity was evident in heterozygous E5V ΔPB hiPS cells compared to wild-type hiPS cells. Furthermore, no significant decrease in CD8+ T-cell-mediated cytotoxicity was evident in homozygous E5V ΔPB hiPS cells compared to and heterozygous *B2M*-deficient hiPS cells.

4.7.4 Assessment of the NK-cell-mediated cytotoxicity

As MHC-I molecules serve as NK-cell inhibitory surface ligands, loss of MHC-I surface expression has the potential to enhance NK-cell-mediated cytotoxicity (D. Wang et al., 2015). To quantify NK-cell mediated cytotoxicity against the generated homozygous and heterozygous E5V ΔPB hiPS cells, the LDH-Cytotoxicity assay was performed (described in section 3.7.2). Figure 42A displays a schematic of the employed experimental co-culture conditions. Figure 42B presents the results of the NK-cell mediated cytotoxicity evaluation. The results showed strong NK-cell cytolytic activity against all tested cell clones. No significant differences in NK-cell mediated cytotoxicity were evident between both homozygous and heterozygous E5V ΔPB hiPS cells and E5Vf (wild-type) hiPS cells.

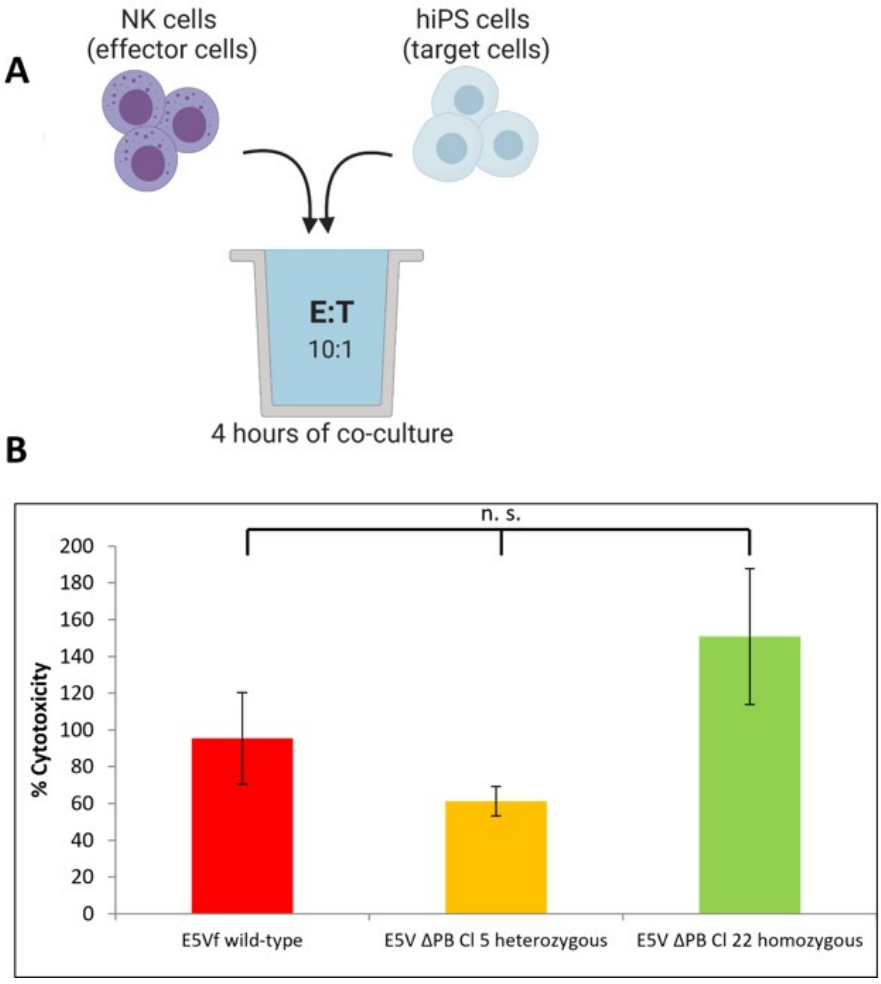

Figure 42: Evaluation of the NK-cell-mediated immune response against the generated *B2M*-deficient hiPS cell clones

(A) Schematic (Created with BioRender.com) showing the experimental setup of the LDH-Cytotoxicity assay. To determine the NK-cell-mediated cytotoxicity, NK-cells (effector cells) were co-cultured with hiPS cells (target cells) for 4 hours at a 10:1 E:T ratio. The Cytotoxicity Detection Kit (LDH) (Roche Applied Science) was employed for cytotoxicity determination and the amount of LDH released in cell culture medium was measured colorimetrically using an ELISA reader. **(B)** Quantification of the NK-cell-mediated cytotoxicity against the generated E5Vf and the generated E5V ΔPB cell lines. The NK-cell-mediated immune response against the generated homozygous (green) and heterozygous (orange) E5V ΔPB cell clones was compared to the response against the E5Vf cell line (wild-type) (red). Representative data from three independent LDH-Cytotoxicity assays performed in triplicates are shown. Deviations in percent cytotoxicity are reported as standard error of the mean. Multiple comparisons were analyzed by One-way ANOVA. **Abbreviations**: NK-cells: natural killer cells; hiPS cells: human induced pluripotent stem cell; E:T ratio: effector to target ratio; LDH: lactate dehydrogenase; ELISA: enzyme-linked immunosorbent assay.

5 Discussion

5.1 Challenges in therapeutic cardiac cell transplantation

Over the last few years, derivates of hiPS cells, named cardiac progenitor cells (CPCs) and cardiomyocytes (CMs) have emerged as a promising source for cardiac cell therapy, as they can be expanded and a high yield of hiPS cell-derived CMs can be produced (Burridge et al., 2014). Several preclinical animal studies have already demonstrated the cardiac regeneration potential of hiPS cell-derived CMs (Lalit, Hei, Raval, & Kamp, 2014). Nevertheless, their transition to clinical application is limited, mainly by immune rejection due to HLA incompatibility (Petrus-Reurer et al., 2021; Thongsin & Wattanapanitch, 2021). Production and subsequent differentiation of autologous patient-specific hiPS cells are costly and time-consuming processes, limiting their use for the treatment of acute diseases (Sato et al., 2015; Mattapally et al., 2018; Malik et al., 2019; Deuse et al., 2019). Thus, generation of an immunotolerant universal donor cell line has the potential to overcome these limitations (Riolobos et al., 2013; W. Zhao et al., 2020). In particular, HLA engineering represents a promising strategy that enables to address the immunological challenges associated with allogeneic cell transplantation (Riolobos et al., 2013; Shi et al., 2020). In addition to graft rejection, inadequate cell fate tracking methods compromise the assessment of graft survival and efficacy following therapeutic cell transplantation (Terrovitis, Smith, & Marbán, 2010; Naumova, Modo, Moore, Murry, & Frank, 2014). Therefore, the CRISPR-Cas9 technology was used to obtain a targeted knockout of the *B2M* gene to establish a hypoimmunogenic hiPS cell line for regenerative therapies, which simultaneously has the potential to monitor functional integration into the recipient's cardiac tissue, as the transplanted cells would show red fluorescence due to the tdTomato integration which previously was done in the parental line.

5.2 Characterization of the parental E5V cell line

Cardiac cell therapy requires production of functional hiPS cell-derived CPCs/CMs in clinical scale quantities to effectively replace damaged cardiac tissue (Burridge et al., 2014; Lalit et al., 2014). To investigate the cardiac differentiation potential of the genetically modified *B2M*-deficient hiPS cell line by subsequent comparisons, stable and reproducible cardiac differentiation of the E5V parental hiPS cell line must be ensured. As expected, upon directed differentiation E5V parental hiPS-cell derived CPCs/CMs robustly expressed the cardiac transcription factors (*NKX2.5*, *TBX5*), and the key CM-specific markers gene expression profile (*MLC2a* and *MLC2v*) described by Burridge and colleagues (Burridge et al., 2014). Similiar to the process of human embryonic heart development, hiPS cells develop consecutively

from the undifferentiated state through the primitive mesoderm to CPCs and further to CMs (Moon et al., 2017; Gao & Pu, 2021). Undifferentiated hiPS cells showed no cardiac-specific gene expression except for low-level gene expression detectable for *TBX5*, which has also been described by others (Assou et al., 2015). From D6 to D21, expression of the analyzed early cardiac transcription factors *NKX2.5* and *TBX5* gradually increased, indicating that differentiating cells have acquired the characteristics of immature cardiac progenitor cells (Burridge et al., 2014; Moon et al., 2017). *MLC2a* is known to be expressed in the developing fetal heart in differentiating cells destined to develop into either atrial or ventricular CMs, and its expression is downregulated during ventricular maturation of CMs (Kubalak, Miller-Hance, O'Brien, Dyson, & Chien, 1994; Bizy et al., 2013). In contrast, *MLC2v* expression during cardiac development and in the adult heart is essentially restricted to the ventricles (O'Brien et al., 1993). In this work, *MLC2a* was induced in hiPS-cell derived CMs as early as D6 and increased continuously, whereas ventricular-specific *MLC2v* was expressed in a delayed manner from D14 on, possibly reflecting the onset of ventricular specification or the presence of different cardiac cell types within the analyzed cell population (Kehat et al., 2001; Kawai et al., 2022; M. Zhang et al., 2015). Notwithstanding progress in developing highly efficient and reproducible directed cardiac differentiation protocols, structural and functional immaturity of hiPS cell derived-CMs still remains a hurdle in cardiac cell therapy (Liew et al., 2020). hiPS cell-derived CMs have been found to display gene expression profiles, structural and electrophysiological characteristics comparable to fetal CMs (Burridge, Keller, Gold, & Wu, 2012; Liew et al., 2020). Consequently, several advances have been made in recent years to improve the maturity of hiPS cell-derived CMs through prolonged culture protocols, biochemical, electrical and environmental stimulation, but a maturity status that disposes of all adult human CMs characteristics has not been achieved yet (Sontayananon, Redwood, Davies, & Gehmlich, 2020; Sacchetto, Vitiello, de Windt, Rampazzo, & Calore, 2020; Liew et al., 2020; J. Li et al., 2021). In this work, staining of cardiac-specific markers showed expression of TNNT2, α-actinin, MLC2a and MLC2v, and displayed formation of sarcomeric patterns, confirming successful cardiac differentiation of the E5V cell line (parental line). No discernible differences in cardiac-specific protein expression was detected between homo- and heterozygous E5V hiPS-cell derived CMs for tdTomato on D30 and D60 of the directed cardiac differentiation protocol, indicating that both genotypes are equally potent to differentiate towards the cardiac lineage. It can be assumed that both alleles of the MLC2v locus are expressed, as no difference between homozygous and heterozygous MLC2v expression could be detected. This means that one should be able to follow the cells in the animal model with a heterozygous MLC2v-tdTomato cell line just as well as with a homozygous cell line. Consistent with results from other groups, immunofluorescence analysis at D30 and D60 confirmed an E5V-derived double positive cell population for MLC2a and MLC2v at the protein level, corresponding to immature CMs with an early ventricular phenotype (Bizy et al., 2013; M. Zhang et al., 2015). However, immunocytochemistry only allows a qualitative statement of the cardiac differential potential. To obtain further quantitative information on the efficient differentiation of CMs and to determine the homogeneity of the cell populations, FACS analyses need to be performed in future experiments (Bhattacharya et al., 2014). For functional characterization of the hiPS cell-derived CMs, their electrophysiological properties and contractile function still need to be investigated. Moreover, cell heterogeneity is an ongoing challenge in differentiated cell pop-

ulations (Waas et al., 2019; Jiang & Lian, 2020; Liew et al., 2020). To further improve the purity of CMs, glucose starvation can be applied (Sharma et al., 2015). This method is based on the difference in glucose metabolism between CMs and non-CMs (Tohyama et al., 2013). Furthermore, the MLC2v-tdTomato feature of the E5V cell line can be used to enrich CMs with a ventricular phenotype using FACS, reducing the heterogeneity of hiPS-derived CMs (Sontayananon et al., 2020). The tdTomato fluorescence in differentiating E5V hiPS cells was generally detectable around D20 of the directed cardiac differentiation protocol and increased over time, highlighting its potential for real-time tracking of cells during cardiac differentiation and examination of their maturation status (Sontayananon et al., 2020). Immunofluorescence analyses at D30 and D60 confirmed that the ventricular expression pattern of the MLC2v-tdTomato knock-in reporter was consistent with endogenous MLC2v expression. These results suggest that the traceable feature of the cell line enables monitoring of ventricular hiPS cell-derived CMs in long-term cell cultures and may contribute to the future use of these cells in *in vivo* cell transplantation studies. FACS analysis was performed to evaluate the MHC-I cell surface expression of E5V parental (wild type) hiPS cells and CMs derived thereof. It was found that 90.9 % of the hiPS cells expressed MHC-I, while only 51.0 % of the hiPS cell-derived CMs were MHC-I positive. In their study, Chen and colleagues analyzed the expression of MHC-I on several hiPS cell lines obtained from human foreskin fibroblasts and their derivatives (stem cell-derived hepatocytes) using mouse anti-human HLA-A,B,C (W6/32) by FACS (H. F. Chen et al., 2015). A high percentage of their analyzed undifferentiated hiPS cells expressed HLA-I molecules (69.5 %), and after spontaneous in vitro differentiation, a gradually decreasing percentage of cells was found to express HLA-I at D7 (29.5 %) and D15 (18.7 %) compared to undifferentiated cells, before levels increased again at D30 (54.3 %) (H. F. Chen et al., 2015). Säljö and colleagues also confirmed high MHC-I expression in undifferentiated hiPS cells (derived from human skin fibroblasts) (Säljö et al., 2017). Except for one cell line, MHC-I expression decreased rapidly during differentiation into hepatocyte-like cells, with expression remaining low from D7 (Säljö et al., 2017). In contrast, during cardiac differentiation, the initial decrease in MHC-I expression was followed by a sharp increase in MHC-I expression from D11 onward (Säljö et al., 2017). The mechanism of these antigenic changes observed during differentiation is not yet known and could be a consequence of different developmental processes, but could also be influenced by the culture conditions and differentiation protocols used (H. F. Chen et al., 2015; Säljö et al., 2017).

5.3 Generation of the *B2M*-deficient cell line

Several strategies for generating hypoimmunogenic hiPS cells have been described, including generation of universal hiPS cells by targeted disruption of the *B2M* gene, production of HLA-homozygous hiPS cells using gene editing approaches and enhancement of immune tolerance by knock-in of specific genes (Q. Ye et al., 2020). Deletion of *B2M*, leading to the elimination of MHC-I surface expression to improve immmunocompatibility, has been performed in both hESCs and hiPS cells (Riolobos et al., 2013; D. Wang et al., 2015; Lu et al., 2013; Karabekian et al., 2015; Feng et al., 2014; Börger et al., 2016; Deuse et al., 2019). So far, numerous gene editing approaches (RNA interference (RNAi), adeno-associated virus (AAV), zinc-finger nuclease (ZFN), transcription activator-like effector nuclease (TALEN) and CRISPR-Cas9)

have been tested, differing mainly in their gene editing efficiency. On the one hand, there is RNAi-mediated *B2M* gene silencing, where gene knockdown was found to be incomplete and of unclear durability (Figueiredo et al., 2013; Karabekian et al., 2015; Börger et al., 2016). On the other hand, there is AAV-mediated gene editing which was also found to reduce but not completely eliminate *B2M* gene expression (Riolobos et al., 2013; Zha et al., 2020). With the advent of gene editing technologies such as ZFN and TALEN, new opportunities to enhance *B2M* disruption in human pluripotent stem cells were offered (Lu et al., 2013; Feng et al., 2014; Zha et al., 2020). However, these technologies have their own limitations, such as low efficacy, complex design and off-target effects (Mandal et al., 2014; D. Wang et al., 2015; Ranjbar et al., 2022). Finally, the development of CRISPR-Cas9 technology, a simple and versatile gene editing tool, aimed to overcome these limitations and has been successfully used by several groups for an effectively targeted knockout of *B2M* (Mandal et al., 2014; Sato et al., 2015; Deuse et al., 2019; Zha et al., 2020; Norbnop et al., 2020; Ranjbar et al., 2022). In humans, the major protein component of the functional B2M protein is encoded by exons 2 and 3 of the *B2M* gene (Reinhart & Pearson, 1993). Shi and colleagues designed *B2M*-deficient hESCs in their study using two custom-made sgRNAs for CRISPR-Cas9 gene editing targeting exon 2 and 3 of the *B2M* gene, a CAG promoter-driven Cas9-P2A-GFP vector and a transient puromycin expression vector. Sequencing of the 7 selected clones revealed that 28.6 % (2/7) were homozygously and 57.1 % (4/7) were heterozygously targeted. After successful Cre-mediated excision of the puromycin resistance cassette, CRISPR-Cas9 technology was employed in this work to also replace exons 2 and 3 of the *B2M* gene in the E5Vf cell line (wild-type) on one or both alleles by a neomycin resistance cassette via homologous recombination. Analysis of gene editing efficiency showed that 26 % (8/31) were edited homozygously and 39 % (12/31) heterozygously, demonstrating solid targeting efficiency. 10 of originally 41 clones were excluded from the analysis due to lack of cell growth, incomplete or incorrect integration of the donor construct or faulty PCR. Besides, investigation of possible genetic alterations is still required in future experiments to rule out off-target mutagenesis (Zha et al., 2020; H. Xu et al., 2019).

5.4 Characterization of the *B2M*-deficient cell line

After successful generation and genotype screening, two homozygous (E5V ΔPB clones 22 and 28) and two heterozygous clones (E5V ΔPB clones 5 and 16) were analyzed by qRT-PCR to evaluate relative gene expression levels of *B2M*. Surprisingly, *B2M* gene expression was highest in the heterozygous E5V ΔPB clone 16, followed by the parental wild-type clone, and lowest in the heterozygous E5V ΔPB clone 5, which could be due to differential allelic gene expression. As expected, no *B2M* expression was detected in both homozygous E5V ΔPB clones 22 and 28. To test the effects of the *B2M* knockout on endogenous cellular B2M protein expression, WB analysis was perfomed. Endogenous B2M protein expression was verified in parental wild-type and heterozygous E5V ΔPB hiPS cell clones. In contrast, no endogenous B2M protein was detected in either homozygous E5V ΔPB hiPS cell clones, confirming successful *B2M* ablation on protein level. Thus, the B2M knockout was detected at the transcriptional level (gene expression) and confirmed at the translational level (protein). In addition, a WB was performed to determine whether knockout of *B2M* had any effect on protein expression of the

other components of the MHC-I complex. This was not the case, as the MHC-I protein was detectable in the WB, but this was also to be expected. Targeted *B2M* knockout has the potential to cause MHC-I cell surface disruption (D. Wang et al., 2015; Drukker et al., 2002). In their study, Hughes and colleagues examined cells in which proper assembly of the MHC-I complex was abrogated by a deficiency of *B2M*, while endogenous MHC-I genes remained unchanged (Hughes, Hammond, & Cresswell, 1997). Synthesized MHC-I heavy chains must fold and associate non-covalently with B2M, which is faciliated by interactions with the chaperones calnexin and calreticulin, before they bind peptides derived from proteasomal degradation of endogenous or exogenous proteins in the endoplasmic reticulum (ER) to form a complex (Hughes et al., 1997; Zimmer et al., 2005; Halenius, Gerke, & Hengel, 2014). Correct and stable MHC-I complex assembly is required prior to the intracellular transport from the ER via Golgi complex to the cell surface (Hughes et al., 1997; Bouvier & Wiley, 1998; Thomas & Tampé, 2021). The absence of B2M prevents important steps of protein from folding and assembly, leading to an unstable MHC-I complex that is no longer transported to the cell surface and consequently removed by a degradation process in the cytosol (Hughes et al., 1997; Burr et al., 2011). To test the functionality of the MHC-I complex, FACS analysis was then performed. In accordance, FACS analyses to assess changes in MHC-I cell surface expression showed detectable MHC-I expression on the parental hiPS line, whereas its expression was reduced in heterozygous E5V ΔPB hiPS cell clones and not detectable on the cell surface of both homozygous E5V ΔPB hiPS cell clones (Riolobos et al., 2013; Zha et al., 2020). Furthermore, immunocytochemistry confirmed these results. The expected membranous pericellular MHC-I staining was demonstrated in parental wild-type and heterozygous E5V ΔPB hiPS cell clones. In contrast, surface MHC-I could not be detected in homozygous E5V ΔPB hiPS cells. The absence of B2M affects the conformation of the MHC-I complex so that it can no longer be recognized. These results highlight the importance of the B2M protein in stabilizing MHC-I on the cell surface and maintaining the native structure of the MHC-I heavy chain (L. Li, Dong, & Wang, 2016). Besides, cell surface expression of MHC-I is enhanced in all cells by stimulation with interferons, so future experiments will need to investigate whether MHC-I expression is not also upregulated after administration of recombinant IFNγ (Zimmer et al., 2005; F. Zhou, 2009; Shklovskaya & Rizos, 2021). Individuals in whom MHC-I cell surface expression is severely reduced due to rare gene mutations may have increased susceptibility to infection but show no defects in non-immune cells or tissues, suggesting that the lack of *B2M* expression is not critical for normal cell or organ function (Zimmer et al., 2005; Karabekian et al., 2015). As described by other groups, hiPS cells retain their characteristics after targeted *B2M* disruption, confirming the feasibility of *B2M* knockout (Zha et al., 2020). Thus, monitoring of general traits such as cell morphology and growth revealed no morphological differences between the edited homozygous and heterozygous E5V ΔPB hiPS cell colonies and the parental line. Furthermore, gene editing did not affect the cardiac differentiation potential of *B2M*-deficient hiPS cells. Consequently, mRNA expression of essential cardiac transcription factors *NKX2.5*, *TBX5*, and key CM-specific markers *MLC2v* and *MLC2a* were comparable to the parental wild-type cell line during directed cardiac differentiation. Immunocytochemistry confirmed these results, showing similar expression of TNNT2, α-actinin, MLC2a and MLC2v as in unedited cells after 30 days of cardiac differentiation. These findings are in accordance with previous studies investigating the effect of *B2M*-deficiency on efficient cardiac

differentiation capacity (Karabekian et al., 2015; Mattapally et al., 2018; Shi et al., 2020).

5.5 Isolation of PBMCs and immune cell subpopulations

Prior to immunological testing, FACS analysis was performed to examine PBMCs and immune cell populations. Three distinct cell populations were identified in the flow cytometric FCS/SSC profile of the peripheral whole blood sample (after red blood cell lysis) based on their size and granularity, corresponding to neutrophils, monocytes, and lymphocytes, which was comparable to analyses performed by other laboratories (Eljaszewicz et al., 2015; Tomas et al., 2019; Rowley, 2012). After separation of PBMCs from peripheral whole blood, the FCS/SSC flow cytometric profile revealed two distinct cell populations corresponding to monocytes and lymphocytes, with no neutrophils (Tomas et al., 2019; Chometon et al., 2020). PBMCs consist of lymphocytes (T-cells, B-cells, and NK-cells), monocytes, and dendritic cells and the frequency of these immune cell subpopulations varies from donor to donor (Kleiveland, 2015). In this work, the distribution of lymphocyte subpopulations within the PBMC fraction was examined with specific antibodies by FACS analysis and revealed a total of 26.9 % CD16+ NK-cells and 44.5 % CD3+ T-cells. The CD3+ T-cell fraction was composed of 11.7 % CD8+ cytotoxic T-cells. A total of 28.6 % CD3- and CD16- cells were detected, corresponding to other immune cell subsets. One the one hand, the interpretation of this result is limited by the fact that only a few CD markers were examined in this experiment, and therefore, the results serve only as an approximate estimate of immune cell frequency without providing an accurate quantitative statement. On the other hand, the CD16 molecule is not specific to NK-cells and is also expressed to some extent on the surface of neutrophils, macrophages, and subsets of T-cells, monocytes, eosinophils, and dendritic cells (Naeim, Nagesh Rao, Song, & Phan, 2018). In general, human peripheral blood NK-cells are CD3 negative and can be divided into two major subsets based on their markers CD16 and CD56: dim (CD56+dim CD16+) NK-cells, which account for more than 90 %, and bright (CD56+bright CD16-) NK-cells, which account for 10 % (Moretta et al., 1989; Lin et al., 2004; Poli et al., 2009). Therefore, the additional use of an anti-CD56 antibody should be considered in future experiments. Isolation of the desired immune cell type based on its specific CD markers is an effective method for cell enrichment and purification from contaminating cells (R. Weiss et al., 2021). In this work, MACS® MicroBead Technology (Miltenyi Biotec) enabled successful enrichment of immune cell subpopulations from PBMCs. Purity assessment by FACS confirmed the high purity of CD3+ T-cells (99.15 %), CD8+ T-cells (98.9 %) and CD16+ NK-cells (97.4 %). Column-based magnetic activated cell sorting has also been successfully used by other groups to enrich immune cell subpopulations of high quality, viability, and without compromising cell function (R. Weiss et al., 2021; Al-Shanti, Steward, Garland, & Rowbottom, 2004; E. Weiss et al., 2020).

5.6 Quantification of the immune response by measuring gene expression of secretory factors and cytokines

5.6.1 Advantages and disadvantages of the assay

As part of this work, a test was established to quantify the immune response by measuring the gene expression of secretory factors and cytokines. The main advantage of using human PBMCs to study the immune response is that they provide a readily available source of immune cells, as they can easily be isolated from peripheral whole blood or buffy coats (Kleiveland, 2015). Cytokines are signalling glycoproteins/peptides produced locally by immune cells, and difficulties in their analysis at the protein level include their instability, short half-life and high vulnerability to post-sampling manipulation (Israelsson et al., 2020). qRT-PCR is therefore a simple and inexpensive method with high sensitivity and reproducibility for the study of gene expression profiles and mRNA quantification of cytokines has been widely used in immunological research (Giulietti et al., 2001; Stordeur et al., 2002). However, since the biological effects of cytokines are determined by their protein/peptide form and not all mRNA signals are translated into proteins, the assessment of mRNA expression of cytokines should be combined with other assays that allow protein quantification (Nicolet, Guislain, & Wolkers, 2017; Israelsson et al., 2020). Furthermore, PBMCs represent mixed cell populations in which the frequency of cell subsets varies among individuals and the expression of subset-specific genes fluctuates (Corkum et al., 2015; Kleiveland, 2015). Thus, isolation of immune cell subpopulations is a valuable approach to identify individual gene expression profiles that are otherwise masked in the whole PBMC population (Corkum et al., 2015). In addition, when using PBMC in *in vitro* experiments, cells lack the environmental stimuli to which they would have been exposed under normal *in vivo* conditions, which should be taken into account when interpreting the results (Kleiveland, 2015).

5.6.2 Evaluation of the immunogenicity of wild-type hiPS cells and hiPS-cell derived CMs

Comparative gene expression analysis of secretory factors and cytokines performed after 3 days of co-culture with PBMCs showed no significant differences for *IFN*γ, *IL10* and *IL2* between immunocompetent wild-type (parental) E5V-hiPS cells and their derived CMs. However, the expression of *GZMB* in PBMCs co-cultured with immunocompetent wild-type (parental) E5V hiPS cells in different E: T ratios (3.125 to 25:1) was significantly higher than in PBMCs stimulated with their derived CMs. These results may indicate a downregulation of hiPS cells immunogeneity upon cardiac differentiation. GZMB is an important mediator of the cytotoxic function of CD8+ T-cells and NK-cells to eliminate allogeneic cells (Chowdhury & Lieberman, 2008). To determine the exact origin of cytokine expression, however, the different subpopulations of immune cells should also be studied individually. Besides, further studies with ELISA are required for accurate quantification of cytokines at the protein level. Whether the differentiation stage of iPS cells affects their immunogenic and immunomodulatory

properties after transplantation is currently the subject of research and controversy (Rossbach et al., 2022). The conflicting information on the immunogenic properties of iPS cell derivatives can be explained in part by the different immunogenicity of the cell types ultimately produced (Tapia & Schöler, 2016; Mehler, Burns, Stauss, Francis, & Moore, 2020). The expression of specific immunogenic antigens during the course of cardiac differentiation could explain the emergence of distinct T-cell- and NK-cell-dependent immune responses directed against the different maturation stages of hiPS cell-derived CPCs/CMs (Bizy & Klos, 2020). Moreover, the immunogenic properties of differentiated hiPS cells could also be influenced by the origin of the somatic parental cells, the quality of reprogramming, and the differentiation protocol used (Tapia & Schöler, 2016; Bizy & Klos, 2020). Therefore, accurate characterization of the immunological phenotype of hiPS cell derivatives is extremely important prior to clinical application (Mehler et al., 2020).

5.7 LDH-Cytotoxicity assay by ELISA readout

5.7.1 Advantages and disadvantages of the assay

A second assay was developed to characterize the cytotoxic T-cell and NK-cell-mediated immune response. The presence of dead cells can be detected by measuring markers that leak from the cytoplasm into the culture medium due to loss of their membrane integrity (Riss, Niles, Moravec, Karassina, & Vidugiriene, 2019). LDH is an enzyme that occurs naturally in the cell cytoplasm (Aslantürk, 2017). LDH release assays therefore provide a reliable, inexpensive and non-radioactive method for analysing lymphocyte-mediated cytotoxic activity against target cells (Weidmann et al., 1995). An advantage of this assay is that the target cells do not need to be additionally labelled with fluorescent dyes before performing the assay (Riss et al., 2019). However, a disadvantage of the assay is that LDH release is not limited to target cells and is also partially released by dying effector cells (Riss et al., 2019).

5.8 Evaluation of the immunogenicity of the *B2M*-deficient cell line

Despite the lack of significance, gene expression levels of *GZMB* and *IFNγ* was higher in PBMCs co-cultured with homozygous *B2M*-deficient E5V ΔPB hiPS cells than in PBMCs co-cultured with heteozygous E5V ΔPB and E5Vf (wild-type) hiPS cells, while *IL10* and *IL2* gene expression was higher in PBMCs co-cultured with E5Vf (wild-type) hiPS cells than in PBMCs co-cultured with homozygous and heterozygous E5V ΔPB hiPS cell clones. However, since PBMCs are mixed cell populations, the origin of the upregulated cytokine response cannot be clearly assigned to a specific immune cell type, and therefore the cytokine response of individual immune cell subpopulations should be investigated in further experiments. Targeted disruption of the *B2M* gene has been found to result in a decrease in CD8+ T-cell-mediated cytotoxicity due to a complete lack of surface MHC-I (D. Wang et al., 2015; Han et al., 2019; Norbnop et al., 2020; W. Zhao et al., 2020). Previously, other groups have used LDH release-based cytolytic assays to quantify the cytotoxicity of CD8+ T-cells and NK-cells (D. Wang

et al., 2015; Shi et al., 2020; Shao et al., 2020). After successful establishment of the LDH assay in this work, the cytotoxic T-cell and NK-cell-mediated immune response against the edited cell clones was analyzed. The homozygous *B2M* gene knockout resulted in a significant reduction in CD8+ T-cell-mediated cytotoxicity compared to wild-type hiPS cells (parental line). However, knockout of only one *B2M* allele was not sufficient to reduce cytotoxicity, highlighting the need for a biallelic knockout to generate hypoimmunogenic hiPS cells. Since in animal models CPCs or CMs are always transplanted and never hiPS cells, in vitro CD8+ T-cell-mediated cytotoxicity against *B2M* knockout hiPS cell-derived CPCs and CMs should also be investigated in next experiments. As MHC-I molecules act as important ligand inhibitors for NK-cells, a potential drawback of this approach could be that, according to the "missing-self theory", MHC-I surface deficiency of donor cells could render them vulnerable to recognition and destruction by NK-cells (Ljunggren & Kärre, 1990; Morvan & Lanier, 2016). Assessment of NK-cell-mediated cytotoxicity showed strong cytolytic activity against all cell clones tested, suggesting that *B2M* gene knockout can not modulate NK-cell-mediated cytotoxicity. These results are in accordance with studies performed by other research groups (D. Wang et al., 2015; Shi et al., 2020; Zha et al., 2020). While *B2M* knockout represents a first solid approach to reduce the T-cell immune response, further genetic modifications are required to fully downregulate the immunogenicity of hiPS cells to finally transplant CPCs and CMs with reduced immunogenicity. It is known that the immune response of NK-cells is regulated by various inhibitory receptors and their ligands and to date, several strategies have been proposed to reduce NK-cell-mediated cytotoxic activity against target cells (Pegram, Andrews, Smyth, Darcy, & Kershaw, 2011). The introduction and overexpression of membrane-bound non-classical HLA class I molecules HLA-E or HLA-G have been shown to protect cells from NK-cell-mediated cytotoxicity via interaction with various NK-cell inhibitor receptors (N. Lee et al., 1998; Rajagopalan & Long, 2012; Gornalusse et al., 2017; Han et al., 2019; Q. Ye et al., 2020). In the extravillous trophoblasts, HLA-G and E are co-expressed and are involved in modulating immune cell function and maintaining immune privilege at the maternal-fetal interface (Kanellopoulos-Langevin, Caucheteux, Verbeke, & Ojcius, 2003; Tersigni et al., 2020). Furthermore, to reduce NK-cell cytotoxicity Xu and colleagues selectively knocked out the HLA-A/-B gene while retaining the HLA-C gene (H. Xu et al., 2019). However, HLA-C can still present T-cell peptides, which could cause possible T-cell activation (H. Xu et al., 2019; Zha et al., 2020). Moreover, proinflammatory cytokines may upregulate transplant-specific MHC-II genes during the immune response against allografts (Kittur et al., 2002). As a result, several research groups have decided to simultaneously eliminate MHC-II expression by targeting its transcription regulator *CIITA* to reduce activation of other immune cells by CD4+ helper T-cells via cytokine release (Mattapally et al., 2018; H. Xu et al., 2019; Deuse et al., 2019; Han et al., 2019). In addition, Deuse and colleagues showed that ectopic overexpression of CD47 minimizes all innate immune responses, including phagocytosis by macrophages (Deuse et al., 2019). Other researchers have found that knocking in immunoregulatory factors (cytotoxic T-lymphocyte antigen 4 (CTLA4) and programmed death ligand-1 (PD-L1)) can further modulate the allogeneic immune response (Rong et al., 2014; Han et al., 2019). Given the complexity of the immune system, a combination of strategies will be required to generate highly immunocompatible hiPS cells and, most importantly, *in vivo* assessment of the survival benefit of these cells represents an important next step. Other aspects that need

to be considered in the future are safety concerns related to the use of hypoimmunogenic hiPS cell-derived cells: the risk of teratoma formation due to transplantation of some still present undifferentiated cells in amounts of transplanted CPCs or CMs, and the therefore increased risk of tumorigenicity. Another issue are viral infections, as cells with MHC-I surface deficiency acquire the ability to evade immune surveillance (Riolobos et al., 2013; Trounson et al., 2019; Shi et al., 2020). Therefore, the possible integration of a suicide gene or the use of a safe-harbour locus could be useful to eliminate this risk (Vanneaux, 2019; Shi et al., 2020). In addition, the optimal differentiation state of hiPS cell-derived CPCs/CMs for transplantation must be determined and, most importantly, the mechanical and electrophysical coupling ability of these cells must be improved to reduce the risk of cardiac arrhythmias (Lalit et al., 2014; Sadahiro, 2019).

6 Conclusion

Genetic manipulation using CRISPR/Cas9 technology efficiently generated *B2M* knockout hiPS cells. The engineered hiPS cells retain their properties after targeted disruption of the *B2M* gene and can efficiently differentiate into immature ventricular cardiomyocytes. *B2M* knockout was able to significantly decrease CD8+ T-cell-mediated cytotoxicity but was unable to reduce the NK-cell-mediated immune response. In conclusion, the generated hiPS cell line exhibits hypoimmunogenic properties for regenerative cell therapy and has the potential to simultaneously monitor ventricular cardiomyocytes after *in vivo* transplantation.

References

Abu-Dawud, R., Graffmann, N., Ferber, S., Wruck, W., & Adjaye, J. (2018, jul). Pluripotent stem cells: induction and self-renewal. *Philosophical Transactions of the Royal Society B: Biological Sciences*, *373*(1750). doi: 10.1098/RSTB.2017.0213

Adan, A., Alizada, G., Kiraz, Y., Baran, Y., & Nalbant, A. (2017, feb). *Flow cytometry: basic principles and applications* (Vol. 37) (No. 2). Taylor and Francis Ltd. doi: 10.3109/07388551.2015.1128876

Alageel, S., Wright, A. J., & Gulliford, M. C. (2016, oct). Changes in cardiovascular disease risk and behavioural risk factors before the introduction of a health check programme in England. *Preventive medicine*, *91*, 158–163. doi: 10.1016/J.YPMED.2016.08.025

Alberts B, Johnson A, Lewis J, & al., E. (2002). T Cells and MHC Proteins. In *Molecular biology of the cell* (4th ed.). New York: Garland Science. Retrieved from `https://www.ncbi.nlm.nih.gov/books/NBK26926/`

Al-Shanti, N., Steward, C. G., Garland, R. J., & Rowbottom, A. W. (2004, jul). Investigation of alpha nascent polypeptide-associated complex functions in a human CD8+ T cell ex vivo expansion model using antisense oligonucleotides. *Immunology*, *112*(3), 397. doi: 10.1111/J.1365-2567.2004.01893.X

Ambrose, J. A., & Singh, M. (2015, jan). Pathophysiology of coronary artery disease leading to acute coronary syndromes. *F1000Prime Reports*, *7*. doi: 10.12703/P7-08

Aslantürk, Ö. S. (2017, dec). In Vitro Cytotoxicity and Cell Viability Assays: Principles, Advantages, and Disadvantages. In *Genotoxicity - a predictable risk to our actual world.* IntechOpen. doi: 10.5772/INTECHOPEN.71923

Assou, S., Pourret, E., Péquignot, M., Rigau, V., Kalatzis, V., Aït-Ahmed, O., & Hamamah, S. (2015, oct). Cultured Cells from the Human Oocyte Cumulus Niche Are Efficient Feeders to Propagate Pluripotent Stem Cells. *Stem Cells and Development*, *24*(19), 2317. doi: 10.1089/SCD.2015.0043

Bar, A., & Cohen, S. (2020, feb). Inducing Endogenous Cardiac Regeneration: Can Biomaterials Connect the Dots? *Frontiers in Bioengineering and Biotechnology*, *8*. doi: 10.3389/FBIOE.2020.00126

Barao, I., & Murphy, W. J. (2003, dec). The immunobiology of natural killer cells and bone marrow allograft rejection. *Biology of Blood and Marrow Transplantation*, *9*(12), 727–741. doi: 10.1016/J.BBMT.2003.09.002

Barbierato, M., Argentini, C., & Skaper, S. D. (2012). Indirect immunofluorescence staining of cultured neural cells. *Methods in molecular biology*, *846*, 235–246. doi:

10.1007/978-1-61779-536-7_21

Barry, J., Hyllner, J., Stacey, G., Taylor, C. J., & Turner, M. (2015, jun). Setting Up a Haplobank: Issues and Solutions. *Current Stem Cell Reports*, *1*(2), 110–117. doi: 10.1007/S40778-015-0011-7

Basu, S., Campbell, H. M., Dittel, B. N., & Ray, A. (2010). Purification of specific cell population by fluorescence activated cell sorting (FACS). *Journal of Visualized Experiments*(41). doi: 10.3791/1546

Batalov, I., & Feinberg, A. W. (2015, may). Differentiation of Cardiomyocytes from Human Pluripotent Stem Cells Using Monolayer Culture. *Biomarker insights*, *10*(Suppl 1), 71–76. doi: 10.4137/BMI.S20050

Bauer, C. R. (2014). Labeling and use of monoclonal antibodies in immunofluorescence: protocols for cytoskeletal and nuclear antigens. *Methods in molecular biology (Clifton, N.J.)*, *1131*, 543–548. doi: 10.1007/978-1-62703-992-5_34

Bedada, F. B., Wheelwright, M., & Metzger, J. M. (2016, jul). Maturation status of sarcomere structure and function in human iPSC-derived cardiac myocytes. *Biochimica et biophysica acta*, *1863*(7 Pt B), 1829–1838. doi: 10.1016/J.BBAMCR.2015.11.005

Beers, J., Gulbranson, D. R., George, N., Siniscalchi, L. I., Jones, J., Thomson, J. A., & Chen, G. (2012, nov). Passaging and colony expansion of human pluripotent stem cells by enzyme-free dissociation in chemically defined culture conditions. *Nature protocols*, *7*(11), 2029–2040. doi: 10.1038/NPROT.2012.130

Benjamin, J. E., Gill, S., & Negrin, R. S. (2010, mar). Biology and clinical effects of natural killer cells in allogeneic transplantation. *Current opinion in oncology*, *22*(2), 130–137. doi: 10.1097/CCO.0B013E328335A559

Bergmann, O., Zdunek, S., Felker, A., Salehpour, M., Alkass, K., Bernard, S., ... Frisén, J. (2015, jun). Dynamics of Cell Generation and Turnover in the Human Heart. *Cell*, *161*(7), 1566–1575. doi: 10.1016/J.CELL.2015.05.026

Bessoles, S., Grandclément, C., Alari-Pahissa, E., Gehrig, J., Jeevan-Raj, B., & Held, W. (2014). Adaptations of natural killer cells to self-MHC class I. *Frontiers in Immunology*, *5*(Jul), 349. doi: 10.3389/FIMMU.2014.00349/BIBTEX

Bharat, A., & Mohanakumar, T. (2007, jul). Allopeptides and the Alloimmune Response. *Cellular immunology*, *248*(1), 31. doi: 10.1016/J.CELLIMM.2007.03.010

Bhattacharya, S., Burridge, P. W., Kropp, E. M., Chuppa, S. L., Kwok, W. M., Wu, J. C., ... Gundry, R. L. (2014, sep). High Efficiency Differentiation of Human Pluripotent Stem Cells to Cardiomyocytes and Characterization by Flow Cytometry. *Journal of Visualized Experiments : JoVE*(91), 52010. doi: 10.3791/52010

Birnbaum, Y., Fishbein, M. C., Luo, H., Nishioka, T., & Siegel, R. J. (1997, nov). Regional Remodeling of Atherosclerotic Arteries: A Major Determinant of Clinical Manifestations of Disease. *Journal of the American College of Cardiology*, *30*(5), 1149–1164. doi: 10.1016/S0735-1097(97)00320-3

Bissell, D. M., Arenson, D. M., Maher, J. J., & Roll, F. J. (1987). Support of cultured hepatocytes by a laminin-rich gel. Evidence for a functionally significant suben-

dothelial matrix in normal rat liver. *The Journal of clinical investigation*, *79*(3), 801–812. doi: 10.1172/JCI112887

Bizy, A., Guerrero-Serna, G., Hu, B., Ponce-Balbuena, D., Willis, B. C., Zarzoso, M., ... Jalife, J. (2013, nov). Myosin light chain 2-based selection of human iPSC-derived early ventricular cardiac myocytes. *Stem cell research*, *11*(3), 1335–1347. doi: 10.1016/J.SCR.2013.09.003

Bizy, A., & Klos, M. (2020, sep). Optimizing the Use of iPSC-CMs for Cardiac Regeneration in Animal Models. *Animals 2020, Vol. 10, Page 1561*, *10*(9), 1561. doi: 10.3390/ANI10091561

Boardman, D. A., Jacob, J., Smyth, L. A., Lombardi, G., & Lechler, R. I. (2016, dec). What Is Direct Allorecognition? *Current Transplantation Reports*, *3*(4), 275. doi: 10.1007/S40472-016-0115-8

Börger, A. K., Eicke, D., Wolf, C., Gras, C., Aufderbeck, S., Schulze, K., ... Figueiredo, C. (2016). Generation of HLA-Universal iPSC-Derived Megakaryocytes and Platelets for Survival Under Refractoriness Conditions. *Molecular Medicine*, *22*, 274. doi: 10.2119/MOLMED.2015.00235

Bouvier, M., & Wiley, D. C. (1998, may). Structural characterization of a soluble and partially folded class I major histocompatibility heavy chain/β2m heterodimer. *Nature Structural Biology*, *5*(5), 377–384. doi: 10.1038/nsb0598-377

Boyd, A. S., Rodrigues, N. P., Lui, K. O., Fu, X., & Xu, Y. (2012, may). Concise Review: Immune Recognition of Induced Pluripotent Stem Cells. *Stem Cells*, *30*(5), 797–803. doi: 10.1002/STEM.1066

Boyette, L. C., & Manna, B. (2021). *Physiology, Myocardial Oxygen Demand*. StatPearls Publishing. Retrieved from `https://www.ncbi.nlm.nih.gov/books/NBK499897/`

Brown, J. C., Gerhardt, T. E., & Kwon, E. (2021, jun). Risk Factors For Coronary Artery Disease. In *Statpearls [internet]* (pp. 1–219). StatPearls Publishing. doi: 10.3109/9781420014570

Brunner, E., Yagi, R., Debrunner, M., Beck-Schneider, D., Burger, A., Escher, E., ... Basler, K. (2019, jun). CRISPR-induced double-strand breaks trigger recombination between homologous chromosome arms. *Life Science Alliance*, *2*(3). doi: 10.26508/LSA.201800267

Burr, M. L., Cano, F., Svobodova, S., Boyle, L. H., Boname, J. M., & Lehner, P. J. (2011, feb). HRD1 and UBE2J1 target misfolded MHC class I heavy chains for endoplasmic reticulum-associated degradation. *Proceedings of the National Academy of Sciences of the United States of America*, *108*(5), 2034–2039. doi: 10.1073/PNAS.1016229108/SUPPL_FILE/PNAS.201016229SI.PDF

Burridge, P. W., Keller, G., Gold, J. D., & Wu, J. C. (2012, jan). Production of De Novo Cardiomyocytes: Human Pluripotent Stem Cell Differentiation and Direct Reprogramming. *Cell Stem Cell*, *10*(1), 16. doi: 10.1016/J.STEM.2011.12.013

Burridge, P. W., Matsa, E., Shukla, P., Lin, Z. C., Churko, J. M., Ebert, A. D., ... Wu, J. C. (2014). Chemically Defined and Small Molecule-Based Generation of Human

Cardiomyocytes. *Nature methods*, *11*(8), 855. doi: 10.1038/NMETH.2999

Cambria, E., Pasqualini, F. S., Wolint, P., Günter, J., Steiger, J., Bopp, A., ... Emmert, M. Y. (2017, dec). Translational cardiac stem cell therapy: advancing from first-generation to next-generation cell types. *NPJ Regenerative Medicine*, *2*(1), 17. doi: 10.1038/S41536-017-0024-1

Chan, C. J., Smyth, M. J., & Martinet, L. (2014, jan). Molecular mechanisms of natural killer cell activation in response to cellular stress. *Cell Death and Differentiation*, *21*(1), 5. doi: 10.1038/CDD.2013.26

Chao, T. H., Chen, I. C., Tseng, S. Y., & Li, Y. H. (2014, sep). Pluripotent Stem Cell Therapy in Ischemic Cardiovascular Disease. *Acta Cardiologica Sinica*, *30*(5), 365.

Chaplin, D. D. (2010, feb). Overview of the Immune Response. *The Journal of allergy and clinical immunology*, *125*(2 Suppl 2), S3. doi: 10.1016/J.JACI.2009.12.980

Charles A Janeway, J., Travers, P., Walport, M., & Shlomchik, M. J. (2001). T cell-mediated cytotoxicity. In *Immunobiology: The immune system in health and disease* (Vol. 5, chap. T cell-med). Garland Science.

Chávez-Galán, L., Arenas-Del Angel, M. C., Zenteno, E., Chávez, R., & Lascurain, R. (2009). Cell death mechanisms induced by cytotoxic lymphocytes. *Cellular molecular immunology*, *6*(1), 15–25. doi: 10.1038/CMI.2009.3

Chen, G., Gulbranson, D. R., Hou, Z., Bolin, J. M., Ruotti, V., Probasco, M. D., ... Thomson, J. A. (2011, may). Chemically defined conditions for human iPSC derivation and culture. *Nature Methods*, *8*(5), 424–429. doi: 10.1038/nmeth.1593

Chen, H. F., Yu, C. Y., Chen, M. J., Chou, S. H., Chiang, M. S., Chou, W. H., ... Ho, H. N. (2015, jan). Characteristic expression of major histocompatibility complex and immune privilege genes in human pluripotent stem cells and their derivatives. *Cell Transplantation*, *24*(5), 845–864. doi: 10.3727/096368913X674639

Chirikian, O., Goodyer, W. R., Dzilic, E., Serpooshan, V., Buikema, J. W., McKeithan, W., ... Wu, S. M. (2021, feb). CRISPR/Cas9-based targeting of fluorescent reporters to human iPSCs to isolate atrial and ventricular-specific cardiomyocytes. *Scientific Reports 2021*, *11*(1), 1–10. doi: 10.1038/s41598-021-81860-x

Chometon, T. Q., Da Silva Siqueira, M., Santacute;anna, J. C., Almeida, M. R., Gandini, M., De Almeida Nogueira, A. C. M., & Antas, P. R. Z. (2020, apr). A protocol for rapid monocyte isolation and generation of singular human monocyte-derived dendritic cells. *PLOS ONE*, *15*(4), e0231132. doi: 10.1371/JOURNAL.PONE.0231132

Chong, J. J., Yang, X., Don, C. W., Minami, E., Liu, Y. W., Weyers, J. J., ... Murry, C. E. (2014). Human Embryonic Stem Cell-Derived Cardiomyocytes Regenerate Non-Human Primate Hearts. *Nature*, *510*(7504), 273. doi: 10.1038/NATURE13233

Chowdhury, D., & Lieberman, J. (2008). Death by a Thousand Cuts: Granzyme Pathways of Programmed Cell Death. *Annual review of immunology*, *26*, 389. doi: 10.1146/ANNUREV.IMMUNOL.26.021607.090404

Choy, J. C. (2010, apr). *Granzymes and perforin in solid organ transplant rejection* (Vol. 17) (No. 4). Nature Publishing Group. doi: 10.1038/cdd.2009.161

Claassen, D. A., Desler, M. M., & Rizzino, A. (2009, aug). ROCK inhibition enhances the recovery and growth of cryopreserved human embryonic stem cells and human induced pluripotent stem cells. *Molecular reproduction and development*, *76*(8), 722–732. doi: 10.1002/MRD.21021

Corkum, C. P., Ings, D. P., Burgess, C., Karwowska, S., Kroll, W., & Michalak, T. I. (2015, aug). Immune cell subsets and their gene expression profiles from human PBMC isolated by Vacutainer Cell Preparation Tube (CPT) and standard density gradient. *BMC Immunology*, *16*(1), 1–18. doi: 10.1186/S12865-015-0113-0/FIGURES/9

Cossarizza, A., Chang, H. D., Radbruch, A., Akdis, M., Andrä, I., Annunziato, F., ... Zimmermann, J. (2017, oct). Guidelines for the use of flow cytometry and cell sorting in immunological studies. *European Journal of Immunology*, *47*(10), 1584–1797. doi: 10.1002/EJI.201646632

Cruz-Tapias, P., Castiblanco, J., & Anaya, J.-M. (2013, jul). Major histocompatibility complex: Antigen processing and presentation. In *Autoimmunity: From bench to bedside [internet]* (chap. 10). Bogota (Colombia): El Rosario University Press.

De Almeida, P. E., Ransohoff, J. D., Nahid, A., & Wu, J. C. (2013, feb). Immunogenicity of Pluripotent Stem Cells and Their Derivatives. *Circulation research*, *112*(3), 549. doi: 10.1161/CIRCRESAHA.111.249243

De Rham, C., & Villard, J. (2014). Potential and limitation of HLA-based banking of human pluripotent stem cells for cell therapy. *Journal of immunology research*. doi: 10.1155/2014/518135

Deepak, S., Kottapalli, K., Rakwal, R., Oros, G., Rangappa, K., Iwahashi, H., ... Agrawal, G. (2007, jul). Real-Time PCR: Revolutionizing Detection and Expression Analysis of Genes. *Current Genomics*, *8*(4), 234. doi: 10.2174/138920207781386960

Deuse, T., Hu, X., Gravina, A., Wang, D., Tediashvili, G., De, C., ... Schrepfer, S. (2019, mar). Hypoimmunogenic derivatives of induced pluripotent stem cells evade immune rejection in fully immunocompetent allogeneic recipients. *Nature biotechnology*, *37*(3), 252. doi: 10.1038/S41587-019-0016-3

Di Franco, S., Amarelli, C., Montalto, A., Loforte, A., & Musumeci, F. (2018, jul). Biomaterials and heart recovery: cardiac repair, regeneration and healing in the MCS era: a state of the heart. *Journal of Thoracic Disease*, *10*(Suppl 20), S2346. doi: 10.21037/JTD.2018.01.85

Donaldson, J. G. (1998, oct). Immunofluorescence Staining. *Current Protocols in Cell Biology*(1), 4.3.1–4.3.6. doi: 10.1002/0471143030.CB0403S00

Doudna, J. A., & Charpentier, E. (2014, nov). Genome editing. The new frontier of genome engineering with CRISPR-Cas9. *Science (New York, N.Y.)*, *346*(6213). doi: 10.1126/SCIENCE.1258096

Dragan, A. I., Pavlovic, R., McGivney, J. B., Casas-Finet, J. R., Bishop, E. S., Strouse,

R. J., ... Geddes, C. D. (2012, jul). SYBR Green I: Fluorescence properties and interaction with DNA. *Journal of Fluorescence*, *22*(4), 1189–1199. doi: 10.1007/s10895-012-1059-8

Drukker, M., Katz, G., Urbach, A., Schuldiner, M., Markel, G., Itskovitz-Eldor, J., ... Benvenisty, N. (2002, jul). Characterization of the expression of MHC proteins in human embryonic stem cells. *Proceedings of the National Academy of Sciences of the United States of America*, *99*(15), 9864–9869. doi: 10.1073/PNAS.142298299

Eljaszewicz, A., Raiter-Smiljanic, A., Szkulmowska, A., Bukowska, D., Derzsi, L., Wojtkowski, M., ... Garstecki, P. (2015, oct). Differentiation of morphotic elements in human blood using optical coherence tomography and a microfluidic setup. *Optics Express*, *23*(21), 27724–27738. doi: 10.1364/OE.23.027724

Eminli, S., Foudi, A., Stadtfeld, M., Maherali, N., Ahfeldt, T., Mostoslavsky, G., ... Hochedlinger, K. (2009, sep). Differentiation stage determines potential of hematopoietic cells for reprogramming into induced pluripotent stem cells. *Nature genetics*, *41*(9), 968–976. doi: 10.1038/NG.428

Eslami, A., & Lujan, J. (2010). Western blotting: sample preparation to detection. *Journal of visualized experiments : JoVE*(44). doi: 10.3791/2359

Feng, Q., Shabrani, N., Thon, J. N., Huo, H., Thiel, A., Machlus, K. R., ... Lanza, R. (2014, nov). Scalable Generation of Universal Platelets from Human Induced Pluripotent Stem Cells. *Stem Cell Reports*, *3*(5), 817. doi: 10.1016/J.STEMCR.2014.09.010

Figueiredo, C., Wedekind, D., Müller, T., Vahlsing, S., Horn, P. A., Seltsam, A., & Blasczyk, R. (2013). MHC Universal Cells Survive in an Allogeneic Environment after Incompatible Transplantation. *BioMed Research International*, 12. doi: 10.1155/2013/796046

Finan, A., & Richard, S. (2015, sep). Stimulating endogenous cardiac repair. *Frontiers in Cell and Developmental Biology*, *3*(SEP), 57. doi: 10.3389/FCELL.2015.00057

Ford, E. S., Ajani, U. A., Croft, J. B., Critchley, J. A., Phil, D., Labarthe, D. R., ... Capewell, S. (2009, oct). Explaining the Decrease in U.S. Deaths from Coronary Disease, 1980â“2000. *The New England Journal of Medicine*, *356*(23), 2388–2398. doi: 10.1056/NEJMSA053935

Frenzel, L. P., Abdullah, Z., Kriegeskorte, A. K., Dieterich, R., Lange, N., Busch, D. H., ... Šarić, T. (2009, feb). Role of natural-killer group 2 member D ligands and intercellular adhesion molecule 1 in natural killer cell-mediated lysis of murine embryonic stem cells and embryonic stem cell-derived cardiomyocytes. *Stem cells (Dayton, Ohio)*, *27*(2), 307–316. doi: 10.1634/STEMCELLS.2008-0528

Froger, A., & Hall, J. E. (2007, jul). Transformation of Plasmid DNA into E. Coli using the heat shock method. *Journal of Visualized Experiments*(6), 253. doi: 10.3791/253

Gao, Y., & Pu, J. (2021, may). Differentiation and Application of Human Pluripotent Stem Cells Derived Cardiovascular Cells for Treatment of Heart Diseases: Promises and Challenges. *Frontiers in Cell and Developmental Biology*, *9*, 921. doi: 10.3389/

fcell.2021.658088

García, M. A. A., Yebra, B. G., Flores, A. L. L., & Guerra, E. G. (2012). The Major Histocompatibility Complex in Transplantation. *Journal of Transplantation*, *2012*, 1–7. doi: 10.1155/2012/842141

Garibyan, L., & Avashia, N. (2013). Polymerase chain reaction. *The Journal of investigative dermatology*, *133*(3), 1–4. doi: 10.1038/JID.2013.1

Gasiunas, G., Barrangou, R., Horvath, P., & Siksnys, V. (2012, sep). Cas9-crRNA ribonucleoprotein complex mediates specific DNA cleavage for adaptive immunity in bacteria. *Proceedings of the National Academy of Sciences of the United States of America*, *109*(39), E2579–E2586. doi: 10.1073/PNAS.1208507109/-/DCSUPPLEMENTAL

George, V., Colombo, S., & Targoff, K. L. (2015, apr). An early requirement for nkx2.5 ensures the first and second heart field ventricular identity and cardiac function into adulthood. *Developmental biology*, *400*(1), 10–22. doi: 10.1016/J.YDBIO.2014.12.019

Gepstein, L. (2002, nov). Derivation and potential applications of human embryonic stem cells. *Circulation research*, *91*(10), 866–876. doi: 10.1161/01.RES.0000041435.95082.84

Ghosh, Z., Wilson, K. D., Wu, Y., Hu, S., Quertermous, T., & Wu, J. C. (2010, feb). Persistent Donor Cell Gene Expression among Human Induced Pluripotent Stem Cells Contributes to Differences with Human Embryonic Stem Cells. *PLoS ONE*, *5*(2). doi: 10.1371/JOURNAL.PONE.0008975

Giulietti, A., Overbergh, L., Valckx, D., Decallonne, B., Bouillon, R., & Mathieu, C. (2001, dec). An Overview of Real-Time Quantitative PCR: Applications to Quantify Cytokine Gene Expression. *Methods*, *25*(4), 386–401. doi: 10.1006/METH.2001.1261

Gleditzsch, D., Pausch, P., Müller-Esparza, H., Özcan, A., Guo, X., Bange, G., & Randau, L. (2019, apr). PAM identification by CRISPR-Cas effector complexes: diversified mechanisms and structures. *RNA biology*, *16*(4), 504–517. doi: 10.1080/15476286.2018.1504546

Gornalusse, G. G., Hirata, R. K., Funk, S. E., Riolobos, L., Lopes, V. S., Manske, G., ... Russell, D. W. (2017, aug). HLA-E-expressing pluripotent stem cells escape allogeneic responses and lysis by NK cells. *Nature biotechnology*, *35*(8), 765. doi: 10.1038/NBT.3860

Green, M. R., & Sambrook, J. (2018, oct). Analysis and Normalization of Real-Time Polymerase Chain Reaction (PCR) Experimental Data. *Cold Spring Harbor protocols*(10), 769–777. doi: 10.1101/PDB.TOP095000

Guo, Y., & Pu, W. T. (2020). Cardiomyocyte Maturation: New Phase in Development. *Circulation research*, *126*(8), 1086. doi: 10.1161/CIRCRESAHA.119.315862

Gupta, T., & Krim, S. R. (2019, dec). Cardiac Transplantation: Update on a Road Less Traveled. *The Ochsner Journal*, *19*(4), 369. doi: 10.31486/TOJ.19.0022

Hackett, C. H., & Fortier, L. A. (2011, aug). Embryonic Stem Cells and iPS Cells:

Sources and Characteristics. *The Veterinary clinics of North America. Equine practice*, *27*(2), 233. doi: 10.1016/J.CVEQ.2011.04.003

Haddad, F., & Baldwin, K. M. (2010). Reverse transcription of the ribonucleic acid: the first step in RT-PCR assay. *Methods in molecular biology*, *630*, 261–270. doi: 10.1007/978-1-60761-629-0_17

Halenius, A., Gerke, C., & Hengel, H. (2014). Classical and non-classical MHC I molecule manipulation by human cytomegalovirus: so many targets-but how many arrows in the quiver? *Cellular Molecular Immunology*, *12*, 139–153. doi: 10.1038/cmi.2014.105

Hamerman, J. A., Ogasawara, K., & Lanier, L. L. (2005, feb). NK cells in innate immunity. *Current opinion in immunology*, *17*(1), 29–35. doi: 10.1016/J.COI.2004.11.001

Han, X., Wang, M., Duan, S., Franco, P. J., Kenty, J. H. R., Hedrick, P., ... Cowan, C. A. (2019, may). Generation of hypoimmunogenic human pluripotent stem cells. *Proceedings of the National Academy of Sciences of the United States of America*, *116*(21), 10441–10446. doi: 10.1073/PNAS.1902566116/-/DCSUPPLEMENTAL

Harper, S. J., Ali, J. M., Wlodek, E., Negus, M. C., Harper, I. G., Chhabra, M., ... Pettigrew, G. J. (2015, oct). CD8 T-cell recognition of acquired alloantigen promotes acute allograft rejection. *Proceedings of the National Academy of Sciences of the United States of America*, *112*(41), 12788–12793. doi: 10.1073/pnas.1513533112

Hasan, A., Khattab, A., Islam, M. A., Hweij, K. A., Zeitouny, J., Waters, R., ... Paul, A. (2015, nov). Injectable Hydrogels for Cardiac Tissue Repair after Myocardial Infarction. *Advanced science*, *2*(11). Retrieved from `https://pubmed.ncbi.nlm.nih.gov/27668147/` doi: 10.1002/ADVS.201500122

Hashimoto, H., Olson, E. N., & Bassel-Duby, R. (2018, oct). Therapeutic approaches for cardiac regeneration and repair. *Nature reviews. Cardiology*, *15*(10), 585. doi: 10.1038/S41569-018-0036-6

Hastings, C. L., Roche, E. T., Ruiz-Hernandez, E., Schenke-Layland, K., Walsh, C. J., & Duffy, G. P. (2015, apr). Drug and cell delivery for cardiac regeneration. *Advanced Drug Delivery Reviews*, *84*, 85–106. doi: 10.1016/J.ADDR.2014.08.006

Hnasko, T. S., & Hnasko, R. M. (2015). The Western Blot. *Methods in Molecular Biology*, *1318*, 87–96. doi: 10.1007/978-1-4939-2742-5_9

Horvath, P., & Barrangou, R. (2010, jan). CRISPR/Cas, the immune system of Bacteria and Archaea. *Science*, *327*(5962), 167–170. doi: 10.1126/SCIENCE.1179555/SUPPL_FILE/167_THUMB.JPG

Hsu, P. D., Lander, E. S., & Zhang, F. (2014, jun). Development and Applications of CRISPR-Cas9 for Genome Engineering. *Cell*, *157*(6), 1262–1278. doi: 10.1016/J.CELL.2014.05.010

Huang, C. Y., Liu, C. L., Ting, C. Y., Chiu, Y. T., Cheng, Y. C., Nicholson, M. W., & Hsieh, P. C. (2019, oct). Human iPSC banking: barriers and opportunities. *Journal of Biomedical Science*, *26*(1). doi: 10.1186/S12929-019-0578-X

Hughes, E. A., Hammond, C., & Cresswell, P. (1997, mar). Misfolded major histocom-

patibility complex class I heavy chains are translocated into the cytoplasm and degraded by the proteasome. *Proceedings of the National Academy of Sciences of the United States of America*, *94*(5), 1896. doi: 10.1073/PNAS.94.5.1896

Ichimura, H., Kadota, S., Kashihara, T., Yamada, M., Ito, K., Kobayashi, H., ... Shiba, Y. (2020, dec). Increased predominance of the matured ventricular subtype in embryonic stem cell-derived cardiomyocytes in vivo. *Scientific Reports*, *10*(1), 11883. doi: 10.1038/S41598-020-68373-9

Ichise, H., Nagano, S., Maeda, T., Miyazaki, M., Miyazaki, Y., Kojima, H., ... Kawamoto, H. (2017, sep). NK Cell Alloreactivity against KIR-Ligand-Mismatched HLA-Haploidentical Tissue Derived from HLA Haplotype-Homozygous iPSCs. *Stem Cell Reports*, *9*(3), 853. doi: 10.1016/J.STEMCR.2017.07.020

Im, K., Mareninov, S., Diaz, M. F. P., & Yong, W. H. (2019). An introduction to Performing Immunofluorescence Staining. *Methods in molecular biology*, *1897*, 299. doi: 10.1007/978-1-4939-8935-5_26

Ingulli, E. (2010, jan). Mechanism of cellular rejection in transplantation. *Pediatric Nephrology*, *25*(1), 61–74. doi: 10.1007/S00467-008-1020-X/FIGURES/2

Ishizaki, T., Uehata, M., Tamechika, I., Keel, J., Nonomura, K., Maekawa, M., & Narumiya, S. (2000). Pharmacological properties of Y-27632, a specific inhibitor of Rho-associated kinases. *Molecular Pharmacology*, *57*(5), 976–983. doi: 10.2/JQUERY.MIN.JS

Israelsson, P., Dehlin, E., Nagaev, I., Lundin, E., Ottander, U., & Mincheva-Nilsson, L. (2020, jul). Cytokine mRNA and protein expression by cell cultures of epithelial ovarian cancer: Methodological considerations on the choice of analytical method for cytokine analyses. *American Journal of Reproductive Immunology*, *84*(1), e13249. doi: 10.1111/AJI.13249

Jia, Y. (2012, jan). Real-Time PCR. *Methods in Cell Biology*, *112*, 55–68. doi: 10.1016/B978-0-12-405914-6.00003-2

Jiang, Y., & Lian, X. L. (2020, mar). Heart regeneration with human pluripotent stem cells: Prospects and challenges. *Bioactive Materials*, *5*(1), 74. doi: 10.1016/J.BIOACTMAT.2020.01.003

Jinek, M., Chylinski, K., Fonfara, I., Hauer, M., Doudna, J. A., & Charpentier, E. (2012, aug). A programmable dual-RNA-guided DNA endonuclease in adaptive bacterial immunity. *Science*, *337*(6096), 816–821. doi: 10.1126/science.1225829

Kanellopoulos-Langevin, C., Caucheteux, S. M., Verbeke, P., & Ojcius, D. M. (2003, dec). Tolerance of the fetus by the maternal immune system: Role of inflammatory mediators at the feto-maternal interface. *Reproductive Biology and Endocrinology*, *1*(1), 1–6. doi: 10.1186/1477-7827-1-121/FIGURES/4

Karabekian, Z., Ding, H., Stybayeva, G., Ivanova, I., Muselimyan, N., Haque, A., ... Sarvazyan, N. (2015, oct). HLA Class I Depleted hESC as a Source of Hypoimmunogenic Cells for Tissue Engineering Applications. *Tissue Engineering. Part A*, *21*(19-20), 2559. doi: 10.1089/TEN.TEA.2015.0105

Kawai, Y., Tohyama, S., Arai, K., Tamura, T., Soma, Y., Fukuda, K., ... Kobayashi, E. (2022, jan). Scaffold-Free Tubular Engineered Heart Tissue From Human Induced Pluripotent Stem Cells Using Bio-3D Printing Technology in vivo. *Frontiers in Cardiovascular Medicine*, 2237. doi: 10.3389/FCVM.2021.806215

Kehat, I., Kenyagin-Karsenti, D., Snir, M., Segev, H., Amit, M., Gepstein, A., ... Gepstein, L. (2001, aug). Human embryonic stem cells can differentiate into myocytes with structural and functional properties of cardiomyocytes. *Journal of Clinical Investigation*, *108*(3), 407. doi: 10.1172/JCI12131

Kepp, O., Galluzzi, L., Lipinski, M., Yuan, J., & Kroemer, G. (2011, mar). Cell death assays for drug discovery. *Nature Reviews Drug Discovery*, *10*(3), 221–237. doi: 10.1038/nrd3373

Khan, F. A., Almohazey, D., Alomari, M., & Almofty, S. A. (2018). Isolation, Culture, and Functional Characterization of Human Embryonic Stem Cells: Current Trends and Challenges. *Stem Cells International*. doi: 10.1155/2018/1429351

Kim, H., Kim, M., Im, S.-K., & Fang, S. (2018). Mouse Cre-LoxP system: general principles to determine tissue-specific roles of target genes. *Laboratory Animal Research*, *34*(4), 147. doi: 10.5625/LAR.2018.34.4.147

Kim, K., Doi, A., Wen, B., Ng, K., Zhao, R., Cahan, P., ... Daley, G. Q. (2010). Epigenetic memory in induced pluripotent stem cells. *Nature*, *467*(7313), 285. doi: 10.1038/NATURE09342

Kittur, D. S., Wilasrusmee, C., Han, W. F., Xu, R., Burdick, J. F., & Adler, W. (2002, aug). Locally derived cytokines and upregulation of MHC class II genes in allografts. *The Journal of Heart and Lung Transplantation*, *21*(8), 882–889. doi: 10.1016/S1053-2498(02)00407-2

Kleinman, H. K., McGarvey, M. L., Liotta, L. A., Robey, P. G., Tryggvason, K., & Martin, G. R. (1982). Isolation and characterization of type IV procollagen, laminin, and heparan sulfate proteoglycan from the EHS sarcoma. *Biochemistry*, *21*(24), 6188–6193. doi: 10.1021/BI00267A025

Kleiveland, C. (2015, jan). Peripheral blood mononuclear cells. *The Impact of Food Bioactives on Health: In Vitro and Ex Vivo Models*, 161–167. doi: 10.1007/978-3-319-16104-4_15/FIGURES/1

Kubalak, S. W., Miller-Hance, W. C., O'Brien, T. X., Dyson, E., & Chien, K. R. (1994, jun). Chamber specification of atrial myosin light chain-2 expression precedes septation during murine cardiogenesis. *Journal of Biological Chemistry*, *269*(24), 16961–16970. doi: 10.1016/S0021-9258(19)89483-8

Laco, F., Woo, T. L., Zhong, Q., Szmyd, R., Ting, S., Khan, F. J., ... Oh, S. (2018, jun). Unraveling the Inconsistencies of Cardiac Differentiation Efficiency Induced by the GSK3β Inhibitor CHIR99021 in Human Pluripotent Stem Cells. *Stem Cell Reports*, *10*(6), 1851–1866. doi: 10.1016/j.stemcr.2018.03.023

Lacy, P., & Stow, J. L. (2011, jul). Cytokine release from innate immune cells: association with diverse membrane trafficking pathways. *Blood*, *118*(1), 9–18. doi: 10.1182/BLOOD-2010-08-265892

Laflamme, M. A., Chen, K. Y., Naumova, A. V., Muskheli, V., Fugate, J. A., Dupras, S. K., ... Murry, C. E. (2007, aug). Cardiomyocytes derived from human embryonic stem cells in pro-survival factors enhance function of infarcted rat hearts. *Nature Biotechnology*, *25*(9), 1015–1024. doi: 10.1038/nbt1327

Lalit, P. A., Hei, D. J., Raval, A. N., & Kamp, T. J. (2014, apr). iPS Cells for Post-myocardial Infarction Repair: Remarkable Opportunities and Challenges. *Circulation research*, *114*(8), 1328. doi: 10.1161/CIRCRESAHA.114.300556

LaRosa, D. F., Rahman, A. H., & Turka, L. A. (2007, jun). The Innate Immune System in Allograft Rejection and Tolerance. *Journal of immunology*, *178*(12), 7503. doi: 10.4049/JIMMUNOL.178.12.7503

Lee, N., Llano, M., Carretero, M., Akiko-Ishitani, Navarro, F., López-Botet, M., & Geraghty, D. E. (1998, apr). HLA-E is a major ligand for the natural killer inhibitory receptor CD94/NKG2A. *Proceedings of the National Academy of Sciences of the United States of America*, *95*(9), 5199–5204. doi: 10.1073/PNAS.95.9.5199

Lee, P. Y., Costumbrado, J., Hsu, C. Y., & Kim, Y. H. (2012, apr). Agarose Gel Electrophoresis for the Separation of DNA Fragments. *Journal of Visualized Experiments : JoVE*(62), 3923. doi: 10.3791/3923

Lemcke, H., Voronina, N., Steinhoff, G., & David, R. (2018). Recent Progress in Stem Cell Modification for Cardiac Regeneration. *Stem Cells International*, *2018*. doi: 10.1155/2018/1909346

Li, J., Lee, J. K., Miwa, K., Kuramoto, Y., Masuyama, K., Yasutake, H., ... Sakata, Y. (2021, feb). Scaffold-Mediated Developmental Effects on Human Induced Pluripotent Stem Cell-Derived Cardiomyocytes Are Preserved After External Support Removal. *Frontiers in Cell and Developmental Biology*, *9*, 255. doi: 10.3389/FCELL.2021.591754/BIBTEX

Li, J., Song, W., Pan, G., & Zhou, J. (2014, jul). Advances in understanding the cell types and approaches used for generating induced pluripotent stem cells. *Journal of Hematology Oncology*, *7*(1), 50. doi: 10.1186/S13045-014-0050-Z

Li, L., Dong, M., & Wang, X. G. (2016, feb). The Implication and Significance of Beta 2 Microglobulin: A Conservative Multifunctional Regulator. *Chinese Medical Journal*, *129*(4), 448. doi: 10.4103/0366-6999.176084

Li, X., Meng, G., Krawetz, R., Liu, S., & Rancourt, D. E. (2008, dec). The ROCK inhibitor Y-27632 enhances the survival rate of human embryonic stem cells following cryopreservation. *Stem cells and development*, *17*(6), 1079–1085. doi: 10.1089/SCD.2007.0247

Li, X. C., & Raghavan, M. (2010, aug). Structure and function of major histocompatibility complex (MHC) class I antigens. *Current opinion in organ transplantation*, *15*(4), 499. doi: 10.1097/MOT.0B013E32833BFB33

Lian, X., Hsiao, C., Wilson, G., Zhu, K., Hazeltine, L. B., Azarin, S. M., ... Palecek, S. P. (2012, jul). Robust cardiomyocyte differentiation from human pluripotent stem cells via temporal modulation of canonical Wnt signaling. *Proceedings of the National Academy of Sciences of the United States of America*, *109*(27), E1848.

doi: 10.1073/pnas.1200250109

Liao, X., Makris, M., & Luo, X. M. (2016, nov). Fluorescence-activated cell sorting for purification of plasmacytoid dendritic cells from the mouse bone marrow. *Journal of Visualized Experiments*(117). doi: 10.3791/54641

Lichter, J. G., Carruth, E., Mitchell, C., Barth, A. S., Aiba, T., Kass, D. A., ... Sachse, F. B. (2014). Remodeling of the Sarcomeric Cytoskeleton in Cardiac Ventricular Myocytes during Heart Failure and after Cardiac Resynchronization Therapy. *Journal of molecular and cellular cardiology*, *72*, 186. doi: 10.1016/J.YJMCC.2014.03.012

Liew, L. C., Ho, B. X., & Soh, B. S. (2020, mar). Mending a broken heart: current strategies and limitations of cell-based therapy. *Stem Cell Research Therapy*, *11*(1), 1–15. doi: 10.1186/S13287-020-01648-0

Lin, A. W., Gonzalez, S. A., Cunningham-Rundles, S., Dorante, G., Marshall, S., Tignor, A., ... Talal, A. H. (2004, aug). CD56+dim and CD56+bright cell activation and apoptosis in hepatitis C virus infection. *Clinical and Experimental Immunology*, *137*(2), 408. doi: 10.1111/J.1365-2249.2004.02523.X

Liu, G., David, B. T., Trawczynski, M., & Fessler, R. G. (2020, feb). Advances in Pluripotent Stem Cells: History, Mechanisms, Technologies, and Applications. *Stem Cell Reviews and Reports*, *16*(1), 3. doi: 10.1007/S12015-019-09935-X

Liu, P., Chen, S., Li, X., Qin, L., Huang, K., Wang, L., ... Pei, D. (2013, jul). Low Immunogenicity of Neural Progenitor Cells Differentiated from Induced Pluripotent Stem Cells Derived from Less Immunogenic Somatic Cells. *PLoS ONE*, *8*(7). doi: 10.1371/JOURNAL.PONE.0069617

Liu, X., Li, W., Fu, X., & Xu, Y. (2017, jun). The Immunogenicity and Immune Tolerance of Pluripotent Stem Cell Derivatives. *Frontiers in Immunology*, *8*(Jun), 645. doi: 10.3389/FIMMU.2017.00645

Ljunggren, H. G., & Kärre, K. (1990). In search of the 'missing self': MHC molecules and NK cell recognition. *Immunology today*, *11*(7), 237–244. doi: 10.1016/0167-5699(90)90097-S

Lodish, H., Berk, A., Zipursky, S. L., Matsudaira, P., Baltimore, D., & Darnell, J. (2000). DNA Cloning with Plasmid Vectors. In *Molecular cell biology* (4th ed.). New York: W. H. Freeman.

Lopez, E. O., Ballard, B. D., & Jan, A. (2021, aug). Cardiovascular Disease. In *Statpearls [internet].* StatPearls Publishing.

Loureiro, A., & Da Silva, G. J. (2019, mar). CRISPR-Cas: Converting A Bacterial Defence Mechanism into A State-of-the-Art Genetic Manipulation Tool. *Antibiotics*, *8*(1). doi: 10.3390/ANTIBIOTICS8010018

Lu, P., Chen, J., He, L., Ren, J., Chen, H., Rao, L., ... Xiao, L. (2013, aug). Generating Hypoimmunogenic Human Embryonic Stem Cells by the Disruption of Beta 2-Microglobulin. *Stem Cell Reviews and Reports*, *9*(6), 806–813. doi: 10.1007/S12015-013-9457-0

Ludwig, T. E., Bergendahl, V., Levenstein, M. E., Yu, J., Probasco, M. D., & Thomson,

J. A. (2006, jul). Feeder-independent culture of human embryonic stem cells. *Nature Methods*, *3*(8), 637–646. doi: 10.1038/nmeth902

Ludwig, T. E., Levenstein, M. E., Jones, J. M., Berggren, W. T., Mitchen, E. R., Frane, J. L., ... Thomson, J. A. (2006, jan). Derivation of human embryonic stem cells in defined conditions. *Nature Biotechnology*, *24*(2), 185–187. doi: 10.1038/nbt1177

Mahmood, T., & Yang, P. C. (2012, sep). Western Blot: Technique, Theory, and Trouble Shooting. *North American Journal of Medical Sciences*, *4*(9), 429–434. doi: 10.4103/1947-2714.100998

Maity, B., Sheff, D., & Fisher, R. A. (2013, jan). Immunostaining. Detection of Signaling Protein Location in Tissues, Cells and Subcellular Compartments. In *Methods in cell biology* (Vol. 113, pp. 81–105). Academic Press Inc. doi: 10.1016/B978-0-12-407239-8.00005-7

Maldonado, M., Luu, R. J., Ramos, M. E., & Nam, J. (2016, sep). ROCK inhibitor primes human induced pluripotent stem cells to selectively differentiate towards mesendodermal lineage via epithelial-mesenchymal transition-like modulation. *Stem Cell Research*, *17*(2), 222–227. doi: 10.1016/J.SCR.2016.07.009

Malik, N. N., Jenkins, A. M., Mellon, J., & Bailey, G. (2019, oct). Engineering strategies for generating hypoimmunogenic cells with high clinical and commercial value. *Regenerative Medicine*, *14*(11), 983–989. doi: 10.2217/RME-2019-0117/ASSET/IMAGES/LARGE/FIGURE1.JPEG

Mandal, P. K., Ferreira, L. M., Collins, R., Meissner, T. B., Boutwell, C. L., Friesen, M., ... Cowan, C. A. (2014). Efficient ablation of genes in human hematopoietic stem and effector cells using CRISPR/Cas9. *Cell Stem Cell*, *15*(5), 643. doi: 10.1016/J.STEM.2014.10.004

Marino, J., Paster, J., & Benichou, G. (2016). Allorecognition by T lymphocytes and allograft rejection. *Frontiers in Immunology*, *7*(Dec). doi: 10.3389/fimmu.2016.00582

Martin, U. (2017). Therapeutic Application of Pluripotent Stem Cells: Challenges and Risks. *Frontiers in Medicine*, *4*(Dec), 1. doi: 10.3389/FMED.2017.00229

Mattapally, S., Pawlik, K. M., Fast, V. G., Zumaquero, E., Lund, F. E., Randall, T. D., ... Zhang, J. (2018, dec). Human Leukocyte Antigen Class I and II Knockout Human Induced Pluripotent Stem Cell-Derived Cells: Universal Donor for Cell Therapy. *Journal of the American Heart Association: Cardiovascular and Cerebrovascular Disease*, *7*(23). doi: 10.1161/JAHA.118.010239

Maximilian Buja, L., & Vela, D. (2008, nov). Cardiomyocyte death and renewal in the normal and diseased heart. *Cardiovascular Pathology*, *17*(6), 349–374. doi: 10.1016/J.CARPATH.2008.02.004

McGuire, P. G., & Seeds, N. W. (1989, jun). The interaction of plasminogen activator with a reconstituted basement membrane matrix and extracellular macromolecules produced by cultured epithelial cells. *Journal of Cellular Biochemistry*, *40*(2), 215–227. doi: 10.1002/JCB.240400210

McKinnon, K. M. (2018, feb). Flow Cytometry: An Overview. *Current protocols in*

immunology, *120*, 5.1.1. doi: 10.1002/CPIM.40

Mehler, V. J., Burns, C. J., Stauss, H., Francis, R. J., & Moore, M. L. (2020, mar). Human iPSC-Derived Neural Crest Stem Cells Exhibit Low Immunogenicity. *Molecular Therapy - Methods and Clinical Development*, *16*, 161–171. doi: 10.1016/j.omtm.2019.12.015

Miltenyi, S., Müller, W., Weichel, W., & Radbruch, A. (1990). High gradient magnetic cell separation with MACS. *Cytometry*, *11*(2), 231–238. doi: 10.1002/cyto.990110203

Miyagawa, S., Fukushima, S., Imanishi, Y., Kawamura, T., Mochizuki- Oda, N., Masuda, S., & Sawa, Y. (2016, jan). Building A New Treatment For Heart Failure-Transplantation of Induced Pluripotent Stem Cell-derived Cells into the Heart. *Current Medicinal Chemistry*, *16*(1), 5. doi: 10.2174/156652321666616011909414 3

Moon, S. H., Bae, D., Jung, T. H., Chung, E. B., Jeong, Y. H., Park, S. J., & Chung, H. M. (2017, may). From Bench to Market: Preparing Human Pluripotent Stem Cells Derived Cardiomyocytes for Various Applications. *International Journal of Stem Cells*, *10*(1), 1. doi: 10.15283/IJSC17024

Moretta, A., Ciccone, E., Tambussi, G., Bottino, C., Viale, O., Pende, D., ... Mingari, M. C. (1989). Surface molecules involved in CD3-negative NK cell function. A novel molecule which regulates the activation of a subset of human NK cells. *International journal of cancer*, *4*(1), 48–52. doi: 10.1002/IJC.2910440713

Morvan, M. G., & Lanier, L. L. (2016, dec). NK cells and cancer: you can teach innate cells new tricks. *Nature Reviews Cancer*, *16*(1), 7–19. doi: 10.1038/nrc.2015.5

Mummery, C. L., Zhang, J., Ng, E. S., Elliott, D. A., Elefanty, A. G., & Kamp, T. J. (2012, jul). Differentiation of Human ES and iPS Cells to Cardiomyocytes: A Methods Overview. *Circulation research*, *111*(3), 344. doi: 10.1161/CIRCRESAHA.110.227512

Naeim, F., Nagesh Rao, P., Song, S. X., & Phan, R. T. (2018). Principles of Immunophenotyping. *Atlas of Hematopathology*, 29–56. doi: 10.1016/B978-0-12-809843-1.00002-4

Nagy, A. (2000). Cre Recombinase: The Universal Reagent for Genome Tailoring. *Genesis*, *26*(2), 99–109. doi: 10.1002/(SICI)1526-968X(200002)26:2

Nakamura, T., Shirouzu, T., Nakata, K., Yoshimura, N., & Ushigome, H. (2019, sep). The Role of Major Histocompatibility Complex in Organ Transplantation- Donor Specific Anti-Major Histocompatibility Complex Antibodies Analysis Goes to the Next Stage. *International Journal of Molecular Sciences*, *20*(18). doi: 10.3390/IJMS20184544

Nathans, D. (1964). PUROMYCIN INHIBITION OF PROTEIN SYNTHESIS: INCORPORATION OF PUROMYCIN INTO PEPTIDE CHAINS. *Proceedings of the National Academy of Sciences of the United States of America*, *51*(4), 585–592. doi: 10.1073/PNAS.51.4.585

Naumova, A. V., Modo, M., Moore, A., Murry, C. E., & Frank, J. A. (2014, aug).

Clinical imaging in regenerative medicine. *Nature biotechnology*, *32*(8), 804. doi: 10.1038/NBT.2993

Newman, M., & Ausubel, F. M. (2016, jul). Introduction to gene editing and manipulation using CRISPR/Cas9 technology. *Current Protocols in Molecular Biology*, 31.4.1–31.4.6. doi: 10.1002/cpmb.14

Nicolet, B. P., Guislain, A., & Wolkers, M. C. (2017, jan). Combined Single-Cell Measurement of Cytokine mRNA and Protein Identifies T Cells with Persistent Effector Function. *The Journal of Immunology*, *198*(2), 962–970. doi: 10.4049/JIMMUNOL.1601531/-/DCSUPPLEMENTAL

Noakes, P. S., & Michaelis, L. J. (2013). Innate and adaptive immunity. In *Diet, immunity and inflammation* (pp. 3–33). Elsevier Ltd. doi: 10.1533/9780857095749.1.3

Norbnop, P., Ingrungruanglert, P., Israsena, N., Suphapeetiporn, K., & Shotelersuk, V. (2020, dec). Generation and characterization of HLA-universal platelets derived from induced pluripotent stem cells. *Scientific Reports*, *10*(1). doi: 10.1038/S41598-020-65577-X

O'Brien, T. X., Lee, K. J., & Chien, K. R. (1993, jun). Positional specification of ventricular myosin light chain 2 expression in the primitive murine heart tube. *Proceedings of the National Academy of Sciences of the United States of America*, *90*(11), 5157. doi: 10.1073/PNAS.90.11.5157

Oikonomopoulos, A., Kitani, T., & Wu, J. C. (2018, jul). Pluripotent Stem Cell-Derived Cardiomyocytes as a Platform for Cell Therapy Applications: Progress and Hurdles for Clinical Translation. *Molecular Therapy*, *26*(7), 1624. doi: 10.1016/J.YMTHE.2018.02.026

Ooi, A., Wong, A., Esau, L., Lemtiri-Chlieh, F., & Gehring, C. (2016, jul). A guide to transient expression of membrane proteins in HEK-293 cells for functional characterization. *Frontiers in Physiology*, *7*(Jul), 300. doi: 10.3389/FPHYS.2016.00300/BIBTEX

Otsuka, R., Wada, H., Murata, T., & Seino, K. I. (2020, jul). Immune reaction and regulation in transplantation based on pluripotent stem cell technology. *Inflammation and Regeneration*, *40*(1), 1–9. doi: 10.1186/S41232-020-00125-8/FIGURES/2

Park, M., & Yoon, Y. S. (2018, nov). Cardiac Regeneration with Human Pluripotent Stem Cell-Derived Cardiomyocytes. *Korean Circulation Journal*, *48*(11), 974. doi: 10.4070/KCJ.2018.0312

Parmacek, M. S., & Epstein, J. A. (2009, jul). Cardiomyocyte Renewal. *The New England journal of medicine*, *361*(1), 86. doi: 10.1056/NEJMCIBR0903347

Pasterkamp, G., Galis, Z. S., & De Kleijn, D. P. (2004, apr). Expansive Arterial Remodeling: Location, Location, Location. *Arteriosclerosis, thrombosis, and vascular biology*, *24*(4), 650. doi: 10.1161/01.ATV.0000120376.09047.FE

Patel, M., & Yang, S. (2010). Advances in Reprogramming Somatic Cells to Induced Pluripotent Stem Cells. *Stem cell reviews*, *6*(3), 367. doi: 10.1007/S12015-010-9123-8

Pawani, H., & Bhartiya, D. (2013, feb). Pluripotent stem cells for cardiac regeneration: Overview of recent advances and emerging trends. *The Indian Journal of Medical Research*, *137*(2), 270.

Pegram, H. J., Andrews, D. M., Smyth, M. J., Darcy, P. K., & Kershaw, M. H. (2011, feb). Activating and inhibitory receptors of natural killer cells. *Immunology and Cell Biology*, *89*(2), 216–224. doi: 10.1038/ICB.2010.78

Peirson, S. N., & Butler, J. N. (2007). RNA Extraction From Mammalian Tissues. In *Circadian rhythms. methods in molecular biology* (Vol. 362, pp. 315–327). Humana Press. doi: 10.1007/978-1-59745-257-1_22

Petrus-Reurer, S., Romano, M., Howlett, S., Jones, J. L., Lombardi, G., & Saeb-Parsy, K. (2021, jun). Immunological considerations and challenges for regenerative cellular therapies. *Communications Biology*, *4*(1), 1–16. doi: 10.1038/s42003-021-02237-4

Pirenne, J., Pirenne-Noizat, F., de Groote, D., Vrindts, Y., Lopez, M., Gathy, R., ... Franchimont, P. (1994, apr). Cytokines and organ transplantation. A review. *Nuclear Medicine and Biology*, *21*(3), 545–555. doi: 10.1016/0969-8051(94)90076-0

Plouffe, B. D., Murthy, S. K., & Lewis, L. H. (2015, jan). Fundamentals and Application of Magnetic Particles in Cell Isolation and Enrichment. *Reports on progress in physics.*, *78*(1), 016601. doi: 10.1088/0034-4885/78/1/016601

Poli, A., Michel, T., Thérésine, M., Andrès, E., Hentges, F., & Zimmer, J. (2009). CD56bright natural killer (NK) cells: an important NK cell subset. *Immunology*, *126*(4), 458. doi: 10.1111/J.1365-2567.2008.03027.X

Polo, J. M., Liu, S., Figueroa, M. E., Kulalert, W., Eminli, S., Tan, K. Y., ... Hochedlinger, K. (2010, aug). Cell type of origin influences the molecular and functional properties of mouse induced pluripotent stem cells. *Nature biotechnology*, *28*(8), 848. doi: 10.1038/NBT.1667

Radcliff, G., & Jaroszeski, M. J. (1998). Basics of Flow Cytometry. *Methods in molecular biology*, *91*, 1–24. doi: 10.1385/0-89603-354-6:1

Rajagopalan, S., & Long, E. O. (2012). KIR2DL4 (CD158d): An activation receptor for HLA-G. *Frontiers in Immunology*, *3*(Aug), 258. doi: 10.3389/FIMMU.2012.00258/BIBTEX

Rajala, K., Pekkanen-Mattila, M., & Aalto-Setälä, K. (2011). Cardiac Differentiation of Pluripotent Stem Cells. *Stem Cells International*, 383709. doi: 10.4061/2011/383709

Ranjbar, M., Amiri, F., Nourigorji, M., Torabizadeh, F., Dara, M., & Dianatpour, M. (2022, dec). B2M gene knockout in HEK293T cells by non-viral delivery of CRISPR-Cas9 system for the generation of universal cells. *Egyptian Journal of Medical Human Genetics*, *23*(1), 1–7. doi: 10.1186/S43042-022-00267-Z/FIGURES/3

Raval, A. N., Kamp, T. J., & Hogle, L. F. (2008, oct). Cellular Therapies for Heart Disease: Unveiling the Ethical and Public Policy Challenges. *Journal of molecular*

and cellular cardiology, *45*(4), 593. doi: 10.1016/J.YJMCC.2007.11.005

Reinhart, J., & Pearson, W. R. (1993, jun). The Structure of Two Murine Class-Mu Glutathione Transferase Genes Coordinately Induced by Butylated Hydroxyanisole. *Archives of Biochemistry and Biophysics*, *303*(2), 383–393. doi: 10.1006/abbi.1993.1299

Richardson, W. J., Clarke, S. A., Alexander Quinn, T., & Holmes, J. W. (2015, oct). Physiological Implications of Myocardial Scar Structure. *Comprehensive Physiology*, *5*(4), 1877. doi: 10.1002/CPHY.C140067

Riolobos, L., Hirata, R. K., Turtle, C. J., Wang, P. R., Gornalusse, G. G., Zavajlevski, M., ... Russell, D. W. (2013). HLA Engineering of Human Pluripotent Stem Cells. *Molecular Therapy*, *21*(6), 1232. doi: 10.1038/MT.2013.59

Riss, T., Niles, A., Moravec, R., Karassina, N., & Vidugiriene, J. (2019, may). Cytotoxicity Assays: In Vitro Methods to Measure Dead Cells. In *Assay guidance manual [internet]* (chap. Cytotoxici). Eli Lilly & Company and the National Center for Advancing Translational Sciences. Retrieved from `https://www.ncbi.nlm.nih.gov/books/NBK540958/`

Roche Diagnostics. (2007). *LDH Cytotoxicity Detection Kit Document 11644793001 Version 10* (Vol. 25) (No. Jan).

Rodríguez-Rodríguez, D. R., Ramírez-Solís, R., Garza-Elizondo, M. A., Garza-Rodríguez, M. D. L., & Barrera-Saldaña, H. A. (2019, apr). Genome editing: A perspective on the application of CRISPR/Cas9 to study human diseases (Review). *International Journal of Molecular Medicine*, *43*(4), 1559. doi: 10.3892/IJMM.2019.4112

Romano, M., Fanelli, G., Albany, C. J., Giganti, G., & Lombardi, G. (2019). Past, Present, and Future of Regulatory T Cell Therapy in Transplantation and Autoimmunity. *Frontiers in Immunology*, *10*(Jan), 43. doi: 10.3389/FIMMU.2019.00043

Rong, Z., Wang, M., Hu, Z., Stradner, M., Zhu, S., Kong, H., ... Fu, X. (2014, jan). An effective approach to prevent immune rejection of human ESC-derived allografts. *Cell stem cell*, *14*(1), 121. doi: 10.1016/J.STEM.2013.11.014

Rossbach, B., Hariharan, K., Mah, N., Oh, S. J., Volk, H. D., Reinke, P., & Kurtz, A. (2022, apr). Human iPSC-Derived Renal Cells Change Their Immunogenic Properties during Maturation: Implications for Regenerative Therapies. *Cells*, *11*(8). doi: 10.3390/CELLS11081328/S1

Roth, G. A., Mensah, G. A., Johnson, C. O., Addolorato, G., Ammirati, E., Baddour, L. M., ... Fuster, V. (2020, dec). Global Burden of Cardiovascular Diseases and Risk Factors, 1990â“2019: Update From the GBD 2019 Study. *Journal of the American College of Cardiology*, *76*(25), 2982–3021. doi: 10.1016/J.JACC.2020.11.010

Rowley, T. (2012, aug). Flow Cytometry - A Survey and the Basics. *Materials and Methods*, *2*. doi: 10.13070/MM.EN.2.125

Ruggeri, L., Mancusi, A., Burchielli, E., Perruccio, K., Aversa, F., Martelli, M. F., & Velardi, A. (2006, oct). Natural killer cell recognition of missing self and

haploidentical hematopoietic transplantation. *Seminars in Cancer Biology*, *16*(5), 404–411. doi: 10.1016/J.SEMCANCER.2006.07.007

Ryu, S. M., Hur, J. W., & Kim, K. (2019, aug). Evolution of CRISPR towards accurate and efficient mammal genome engineering. *BMB Reports*, *52*(8), 475–481. doi: 10.5483/BMBRep.2019.52.8.149

Sacchetto, C., Vitiello, L., de Windt, L. J., Rampazzo, A., & Calore, M. (2020, may). Modeling Cardiovascular Diseases with hiPSC-Derived Cardiomyocytes in 2D and 3D Cultures. *International Journal of Molecular Sciences*, *21*(9). doi: 10.3390/IJMS21093404

Sadahiro, T. (2019, dec). Cardiac regeneration with pluripotent stem cell-derived cardiomyocytes and direct cardiac reprogramming. *Regenerative Therapy*, *11*, 95–100. doi: 10.1016/J.RETH.2019.06.004

Säljö, K., Barone, A., Mölne, J., Rydberg, L., Teneberg, S., & Breimer, M. E. (2017, oct). HLA and Histo-Blood Group Antigen Expression in Human Pluripotent Stem Cells and their Derivatives. *Scientific Reports*, *7*(1), 1–14. doi: 10.1038/s41598-017-12231-8

Sander, J. D., & Joung, J. K. (2014). CRISPR-Cas systems for genome editing, regulation and targeting. *Nature biotechnology*, *32*(4), 347. doi: 10.1038/NBT.2842

Sato, T., Akatsuka, H., Yamaguchi, Y., Miyashita, K., Tanaka, M., Tamaki, T., ... Kimura, M. (2015). Establishment of β-2 microglobulin deficient human iPS cells using CRISPR/Cas9 system. *Integrative Molecular Medicine*, *2*(6). doi: 10.15761/IMM.1000171

Schaun, M. I., Eibel, B., Kristocheck, M., Sausen, G., Machado, L., Koche, A., & Markoski, M. M. (2016). Cell Therapy in Ischemic Heart Disease: Interventions That Modulate Cardiac Regeneration. *Stem Cells International*, *2016*. doi: 10.1155/2016/2171035

Scheiner, Z. S., Talib, S., & Feigal, E. G. (2014, feb). The Potential for Immunogenicity of Autologous Induced Pluripotent Stem Cell-derived Therapies. *The Journal of Biological Chemistry*, *289*(8), 4571. doi: 10.1074/JBC.R113.509588

Segers, V. F., & Lee, R. T. (2008, feb). Stem-cell therapy for cardiac disease. *Nature*, *451*(7181), 937–942. doi: 10.1038/nature06800

Shao, L., Zhang, Y., Pan, X., Liu, B., Liang, C., Zhang, Y., ... Li, Y. (2020, mar). Knockout of beta-2 microglobulin enhances cardiac repair by modulating exosome imprinting and inhibiting stem cell-induced immune rejection. *Cellular and Molecular Life Sciences*, *77*(5), 937–952. doi: 10.1007/S00018-019-03220-3/FIGURES/8

Sharma, A., Li, G., Rajarajan, K., Hamaguchi, R., Burridge, P. W., & Wu, S. M. (2015, mar). Derivation of Highly Purified Cardiomyocytes from Human Induced Pluripotent Stem Cells Using Small Molecule-modulated Differentiation and Subsequent Glucose Starvation. *Journal of Visualized Experiments : JoVE*(97), 52628. doi: 10.3791/52628

Shi, L., Li, W., Liu, Y., Chen, Z., Hui, Y., Hao, P., ... Zhang, X. (2020, nov). Generation

of hypoimmunogenic human pluripotent stem cells via expression of membrane-bound and secreted β2m-HLA-G fusion proteins. *Stem Cells*, *38*(11), 1423–1437. doi: 10.1002/STEM.3269

Shiba, Y., Hauch, K. D., & Laflamme, M. A. (2009, aug). Cardiac Applications for Human Pluripotent Stem Cells. *Current pharmaceutical design*, *15*(24), 2791. doi: 10.2174/138161209788923804

Shklovskaya, E., & Rizos, H. (2021, jul). MHC Class I Deficiency in Solid Tumors and Therapeutic Strategies to Overcome It. *International Journal of Molecular Sciences*, *22*(13). doi: 10.3390/IJMS22136741

Silver, S. E., Barrs, R. W., & Mei, Y. (2021, nov). Transplantation of Human Pluripotent Stem Cell-Derived Cardiomyocytes for Cardiac Regenerative Therapy. *Frontiers in Cardiovascular Medicine*(Nov), 1620. doi: 10.3389/FCVM.2021.707890

Sontayananon, N., Redwood, C., Davies, B., & Gehmlich, K. (2020, nov). Fluorescent PSC-Derived Cardiomyocyte Reporter Lines: Generation Approaches and Their Applications in Cardiovascular Medicine. *Biology*, *9*(11), 1–24. doi: 10.3390/BIOLOGY9110402

Staerk, J., Dawlaty, M. M., Gao, Q., Maetzel, D., Hanna, J., Sommer, C. A., ... Jaenisch, R. (2010). Reprogramming of peripheral blood cells to induced pluripotent stem cells. *Cell stem cell*, *7*(1), 20. doi: 10.1016/J.STEM.2010.06.002

Steimle, J. D., & Moskowitz, I. P. (2017, dec). TBX5: A Key Regulator of Heart Development. *Current topics in developmental biology*, *122*, 195. doi: 10.1016/BS.CTDB.2016.08.008

Steyer, B., Bu, Q., Cory, E., Jiang, K., Duong, S., Sinha, D., ... Saha, K. (2018, feb). Scarless Genome Editing of Human Pluripotent Stem Cells via Transient Puromycin Selection. *Stem Cell Reports*, *10*(2), 642. doi: 10.1016/J.STEMCR.2017.12.004

Stordeur, P., Poulin, L. F., Craciun, L., Zhou, L., Schandene, L., De Lavareille, A., ... Goldman, M. (2002). Cytokine mRNA quantification by real-time PCR. *Journal of Immunological Methods*, *259*, 55–64.

Strober, W. (1997, mar). Trypan Blue Exclusion Test of Cell Viability. *Current Protocols in Immunology*, *21*(1), A.3B.1–A.3B.2. doi: 10.1002/0471142735.IMA03BS21

Sun, N., Yazawa, M., Liu, J., Han, L., Sanchez-Freire, V., Abilez, O. J., ... Wu, J. C. (2012, apr). Patient-specific induced pluripotent stem cells as a model for familial dilated cardiomyopathy. *Science Translational Medicine*, *4*(130), 130ra47. doi: 10.1126/scitranslmed.3003552

Sweeney, H. L., & Hammers, D. W. (2018, feb). Muscle Contraction. *Cold Spring Harbor Perspectives in Biology*, *10*(2). doi: 10.1101/CSHPERSPECT.A023200

Takahashi, K., Tanabe, K., Ohnuki, M., Narita, M., Ichisaka, T., Tomoda, K., & Yamanaka, S. (2007, nov). *Induction of pluripotent stem cells from adult human fibroblasts by defined factors* (Vol. 131) (No. 5). Cell. doi: 10.1016/J.CELL.2007.11.019

Takahashi, K., & Yamanaka, S. (2006). Induction of Pluripotent Stem Cells from Mouse

Embryonic and Adult Fibroblast Cultures by Defined Factors. *Cell*, *126*(4), 663–676. doi: 10.1016/j.cell.2006.07.024

Tang, Q., & Bluestone, J. A. (2013). Regulatory T-Cell Therapy in Transplantation: Moving to the Clinic. *Cold Spring Harbor Perspectives in Medicine*, *3*(11). doi: 10.1101/CSHPERSPECT.A015552

Tapia, N., & Schöler, H. R. (2016, sep). Molecular Obstacles to Clinical Translation of iPSCs. *Cell Stem Cell*, *19*(3), 298–309. doi: 10.1016/J.STEM.2016.06.017

Taylor, C. J., Bolton, E. M., & Bradley, J. A. (2011, jul). Immunological considerations for embryonic and induced pluripotent stem cell banking. *Philosophical Transactions of the Royal Society of London. Series B, Biological Sciences*, *366*(1575), 2312. doi: 10.1098/RSTB.2011.0030

Terrovitis, J. V., Smith, R. R., & Marbán, E. (2010, feb). Assessment and Optimization of Cell Engraftment after Transplantation into the Heart. *Circulation research*, *106*(3), 479. doi: 10.1161/CIRCRESAHA.109.208991

Tersigni, C., Meli, F., Neri, C., Iacoangeli, A., Franco, R., Lanzone, A., ... Di Simone, N. (2020, jul). Role of Human Leukocyte Antigens at the Feto-Maternal Interface in Normal and Pathological Pregnancy: An Update. *International Journal of Molecular Sciences*, *21*(13), 1–13. doi: 10.3390/IJMS21134756

Thomas, C., & Tampé, R. (2021, jun). MHC I assembly and peptide editing - chaperones, clients, and molecular plasticity in immunity. *Current Opinion in Immunology*, *70*, 48–56. doi: 10.1016/J.COI.2021.02.004

Thomson, J. A., Itskovitz-Eldor, J., Shapiro, S. S., Waknitz, M. A., Swiergiel, J. J., Marshall, V. S., & Jones, J. M. (1998, nov). Embryonic Stem Cell Lines Derived from Human Blastocysts. *Science*, *282*(5391), 1145–1147. doi: 10.1126/SCIENCE.282.5391.1145

Thongsin, N., & Wattanapanitch, M. (2021, oct). Generation of B2M bi-allelic knockout human induced pluripotent stem cells (MUSIi001-A-1) using a CRISPR/Cas9 system. *Stem cell research*, *56*. doi: 10.1016/J.SCR.2021.102551

Timmis, A., Townsend, N., Gale, C. P., Torbica, A., Lettino, M., Petersen, S. E., ... Bardinet, I. (2020, jan). European Society of Cardiology: Cardiovascular Disease Statistics 2019. *European Heart Journal*, *41*(1), 12–85. doi: 10.1093/EURHEARTJ/EHZ859

Tohyama, S., Hattori, F., Sano, M., Hishiki, T., Nagahata, Y., Matsuura, T., ... Fukuda, K. (2013, jan). Distinct metabolic flow enables large-scale purification of mouse and human pluripotent stem cell-derived cardiomyocytes. *Cell Stem Cell*, *12*(1), 127–137. doi: 10.1016/J.STEM.2012.09.013

Tomas, C., Lodge, T. A., Potter, M., Elson, J. L., Newton, J. L., & Morten, K. J. (2019, dec). Assessing cellular energy dysfunction in CFS/ME using a commercially available laboratory test. *Scientific Reports*, *9*(1). doi: 10.1038/S41598-019-47966-Z

Tonsho, M., Michel, S., Ahmed, Z., Alessandrini, A., & Madsen, J. C. (2014). Heart Transplantation: Challenges Facing the Field. *Cold Spring Harbor Perspectives in*

Medicine, *4*(5). doi: 10.1101/CSHPERSPECT.A015636

Trounson, A., Boyd, N. R., & Boyd, R. L. (2019, apr). Toward a Universal Solution: Editing Compatibility into Pluripotent Stem Cells. *Cell Stem Cell*, *24*(4), 508–510. doi: 10.1016/J.STEM.2019.03.003

Umekage, M., Sato, Y., & Takasu, N. (2019, sep). Overview: an iPS cell stock at CiRA. *Inflammation and Regeneration*, *39*(1). doi: 10.1186/S41232-019-0106-0

Ungrin, M. D., Joshi, C., Nica, A., Bauwens, C., & Zandstra, P. W. (2008, feb). Reproducible, Ultra High-Throughput Formation of Multicellular Organization from Single Cell Suspension-Derived Human Embryonic Stem Cell Aggregates. *PLoS ONE*, *3*(2). doi: 10.1371/JOURNAL.PONE.0001565

Vanneaux, V. (2019, sep). Induced Pluripotent Stem Cells for Clinical Use. In *Update on mesenchymal and induced pluripotent stem cells.* IntechOpen. doi: 10.5772/INTECHOPEN.88878

Vernardis, S. I., Terzoudis, K., Panoskaltsis, N., & Mantalaris, A. (2017, feb). Human embryonic and induced pluripotent stem cells maintain phenotype but alter their metabolism after exposure to ROCK inhibitor. *Scientific Reports*, *7*(1), 1–11. doi: 10.1038/srep42138

Volarevic, M., Wu, C. H., Smolic, R., Andorfer, J. H., & Wu, G. Y. (2007, nov). A novel G418 conjugate results in targeted selection of genetically protected hepatocytes without bystander toxicity. *Bioconjugate chemistry*, *18*(6), 1965–1971. doi: 10.1021/BC700277D

Vukicevic, S., Kleinman, H. K., Luyten, F. P., Roberts, A. B., Roche, N. S., & Reddi, A. H. (1992, sep). Identification of multiple active growth factors in basement membrane matrigel suggests caution in interpretation of cellular activity related to extracellular matrix components. *Experimental Cell Research*, *202*(1), 1–8. doi: 10.1016/0014-4827(92)90397-Q

Waas, M., Weerasekera, R., Kropp, E. M., Romero-Tejeda, M., Poon, E. N., Boheler, K. R., ... Gundry, R. L. (2019, feb). Are These Cardiomyocytes? Protocol Development Reveals Impact of Sample Preparation on the Accuracy of Identifying Cardiomyocytes by Flow Cytometry. *Stem Cell Reports*, *12*(2), 395. doi: 10.1016/J.STEMCR.2018.12.016

Walsh, P. T., Strom, T. B., & Turka, L. A. (2004). Routes to Transplant Tolerance versus Rejection: The Role of Cytokines. *Immunity*, *20*(2), 121. doi: 10.1016/S1074-7613(04)00024-X

Wang, D., Quan, Y., Yan, Q., Morales, J. E., & Wetsel, R. A. (2015, oct). Targeted Disruption of the β2-Microglobulin Gene Minimizes the Immunogenicity of Human Embryonic Stem Cells. *Stem Cells Translational Medicine*, *4*(10), 1234–1245. doi: 10.5966/sctm.2015-0049

Wang, Y., Chou, B. K., Dowey, S., He, C., Gerecht, S., & Cheng, L. (2013, nov). Scalable expansion of human induced pluripotent stem cells in the defined xeno-free E8 medium under adherent and suspension culture conditions. *Stem cell research*, *11*(3), 1103. doi: 10.1016/J.SCR.2013.07.011

Waseem, S., Allen, M. A., Schreier, S., Udomsangpetch, R., & Bhakdi, S. C. (2014, may). Antibody-Conjugated Paramagnetic Nanobeads: Kinetics of Bead-Cell Binding. *International Journal of Molecular Sciences*, *15*(5), 8821. doi: 10.3390/IJMS15058821

Weidmann, E., Brieger, J., Jahn, B., Hoelzer, D., Bergmann, L., & Mitrou, P. S. (1995, mar). Lactate dehydrogenase-release assay: a reliable, nonradioactive technique for analysis of cytotoxic lymphocyte-mediated lytic activity against blasts from acute myelocytic leukemia. *Annals of hematology*, *70*(3), 153–158. doi: 10.1007/BF01682036

Weiss, E., Schlegel, J., Terpitz, U., Weber, M., Linde, J., Schmitt, A. L., ... Loeffler, J. (2020, sep). Reconstituting NK Cells After Allogeneic Stem Cell Transplantation Show Impaired Response to the Fungal Pathogen Aspergillus fumigatus. *Frontiers in Immunology*, *11*, 2117. doi: 10.3389/FIMMU.2020.02117/BIBTEX

Weiss, R., Gerdes, W., Berthold, R., Sack, U., Koehl, U., Hauschildt, S., & Grahnert, A. (2021, nov). Comparison of three CD3-specific separation methods leading to labeled and label-free T cells. *Cells*, *10*(11). doi: 10.3390/CELLS10112824/S1

Xu, C., Police, S., Rao, N., & Carpenter, M. K. (2002, sep). Characterization and enrichment of cardiomyocytes derived from human embryonic stem cells. *Circulation Research*, *91*(6), 501–508. doi: 10.1161/01.RES.0000035254.80718.91

Xu, H., Wang, B., Ono, M., Kagita, A., Fujii, K., Sasakawa, N., ... Hotta, A. (2019, apr). Targeted Disruption of HLA Genes via CRISPR-Cas9 Generates iPSCs with Enhanced Immune Compatibility. *Cell Stem Cell*, *24*(4), 566–578.e7. doi: 10.1016/J.STEM.2019.02.005/ATTACHMENT/34B5807D-C4DA-4A48-A67D-21C64BD91BD9/MMC7.XLS

Yawata, M., Yawata, N., Draghi, M., Partheniou, F., Little, A. M., & Parham, P. (2008, sep). MHC class I specific inhibitory receptors and their ligands structure diverse human NK-cell repertoires toward a balance of missing self-response. *Blood*, *112*(6), 2369. doi: 10.1182/BLOOD-2008-03-143727

Ye, L., Chang, Y. H., Xiong, Q., Zhang, P., Zhang, L., Somasundaram, P., ... Zhang, J. (2014, dec). Cardiac repair in a porcine model of acute myocardial infarction with human induced pluripotent stem cell-derived cardiovascular cell populations. *Cell Stem Cell*, *15*(6), 750. doi: 10.1016/J.STEM.2014.11.009

Ye, Q., Sung, T. C., Yang, J. M., Ling, Q. D., He, Y., & Higuchi, A. (2020, dec). Generation of universal and hypoimmunogenic human pluripotent stem cells. *Cell Proliferation*, *53*(12), e12946. doi: 10.1111/CPR.12946

Zha, S., Tay, J. C. K., Zhu, S., Li, Z., Du, Z., & Wang, S. (2020). Generation of Mesenchymal Stromal Cells with Low Immunogenicity from Human PBMC-Derived β2 Microglobulin Knockout Induced Pluripotent Stem Cells. *Cell Transplantation*, *29*. doi: 10.1177/0963689720965529

Zhang, M., Schulte, J. S., Heinick, A., Piccini, I., Rao, J., Quaranta, R., ... Greber, B. (2015, may). Universal Cardiac Induction of Human Pluripotent Stem Cells in Two and Three-Dimensional Formats: Implications for In Vitro Maturation. *Stem*

Cells, *33*(5), 1456–1469. doi: 10.1002/STEM.1964

Zhang, Z., & Nam, Y. J. (2018, oct). Generation of MLC-2v-tdTomato knock-in reporter mouse line. *Genesis*, *56*(10), e23256. doi: 10.1002/dvg.23256

Zhao, M., Tang, Y., Zhou, Y., & Zhang, J. (2019, dec). Deciphering Role of Wnt Signalling in Cardiac Mesoderm and Cardiomyocyte Differentiation from Human iPSCs: Four-dimensional control of Wnt pathway for hiPSC-CMs differentiation. *Scientific Reports*, *9*(1). doi: 10.1038/S41598-019-55620-X

Zhao, T., Zhang, Z. N., Rong, Z., & Xu, Y. (2011, may). Immunogenicity of induced pluripotent stem cells. *Nature*, *474*(7350), 212–215. doi: 10.1038/nature10135

Zhao, W., Lei, A., Tian, L., Wang, X., Correia, C., Weiskittel, T., ... Zhang, J. (2020, jun). Strategies for Genetically Engineering Hypoimmunogenic Universal Pluripotent Stem Cells. *iScience*, *23*(6), 101162. doi: 10.1016/J.ISCI.2020.101162

Zheng, Q., Cai, X., Tan, M. H., Schaffert, S., Arnold, C. P., Gong, X., ... Huang, S. (2014, sep). Precise gene deletion and replacement using the CRISPR/Cas9 system in human cells. *BioTechniques*, *57*(3), 115–124. doi: 10.2144/000114196

Zhou, F. (2009). Molecular mechanisms of IFN-gamma to up-regulate MHC class I antigen processing and presentation. *International reviews of immunology*, *28*(3-4), 239–260. doi: 10.1080/08830180902978120

Zhou, Y., Singh, A. K., Hoyt, R. F., Wang, S., Yu, Z., Hunt, T., ... Horvath, K. A. (2014). Regulatory T cells enhance mesenchymal stem cell survival and proliferation following autologous cotransplantation in ischemic myocardium. *Journal of Thoracic and Cardiovascular Surgery*, *148*(3), 1131–1137. doi: 10.1016/J.JTCVS.2014.06.029

Zhu, W. Z., Hauch, K. D., Xu, C., & Laflamme, M. A. (2009, jan). Human Embryonic Stem Cells and Cardiac Repair. *Transplantation reviews*, *23*(1), 53. doi: 10.1016/J.TRRE.2008.05.005

Zimmer, J., Andrès, E., Donato, L., Hanau, D., Hentges, F., & de la Salle, H. (2005, oct). Clinical and immunological aspects of HLA class I deficiency. *QJM*, *98*(10), 719–727. doi: 10.1093/QJMED/HCI112

Zwi-Dantsis, L., Huber, I., Habib, M., Winterstern, A., Gepstein, A., Arbel, G., & Gepstein, L. (2013, jun). Derivation and cardiomyocyte differentiation of induced pluripotent stem cells from heart failure patients. *European Heart Journal*, *34*(21), 1575–1586. doi: 10.1093/EURHEARTJ/EHS096

Supplement

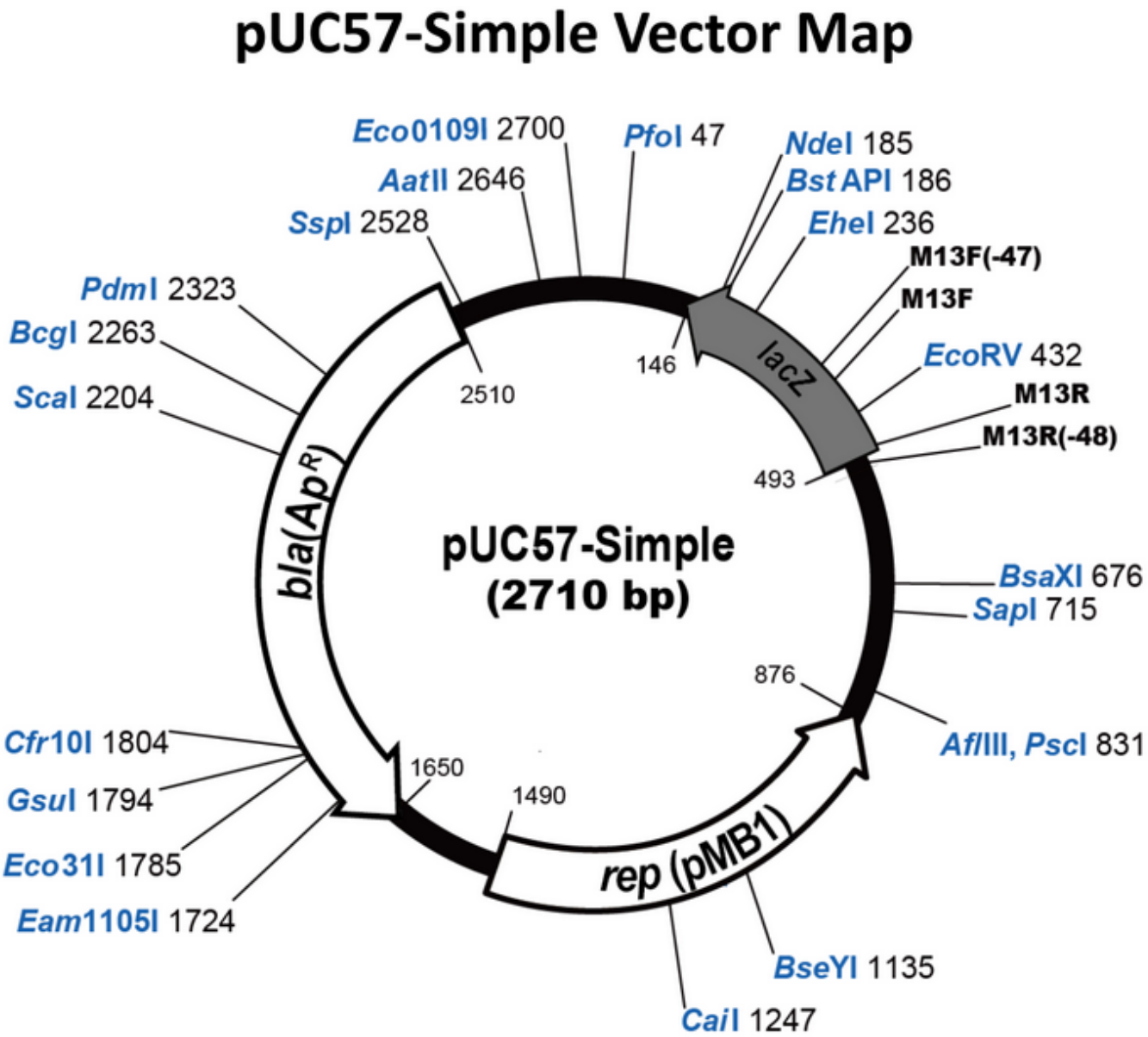

Figure S1: pUC57-Simple vector map (GenScript, Piscataway, NJ)

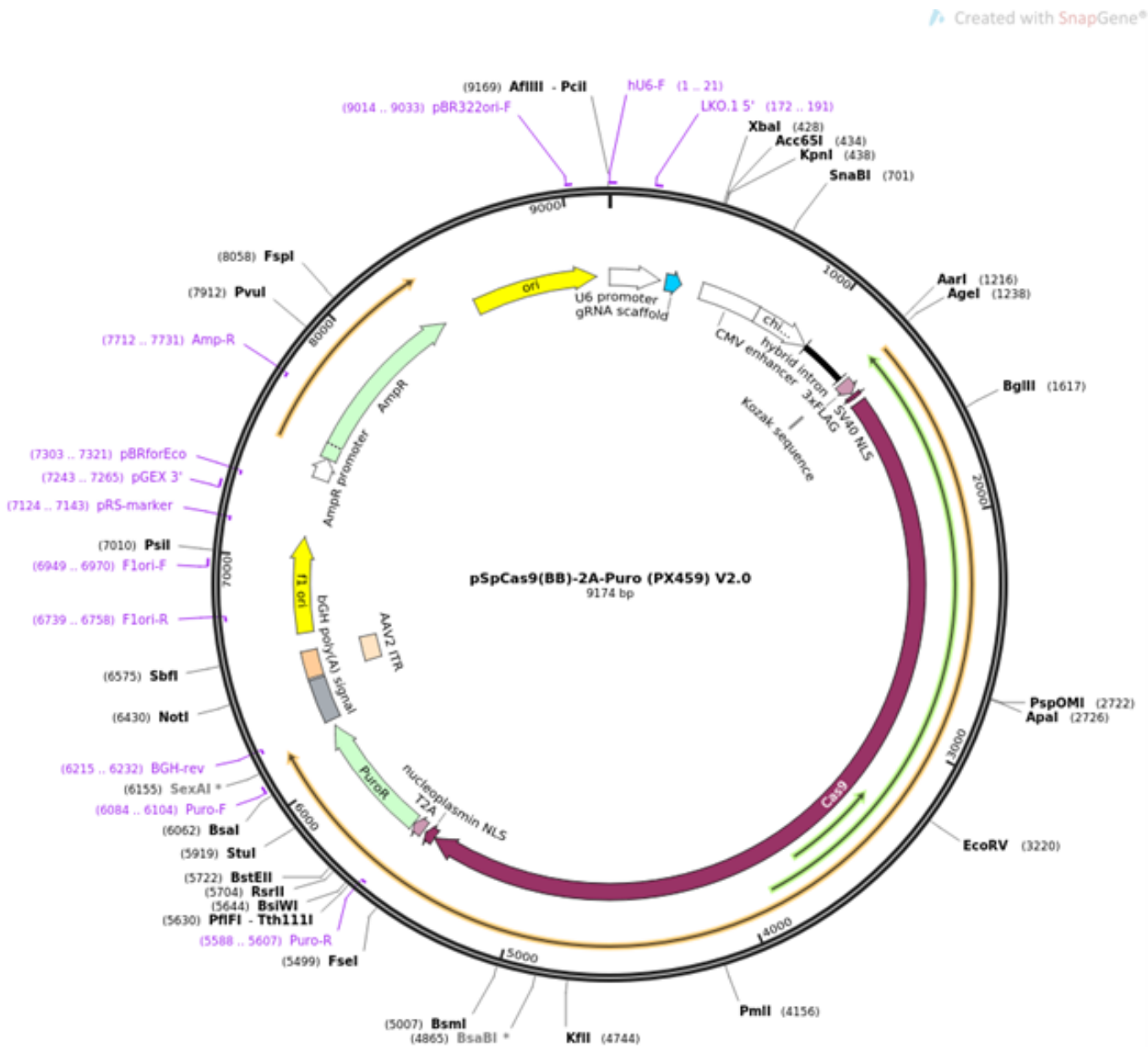

Figure S2: pSpCas9(BB)-2A-Puro (pX459) V2.0 vector map (Addgene, Watertown, MA)

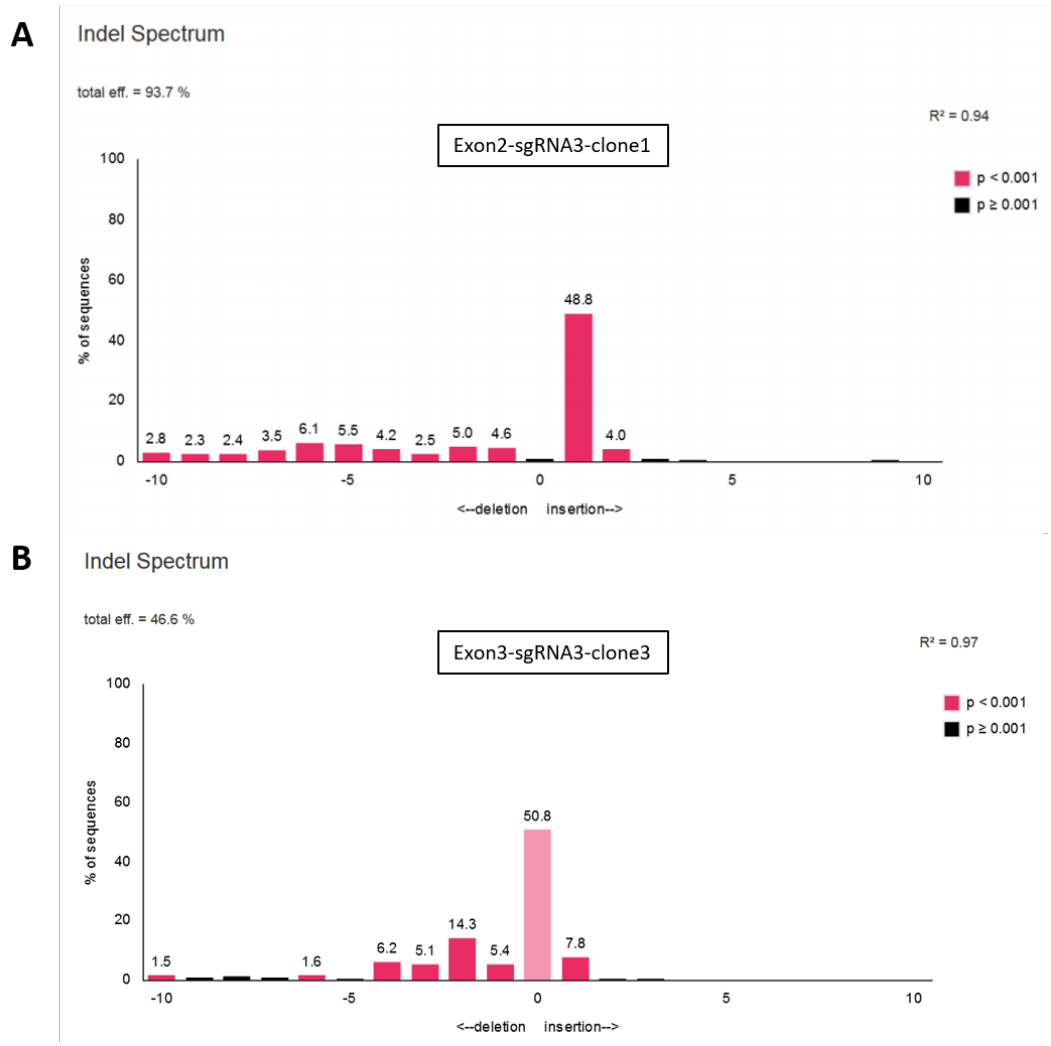

Figure S3: Analysis of sgRNA cleavage efficiency
(A) Exon 2 sgRNA 3 clone 1 cleavage efficiency. **(B)** Exon 2 sgRNA 3 clone 3 cleavage efficiency.

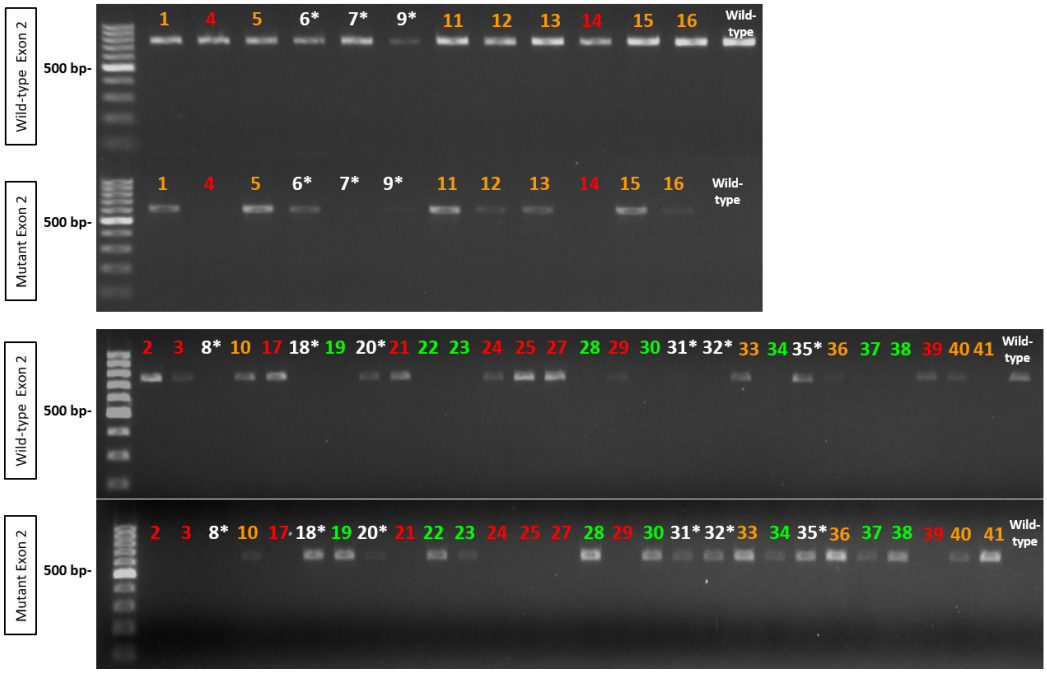

Figure S4: Agarose gel electrophoresis to confirm the *B2M* Exon 2 knockout

Agarose gel electrophoresis to confirm the B2M Exon 2 knockout and the knock-in of the neomycin resistance. The upper gel shows the detection of wild-type alleles using primer set B2M Exon 2 (WT) (B2M Ex2 GT Fwd2/ B2M Ex2 Exon GT Rev1) which led to a 763 bp amplicon. The lower gel shows the detection of mutant alleles using primer set B2M Exon 2 (KO) (B2M Ex2 GT Fwd2/ B2M Ex2 GT Neo R1) which led to a 652 bp amplicon. Clones identified with a homozygous genotype were marked in green. Clones identified with a heterozygous genotype were marked in orange. Clones identified with a wild-type genotype were marked in red. No PCR product or unefficient gene editing were marked with a $*$. Non-edited E5Vf hiPS cells (wild-type) served as a negative control.

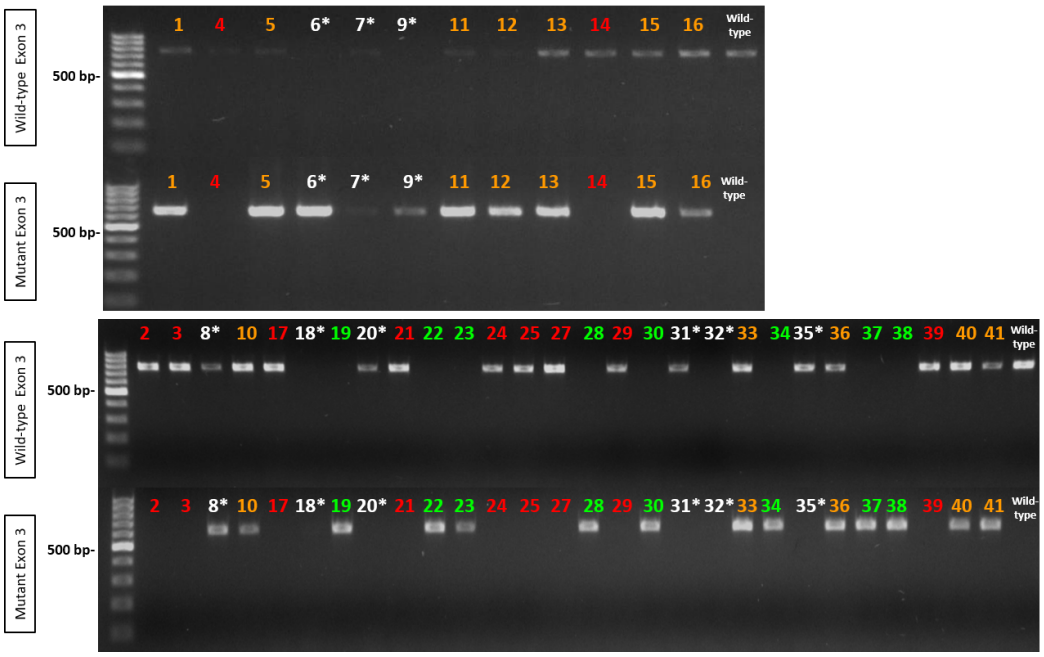

Figure S5: Agarose gel electrophoresis to confirm the *B2M* Exon 3 knockout

Agarose gel electrophoresis to confirm the B2M Exon 3 knockout and the knock-in of the neomycin resistance. The upper gel shows the detection of wild-type alleles using primer set B2M Exon 3 (WT) (B2M Ex3 GT Fwd1/ B2M Ex3 GT Rev3) which led to a 767 bp amplicon. The lower gel shows the detection of mutant alleles using primer set B2M Exon 3 (KO) (B2M Ex3 Neo F2/ B2M Ex3 GT Rev3) which led to a 659 bp amplicon. Clones identified with a homozygous genotype were marked in green. Clones identified with a heterozygous genotype were marked in orange. Clones identified with a wild-type genotype were marked in red. Probes showing no PCR product or unefficient gene editing were marked with a ∗. Non-edited E5Vf hiPS cells (wild-type) served as a negative control.

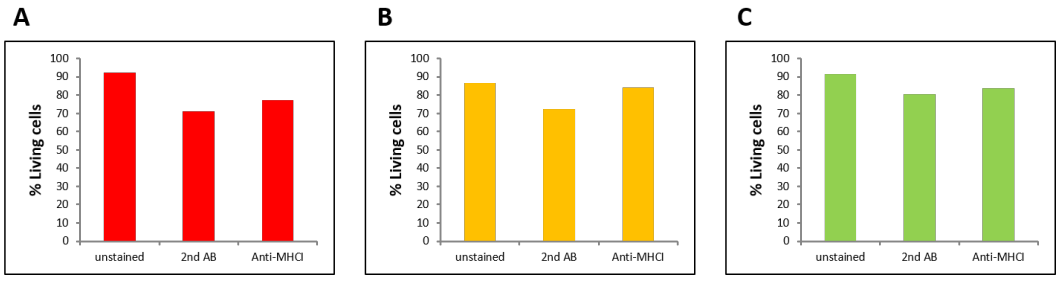

Figure S6: Quantitative determination of cell viability based on FACS analysis

(A) Cell viability of non-edited E5Vf hiPS cell (wild-type) samples (red). **(B)** Cell viability of heterozygous E5V ΔPB hiPS cell samples (orange). **(C)** Cell viability of heterozygous E5V ΔPB hiPS cell samples (green). The percentage of living cells was determined by adding DAPI to all samples immediately before FACS analysis. **Abbreviations**: FACS: fluorescence-activated cell sorting; hiPS cells: human induced pluripotent stem cells; DAPI: 4',6-diamidino-2-phenylindole

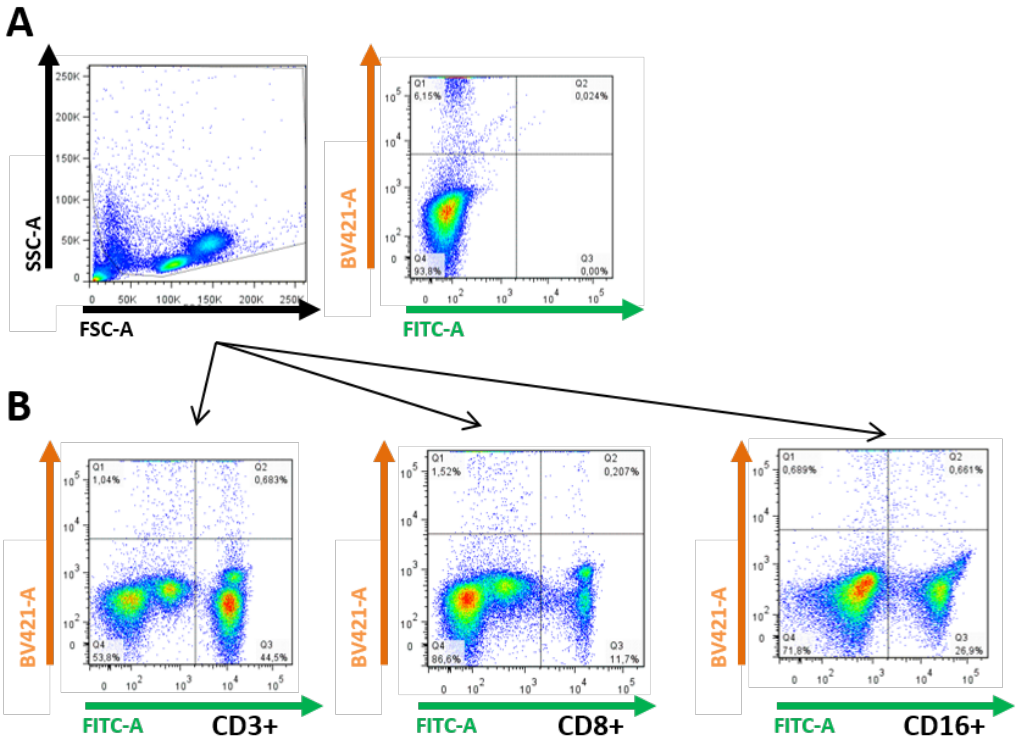

Figure S7: FACS analysis for relative quantification of lymphocyte subpopulations frequencies within the PBMC fraction

(A) Representative FACS anaylsis of unstained PBMCs (control). **(B)** Representative FACS anaylsis of PBMCs stained with specific antibodies (CD3-FITC, CD8-FITC, CD16-FITC, human, Miltenyi Biotec) labelling their respective CD markers. A sequential gating strategy for each flow panel was performed based on the unstained PBMC control sample. Gating of FITC (CD3, CD8 and CD16) positive cells enabled to determine the different lymphocyte subpopulation frequencies. **Abbreviations**: FACS: fluorescence-activated cell sorting; CD: cluster of differentiation

Acknowledgements

First and foremost, I would like to express my deep and sincere gratitude to my supervisor, Prof. Dr. med. Markus Krane, for his continuous and overwhelming support throughout this project. He always took time to read my research reports and discuss my results, gave me insightful comments and suggestions on my experiments and encouraged me to pursue an academic career. The commitment and scientific interest he showed, in addition to his normal clinical routine, cannot be taken for granted and have my deep respect.

Besides, I am extremely grateful to my mentor PD Dr. rer. nat. Harald Lahm for the outstanding supervision of my dissertation. He always provided me with valuable advice and generously shared his knowledge and experience. His guidance in planning and conducting experiments, his incredible patience and his efforts to answer my millions of questions have helped me immeasurably throughout the experimental and writing process of this thesis.

I would like to extend my sincere thanks to Dr. rer. nat. Martina Dreßen, who was like a second mentor to me and always showed great interest in my dissertation. She consistently provided valuable comments and brilliant guidance, helped me with data analysis and put a lot of time and effort into correcting my dissertation.

I am also indebted to Irina Neb and Claudia Abou-Ajram, who were always ready to help when there was a problem. I would like to thank them for their support and help with cell culture and for sharing their technical laboratory knowledge with me.

In addition, I would also like to thank Nicole Beck, who always picked out the best PBMCs for my experiments.

My thanks should also go to Dr. med. Elda Dzilic for kindly providing the cell line, which I was allowed to use for further genetic manipulations and experiments.

Furthermore, I would like to thank my co-doctoral students Paul Heinrich and Kathrin Krähschütz and my lab colleagues Tatjana Luzius and Luis de la Osa de la Rosa, for the numerous scientific and friendly discussions.

I would also like to thank all the other members of the working group for their good and friendly cooperation.

On a personal note, I would like to thank my family, especially my parents, for their unconditional support and encouragement. Their belief in me has kept my spirits and motivation high during my lab work and the writing process. My special thanks go to my mother, who

helped me a lot in proofreading my English and to my boyfriend, who not only supported me morally but also got personally involved by donating blood for my experimental work.